Final Report

AE3200 Design Synthesis Exercise

Faculty of Aerospace Engineering; TU Delft, June 21st 2022

L.O.V.E. mission - *Life On Venus Exploration*

Julian Rothenbuchner	5115221	Felice ten Voorde	4781597
Austin Phillips	5078814	Nora van den Heuvel	5042291
Thijs Goetzee	4539907	Dominique Nieuwenhuizen	5092337
Sowndariya Dhiyaneeswaran	4816277	Addick Land	4557344
Justin Bos	5079268	Carlos Castro Garcia	5003105

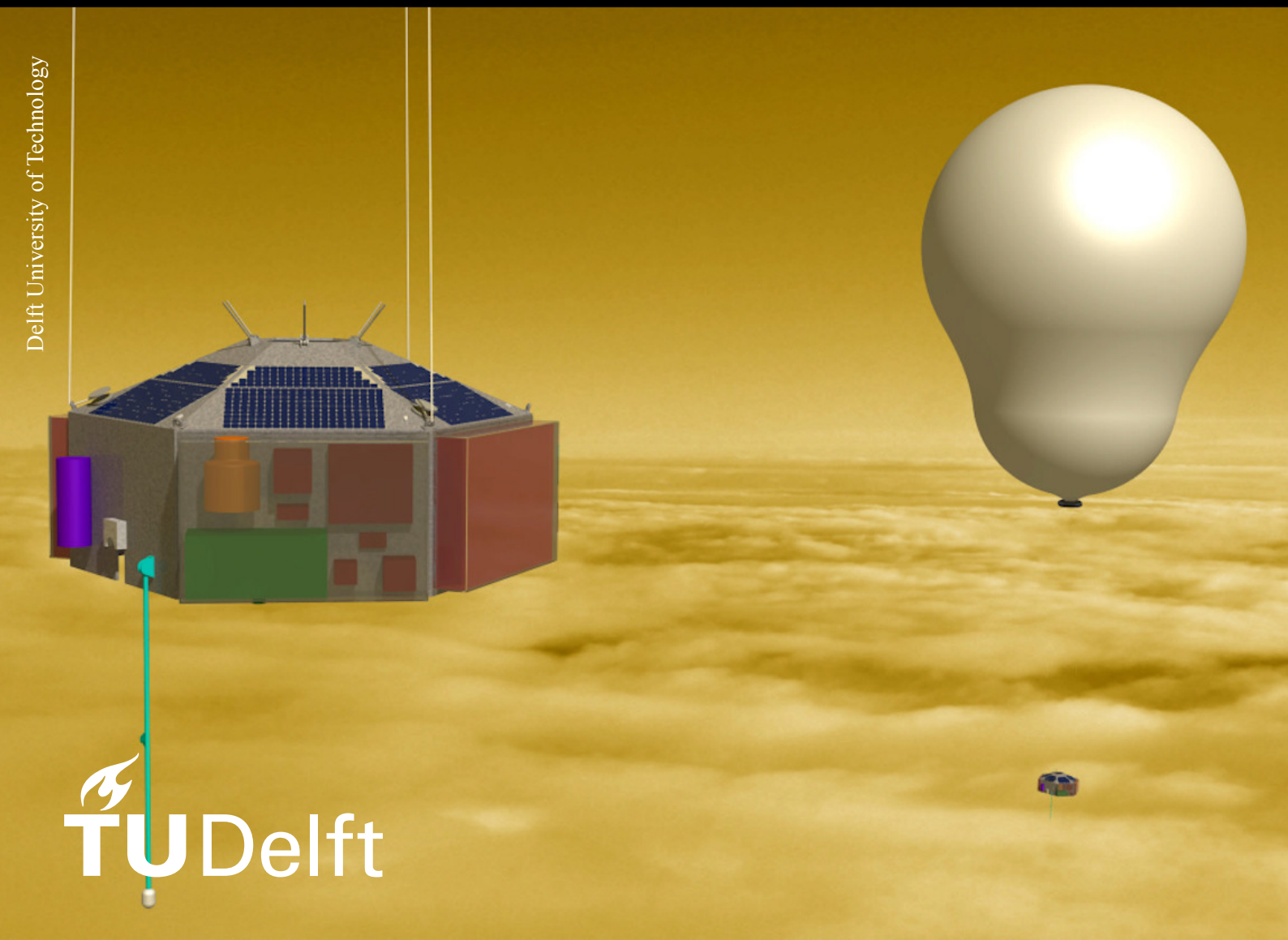

Delft University of Technology

TU Delft

Executive Overview

This chapter presents the executive overview for the Final Report of the L.O.V.E. mission or Life On Venus Exploration mission. The Final Report build up on the Midterm Report which was previously written for the LOVE mission [2].

Mission Description
The LOVE mission is an unmanned scientific mission to Venus which aims at performing long-term in-situ measurements in the Venusian atmosphere. It has a target launch date in April 2031 which would result in the mission being completed in March 2032. It has a budget of 630 million FY2022 Euros. The main scientific objective of the LOVE mission aims at investigating the existence of airborne microbial life within the main cloud deck, which lies 50-70 km above the Venusian surface. Furthermore, the LOVE mission encompasses a secondary scientific objective of investigating the Venusian atmosphere. This atmospheric profiling focuses on the Solar tides that are expected to be one of the main driving forces behind the atmospheric circulation. The degree of atmospheric circulation on Venus is known as the superrotation phenomenon where the atmosphere spins around Venus 60 times faster than the planet itself rotates in that same direction.

Mission Objectives, Requirements and Market Analysis
In Chapter 2 the mission objectives and requirements are reported along with a market analysis. During the previous phases of the project, starting from the mission need statement, two main scientific objectives were derived, namely that "The mission shall investigate the existence of airborne microbial life on Venus" and that "The mission shall investigate the Venusian atmosphere with a focus on the Solar tides partially driving atmosphere circulation". From here a stakeholders analysis was performed to identify the requirements necessary to perform the mission and the constrains in which it had to be done. This led to the generation of 17 stakeholder requirements, which were then translated into about 91 mission level requirements, of which 25 were identified as key requirements. Some of the most important ones are the fact that the mission has to perform measurements inside the atmosphere of Venus for 200 $days$, an at different altitudes ranging from 50-62 km. The type of measurements also were crucial as they dictated the payload instruments selected for the mission, and hence the systems that were necessary to support these instruments.

The market analysis performed showed a small rise in the missions to Venus in the last two decades, although projections indicate this rise is destined to slow down in the 2020-2032 period. Moreover it was found that NASA plans to dedicate more budget to ground based observation, rather than planetary exploration. Although it is argued that the quality of in-situ measurements is much higher than remote investigations, the LOVE mission's 630 million Euros budget can only be justified if the exploration of the Venusian planet is given higher priority in the coming years. One aspect that could tip the scale on this decision is the fact that LOVE has the potential to offer the first finding of extraterrestrial life in the history of mankind, an achievement that is difficult to put a price tag on.

Mission Architecture
In Chapter 2 the architecture of the mission is analyzed. It will consist of six space segments, namely the launch vehicle (LAV), transfer vehicle (TRV), relay satellites (REL), entry and descent vehicle (EDV), the spacecraft bus (SCB), and the payload (PLD). For the purpose of this project only REL, EDV, SCB and PLD were analysed in detail. Although not a physical segment the path of the spacecraft bus on Venus (PAT), the orbit (ORB) and the transfer trajectory to Venus (TRA) were also analyzed. These segments are complemented by the subject of the scientific research, Venus (VEN), the ground segment, composed of the missions operations (MIO), and the command control and communications (CCC), and the end user (PSC).

Despite not being analysed in detail, the TRV was sized based on the the mass and dimensions of the EDV, and it turn this allowed to make a preliminary selection of the launcher vehicles. A wet mass of 217 kg was estimated for the TRV, which together with the total mass of 969 kg of the SCB and EDV combination led to the selection of the Falcon 9 launcher by SpaceX.

Mission Geometry

The geometry of the LOVE mission is analysed in Chapter 2. This consists of three distinct segments: the path of the SCB on Venus, the orbits of the two RELs and the transfer. The spacecraft bus path consists of so-called cycles which begin at the upper altitude limit of 62000 m. After a resting phase that is used to adjust the spacing of the paths relative to each other lasting 876.2 s, a descent phase of constant descent velocity begins, where the SCB descends at -0.5 m/s. After a resting phase at the lower altitude bound of 50000 m. Subsequently, the path follows a constant velocity ascent at 3.5 m/s. these cycles are concatenated to form the path of the SCB. The ground track of this path is at 0 ° latitude. The path will result in subsequent circumnavigations of Venus' equator taking 22 cycles. This path is set to be offset by 30 ° every circumnavigation to improve the coverage of the path. This means that every 12 circumnavigations, the path repeats. The mission operational phase consists of two such repeats, enabling the mission to survey the Venusian atmosphere at high spatial resolution, while also enabling inferences to be made about the temporal evolution of the phenomena observed. The path is shown in Figure 2 After that, the SCB will follow a descending path, crashing into the surface of Venus as part of SCB decommissioning.

The relay orbits are two circular orbits with an inclination of 30.67 ° and an altitude of 1701 $\pm$ 20 km above the Venusian surface. The inclination is chose so that the ground track of the relay satellites continuously covers the path of the SCB, while also respecting ranging and navigation requirements. The right ascensions as well as the mean anomalies at a certain point in time of the ascending nodes of the two orbits are offset by 90 ° to optimize the contact time between the SCB and REL. The geometry is shown in Figure 1. At the end of the operation of the RELs, the periapse of the orbit is reduced to 200 km, causing the relays to burn up in the atmosphere of Venus.

The transfer segment begins in the year 2031 (1st of April) with launch from Earth. The transfer duration is 146 $days$, following a Hohmann trajectory. As the integrated TRV-EDV-SCB-PLD stack and the two RELs travel to Venus separately, it is critical that the two relays are operational so that they can transmit data during the atmospheric entry of the EDV. Therefore, both relays have to perform phasing maneuvers to ensure that they arrive at Venus at least 12 hrs ahead of the rest of the space segment. From there, the EDV descends into Venus directly from its hyperbolic orbit. Also included in the transfer trajectory is the descent of all EDV hardware towards the Venusian surfaces as part of their decommissioning.

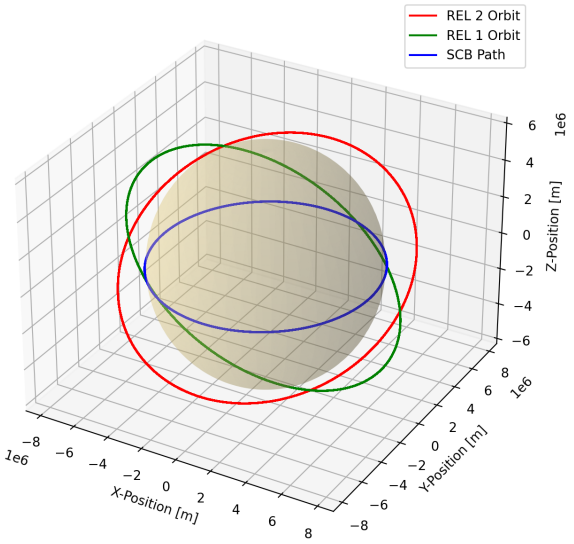

Figure 1: The REL orbits and path of the SCB.

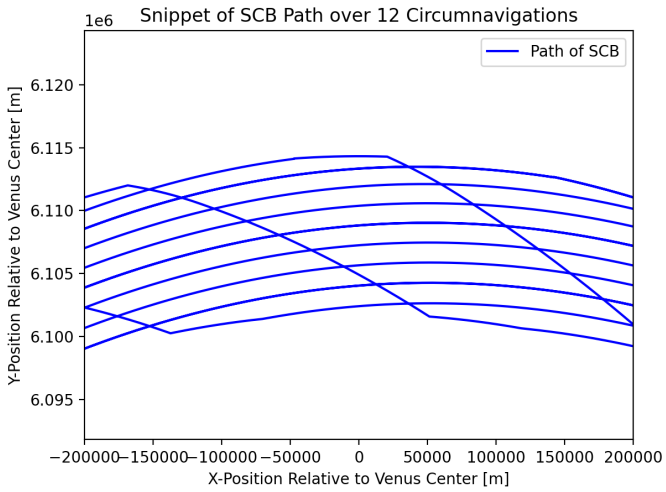

Figure 2: Path of the SCB over the mission duration.

Analysis of the mission geometry yielded several crucial results. Firstly, by determining the relative position of Earth, Sun and Venus (cf. Figure 2), the evolution of distances, eclipse durations and communication contact times can be derived. The results are shown in Figure 2.17, Figure 2.21 and Figure 2.16. Furthermore, the attenuation of RF signals by the Venusian atmosphere is modelled, showing a peak attenuation of 9 dB.

Mission Operations

Chapter 2 discusses the mission operations concept. While the mission constituents, as with any deep space mission, need to act largely autonomously, and the SCB will largely follow a pre-programmed path as described above, various forms of operator interaction with the system need to be considered. Firstly, as many aspects

of the Venusian environment are unknown, it is practically certain that the mission operators will adapt the scheduling of measurements and steering of the SCB to adapt to new learnings. Here, the concept, in line with heritage science missions is that the mission operators will deliver the data to the end user (the scientists), which will request changes to the way the mission is operating. After validating the feasibility of the proposal and adjusting it accordingly, the mission operations will then command the SCB to change its behaviour.

The other major case where operator interaction is required is to deal with contingency scenarios, where the system behavior and performance deviates from expectations, for example as the result of a system failure. Here, the mission operations will receive the housekeeping data, analyse the cause of the error, determine a method to deal with the fault, and command the affected system to change its configuration or behavior to compensate for the error as best as possible.

Mission Reliability and Risk
The reliability and risk analysis is reported in Chapter 2. To provide a quantifiable estimate on the mission reliability, a quantifiable technical risk method was performed. This resulted in a bottom-up approach where the risk of failure of each system's components were first analyzed, and then flowed up to the subsystems, systems, and finally the mission. For each of the components, three failure modes were identified: due to a minor anomaly/degradation, due to a major anomaly/degradation, and due to total failure of the component. The impact of these failures on the performance of the mission was quantified based on how much of the mission was lost, from 1% to 100% in steps. The most challenging aspect of the technical risk was quantifying the probability of a failure occurring, which was ultimately determined using statistical information on spacecraft failures. Mitigation strategies were also employed to reduce the risk of each system. This ultimately led to a mission reliability of 90.06%, which is compliant with the mission and stakeholder requirements.

Mission Resource Analysis
Chapter 2 also covers the analysis of the resources required for the mission. This yielded a development timeline to be concluded in 2031, an overall mission cost of 630 FY2022 M€, a total mission wet mass of 1602.81 kg and a probability of mission success of 0.901. All resource requirements are compliant with partially adjusted mission and customer requirements.

Payload
In Chapter 3 the payload is reported in detail. This is mainly constituted by 6 scientific instruments: the Radiation Assessment Detector (RAD), the Tunable Laser Spectrometer (TLS), the Rover Environmental Monitoring Station (REMS), the Venus Spectrometer (VenSpec), a nephelometer, and finally the Life Signature Detection Polarimeter (LSDpol). These six instruments aim at collecting data which will provide evidence of the existance (or lack thereof) of life on Venus, with the REMS collecting data every 8.6 s, and the other instruments taking measurements simultaneously every 4 hrs, while the SCB is on the descending part of the path. This payload has a total mass of 49.87 kg, consuming 88.98 W.

Spacecraft Bus
In Chapter 4 the detailed design of the spacecraft bus (SCB) and all its subsystems is described. This concept was sized in detail to prove that the concept proposed for the SCB of the LOVE mission is feasible.

The spacecraft bus is a pumped hydrogen gas balloon with a gondola structure to carry the payload. The SCB is able to change its altitude by pumping the hydrogen gas between the a zero pressure and super pressure balloon. This balloon module is controlled by a pump and valve system. The driving factor for the design of this control system is the requirement for the SCB to be able to follow a specified path with an ascent speed of 3.5 m/s and a descent speed of 0.5 m/s. The balloon is deployed using a cable running through the center of the balloon that connects the entry and descent vehicle to the spacecraft bus.

The zero pressure balloon will be made of Kapton Type 250FN029, have a radius of 6.31 m and a mass of 49.82 kg. The super pressure balloon will be made of Vectran Type NT, have a radius of 3.15 m and a mass of 27.19 kg. The total hydrogen gas that will initially be in the balloon module is 14.63 kg. The reserve tank will store 1.15 kg of hydrogen. The pump will be able to pump 200 L of hydrogen gas per minute. The vent will have a diameter of 20 mm. The mail hydrogen tank will have a volume of 0.626 m^3, and a mass of 77.4 kg. The

reserve tank will be shaped like a toroid. The inner diameter will be 0.088 m and the outer diameter will be 0.32 m. The mass of the reserve tank will be 23.6 kg.

The gondola of the SCB supports all of the payload of this mission. The gondola does this by providing electrical power, structural integrity and thermal control. The gondola also provides space for the hydrogen tank used to inflate the balloon module during deployment, the batteries, the solar arrays and the antenna.

The gondola will have a total mass of 166 kg excluding the gas tank. The structure will be made of a sandwich structure composed of an aluminium honeycomb and aluminium face sheet. The SCB will have an area of 0.74 m^2. The average electrical power of the SCB will be 84.5 W and it will have a battery capacity of 8033 W. The on board data storage of the SCB is 512 Mb. The SCB is able to communicate with the relay satellite with an uplink frequency of 390 MHz and a downlink frequency of 438 GHz.

The total estimated cost for the SCB is 192 Million euros FY2022. The reliability of the SCB is 96%. The position and velocity error of the SCB is 87000 m and 0.92 m/s. The total power of the SCB is 1864 Wh. The total mass of the SCB is 441 kg. The operating temperature range is 253.15-313.15 K.

Entry and Descent Vehicle

Chapter 5 introduces the design of the EDV. The vehicle consists of a sphere-cone shape with a 50 ° half-angle and a radius of 1.4 m, its overall mass was estimated to be 528 kg. The main components of the EDV, in terms of weight and importance are the thermal and structural subsystems. For the thermal shielding an ablative heat shield 6.2 cm thick and made of PICA was selected, yielding a mass of 116 kg for the shield. The backshell of the EDV is protected by a layer of Mylar aluminium blanket. The structural subsystem of the EDV was sized following a rough approach and estimate to be about 292 kg.

The entire entry trajectory of the EDV was modelled with a Python code, yielding important values such as total heating, peak heating, and peak g load. The entry follows directly from the transfer to Venus and has therefore a large velocity of 11.4 km/s and an angle of 9.2°. The EDV does not have a attitude determination and control system of its own and relies therefore on a strategically placed center of gravity to remain stable during entry. Moreover the TRV, before releasing the EDV in its trajectory into the planet, performs a spin stabilisation procedure to increase the EDV's stability.

During the descent a main parachute, pulled by a drogue parachute will slow the EDV down to allow for lowering of the SCB and the inflation of the balloon to begin. Only when the balloon is partially inflated will the EDV release the SCB and the latter continue the inflation process.

Relay Satellites

In Chapter 6 the design of the REL is discussed. The two RELs have the main two functions of providing data transmission and ranging to the SCB. On a high level, the REL consists of 8 subsystems. The most important subsystem for the REL's function is the Telemetry and Command (TNC) subsystem, which is responsible for receiving 352567.5 $kbit$ of science and housekeeping data per 24 hrs from the SCB, and transmit it to the ground stations. This is done using a flight-proven IRIS V2 radio, utilizing an omnidirectional UHF antenna to communicate with the SCB, and a high-gain X-Band antenna for the communication with Earth. For getting commands to the SCB, the system works in reverse. Furthermore, the UHF link can be used to generate highly precise location of the SCB on Venus using ranging. At the same time, the TNC subsystem also supports the ranging of the REL from the ground segment.

The onboard data handling (OBD) system is responsible for caching up to 64 MB data from the SCB until it can be transmitted, and operate the REL. It consists of a Flash storage and a flight-proven Texas Instruments MSP430 processor. The attitude of the REL is maintained by the attitude determination and control (ADC) system which points the REL with an accuracy of $\pm$1.75 ° to enable communication with Earth. It uses momentum wheels and cold gas thrusters for attitude control and sun and star sensors for attitude determination. This is integrated in the Xact-50 ADCS module with a separate RCS system. This systems also maintains the operational orbit, making small corrections. For larger maneuvers, the propulsion (PRP) subsystem is available. It consists of a Bi-Propellant thruster with an I_{SP} of 319 s and a thrust of 400 N, which is pressure-fed from two spherical fuel tanks which make up the majority of the REL volume. This subsystem will provide the ΔV required for orbital insertion and deorbiting.

The electric power system provides the REL subsystems mentioned above with electrical power and energy. It consists of a pointed GaAs solar panel with an area of 0.07 m^2 and a mass of 0.321 kg, providing a peak power of 55.38 W. It is supplemented by a 35.74 Wh Li-Ion battery, with the entire EPS providing an average power of 49.46 W. This is all held together by a cubical structure, and thermally protected with multi-layer insulation and a radiator. The overall dry mass of the REL is 19.16 kg, with the overall size being 0.8x0.35x0.35 m.

Sustainable Development Strategy
Lastly, Chapter 7 the sustainability of the LOVE mission is treated. In order to easily approach this subject, the topic of sustainability was divided into three main branches. These are 'Environmental Sustainability', 'Economic Sustainability' and 'Social Sustainability' which discuss the environmental, the economic and the social impact of the LOVE mission. The 'Environmental' aspect is treated for both the Earth's environment as well as non-Earth (e.g. Venus). The 'Economic' aspect of sustainability regards the effect of the mission on the economy nationwide, as well as internationally. Finally, the 'Social' branch was treated, which deals with the effects the mission could have on society.

Nomenclature

Abbreviations

ADC	Attitude Determination and Control System
AIT	Assembly Integration and Testing
AOC	Attitude and Orbit Determination System
BAT	Batteries
BDM	Boom Deployment Mech
BIN	Backshell Insulation
BLM	Balloon Module
BPT	Bipropellant Tank
CAD	Computer Aided Design
CCC	Command, Control, and Communications Architecture
CCDH	Command, Control and Data Handling System
CES	Cutting of EDV from SCB
cf.	Compare
CGT	Cold Gas Tank
CLS	Cutting of lowering mech, for SCB
COM	Center of Mass
COV	Cover
CPU	Central Processing Unit
CR	Cost Risk
CSA	Constitutient/Member States of the National Space Agency
DGB	Disk-Gap Band
DRP	Drogue Parachute
DSE	Design Synthesis Exercise
DSN	Deep Space Network
ECSS	European Cooperation for Space Standardization
EDF	Entry & Descent Float
EDV	Entry & Descent Vehicle
EIRP	Effective Isotropic Radiative Power
EOL	End of Life
EPS	Electrical Power System
ESA	European Space Agency
FEM	Finite Element Analysis
GON	Gondola
GLM	Lowering mech for the Gondola
GND	Ground System

GNP	General Public
GRS	Ground Segment
HEO	High Elliptical Orbit
HES	Heat Shield
HEM	Heat Shield Deployment Mech
HGA	High Gain Antenna
HYD	Hydrogen
ID	Identification
INA	Insurance Agencies
INS	Insulation
IMU	Inertial Measurement Unit
IST	Internal Structure
JPL	Jet Propulsion Laboratory
LAC	Location Attitude Control
LAD	Location Attitude Determination
LAV	Launch Segment
LFT	Lifting System
LGA	Low Gain Antenna
LMS	Lowering mech, for SCB
LNA	Low Noise Amplifier
LOVE	Life On Venus Exploration
LSDpol	Life Signature Detection Polarimeter
LVO	Low Venus Orbit
LVP	Launch Vehicle Supplier
MAP	Main Parachute
MCO	Mission Concept
MDP	Mission Data Processor
MEC	Mechanisms
MEM	Memory
MIO	Mission Operations
MLI	Multi-Layer Insulation
MNI	Manufacturing Parties
MNS	Mission Need Statement
MOG	Mission Operations Group
MRL	Manufacturing Readiness Level
MTA	Main Tank
MVO	Medium Venus Orbit

NASA	National Aeronautics and Space Administration
NAV	Navigation System
NEP	Nephelometer
NPH	Nephelometer
NSA	National Space Agency
ORB	Orbit
OBD	Onboard Data Handling System
OCS	Carbonyl Sulfide
OUS	Outer Shell
PAC	Position and Attitude Control System
PAR	Parachute
PAT	Path of the Spacecraft Bus
PCM	Parachute Cover Opening Mechanism
PIP	Heat Pipe
POL	Polarimeter
RAAN	Right Ascension of the Ascending Node
RAD	Ionising Radiation detector
RCS	Reaction and Control System
REL	Relay Satellite
REM	Rover Environmental Monitoring Station
PAT	Path
PCB	Phase Change Balloon
PCD	Power Control and Distribution
PLD	Payload
POS	Project Objective Statement
PRP	Propulsion System
PSC	Planetary Scientists and Scientific Community
PUHE	Pumped Helium Balloon
PVS	Pump Valve System
RCS	Resilient Composite System
REL	Relay Satellite
RF	Radio Frequency
RGB	Ropes Gondola to Balloon
RIB	Radioactive Ion Beam
ROM	Read Only Memory
RSL	Received Signal Level
RTA	Ready To Assemble
RWL	reaction wheel
SAR	Solar array
SC	Spacecraft

SCB	Spacecraft Bus
SNR	Standards & Regulations
SNR	Signal-to-Noise Ratio
SMAD	Space Mission Analysis and Design
SOA	Solar array
SPB	Super pressure balloon
SPI	On-Ground Infrastructure
SPOF	Single Point Of Failure
SR	Schedule Risk
SSE	Space Segment
SSPA	Solid-State Power Amplifier
STK	Star Tracker
STO	Storage
STR	Structures & Mechanisms System
SUN	Sun sensors
TBD	To be determined
THE	Thermal Management System
THR	Main engine
TLS	Tunable Laser Spectrometer
TNC	Transmit and communication
TPS	Thermal Protection System
TR	Technical Risk
TRA	Trajectory
TRL	Technology Readiness Level
TRN	Transfer
TRM	Tank release mechanism
TRS	Transportation
TRV	Transfer Vehicle
TRX	Iris transponder
TS	Thermal System
TT&C	Telemetry, Tracking and Command System
TUB	Tube
UHF	Ultra High Frequency
USD	US Dollar
UV	Ultra-Violet
VAMP	Variable Altitude Maneuverable Platform
VEC	VenSpec
VEN	Subject (Venus)
VNV	Verification and Validation Entity
VSC	VenSpec
ZPB	Zero pressure balloon
2D	2 Dimensions

Symbols

Symbol:	Definition:	Unit:
a	Albedo factor	$[-]$
a_{bias}	Bias Acceleration	$[m/s^2]$
A_i	Projected area	$[m^2]$
A	Inner tank surface area	$[m^2]$
c	Speed of light	$[m/s]$
C_D	Drag coefficient	$[-]$
cp_s	Centre of (solar) pressure	$[m]$
cm	Centre of mass	$[m]$
C_X	Opening load factor	$[-]$
D_0	Drag force	$[N]$
E	Elastic modulus	$[Pa]$
err_p	Position Error	$[m]$
err_v	Velocity Error	$[m/s]$
F_D	Drag force	$[N]$

Symbol:	Definition:	Unit:
F_{Peak}	Peak shock force	$[N]$
I	Mass moment of inertia	$[kgm^2]$
I_sp	Specific impulse	$[s]$
J_i	Intensity	$[Wm^{-2}]$
m	Mass	$[kg]$
q	Heat flux	$[W/m^2]$
Q	Heat	$[J]$
q_{max}	Maximum dynamic pressure	$[Pa]$
$q*$	Reflectivity	$[-]$
R	Orbital radius	$[m]$
S	Surface	$[m^2]$
S_0	Nominal surface area	$[m^2]$
T	Temperature	$[K]$

Symbol:	Definition:	Unit:
T_{IR}	Effective radiating temperature	$[K]$
V	Velocity	$[m/s]$
h	Stored momentum	$[Nms]$
V_p, V_{pres}, V	Volume	$[m^3]$
r	Range	$[m]$
r	Reliability of component	$[-]$
$\dot{r}$	Range Rate	$[m/s]$
R_{gas}	Specific gas constant	$[-]$
p	Pressure	$[Pa]$
υ	Poisson's ratio	$[-]$
X_1	Force reduction factor	$[-]$
$t_{eclipse}$	Eclipse Time	$[s]$
α	Solar absorptivity	$[-]$
α_{sun}	Solar Azimuth Angle	$[-]$
ϵ	Thermal emissivity	$[-]$
ρ	Density	$[kg/m^3]$
γ_{SUN}	Solar Elevation Angle	$[-]$
σ	Stefan Boltzmann constant	$[Wm^{-2}K^{-4}]$
T_s	Solar radiation torque	$[Nm]$
Φ	Average solar flux	$[W/m^2]$
ϕ	Solar incidence angle	[°]
μ	Gravitational parameter	$[m^3s^-2]$
θ	Body Yaw Angle	$[-]$
$\dot{\theta}$	Body Yaw Rate	$[-]$
ϕ	Body Pitch Angle	$[-]$
$\dot{\phi}$	Body Pitch Rate	$[-]$
ψ	Body Roll Angle	$[-]$
$\dot{\psi}$	Body Roll Rate	$[-]$
ζ	Angle between principal Z-axis and local vertical/roll	[°]
$\dot{Q}$	Heat Flux	$[J/s]$

Symbol:	Definition:	Unit:
k_{eff}	Thermal conductivity	[-]
t	Thickness	[m]
t	Time	$[s]$
σ	Structural Stress	[-]
ΔV	Change in velocity	$[m/s]$
n	Number of parallel components	$[-]$
n	Number of stringers	$[-]$
R_p	Reliability of parallel system	$[-]$
n_gas	Moles of hydrogen	$[mol]$
μ	Permeability	$[kg/ms]$
μ	Permeability	$[mL/(m^224hMPA]$
h_c	Convective heat coefficient	$[W/(m^2K)]$
Ra_L		[-]
η	Efficiency	$[-]$
D	Characteristic size	$[m]$
β	Thermal expansion coefficient	$[1/K]$
k	Thermal conductivity	$[W/(mK)]$
π	Pi	$[-]$
P_{cr}	Critical buckling load	$[N]$
b	Width of buckling panel	$[m]$
h	Height of buckling panel	$[m]$
R_N	Radius of the nose of the sphere-cone	$[m]$
ϵ	Emissivity	$[-]$
C_{abl}	Heat capacity of the ablator	$[J/kgK]$
g	Gravititational acceleration on Earth	$[m/s^2]$
M_{gas}	Propellant mass	$[kg]$
SF	Safety factor	$[-]$
r	Pressurant tank radius	$[m]$

Contents

1 Introduction

Finding life beyond Earth has long been a major driver for the exploration of outer space, if not the greatest one. To discover whether humanity truly is unique in the Universe would have a massive impact on mankind's physiology. After all, if it could be conclusively proven that in one single solar system life started twice, independently of each other and in different environments, it would all but confirm that the cosmos must be full of other lifeforms. That humanity is, in fact, not alone. However, so far most missions towards answering this question have been focused on the bodies further away from the Sun than Earth is; the subsurface of Mars, the oceans of Jupiter's moon Europa, the geysers of Saturn's moon Enceladus are all seen as key destinations for the next generation of scientific exploration missions. However, while most efforts continue to be focused on these bodies, Earth's closest neighbour might have been hiding its own answers all along...

Venus, the second planet from the sun, has long been dismissed as a candidate for life of any sort. Ever since the early explorer probes plunged through its sulfuric, highly corrosive and crushingly dense atmosphere in the 60's and 70's, and reached its scorching hot, lead-melting surface, Venus has been written off as a hellish place where no life could ever survive, let alone develop. Recently though, better studies of its atmosphere have provided surprising new information: there are altitudes where the pressure and temperature are accomodating to potentia life. In recent years, potential life on Venus has come to the fore of science with the discovery of biomarkers - molecules that are thought to only be generated by lifeforms- like Phosphine, has possibly occured. If true, this would indicate something that would have previously been unthinkable: life in the clouds of Venus, "Earth's Evil Twin". However, the only way to settle this argument decisively is to send a mission there to study, traverse and measure the atmosphere of Venus over an extended period of time, something which has never been done before. As an added bonus, such a mission, if performed, would also be of great use in helping to better understand the clouds and winds of Venus, both of which have characteristics that have puzzled scientists for decades, but which cannot be adequately studied by observations from above the atmosphere due to the thick and dense cloud layers. Thus a spacecraft operating in the Venusian atmosphere would help answer this mystery as well. Therefore, this report aims to document and present the design of a mission that would address these objectives, with an eye on further development, analysis and refining of the design.

The report is structured as follows: first Chapter 2 gives a broad overview of the complete mission, followed by the individual detailed design of the payload, spacecraft bus, entry and descent vehicle and relay satellite(s) in Chapter 3, Chapter 4, Chapter 5 and Chapter 6 respectively. Chapter 7 deals with strategies and choices regarding sustainability, while Chapter 8 contains the conclusion.

2 Mission Design

The LOVE mission aims to achieve highly complex scientific goals. To properly comprehend the design choices made in the final design it is crucial to understand the objectives, the stakeholders involved, the requirements set on the mission and on the single segments and the way these segments interact with each other to achieve the common goal.

This chapter focuses on a mission-level overview, beginning with an operational analysis in Section 2.1, which focuses on the reasons behind the mission and its place in the market, followed by the mission architecture and

functional analysis in Section 2.2, which also introduces the mission architecture. Then Section 2.3 provides an overview of the key requirements that heavily drive the design of LOVE, and Section 2.4 introduces the geometry of the mission. Following are Sections 2.5 and 2.6, which discuss the concept of the mission and the operational procedures respectively. Finally Section 2.7 analyses the risk and reliability of the mission and the single elements, while Section 2.8 addresses the resources available and gives an outlook on future developments of LOVE.

2.1. LOVE Mission Operational Capability Analysis

In order to define what the objectives and capabilities of the LOVE mission are, firstly the mission need statement is briefly provided and discussed in Subsection 2.1.1, secondly the scientific goals and stakeholders requirements are derived in Subsection 2.1.2, and finally the market analysis is discussed in Subsection 2.1.3.

2.1.1. Mission Need Statement

The mission need statement expresses in general terms the need that generated the necessity for the mission. It is used to give context to and derive stakeholder requirements and scientific objectives and brings the entire mission design together into one condensed sentence. The LOVE's mission need statement is as follows:

Design a realistic mission to search for potential traces of bacterial life on Venus, while improving the current knowledge on the planet, by ten students in ten weeks.

2.1.2. Scientific Goals and Stakeholder Requirements

The top level scientific goals have been iterated and summarised into two main objectives presented in Table 2.1.

Table 2.1: Scientific objectives.

ID:	Objective:
SCI-OBJ-1	The mission shall investigate the existence of airborne microbial life on Venus.
SCI-OBJ-2	The mission shall investigate the Venusian atmosphere with a focus on the Solar tides partially driving atmosphere circulation.

After identifying, analyzing and prioritizing all stakeholders involved in the mission their needs are translated into requirements, as reported in Table 2.2. It shall be noted that NSA-REQ-1 and NSA-REQ-9 are based on current similar missions such as NASA's VERITAS [27], and are agreed upon after discussion with the clients.

Table 2.2: Stakeholder requirements.

Req. ID:	Description:	Science objective:
	Planetary Scientists	
PSC-REQ-1	The mission shall investigate the presence of biomarkers in the Venusian atmosphere.	SCI-OBJ-1
PSC-REQ-2	The mission shall investigate the habitability of Venus.	SCI-OBJ-1
PSC-REQ-3	The mission shall find evidence to disprove other sources as the dominant producers of biomarkers.	SCI-OBJ-1
PSC-REQ-4	The mission shall investigate the Venusian atmosphere at low altitudes (below the main cloud deck).	SCI-OBJ-2
PSC-REQ-5	The mission shall investigate the Venusian atmosphere at medium altitudes (within the main cloud deck).	SCI-OBJ-2
	National Space Agency	
NSA-REQ-1	The mission shall be compliant with cost limitations stipulated by M class missions.	
NSA-REQ-2	The scientific mission shall have an overall realibility of 90%.	
NSA-REQ-3	The mission shall safeguard the ability to effectively execute future space missions.	
NSA-REQ-4	The mission shall safeguard the ability to perform science on Venus.	
NSA-REQ-5	The mission should minimize the use of scarce, high-impact resources.	
NSA-REQ-6	The mission shall adhere to applicable national and international standards and regulations.	
NSA-REQ-7	The mission shall be launchable using existing and foreseeable launchers.	
NSA-REQ-8	The mission shall return data to scientists through an easy-to-use interface.	

NSA-REQ-9	The mission shall return data to scientists before 2035.
	Mission Operations Group
MOG-REQ-1	The operations of the mission shall be simple.
	Manufacturing parties
MNI-REQ-1	The production and assembly processes for the mission shall be simple to carry out.
	Launch vehicle
LVP-REQ-1	The mission shall attain to the standards and regulations specified by the launcher vehicle.

2.1.3. Market Analysis

In previous phases of the project [1] a market analysis has been performed to understand where LOVE can be placed in the bigger picture of the global space economy and more specifically space exploration. In this section a summary of previous findings of current and future market trends is provided along with competition and updated information on the current mission costs.

Market Definition, Current and Future Trends

Despite the global space economy, including research, exploration and utilisation, being valued at 423.8 billion USD in 2019 [79], it lacks a clear market measurement and assessment, so much that space is not even recognised in the international standards of industrial classification [74]. The best way to approach the analysis of the market for planetary exploration is done by looking at M-class mission similar to LOVE. When looking at Venus missions to this planet have been consistent over the past 7 decades [62], suffered a reduction in the last years and only lately projections suggest the trend is picking up again, as it can be seen in Figure 2.2.

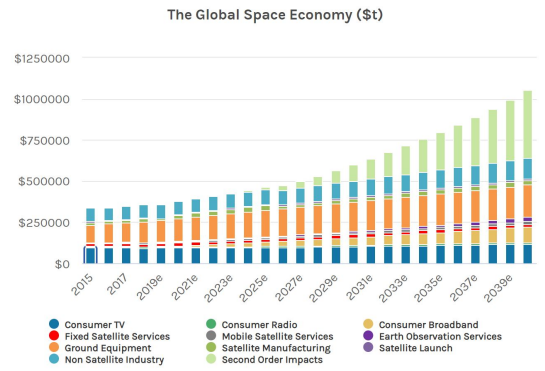

Figure 2.1: Cost trends in the global space economy [79].

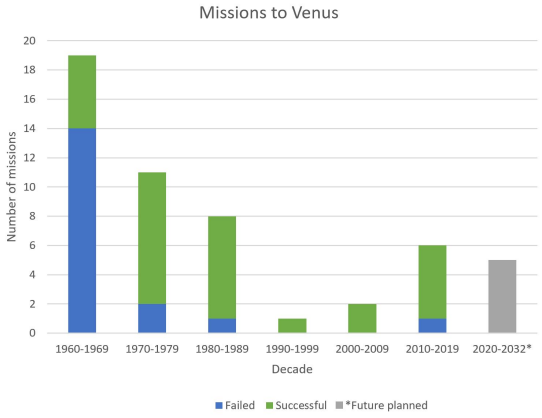

Figure 2.2: Number of missions launched or to be launched to Venus by decade.

In the space exploration market trends suggest a reduction of mission costs as a result of improvements in technology [74]. However this does not necessarily translate to more planetary exploration since the space institutional domain has the lowest budget for the foreseeable future and the largest market failure risks.

Upcoming Missions to Venus and Alternative Services

The upcoming Venus missions that are identified are: VERITAS, DAVINCI+, Venera-D, EnVision, and Shukrayaan. These missions are a mix of probes and orbiters but these two methods are not the only option. NASA allocates a larger budget for 2021 of 580 million USD for ground based observations, compared to 447.7 million USD dedicated for planetary exploration. In the latter only 10 million USD is actually reserved for missions to Venus (more budget requests are being made) [61]. It shall be noted that merely comparing budgets does not take into account the different quality of the obtained information since using orbiters/landers/probes definitely yield much more valuable information than ground based observations.

Position of LOVE within the Market

As discussed in previous reports ”Compared to other missions, this project is similar in the goals of trying to understand the atmospheric science of Venus as well as having a similar timeline. However, only Venera-D is

studying the circulation of the atmosphere in particular. In addition, this project aims to look at signs of life and habitability by analysing specific chemical markers and comparing them against each other based on recent studies - not all of which is covered by competing missions. Decreasing launch costs and the huge knowledge gap in what is actually known about Venus, despite the number of successful missions, seem to make all of these missions complementary to one another, by potentially providing a more comprehensive view of the planet." Some of the positive and negative aspects of this project are highlighted in the Strengths, Weaknesses, Opportunities and Threats (SWOT) diagram as in Figure 2.3 showing how it fares as compared to other projects of this level. [1]. With an overall estimated cost of 524M Euros LOVE places itself on the high end of the current budget estimations. The economical feasibility of this mission is highly dependent on future budget increases and a higher prioritization of planetary research by space agencies, an assumption lightly supported by Figure 2.2. What LOVE has to offer other than high quality in-situ scientific data on Venus, especially compared to previous and similar missions, is the chance of finding life outside of Earth for the first time in the history of mankind; an objective that can arguably justify the large cost.

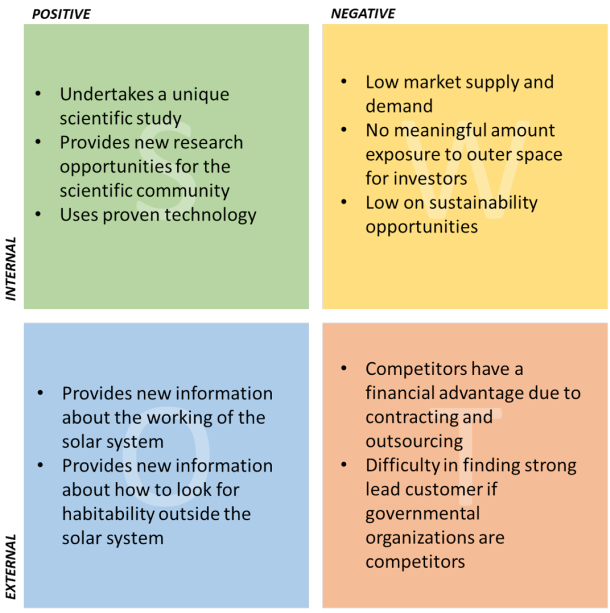

Figure 2.3: Strengths, Weaknesses, Opportunities and Threats (SWOT) diagram.

2.2. Mission Architecture and Functional Analysis

In this section the mission architecture is treated in Subsection 2.2.1, followed by the functional analysis in Subsection 2.2.2.

2.2.1. Mission Architecture and Boundaries

The mission architecture specifies all segments of the mission that together achieve the objectives of the mission. Proper definition of this architecture is crucial in order to properly define interfaces and requirements for the systems. All high-level segments of the mission are tabulated below in Table 2.3.

Table 2.3: Mission architecture and segments the LOVE mission.

Segment:		**Description Tradeable**
1. Subject (Venus)	Segment with which the System interacts to achieve mission objectives.	No
Space Segment		
2. Payload	Part of Space Segment that interacts with the Subject	No
3. Spacecraft Bus	Segment supporting the payload.	Yes
4. Relay Satellite	Segment relaying communications between the SCB and CCC.	Yes
5. Entry & Descent Vehicle	Segment protecting payload and SCB during Venus Entry	Yes
6. Transfer Vehicle	Segment supporting entry and descent vehicle during Transfer	No
Ground Segment		
7. Mission Operations	Segment operating all other segments	No

Table 2.3: Mission architecture and segments the LOVE mission.

Segment:		Description Tradeable
8. Command, Control, and Communications Architecture (CCC)	Elements on ground enabling communication with the space segment.	No
Trajectory		
9. Path	Trajectory of the SCB in Venus atmosphere	No
10. Orbit	Trajectory of the relay satellites around Venus.	No
11. Transfer	Trajectory of space segment between Earth and Venus	No.
12. Launch Segment	Launch Vehicle for Space Segment.	Yes
Mission Concept	How all segments fit together to achieve mission objectives	Yes

Furthermore, it is important to consider how the mission segments interact throughout the mission and how the entire mission interacts with externals such as stakeholders. To that end, for each mission phase specified in Figure 2.7 a system interface and boundary diagram is generated. Figure 2.4 shows an exemplary mission architecture for the operational phase:

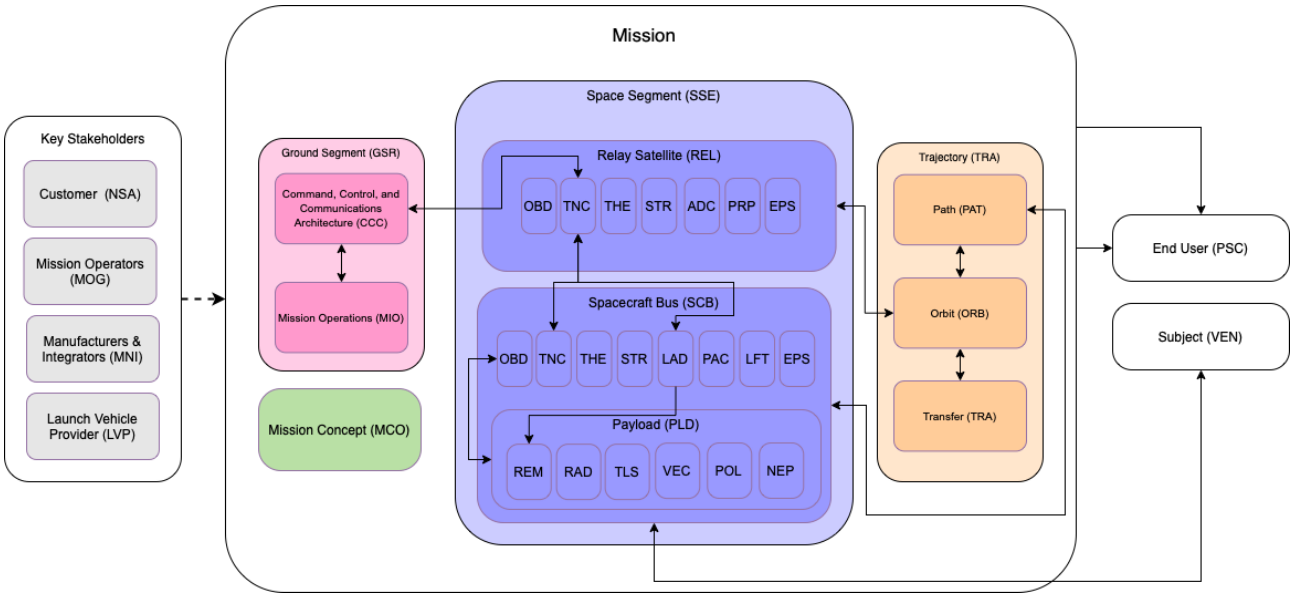

Figure 2.4: The mission architecture of the LOVE mission during the operational phase.

The figure above shows that the mission mainly interacts with the User and the Subject, whereas stakeholders influence the design and execution of the mission.

2.2.2. Functional Analysis

During previous phases of the project, a preliminary functional analysis of the mission has been performed. In this analysis, the actions that need to be carried out by the various segments of the mission are placed in a time sequence in the functional flow diagram, and in a hierarchical structure in the functional flow breakdown structure. The mission is divided into seven different phases, shown in Figure 2.7, which highlight the stakeholders and the elements involved.

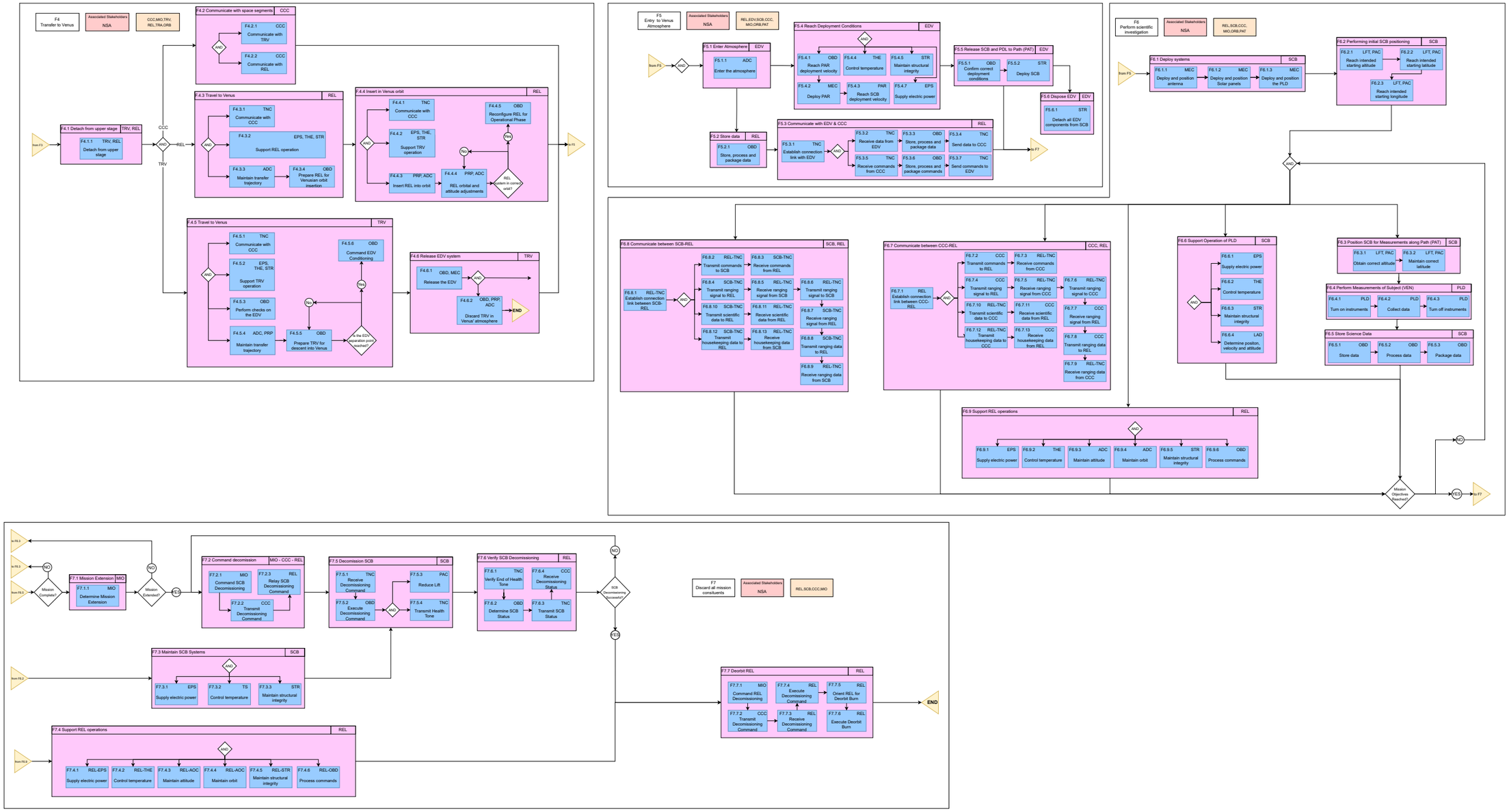

Figure 2.5: Functional flow diagram of detailed mission design.

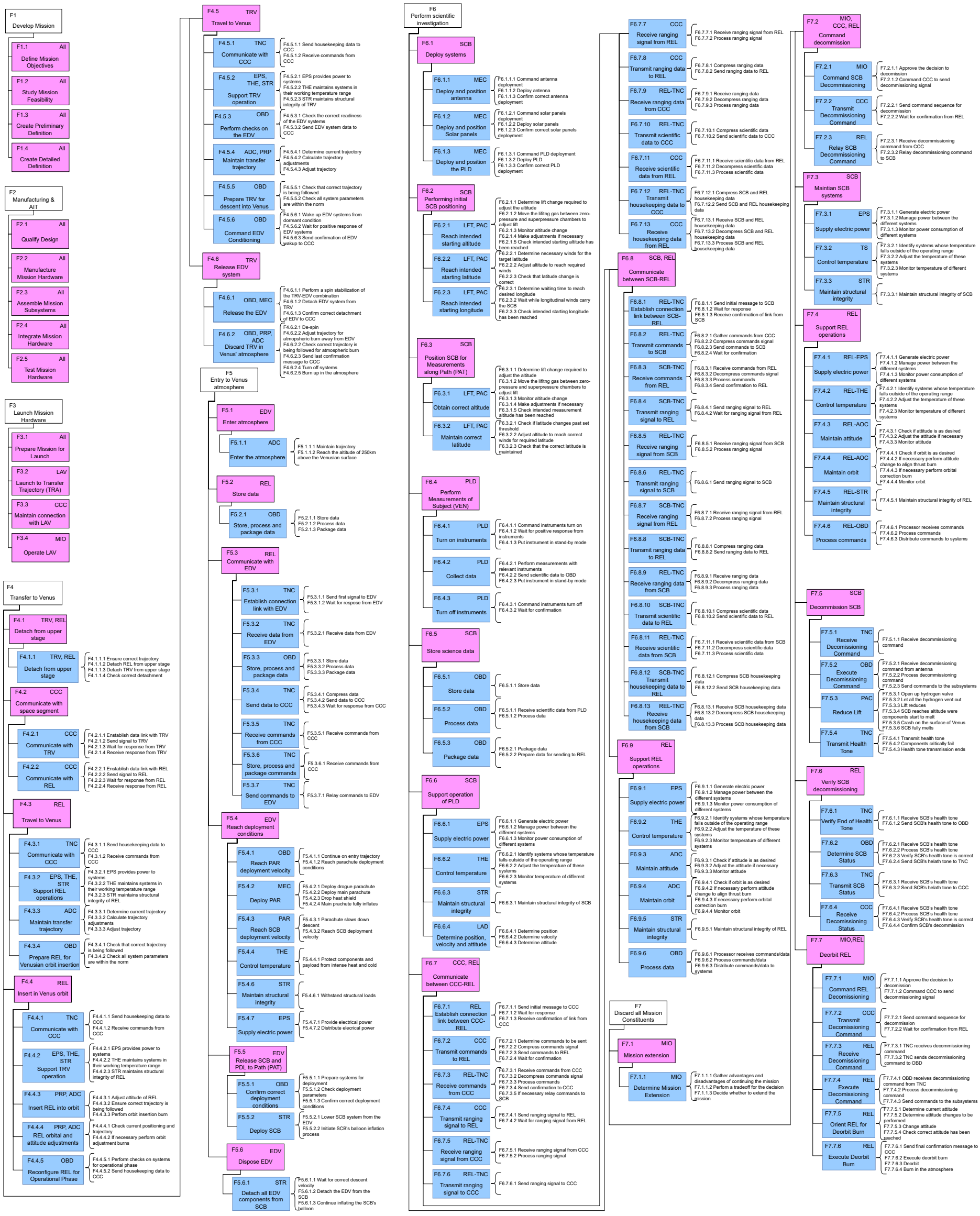

Figure 2.6: Functional flow breakdown structure of detailed mission design.

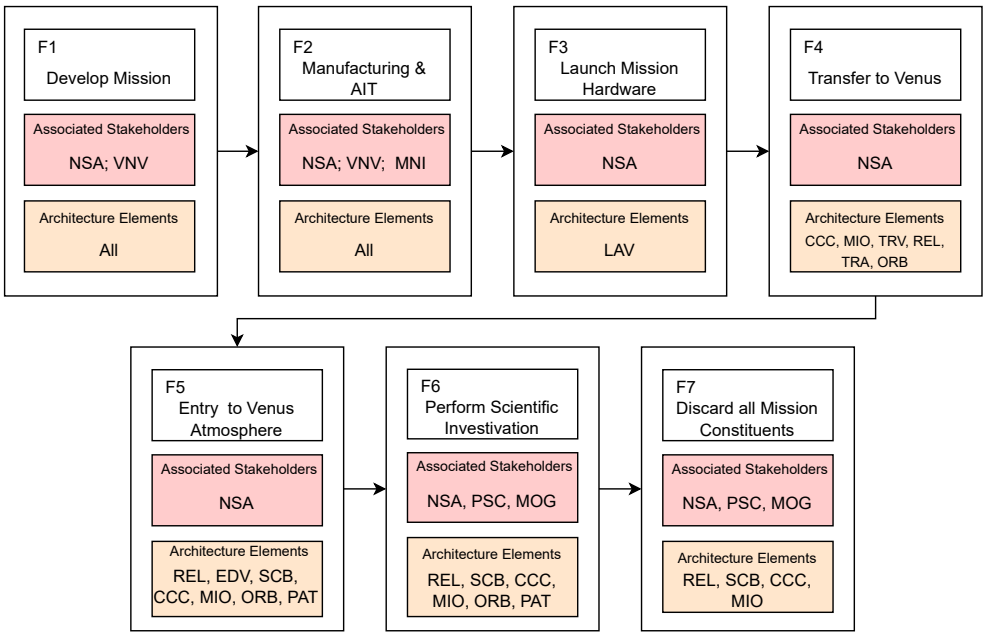

Figure 2.7: Phases of the LOVE mission.

Due to the purpose of this project, only phases F5 to F7 have been designed in detail. Phase F4 is still included in the detailed functional analysis, due to specific concept choices that have been made regarding the transfer to Venus. Since the space segments travel independently to the planet it is deemed important to still analyse the functions of phase F4 to gain insights into the start of F5.

Figure 2.5 and Figure 2.6 show respectively the detailed functional flow diagram and the detailed functional flow breakdown structure for phases F4 to F7.

2.3. Mission Requirements Definition

In order to begin designing the mission segments in further detail, the results of the mission operational analysis (mission need statement, objectives, stakeholder requirements and market analysis) must first be combined with the results obtained in the mission logical analysis (functional flow & block diagram, mission architecture) to form the mission requirements. This is done through the intermediate step of creating a requirements breakdown tree. Then, the mission requirements are continuously updated to stay consistent with the design. However, one must keep in mind that as the design progresses, the ability to adjust requirements diminishes. that Once the mission requirements are established, it is important to identify key requirements which have a larger-than-average impact on the fulfilment of the mission objectives, and driving requirements, which impact the design stronger than other requirements.

In Table 2.4, the key and driving mission requirements are shown. Driving requirements are marked with '[!]'. It is important to realise that the requirements displayed in the following (and, in fact, throughout the report) do not represent the full list of 1451 requirements (of which 83 mission-level, 66 trajectory, 601 systems-level and 701 subsystems-level) that have been generated.

As can be seen, the mission must circumnavigate the Venusian equator at an altitude between 50000 and 62500 m for 200 $days$ while continuously sweeping this altitude range. The mission measures temperature, pressure and wind patterns present in the atmosphere. Furthermore, the mission looks for signs of life by looking for biomarkers (OCS, Ammonia, Phosphine) and substances enabling the presence of life (Water, Ammonia) as well as potential false positives in the detection of biomarkers such as Sulfur Dioxide. Furthermore, the mission searches for life by measuring the circular polarization of light using the unichirality property common to life forms on Earth. Moreover, the aerosol properties of the atmosphere are investigated.

Table 2.4: The key mission requirements, driving requirements are marked with [!].

ID:	Description:	Rationale:
MIS-REQ-2.1	[!] The mission shall perform measurements of the middle atmosphere (main cloud deck) between 50 km and 62 km of altitude.	Altitude range of the main cloud deck, where measurements are desired
MIS-REQ-2.2	[!] The mission shall take measurements at a latitude of 0 ° $\pm$ 5 °.	Fulfilment of mission requirements requires equatorial trajectory to ensure consistent local time for subsequent circumnavigations.
MIS-REQ-2.4	The mission shall conduct 2 measurement cycles sweeping each defined path.	Repeating of path allows for investigation of temporal evolution of measurements.
MIS-REQ-2.9	The mission shall be able to measure atmospheric temperature with an accuracy of at least 1 K.	Required for climate analysis, accuracy quantification taken from [49].
MIS-REQ-2.10	The mission shall be able to measure atmospheric pressure with an accuracy of at least 1 $mbar$.	Required for climate analysis, accuracy taken from [49] and [16].
MIS-REQ-2.12	The mission shall be able to measure meridional (North-South) wind speed magnitudes with an accuracy of at least 1.1 m/s.	Part of atmospheric and wind profiling. Sized to be able to detect expected meridional winds [6].
MIS-REQ-2.13	The mission shall be able to measure zonal (East-West) wind speed magnitudes with an accuracy of at least 1.1 m/s.	Part of atmospheric and wind profiling. Sized to be able to detect expected zonal winds [6].
MIS-REQ-2.14	The mission shall be able to measure vertical wind speed magnitudes with an accuracy of at least 1.1 m/s.	Part of atmospheric and wind profiling. Sized to be able to detect expected vertical winds [6].
MIS-REQ-2.16	The mission shall be able to determine the latitude at which measurements are taken on Venus with an accuracy of at least 1°.	Required for the usefulness of measurements. Furthermore, required to have sufficient knowledge of local time.
MIS-REQ-2.18	The mission shall be able to measure meridional (North-South) wind speed magnitudes with a sensitivity of at least 0.1 m/s.	Part of atmospheric and wind profiling. Sized to be able to detect expected meridional winds [6].
MIS-REQ-2.19	The mission shall be able to measure zonal (East-West) wind speed magnitudes with a sensitivity of at least 0.1 m/s.	Part of atmospheric and wind profiling. Sized to be able to detect expected zonal winds [6].
MIS-REQ-2.20	The mission shall be able to measure vertical wind speed magnitudes with a sensitivity of at least 1.1 m/s.	Part of atmospheric and wind profiling. Sized to be able to detect expected vertical winds [6].
MIS-REQ-3.1	The mission shall measure the concentration levels of phosphine with a sensitivity of at least 1 ppb.	As to accurately find the concentration of phosphine where ppb refers to parts per billion. Phosphine is a byproduct of certain lifeforms when found in a non-oxygenated environment, thus they can be evidence for life.
MIS-REQ-3.5	[!] The mission shall measure the concentration levels of phosphine over a period of at least 200 Earth days.	he minimum period of time for which the customer wants continuous measurements.

Table 2.4: The key mission requirements, driving requirements are marked with [!].

ID:	Description:	Rationale:
MIS-REQ-3.7	The mission shall measure the concentration levels of ammonia with an accuracy of at least 1 ppm.	The presence of ammonia may raise pH levels to levels terrestrial extremophiles are able to survive, also according to source. Ammonia may be a byproduct of some cyanobacteria according to [7]
MIS-REQ-3.11	The mission shall measure the concentration levels of carbonyl sulfide with a sensitivity of at least 1 ppm.	The accuracy is determined to be max of 1 ppm as based on [96]. The presence of carbonyl sulfide may indicate life is present in the atmosphere, as it is a compound difficult to be naturally manufactured.
MIS-REQ-3.16	The mission shall be able to measure circular polarization with an accuracy of at least 10^{-4} $C \cdot m^{-2}$.	Homochirality is a unique property of all biochemical life. Scattered light microbial polarization levels are in the range pc $\approx 10^{-3}$ to 10^{-4} $C \cdot m^{-2}$. The accuracy and sensitivity of the instrument should therefore be at least 10^{-4} to accurately detect the circular polarization. [64].
MIS-REQ-4.1	The mission shall measure the concentration levels of sulfur dioxide with a sensitivity of at least 10 ppb.	According to [28] the concentration that can be found in Venus of SO2 is from 100 ppb down to 10 ppb.- The presence of sulfur dioxide could give a false positive for phosphine in spectroscopy.
MIS-REQ-4.7	The mission shall measure the concentration levels of water with an accuracy of at least 10 ppm.	This accuracy value is based on the sensitivity value, a rough estimate. Water activity is an indicator for the viability of life for extremophiles, thus it is useful to measure the water contents of Venus' clouds according to [35].
MIS-REQ-4.12	The mission shall measure ultraviolet irradiance with an accuracy of at least $1 \cdot 10^{-7}$ UV:PAR.	According to [67], the ultraviolet radiation is in the order of magnitude of 10^{-7} UV:PAR.According to [63], UV imaging shows markings caused by aerosols, but it is not known whether these aerosols are biological or not in nature.
MIS-REQ-4.17	The mission shall measure the radiation incidence on Venus with an accuracy of at least 0.01 Gy	According to [67], the magnitude at which radiation no longer is a threat to the formation of life is 0.01 Gy, where Gy are Gray, which is J/kg. The Venusian atmosphere is hit by ionising radiation due to its lack of magnetic field. This radiation hinders the ability of the Venusian environment to develop life, thus it is imperative to know whether at a certain location life is even able to develop, as this helps determine if the biomarkers are false positives or not.
MIS-REQ-4.21	The mission shall measure the presence of aerosols with an accuracy of at least 150 nm.	The minimum accuracy displayed by the pioneer nephelometer [69].
MIS-REQ-5.1	The mission shall detect natural olivine with a minimum particle volume of at least 0.1 mm^3	The volume of olivine crystals is measured to increase with time, and the range measured for the detection of natural olivine is from 0.1–4 mm^3
MIS-REQ-5.4	[!] The mission shall take a measurement for olivine every 4 hrs for the duration of the mission lifetime.	The 4 hrs interval is done according to the [85], which had instruments which took measurements every 4 hrs.

Table 2.4: The key mission requirements, driving requirements are marked with [!].

ID:	Description:	Rationale:
MIS-REQ-8.1	[!] The total mission cost shall not exceed 630 million Euros (FY2022).	Result of needing to fit M-Class mission regulation, adjusted for subsequent cost analysis.
MIS-REQ-9.1	[!] The spacecraft shall have a probability of 90% of achieving the mission level science requirements.	Customer requirement.

2.4. Mission Geometry Design and Analysis

In order to analyse and design the LOVE mission systems in more detail, further insight into the geometry of the mission is required. Mission geometry analysis includes the analysis of the position of mission segments and relevant planetary bodies relative to each other, with the ultimate goal of deriving distances between the mission elements, eclipse and contact times and the irradiation environment of the various mission elements. This allows for systems to be sized and their performance to be validated. However, the analysis presented here is not intended to be an exact trajectory design and optimisation. The mission constituents considered in the analysis include the two relay satellites, the transfer vehicle, the entry and descent vehicle, the SCB and two ground stations, as well as Venus and Earth. Consequently, the trajectory elements to be considered are the path of the SCB on Venus, the orbits of the RELs and the transfer to Venus. In the following section, the individual elements defining the mission geometry are presented in detail. Firstly, an overview is presented. Then, the SCB, REL orbit and transfer trajectory are discussed in detail.

2.4.1. Spacecraft Bus Path Design and Parametrisation

The specification of the SCB path is mainly driven by the scientific requirements with respect to generating altitude profiles of the various measurements, but also considering ease of control and communication. The latter constraint dictates circumnavigating equatorially, as this allows for the most consistent coverage with the relays. It consists, on a high level, of an operational phase and a decommissioning section subsequent to the operational phase. The former is divided into cycles which consist of an ascent phase, a descent phase and rest periods separating ascent and descent. The latter consists of a descent of the SCB to the Venusian surface. As with other mission segments, requirements are imposed on the path, the most important of which are shown in Table 2.5.

Table 2.5: The key path requirements specifying the trajectory of the SCB.

ID	Description	Rationale
PAT-REQ-2.1	Meas	Required to comply with MIS-REQ-3.5
PAT-REQ-3.1	The operational element of the path shall consist of subsequent circumnavigations of Venus.	Required to fulfill mission objectives of mapping the wind patterns and searching for chemicals.
PAT-REQ-3.2	The operational element shall remain within 0 ± 5 ° of latitude.	Required to ensure consistent data transmission between SCB and relay throughout mission.
PAT-REQ-3.3	The operational element of the path shall feature no less than 22 cycles per one circumnavigation.	Required to achieve sufficient spatial resolution. Result of iterative design to achieve even distribution of path repeats.
PAT-REQ-3.4	The operational element of the path shall repeat every 12 circumnavigations.	Required to achieve sufficient spatial resolution. Result of iterative design to achieve even distribution of path repeats.
PAT-REQ-3.5	The rest time at the lower altitude bound shall be 1175.8 ± 10 s.	Required to ensure consistent longitudinal spread of the path
PAT-REQ-3.6	The rest time at the lower altitude bound shall be 876.2 ± 10 s.	Required to be ensure consistent longitudinal spread of the path

PAT-REQ-3.7	The descent velocity shall be 0.5 ± 0.1 m/s.	Required to sweep the altitude range of interest. Quantification is result of PAC and LFT sizing.
PAT-REQ-3.8	The ascent velocity shall be 3.5 ± 0.5 m/s.	Required to sweep the altitude range of interest. Quantification is result of PAC and LFT sizing.
PAT-REQ-3.9	The upper bound of the altitude shall be 62000 m above Venus Mean Sea Level.	Required to sweep the altitude range of interest. Quantification is result of LFT sizing.
PAT-REQ-3.10	The lower bound of the altitude shall be 50000 m above Venus Mean Sea Level.	Required to sweep the altitude range of interest. Quantification is result of LFT sizing.

The geometry of the path is generated and analysed under the following assumptions:

1. The SCB velocity is equal to the wind velocity.
2. Non-zonal winds are negligible.
3. Winds are independent of location and time.

The model is verified against analytical calculation of travel velocity based on circulation models from literature. Furthermore, the velocity model is validated against wind models from literature. It is found that while the model may not be used to accurately predict the exact ground track, latitudinal deviations from the path are sufficiently small for this model to be valid for power and link budget analysis. The altitude profile of a singular measurement cycle is plotted in Figure 2.8.

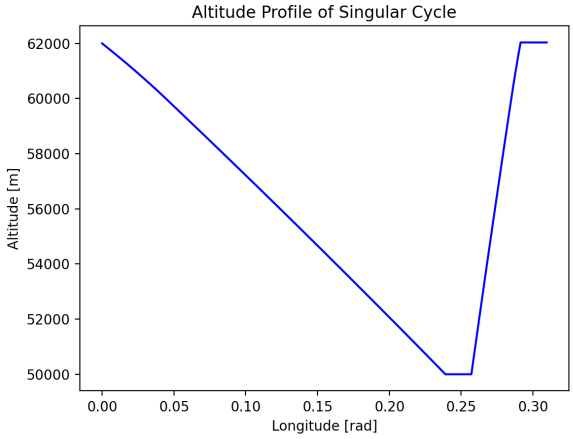

Figure 2.8: The altitude profile over one cycle of the SCB path.

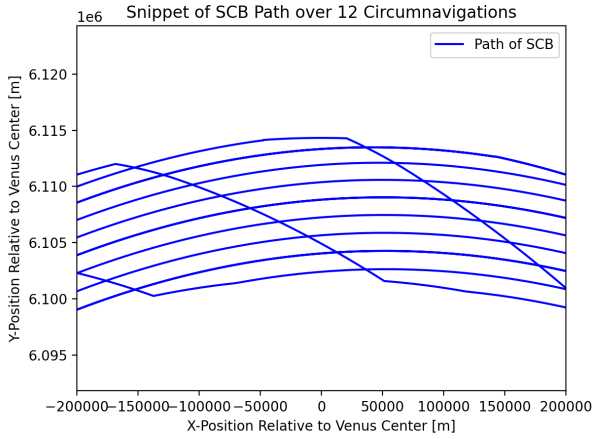

Figure 2.9: A section of the path of the SCB showing spacing.

These cycles are then concatenated into the path of the SCB to form the path. A segment of the path is displayed in Figure 2.9. It can be seen that the descent phase accounts for the majority of longitude travelled by the spacecraft. This leads to most of the area of interest (the altitude range between 50 and 62 km) being covered during that part of the cycle, which has implications for the measurement strategy outlined in Section 2.6. Furthermore, the time for one science cycle is computed to be 93.7 $days$, meaning that within the 200 $days$ duration required for the chemical measurements, there are indeed two science cycles.

2.4.2. Relay Orbit Design

The orbit trajectory segment consists of the operational orbits of the two RELs, and the subsequent deorbiting trajectories. The specification of the operational segment is driven in large parts by the required ground path, which must cover the path of the SCB for all parts of the orbit, and ranging considerations. The first consideration favors an orbit design featuring low inclination, while the latter strongly favors higher inclinations. It is important to note that each REL has a different orbit which is specified separately. Ultimately, the two orbits are identical in all aspects, except for the declination of the ascending node. Consequently, the key requirements of the REL orbit are as shown in Table 2.6:

Table 2.6: The key orbit requirements specifying the trajectory of the relay satellites.

ID	Description	Rationale
ORB-REQ-4.2	The inclination of ORB-REL-1 shall be no more than 30.7°.	Enables ranging of REL and SCB - Function F6.7 and F6.9 and constant coverage of the SCB.
ORB-REQ-4.3	The inclination of ORB-REL-2 shall be no more than 30.7°.	Enables ranging of REL and SCB - Function F6.7 and F6.9 and constant coverage of the SCB.
ORB-REQ-4.4	The declinations of the ascending node of ORB-RE1 and ORB-REL-2 shall be offset by 90 $\pm$ 5 °.	Required for optimal coverage of the SCB path.
ORB-REQ-4.5	The apoapsis of ORB-REL-1 shall be 1701 $\pm$ 20 km above Venus' surface.	Orbital altitude for ideal gap time and data transmission.
ORB-REQ-4.6	The periapsis of ORB-REL-1 shall be 1701 $\pm$ 20 km above Venus' surface.	Orbital altitude for ideal gap time and data transmission.
ORB-REQ-4.9	The periapsis of ORB-REL-1 shall be no more than 100 km above Venus' surface.	Required for guaranteed deorbiting.

For the analysis of the orbit, the following assumptions are made:

1. The Venusian gravity field is identical to that of a point mass.
2. Non-gravitational forces are 0.
3. The minimum elevation of the REL with respect to the SCB is 5°.

Under these assumptions, the orbit geometry is generated, verified by comparison with analytical calculation of orbit periods and validated through inspection of the mission geometry and position over time. While these assumptions mean that the orbit stays perfectly constant during the mission duration, which is not entirely accurate to real life, the code is still considered valid due to a) Venus' J2 perturbation being very small and b) ample ΔV budgets allocated to station keeping for countering other disturbances. The model yields a geometry as shown in Figure 2.10, showing both the path of the SCB and the two REL orbits.

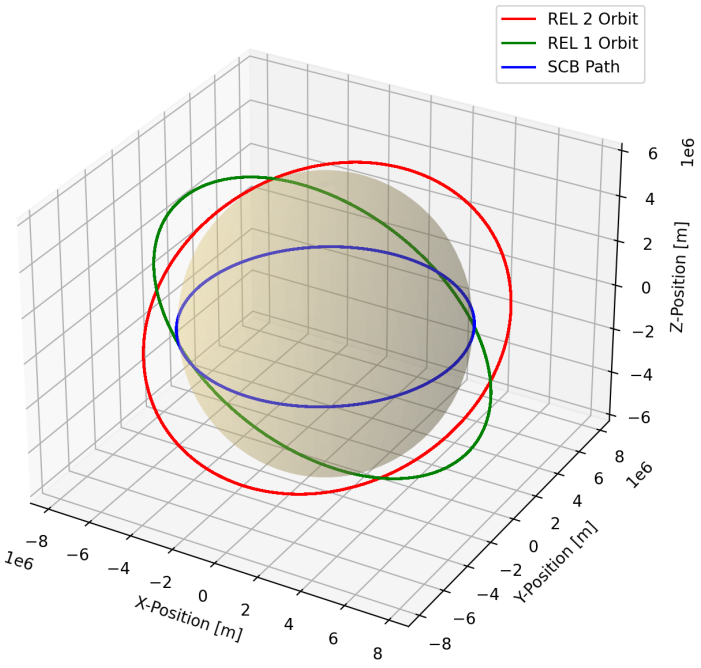

Figure 2.10: The geometry of two REL orbits and the path of the SCB.

2.4.3. Transfer Trajectory Design

The transfer trajectory consists of the trajectories that the two RELs and the transfer stack (the SCB, integrated into the EDV and mounted to the TRV) are using to go to Venus. This trajectory segment begins with the separation of the mission hardware from the launch vehicle. The transfer trajectories of the two RELs end with orbital insertion to Venus, whereas the one of the transfer stack ends when crossing the orbital path of the RELs, shortly before atmospheric entry. The design of the transfer trajectory is expected to be driven mainly by the timing of the arrival of the RELs ahead of the transfer stack, and by the minimisation of the ΔV requirements. In Table 2.7, the main requirements defining the transfer are tabulated:

Table 2.7: The key transfer trajectory requirements.

ID	Description	Rationale
TRA-REQ-3.2	The TRA-REL-1 segment shall end no less than 12 hours before the end of TRA-TRV.	Enables support of EDV and SCB during EDF, called for by F5.2.
TRA-REQ-3.3	The TRA-REL-2 segment shall end no less than 12 hours before the end of TRA-TRV.	Enables support of EDV and SCB during EDF, called for by F5.2.

In order to define the mission geometry, assumptions are first made on the movement and position of Earth and Venus and the chosen transfer, influencing the timing of the mission and hence the mission geometry.

1. The transfer trajectory is a perfect Hohmann transfer.
2. The transfer trajectory duration is equal to a perfectly planar manoeuvre.
3. The mission is ready to launch at the beginning of 2031.

The results of the transfer analysis are verified against the synodic period of Earth and Venus and against analytical calculation of transfer times, and validated using the transfer trajectory geometries of the Venus Express mission. This results in three window options for the mission between 2031 and 2035: one in 2031.25 (March), one in 2032.85 (October) and one in 2034.43 (May). The launch window chosen for the geometry analysis of the mission is the one in 2031. The time for the transfer is estimated to be $1.26 \cdot 10^7$ s or 146 $days$. No further detailed analysis of the transfer is performed since this is not the focus of this design exercise.

2.4.4. Results of the Mission Geometry Analysis

Now, the results of the mission geometry are provided. Firstly, the overall geometry, then the eclipse and contact times relevant for communications and power generation.

Earth-Venus Position and Distance during Mission

Having derived the timing of the transfer to Venus and the operational phase of the mission, the relative positions of Earth and Venus during the mission can be determined. The result of this is shown in Figure 2.11 and Figure 2.12:

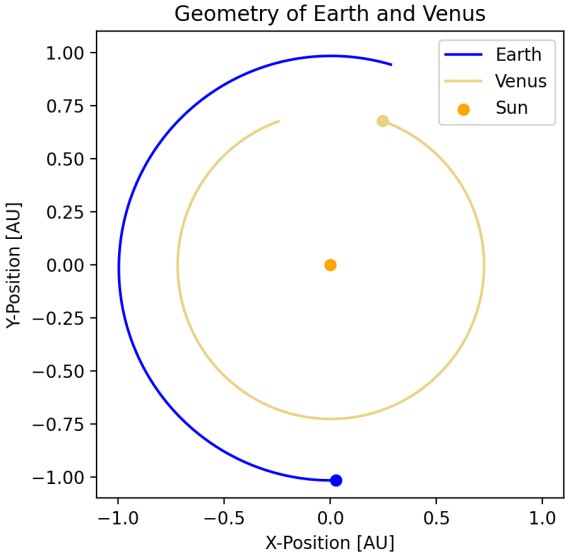

Figure 2.11: The position of Earth and Venus during the operational phase of the mission.

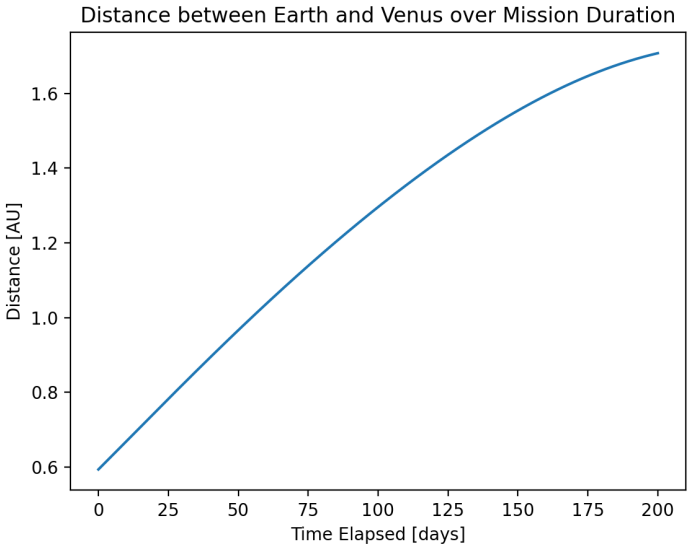

Figure 2.12: The distance between Earth and Venus during the operational phase of the mission

The outputs of this analysis are relevant for the sizing of the REL-TNC and REL-OBD sizing described in Section 6.7 and Section 6.11 respectively.

Relay Overpass Geometry

The first set of results regarding the REL overpass geometry relates to the analysis of a singular overpass, since it relates to the communications link between the RELs and the SCB. Firstly, the elevation angle of the REL as seen from the SCB is important for determining communications eclipse times. Moreover, the distance between

the REL and the SCB is important to determine the free space loss, as well as the path length of the signal in the atmosphere, which is important for the atmospheric attenuation. An assumption is introduced at this point:

1. Atmospheric attenuation is constant throughout the atmosphere of Venus and equal to the attenuation at 50 km.

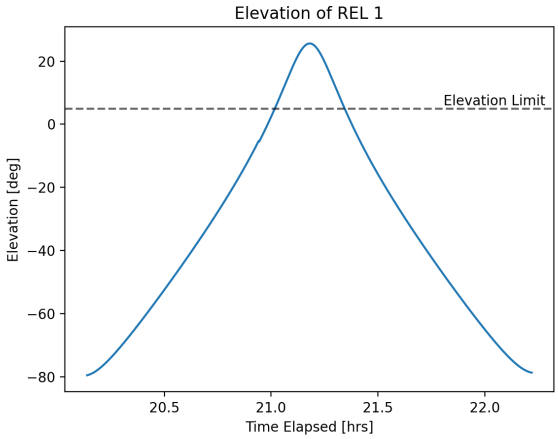

Figure 2.13: The elevation of REL-1 relative to the SCB.

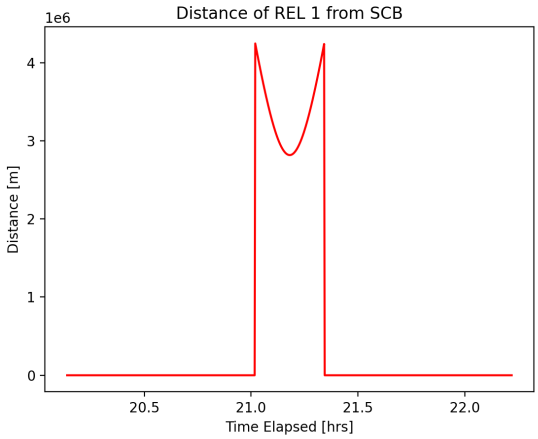

Figure 2.14: The distance between REL-1 and the SCB.

This results in the following results, verified through hand calculations and validated through inspection, showing validity within the requirements of communication analysis: Figure 2.13 shows the elevation of the REL relative to the SCB during a communication overpass. Then, Figure 2.14 shows the distance between the REL and the SCB during the overpass, with the distance being set to 0 if the REL's elevation is below a threshold. The atmospheric attenuation is plotted analogously in Figure 2.15, showing a maximum attenuation of 9 dB at the beginning of the overpass. Next up, Figure 2.16 shows the eclipse and contact times for the two RELs, Figure 2.17 shows the combined contact and eclipse times and Figure 2.18 shows the evolution of the minimum distance between the REL and the SCB over the mission duration. The results obtained are verified by cross-referencing with the verified and validated data on the distance and eclipse conditions between the two RELs and the SCB.

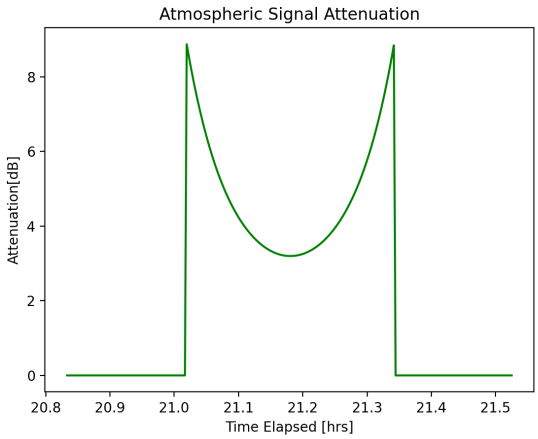

Figure 2.15: The atmospheric attenuation during the overpass.

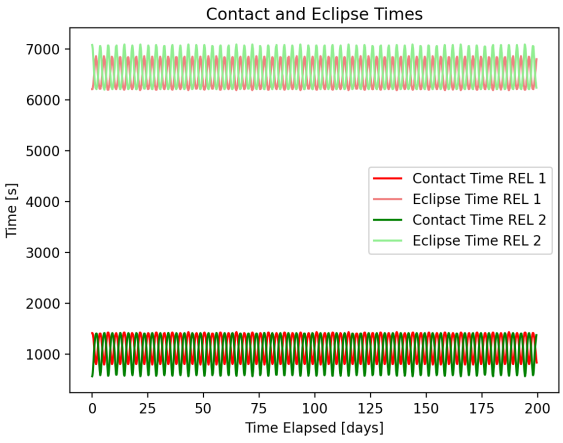

Figure 2.16: Evolution of eclipse and contact times between the REL and the SCB.

The eclipse time varies as the SCB circumnavigates Venus. The critical sizing case can be found when the contact time is minimal. The minimal contact time for one relay is 560 s and the maximal eclipse duration is 7090 s. For the constellation of two relays, the minimal contact time stays unchanged,but the maximum combined eclipse time is reduced to 2920 s. The results of this analysis are used in Section 4.7, Section 4.11 and Section 6.7.

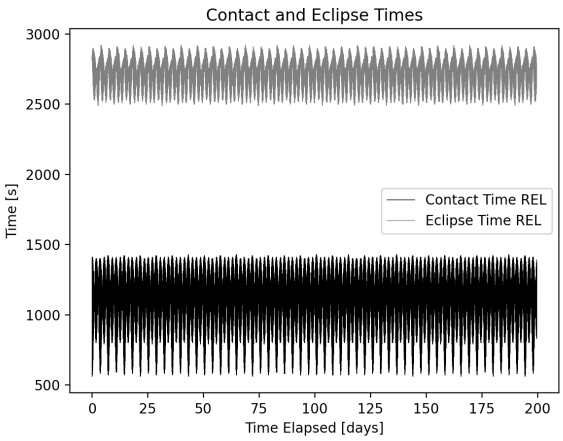

Figure 2.17: Evolution of eclipse and contact times between both RELs and the SCB.

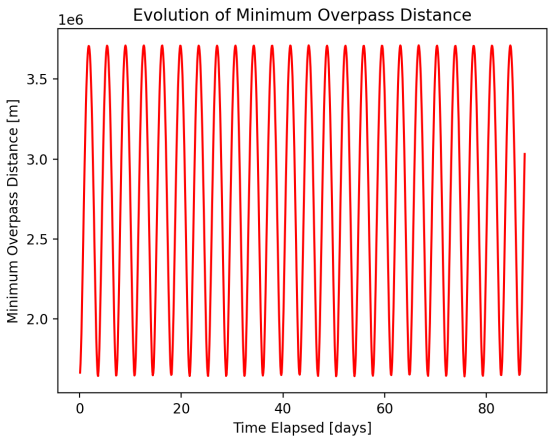

Figure 2.18: Evolution of the minimum distance between the REL and the SCB.

Earth Eclipse Times

In order to better understand how the link budget between the REL and the ground station changes over the mission duration, an analysis is performed on how the eclipse and contact times evolve over the course of the mission. The eclipses here are a result of both the REL orbit and ground station geometry. This yields the graphs shown in Figure 2.19 and Figure 2.20:

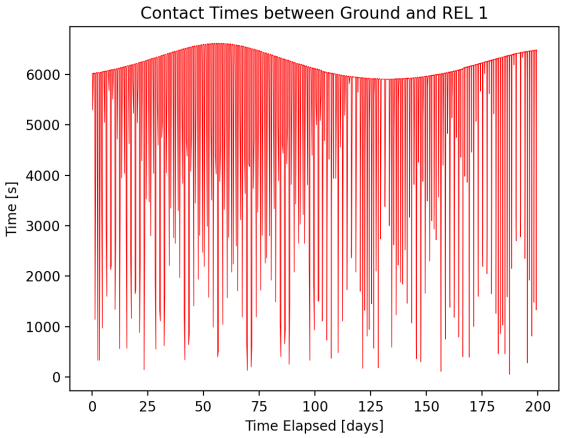

Figure 2.19: The contact times between REL-1 and the ground segment, other REL and ground station removed for clarity

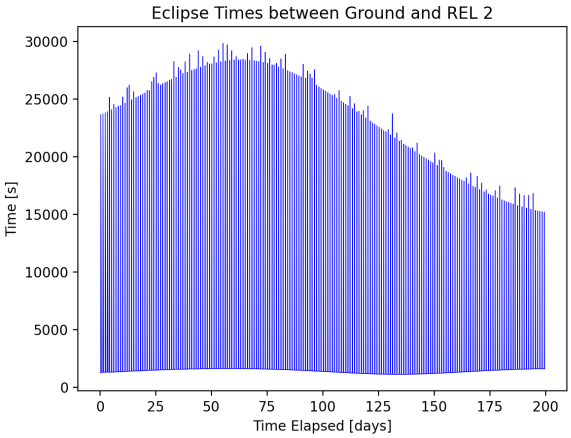

Figure 2.20: The eclipse times between REL-2 and the ground segment, other REL and ground station removed for clarity

It can be seen that the contact times vary as a result of the variations in constellation of Venus and Earth, interrupted by the REL going into eclipse. The worst-case (maximal) eclipse is between the ground segment and REL-2 and lasts 29850 s. The wors-case (minimal) contact time is between REL-1 and the ground segment: 50 s. The long-term variation visible in the graphs is the result of the axis tilt of Earth and the changing relative positions of Venus and Earth. The shorter-term variations are due to the fact that there is a high-frequency eclipse condition, caused by the orbital motion of the relays around Venus, overlaid with a low-frequency eclipse condition caused by the Earth. The results are verified by comparing the eclipse times to the length of one day and the orbital period of the REL. The results of this analysis are used in the sizing of the REL-OBD and REL-TNC shown in Section 6.7 and Section 6.8.

Solar Irradiation of Relay Satellites

The solar irradiation and eclipse time experienced by the RELs is important when considering the REL-EPS and REL-THE sizing and design. In this analysis, the distance between the RELs and the sun, as well as their eclipse times are analysed. Verification and validation is performed by comparing the results of the solar distance calculation to hand calculations, and the eclipse analysis is verified by cross-checking with hand calculations of the eclipse angle and time and validated through visual inspection of the resultant graphs.

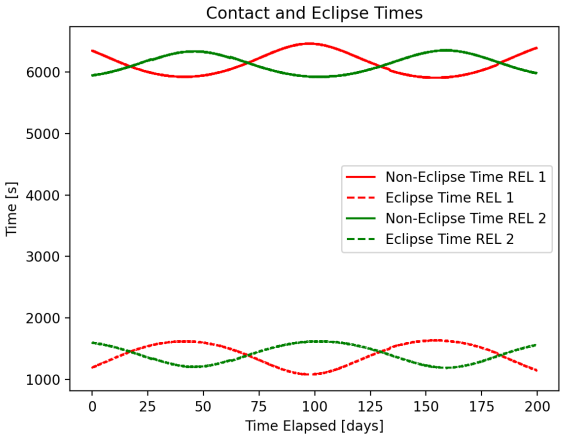

Figure 2.21: Evolution of eclipse and contact times between the REL and the Sun.

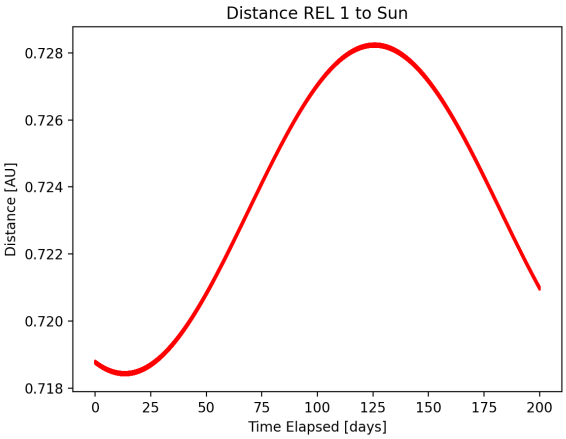

Figure 2.22: Evolution of distance between REL-1 and Sun.

It is shown in Figure 2.21 that the eclipse duration varies throughout the mission for both RELs, which is a result of Venus' motion around the sun, with a minimum at around 40 $days$ into the mission. This condition is critical for the EPS sizing. Furthermore, as Figure 2.22 shows, the distance to the Sun reaches a minimum at around 15 days into the mission, while being maximal around 130 $days$ into the mission. These results are relevant to both the design and sizing of the REL-EPS treated in Section 6.11 and REL-THE, discussed in Section 6.14.

Model Limitations, Verification and Validation

The mission geometry tools are all initially verified by comparison to analytical results. For example, it is verified that the orbital period matches the one obtained using orbital equations. Validation is also done through comparison with results obtained in simpler (often 2D) analyses and reference missions, namely Venus Express where applicable. Furthermore, validation is performed through inspection of the results, ensuring that the resulting graphs are smooth and any variations can be accounted for.

Overall, it is found that the model is valid for orbits with low-medium eccentricities (<0.9) and for the purposes of eclipse, communication and irradiation analysis. It is not fit for orbital trajectory simulation as, in order to save computational resources, only one orbit is propagated, and the subsequent orbits are concatenated.

2.5. Mission Concept Definition and Description

In the following segments, the mission concept is analysed and traded, and the design of the TRV, a mission segment not treated in detail, is discussed. Finally, the overall mission concept is presented.

2.5.1. Mission Transfer Strategy Trade-Off

After the completion of major mission trades, major alternatives are considered. As a result of this analysis with regards to the mission architecture, two alternative options for realising the transfer to Venus (which so far has not been considered in detail) are considered:

The first option is to keep the RELs attached to the TRV, perform a capture manoeuvre in this configuration, and then perform the descent of the EDV. Furthermore, the TRV then deploys both RELs into their respective orbits. Since this option is presupposed through tutor requirements [1], this option has been treated as the baseline. The second option considered is to detach the RELs from the LAV, with them subsequently entering orbit around Venus. The TRV then enters the Venusian atmosphere directly from a hyperbolic trajectory. The results of the final trade-off are shown below in Table 2.8, with the method used being the same as in [2].

The baseline option results having the entire EDV mass undergo the Venus orbital insertion burn ($\Delta V = 3\ km/s$), and the TRV changing the RAAN of is orbit ($\Delta V = 2.3\ km/s$), resulting in a huge propellant mass requirement of almost 20000 kg, which also increases the structural mass. This means that the mission, with a total mass of 21347 kg can not be launched on any currently available launcher, not fulfilling a customer requirement. On the other hand, performing maneuvers of large spacecrafts in deep space is well-explored, lowering the risk and schedule. Furthermore the entry energy of the EDV is relatively low.

Option 2 increases the complexity and mass of the two RELs, since they now have to perform the capture

manoeuvre. On the other hand, they can insert directly into their target orbital planes, meaning highly reduced total mission mass of 1187 kg, with an accompanying reduction in cost. Furthermore, the criticality of each entry manoeuvre is reduced. On the other hand, having a small spacecraft performing large manoeuvres is a relatively novel capability, leading to an increase in risk and schedule. Moreover, the entry energy of the EDV is increased, with implications on the heat shield sizing.

Table 2.8: The trade-off between baseline and new transfer strategy.

	Risk (30%):	Performance (20%):	Sch. (5%):	Cost (40%):	Sus. (5%):	Final Score:
Baseline: Integrated Transfer	2.00	0.00	2.00	0.72	1.00	**1.08**
Separating Relays	2.00	2.00	1.56	1.50	2.00	**1.83**

After a sensitivity analysis adjusting the weights to even weighting (with each criterion having a weight of 0.2) and investigating how a mass change of the EDV might change the result, the separating REL is selected based on a highly robust trade-off result. The latter option is the only feasible one, and even though there are deficiencies in cost and schedule, these are correctable. The former factor has already been corrected in the subsequent detailed design, with the mission cost decreasing significantly from the estimate used in this trade-off.

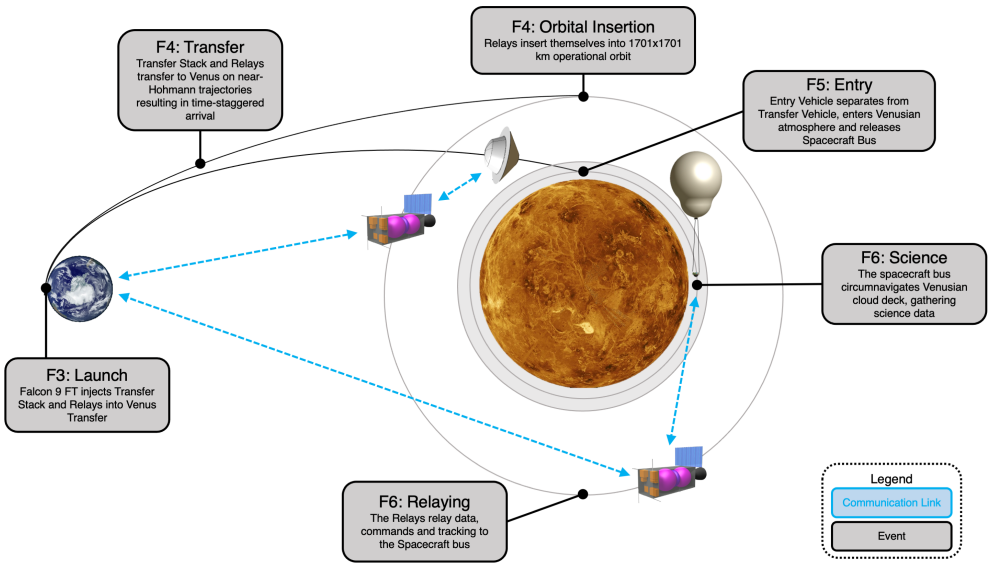

Figure 2.23: ConOps Diagram for the LOVE mission.

2.5.2. Mission Design Overview

In the following subsection the results of the mission-level design efforts, including an operational analysis through the definition of the mission needs, the stakeholder requirements and science objectives, a logical analysis through the creation of the mission architecture, the functional flow and functional breakdown, a physical analysis of the mission geometry, a risk analysis and the requirements definition are presented. The design solutions represent the results of systems-level trades performed in [2]. Firstly, Figure 2.23 shows the mission concept of operations and Figure 2.24 shows the timeline of the mission.

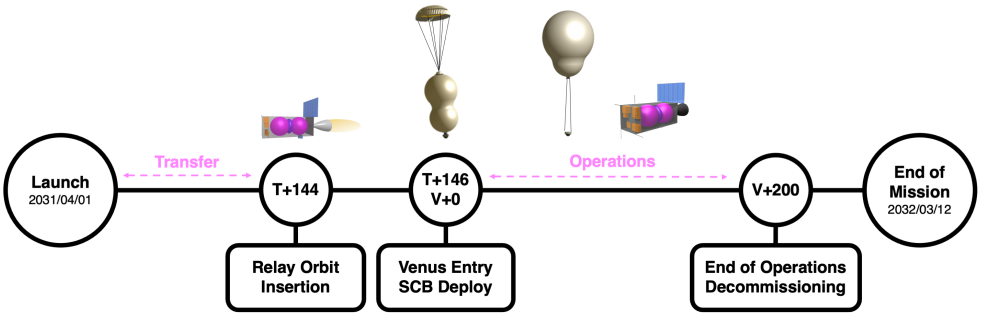

Figure 2.24: Timeline Diagram for the LOVE mission.

Next up, Table 2.9 shows the constituents of the mission and their design. It can be seen from the table above that the two ground stations in Goldstone and Madrid - part of the Deep Space Network, are chosen for the CCC. They are chosen based on their heritage in supporting deep space missions and their locations providing overall low eclipse times for communications.

Table 2.9: Mission concept of the LOVE mission.

Segment:	**Selected Concept**
1. Subject (Venus)	/
Space Segment	
2. PLD	Combined science package consisting of REMS (environmental monitoring), RAD (radiation dosimeter), TLS (tunable laser spectrometer), NEP (nephelometer), VenSpec (spectrometer) and LSD (polarimeter).
3. SCB	Pumped helium balloon with suspended gondola.
4. Relay Satellite	Two SmallSats featuring an IRIS V2 radio, pointed solar panels and bipropellant propulsion.
5. Entry & Descent Vehicle	A passively controlled, sphere-conical capsule using a conventional heat shield and parachute.
6. Transfer Vehicle	Conventional Propulsion, mounted to the backside of EDV.
Ground Segment	
7. Mission Operations	A missions operation group scheduling science investigations and interfacing with users.
8. Command, Control, and Communications Architecture	DSN Ground Stations at Goldstone and Madrid
Trajectory	
9. Path	A 2D path at 0° latitude, sweeping between 50 and 62.5 km in altitude for 200 $days$. 22 altitude cycles per circumnavigation, repeating the path every 12 circumnavigations,
10. Orbit	A 1721 km circular orbit with a 30.67° inclination, with the RAAN of the two REL orbits offset by 180°.
11. Transfer	A Hohmann Transfer, a separate transfer of the transfer stack and the RELs, with the RELs arriving ahead of transfer stack.
12. Launch Segment	Falcon 9 FT

Table 2.9: Mission concept of the LOVE mission.

Segment:	Selected Concept
Mission Concept	The LAV launches the TRV containing an entry capsule with the SCB and two RELs to a Hohmann transfer orbit. The two RELs enter their respective orbits 12 hrs before arrival of the EDV. The TRV gets jettisoned ahead of the hyperbolic entry of the EDV. After the atmospheric entry of the EDV, it releases a pumped helium balloon which circumnavigates the Venusian equator for 200 $days$. The communication and ranging are done using the two smallsat RELs.

2.6. Mission Operations and Data Flow Analysis

This section documents the mission operations concept, the data transmission concepts, and the communications / data flow diagram which encapsulates the data management aspect of the mission.

2.6.1. Mission Operations Concept

While an exact mission operations concept is beyond the scope of the detail provided in this report, a high-level mission operations concept needs to be made in order to inform communication and data flow diagrams which in turn directly influence OBD and TNC design of the space segment. An overview over the operations is provided in Figure 2.25

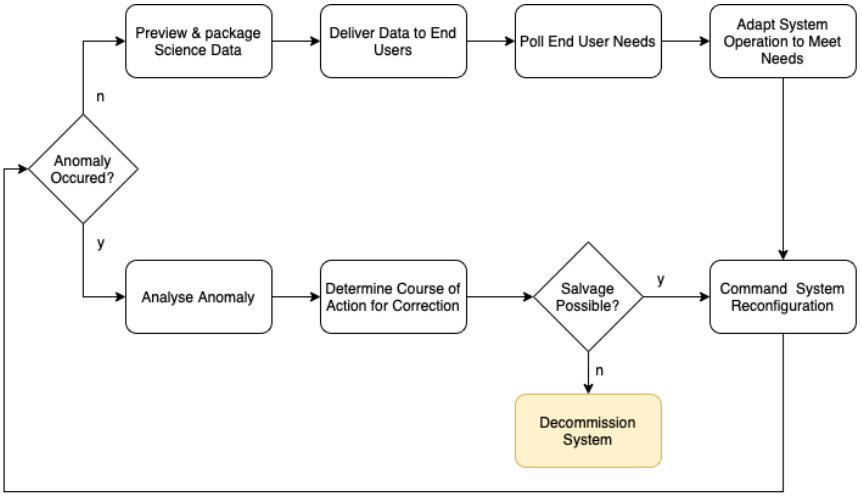

Figure 2.25: Mission Operations Flow Chart.

During nominal operations, each instrument within the payload of the SCB is programmed to take a measurement every certain amount of time, generating data. This data is packaged along with housekeeping data, transmitted through the RELs to the CCC, which sends all of the data to Mission Operations (MIO) where it is displayed to the end user. This is done with high autonomy on the side of the entire system, which is required for deep space mission which are subject to significant communication delays and data budget limitations. However, human interaction with the system is still crucial in ensuring that the mission is a success in two main scenarios: firstly, in order to change the mode of operation of the system in response to scientific results, and secondly, for reacting to anomalies and to handle contingency situations.

For the former, the MIO analyses the data that is returned together with the End User, and poll the End User for requests with regards to SCB operations. After analysing these requests and coming up with an implementation strategy, the appropriate commands are given to the space segment to, for example, remain in a certain altitude range for a longer amount of time.

In the event that any anomalies are detected via the housekeeping data transmitted by the SCB / RELs, changes to the mission can be inputted as commands into the MIO, which transmits them to the necessary system. This is shown in more detail in the maintenance flow diagram in [2].

2.6.2. Mission Data Transmission Concept

During the operational phase of the mission, the payload on the SCB produces approximately 47 Gb worth of scientific data which must be transmitted to Earth in order to analyse it in detail. This data is relayed to 2 different ground stations (Madrid and Goldstone Deep Space Communication Complexes) via a dual REL system (REL-

1 & REL-2), whose trajectories are described in Figure 2.4.4. During a relay overpass, the spacecraft receives commands and transmits as much scientific data as possible. Once it is transmitted to the REL, it in turn transmits it to one of the two ground stations, which in return sends back commands for both the REL and the SCB subsystems.

In order to verify the viability of these communication links and to size the OBD subsystems for all systems, a communications model for the entire mission is made in python. This model based itself off of the bitrates of scientific instruments to generate the total SCB data, as well as the data obtained from the mission geometry analysis. This model simulates the data transmission between the SCB and the RELs, and the data transmission between the RELs and the CCC, and a sample of what can be found in the output of this model can be seen in Figure 2.26.

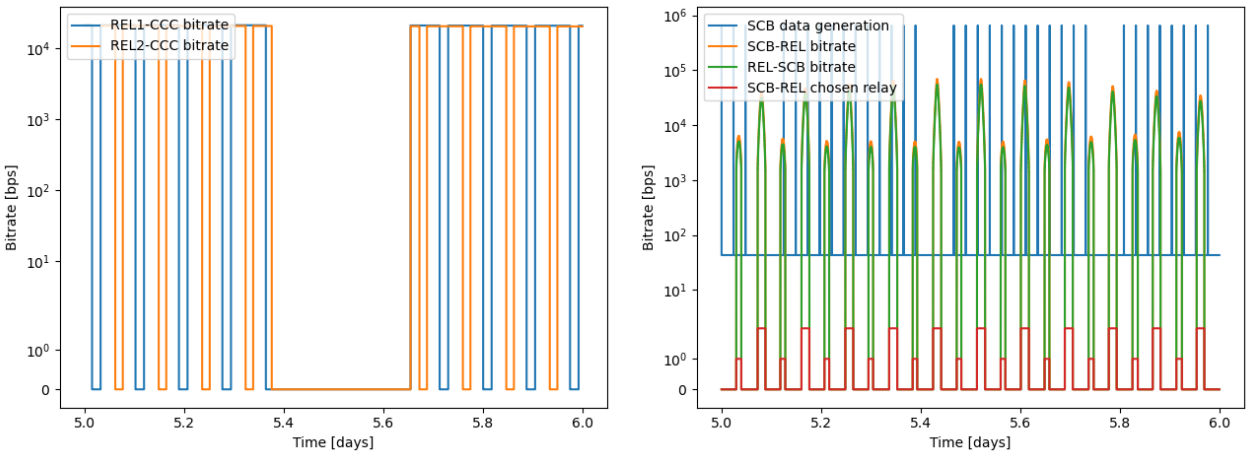

(a) Bitrates between REL-1 and REL-2 to CCC, from day 5 to 6 of the mission.

(b) Data generation on SCB, RELs to SCB and SCB to RELs bitrates, along with an indicator for the chosen relay plotted over time.

Figure 2.26: Graphs from the communications model.

In Figure 2.26b the red line is an indicator of which REL the SCB is communicating to, where 1 means it is communicating to REL-1 and 2 means communicating to REL-2 (0 meaning no communication at all). The SCB-REL and REL-SCB bitrates shown are the available bitrates, however data transfer does not always make use of the entirety of the overpass time. Further analysis is also done for the communications between the RELs and the CCCs, and while some of this analysis can be seen in Figure 2.26a, not all of the results are included, in order to be concise.

Apart from communications, the RELs also do ranging using Doppler to determine the position of the SCB. This is done by appending ranging bits to data packages before being sent to the SCB. When these bits are returned to the REL by the SCB, the REL can accurately determine the full position of the spacecraft, and can communicate this to both the SCB itself or the ground stations. Ranging is also done between the CCC and the REL in a similar manner, using Doppler as well. This is all shown in Figure 2.29.

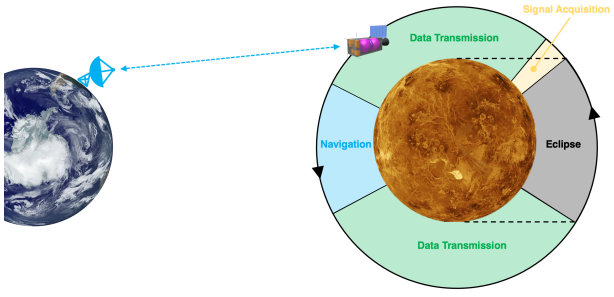

Figure 2.27: Overpass strategy for the REL-CCC link

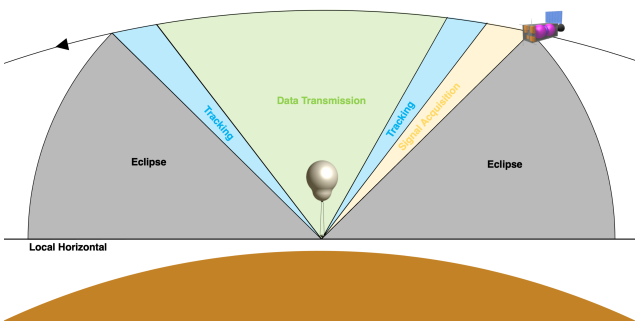

Figure 2.28: Overpass strategy for the REL-SCB link

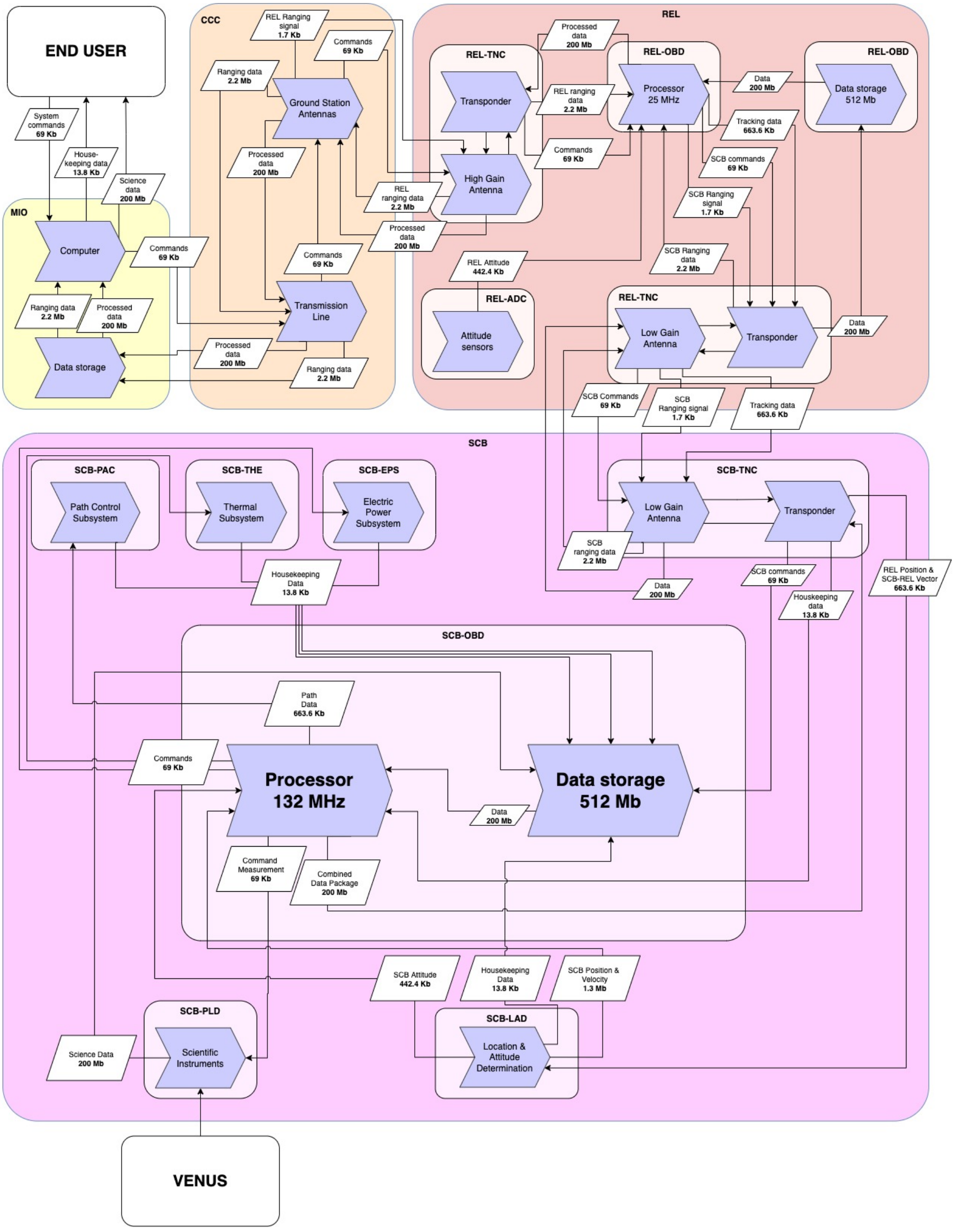

Figure 2.29: Communications & data flow diagram, showing data volumes (data generated per 24 hrs).

2.6.3. Communications and Data Flow Diagram

In Figure 2.29 the data flows between the many different elements of the mission are displayed. In this diagram it is assumed that the ranging is done through Doppler ranging, and that the ranging bits are appended to the data packages. Furthermore, the compression factor is assumed to be 50 [17]. Many of the data volumes are estimated using literature [13].

2.7. Mission Risk Analysis

The technical risk assessment of the LOVE mission, and subsequently the systems and subsystems, consists of identifying the risks, mitigating the crucial risks and setting up contingency plans in the case these risks occur. In order to ultimately obtain an evaluation of the reliability of the different systems, the risks are limited to the subsystem failure cases.

To identify risks, the functions for each subsystem must be determined and the components therein must be specified. Each component of the mission presents a risk of failure. To determine the impact of each failure case, the subsystem-level functions must be derived from the functional analysis in Section 2.2. From this, the functions can be grouped per component and the impact of component failure on the mission loss can be evaluated. The definition of the levels of impact can be seen in Table 2.10. While the impact of a risk is often straightforward to estimate, the probability of that risk occurring is much more difficult to determine.

Table 2.10: Definition of technical risk impact levels.

Impact Definition			
Bin	**Qualitative Def.**	**Mission Loss (%)**	**Mission Loss (-)**
1	Very low	1.00	0.01
2	Low	10.00	0.1
3	Moderate	50.00	0.5
4	High	90.00	0.9
5	Very high	100.00	1

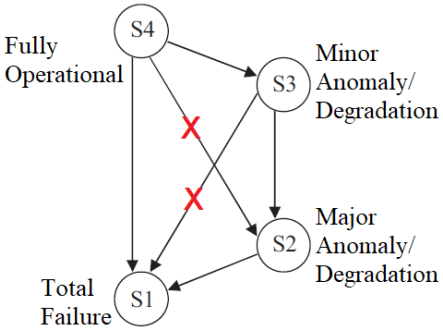

Figure 2.30: Component failure states.

Based on statistical information provided in [71], the probabilities of different failure modes can be estimated for the mission lifetime of 200 $days$. The failure of a component has been subdivided into three types of failures: due to a minor anomaly/degradation, a major anomaly/degradation, or a total failure. These different states can be seen in Figure 2.30. For the purpose of this analysis, only the failures that result in the component no longer being fully operational are considered. Hence, only the risk of going from fully operational (4) to either minorly degradated (3) $R43$, majorly degradated (2) $R42$, and total failure (1) $R41$ are considered.

From the obtained probabilities and specified impacts, the risks can be calculated. To obtain the mission-level risk, a bottom-up approach must be taken: determining the risks of the components-subsystems-systems-mission. The former three steps are performed for SCB, EDV, and REL in Section 4.6, Section 5.7 and Section 6.6, respectively. This leads to the mission technical risk results before and after mitigation, provided in Table 2.11. One can see that without mitigation, the mission does not fulfill the requirement of possessing a 90% probability of achieving the mission level science requirements (MIS-REQ-9.1 in Table 2.4). Thus, risk mitigation is required.

Two approaches have been proposed: performing more analysis and testing of the component to reduce the probability of failure, and / or adding redundancy to reduce the overall risk. The latter is more effective at mitigating the risk, however it is not feasible for components with a high mass / volume, since this considerably changes the design. In that case, the former is more useful. To estimate the effect of adding redundancy, a redundant system is equivalent to a parallel system. Whereas in serial systems, as is the case for the mission systems, where the overall reliability is dependent on each component, a parallel system remains unaffected by the failure of redundant components. The reliability of a parallel system can be calculated using Equation 2.1, where r is the reliability of the component and n is the number of components in parallel (for this report, n=2). Applying these two mitigation strategies to the high-risk components of each systems leads to the technical results after mitigation shown in Table 2.11. Now, the reliability fulfills MIS-REQ-9.1 and the mission is compliant.

$$R_p = 1 - (1 - r)^n \tag{2.1}$$

Table 2.11: Mission technical risk results.

	Mission Achieved (%)	
System	**Before Mitigation**	**After Mitigation**
LAV	100.00	100.00
TRV	99.50	99.50
EDV	91.61	97.67
SCB	94.17	95.99
REL	97.05	97.39
PLD	99.14	99.14
Total	**82.59**	**90.06**

Even with mitigation strategies, failures can still occur. To decrease the impact after a risk has already occurred, contingency plans are set up beforehand. Contingency planning does not occur at a mission-level since the technical risk assessment is a bottom-up approach as specified before, but is discussed at the systems-level.

2.8. Mission Resource Analysis

In the following, the resource requirements of the mission are analysed. These resources include schedule, cost and technical budgets such as mass and volume. This is important in order to ensure that sufficient resources are allocated to the upcoming development phase and that the mission is compatible with the limitations imposed by the mission requirements.

2.8.1. Project Design and Development Logic

Figure 2.31 depicts the steps to be taken after the completion of the DSE. A more thorough analysis of the development production phase can be found in the production plan, in Figure 2.32. This figure also shows the allocation of the available schedule. For a more detailed look into the mission itself, refer to Figure 2.6 which contains the functional flow breakdown structure.

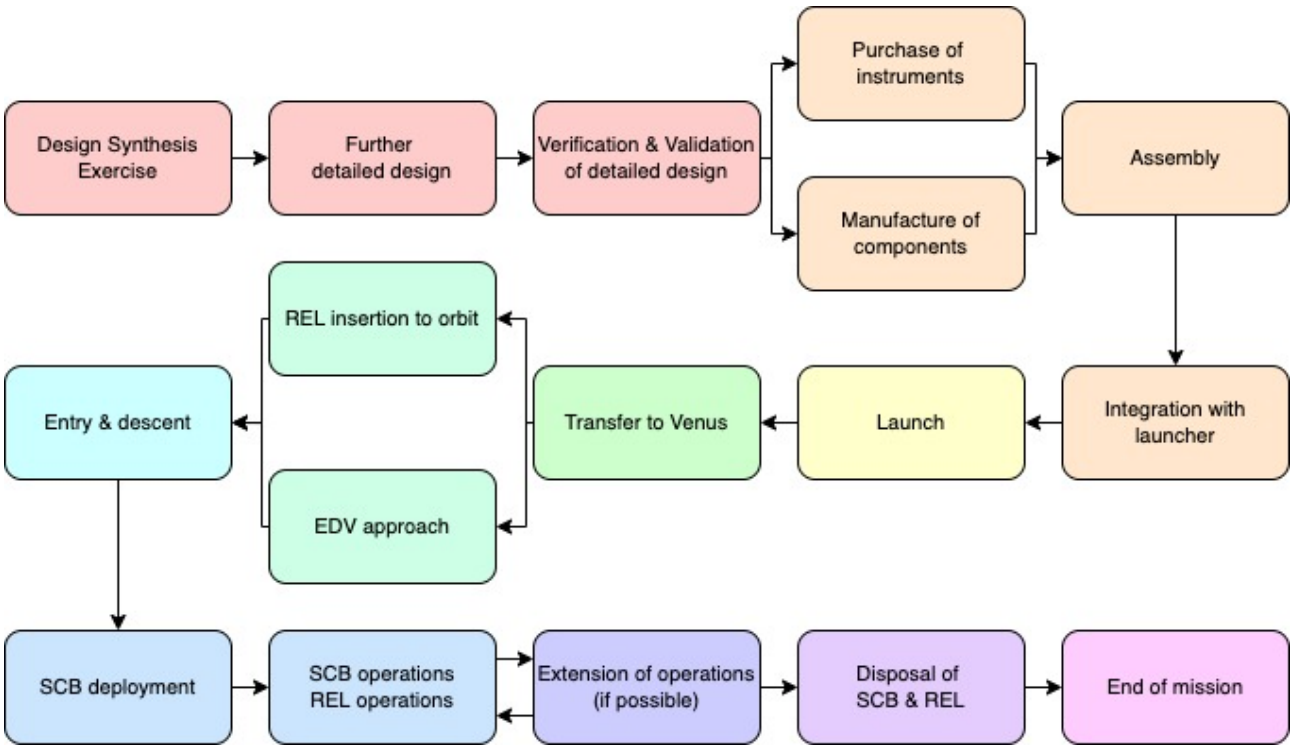

Figure 2.31: The project design & development logic of the LOVE mission.

System	Subsystem	Component full name	Component acronym	2028								2029												2030									
				May	June	July	August	September	October	November	December	January	February	March	April	May	June	July	August	September	October	November	December	January	February	March	April	May	June	July	August	September	October
SCB	SCB-STR	Gondola	GON	Prepare facilities for production and assembly of SCB	GON materials - select supplier	GON materials - place order	GON - production				GON - testing												SCB-STR - Subsystem assembly and integration	SCB-STR - Subsystem testing									
		Balloon module	BLM		BLM materials - select supplier	BLM materials - place order	BLM - production				BLM - testing																						
		Ropes - gondola to balloon	RGB		RGB - select supplier	RGB - place order	RGB - production by external company (off-the-shelf)		RGB - shipping		RGB - testing																						
		Rope - inside balloons	RIB		RIB - select supplier	RIB - place order	RIB - production by external company (off-the-shelf)		RIB - shipping		RIB - testing																						
		Rope - SCB lowering	RSL		RSL - select supplier	RSL - place order	RSL - production by external company (off-the-shelf)		RSL - shipping		RSL - testing																						
	SCB-EPS	Solar array	SOA				SOA - select supplier	SOA - place order	SOA - production by external company (off-the-shelf)		SOA shipping		SOA - hardware testing		SOA - software integration		SOA - software testing						SCB-EPS - Subsystem assembly and integration	SCB-EPS - Subsystem testing									
		Batteries	BAT				BAT - select supplier	BAT - place order	BAT - production by external company (off-the-shelf)		BAT shipping		BAT - hardware testing		BAT - software integration		BAT - software testing																
	SCB-OBD	Power distribution	PCD				PCD - select supplier	PCD - place order	PCD - production by external company (off-the-shelf)		PCD - shipping		PCD - hardware testing				PCD - software testing						SCB-OBD - Subsystem assembly and integration	SCB-OBD - Subsystem testing									
		Processor (RAD750 6U)	CPU				CPU - select supplier	CPU - place order	CPU - production by external company (off-the-shelf)		CPU - shipping	PCD - software writing			PCD - software integration																		
	SCB-TNC	Flash memory	ROM				ROM - select supplier	ROM - place order	ROM - production by external company (off-the-shelf)		ROM shipping	CPU - software writing	ROM - hardware testing		CPU - software integration		CPU- software testing																
		LGA	LGA						LGA - select supplier	LGA - place order	LGA - production by external company (off-the-shelf)		ROM - hardware testing		ROM - software integration		ROM - software testing						SCB-TNC - Subsystem assembly and integration	SCB-TNC - Subsystem testing									
		IRIS	TRX						TRX - select supplier	TRX - place order	TRX - production by external company (off-the-shelf)		LGA - shipping		LGA - hardware testing																	
	SCB-LAD	LN200s	IMU									IMU - select external company	TRX - shipping	TRX - software writing	TRX - hardware testing	TRX - software integration	TRX - software testing						SCB-ADC - Subsystem assembly and integration	SCB-ADC - Subsystem testing									
		6x Sun sensors	SUN									SUN - select external company	IMU - place order	IMU - production by external company (off-the-shelf)		IMU - shipping		IMU - testing															
	SCB-THE	Instruments cover	COV							COV - select external company for production			SUN - place order	SUN - production by external company (off-the-shelf)		SUN - shipping		SUN - testing															
		Heat pipes	PIP						PIP - select supplier	PIP - place order	PIP - production by external company (off-the-shelf)		COV - place order	COV - production by external company		COV - shipping		COV - testing		SCB - components production buffer time		SCB-THE - Subsystem assembly and integration	SCB-THE - Subsystem testing	SCB - Subsystems buffer time	SCB - Final assembly and integration		SCB - Final testing of the integrated system			SCB - Buffer time	
	SCB-PLD	RAD	RAD		RAD - confirm supplier	RAD - place order	RAD - produce individual components			RAD - individual component testing		RAD - component integration	PIP - shipping		PIP - hardware testing																	
		TLS	TLS		TLS - confirm supplier	TLS - place order	TLS - produce individual components			TLS - individual component testing		TLS - component integration	RAD - shipping		RAD - complete instrument testing								SCB-EPS - Subsystem assembly and integration	SCB-PLD - Subsystem testing									
		REMS	REM		REM - confirm supplier	REM - place order	REM - produce individual components			REM - individual component testing		REM - component integration	TLS - shipping		TLS - complete instrument testing																	
		VenSpec	VSC		VSC - confirm supplier	VSC - place order	VSC - produce individual components			VSC - individual component testing		VSC - component integration	REM - shipping		REM - complete instrument testing																	
		Nephelometer	NPH		NPH - confirm supplier	NPH - place order	NPH - produce individual components			NPH - individual component testing		NPH - component integration	VSC - shipping		VSC - complete instrument testing																	
		LSDpol	LSD		LSD - confirm supplier	LSD - place order	LSD - produce individual components			LSD - individual component testing		LSD - component integration	NPH - shipping		NPH - complete instrument testing																	
	SCB-LFT	Reserve tank	RTA				RTA - select external company for production		RTA - place order	RTA - production by external company (complex custom design)			LSD - shipping		LSD - complete instrument testing																	
		Pump and valve system	PVS		PVS materials - select supplier		BDM materials - place order	BDM - shipping		BDM - production			RTA - shipping		RTA - testing		RTA - filling															
		Hydrogen (total)	HYD										BDM - testing																			
		Main tank	MTA		MTA - place order	MTA - production by external company (custom, but close to off-the shelf, design)			MTA - shipping		MTA - testing				HYD - place order	HYD - shipping		HYD - filling					SCB-LFT - Subsystem assembly and integration	SCB-LFT - Subsystem testing									
		Superpressure balloon	SPB						SPB materials - select supplier	SPB materials - place order	SPB materials - production by external company (off-the-shelf)							MTA - filling														
		Zero pressure balloon	ZPB						ZPB materials - select supplier	ZPB materials - place order	ZPB materials - production by external company (off-the-shelf)		SPB materials - shipping		Production of SPB gores	SPB - assembly and integration	SPB - testing															
	SCB-MEC	Boom deployment mech.	BDM				BDM materials - select supplier	BDM materials - place order	BDM - shipping		BDM - production		ZPB materials - shipping		Production of ZPB gores	ZPB - assembly and integration	ZPB - testing															
		Tank release mech.	TRM				TRM materials - select supplier	TRM materials - place order	TRM - shipping		TRM - production			BDM - testing									SCB-MEC - Subsystem assembly and integration	SCB-MEC - Subsystem testing									
		Lowering mech. for the gondola	GLM								GLM materials - select supplier	GLM materials - place order		TRM - testing																	
EDV	EDV-STR	Internal structure	IST	Prepare facilities for production and assembly of EDV	HES tile materials - select supplier	HES tile materials - place order	HES tile materials - shipping		HES single tile - produce and assemble	Testing of single HES tile	Place order for entire HES	GLM - shipping		GLM - production			GLM - testing						EDV-STR - Subsystem assembly and integration	EDV-STR - Subsystem testing	EDV - Subsystem buffer time	EDV - final assembly and integration		EDV - final testing of the integrated system			EDV- Buffer time	
		Outer shell	OUS								IST - select supplier	IST - place order	Shipping of components for a single HES tile		Production of HES tiles	HES - assembly and integration	HES - testing															
	EDV-EPS	Battery	BAT								OUS - select supplier	OUS - place order	IST - production by external company	IST components - shipping		IST - assembly and integration	IST - testing															
		Power distribution	PCD										OUS- production by external company	OUS components - shipping		OUS - assembly and integration	OUS - testing															
	EDV-OBD	Microcontroller	CPU								BAT - select supplier	BAT - place order	BAT - production by external company (off-the-shelf)		BAT shipping		BAT - hardware testing		BAT - software integration		BAT - software testing		EDV-EPS - Subsystem assembly and integration	EPV-EPS - Subsystem testing									
		Flash memory	ROM								PCD - select supplier	PCD - place order	PCD - production by external company (off-the-shelf)		PCD - shipping		PCD - hardware testing				PCD - software testing											
	EDV-TNC	Transponder (IRIS V2)	TRX											PCD - software writing			PCD - software integration															
		Antenna (LGA x 4)	LGA								CPU - select supplier	CPU - place order	CPU - production by external company (off-the-shelf)		CPU - shipping		CPU - hardware testing				CPU- software testing		EDV-OBD - Subsystem assembly and integration	EDV-OBD - Subsystem testing									
	EDV-THE	Heat shield	HES											CPU - software writing			CPU - software integration															
		Backshell insulation	BIN								ROM - select supplier	ROM - place order	ROM - production by external company (off-the-shelf)		ROM shipping		ROM - hardware testing		ROM - software integration		ROM - software testing											
		Drogue parachute	DRP														TRX - software writing		TRX - software integration		TRX - software testing		EDV-TNC - Subsystem assembly and integration	EDV-TNC - Subsystem testing									
	EDV-PAR	Main parachute	MAP								TRX - place order	TRX - production by external company (off-the-shelf)																				
														TRX - shipping		TRX - hardware testing															
	EDV-MEC	Heat shield deployment mech.	HEM								LGA - place order	LGA - production by external company (off-the-shelf)		LGA - shipping		LGA - hardware testing															
		Parachute cover opening mech.	PCM																				EDV-THE - Subsystem assembly and integration	EDV-THE - Subsystem testing									
		Mortar for drogue parachute	MDP								BIN - select external company for production		BIN - place order	BIN - production by external company		BIN - shipping		BIN - testing		EDV - components production buffer time											
		Lowering mech. for SCB	LMS								DRP - select external company for production		DRP - place order	DRP - production by external company		DRP - shipping		DRP - testing				EDV-PAR - Subsystem assembly and integration	EDV-PAR - Subsystem testing									
		Cutting of lowering mech. for SCB	CLS								MAP - select external company for production		MAP - place order	MAP - production by external company		MAP - shipping		MAP - testing														
		Cutting of EDV from SCB	CES										HEM components - select supplier	HEM components - select supplier	HEM - shipping of components		HEM production	HEM - assembly and integration	HEM - testing													
													PCM components - select supplier	PCM components - select supplier	PCM - shipping of components		PCM - production	PCM - assembly and integration	PCM - testing													
												MDP components - select supplier	MDP components - select supplier	MDP - shipping of components		MDP production	MDP - assembly and integration	MDP - testing													
													LMS components - select supplier	LMS components - select supplier	LMS - shipping of components		LMS production	LMS - assembly and integration	LMS - testing													
													CLS components - select supplier	CLS components - select supplier	CLS - shipping of components		CLS production	CLS - assembly and integration	CLS - testing													
													CES components - select supplier	CES components - select supplier	CES - shipping of components		CES production	CES - assembly and integration	CES - testing													
REL	REL-STR	Tube	TUB	Prepare facilities for production and assembly of REL						TUB - select external company for production		TUB - place order	TUB - production by external company	TUB - shipping		TUB - testing																	
		Cover	COV							COV - select external company for production		COV - place order	COV - production by external company	COV - shipping		COV - testing																	
	REL-EPS	Power control & distribution	PCD						PCD - place order	PCD - production by external company (off-the-shelf)	PCD - shipping		PCD - hardware testing				PCD - software testing															
		Battery	BAT						BAT - place order	BAT - production by external company (off-the-shelf)	BAT shipping		PCD - software writing		PCD - software integration								REL-EPS - Subsystem assembly and integration	REL-EPS - Subsystem testing									
		Solar array	SOA						SOA - place order	SOA - production by external company (off-the-shelf)	SOA shipping		BAT - hardware testing		BAT - software integration		BAT - software testing															
	REL-OBD	Processor	CPU						CPU - place order	CPU - production by external company (off-the-shelf)	CPU - shipping		SOA - hardware testing		SOA - software integration		SOA - software testing															
		Flash memory	ROM						ROM - place order	ROM - production by external company (off-the-shelf)	ROM shipping		CPU - hardware testing				CPU- software testing						REL-OBD - Subsystem assembly and integration	REL-OBD - Subsystem testing									
												CPU - software writing			CPU - software integration																	
	REL-TNC	Iris Transponder	TRX							TRX - place order	TRX - production by external company (off-the-shelf)		ROM - hardware testing		ROM - software integration		ROM - software testing															
		High gain antenna	HGA							HGA - place order	HGA - production by external company (off-the-shelf)			TRX - software writing		TRX - software integration		TRX - software testing														
		Low gain antenna	LGA							LGA - place order	LGA - production by external company (off-the-shelf)		TRX - shipping		TRX - hardware testing								REL-TNC - Subsystem assembly and integration	REL-TNC - Subsystem testing									
	REL-THE	Heat pipe	PIP							PIP - place order	PIP - production by external company (off-the-shelf)		HGA - shipping		HGA - hardware testing																	
		Radiator	RAD							RAD - place order	RAD - production by external company (off-the-shelf)		LGA - shipping		LGA - hardware testing																	
		Multilayer insulation	MLI							INS - place order	INS - production by external company (off-the-shelf)		PIP - shipping		PIP - hardware testing																	
	REL-MEC	-	-										RAD - shipping		RAD - hardware testing								REL-THE - Subsystem assembly and integration	REL-THE - Subsystem testing									
													INS - shipping		INS - hardware testing																	
	REL-ADC	Star tracker	STK						STK - place order	STK - production by external company (off-the-shelf)	STK - shipping												-	-									
		Reaction wheel	RWL						RWL - place order	RWL - production by external company (off-the-shelf)	RWL - shipping		STK - hardware testing		STK - software integration		STK - software testing															
												RWL - software writing			RWL - software integration								REL-ADC - Subsystem assembly and integration	REL-ADC - Subsystem testing									
	REL-PRP	Bipropellant tank	BPT							BPT - select external company for production		BPT - place order	RWL - hardware testing		RWL - software testing																	
		Cold gas tank	CGT							CGT - select external company for production		CGT - place order	BPT - production by external company	BPT - shipping		BPT - testing																
		Main engine	THR						THR - place order	THR - production by external company (off-the-shelf)	THR - shipping		CGT - production by external company	CGT - shipping		CGT - testing																
		RCS	RCS						RCS - place order	RCS - production by external company (off-the-shelf)	RCS - shipping		THR - hardware testing				THR - software testing						REL-PRP - Subsystem assembly and integration	REL-PRP - Subsystem testing									
												RCS - software writing			RCS - software integration																	

Figure 2.32: The production plan of the LOVE mission.

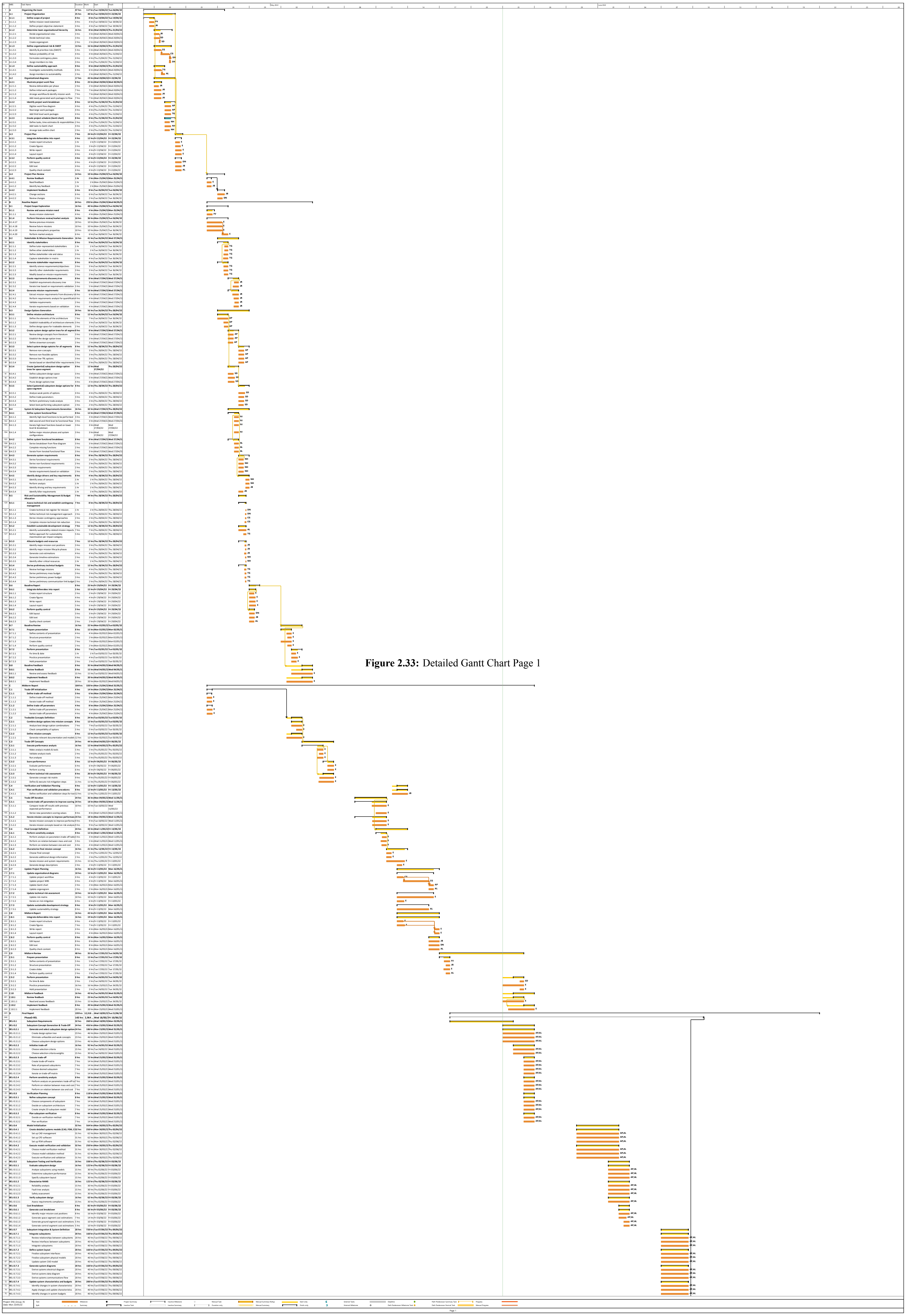

Figure 2.33: Detailed Gantt Chart Page 1

ID	WBS	Task Name	Duration	Work	Start	Finish
76	REL-D.7.4.4	Apply changes and update budgets	20 hrs	40 hrs	Tue 07/06/22	Thu 09/06/22
77	**REL-D.8**	**Model Iteration**	**8 hrs**	**186 hrs**	**Thu 09/06/22**	**Thu 09/06/22**
78	**REL-D.8.1**	**Update systems models**	**8 hrs**	**58 hrs**	**Thu 09/06/22**	**Thu 09/06/22**
79	REL-D.8.1.1	Update CAD management	7 hrs	14 hrs	Thu 09/06/22	Thu 09/06/22
80	REL-D.8.1.2	Update CFD software	7 hrs	14 hrs	Thu 09/06/22	Thu 09/06/22
81	REL-D.8.1.3	Update FEM software	7 hrs	14 hrs	Thu 09/06/22	Thu 09/06/22
82	**REL-D.8.2**	**Execute model verification and validation**	**8 hrs**	**112 hrs**	**Thu 09/06/22**	**Thu 09/06/22**
83	REL-D.8.2.1	Choose model verification method	16 hrs	32 hrs	Wed 08/06/22	Thu 09/06/22
84	REL-D.8.2.2	Choose model validation method	16 hrs	32 hrs	Wed 08/06/22	Thu 09/06/22
85	REL-D.8.2.3	Execute verification and validation	16 hrs	32 hrs	Wed 08/06/22	Thu 09/06/22
86	**REL-D.9**	**System Testing and Verification**	**16 hrs**	**240 hrs**	**Thu 09/06/22**	**Fri 10/06/22**
87	**REL-D.9.1**	**Evaluate system configuration**	**16 hrs**	**64 hrs**	**Thu 09/06/22**	**Fri 10/06/22**
88	REL-D.9.1.1	Analyze systems using models	8 hrs	16 hrs	Thu 09/06/22	Thu 09/06/22
89	REL-D.9.1.2	Determine systems performance	8 hrs	16 hrs	Fri 10/06/22	Fri 10/06/22
90	**REL-D.9.2**	**Characterize RAMS**	**16 hrs**	**80 hrs**	**Thu 09/06/22**	**Fri 10/06/22**
91	REL-D.9.2.1	Reliability analysis	8 hrs	16 hrs	Thu 09/06/22	Thu 09/06/22
92	REL-D.9.2.2	Fault tree analysis	8 hrs	16 hrs	Fri 10/06/22	Fri 10/06/22
93	REL-D.9.2.3	Safety assessment	8 hrs	16 hrs	Fri 10/06/22	Fri 10/06/22
94	**REL-D.9.3**	**Verify system configuration**	**16 hrs**	**96 hrs**	**Thu 09/06/22**	**Fri 10/06/22**
95	REL-D.9.3.1	Assess requirements compliance	16 hrs	48 hrs	Thu 09/06/22	Fri 10/06/22
268		**Phase0-SCB**	**143 hrs**	**4,443 ...**	**Wed 18/05/22**	**Fri 10/06/22**
1	**SCB-D.1**	**Subsystem Requirements**	**32 hrs**	**390 hrs**	**Wed 18/05/22**	**Mon 23/05/22**
2	**SCB-D.1.1**	**Iterate preliminary subsystem requirements**	**24 hrs**	**210 hrs**	**Wed 18/05/22**	**Fri 20/05/22**
3	SCB-D.1.1.1	Iterate functional analysis	23 hrs	69 hrs	Wed 18/05/22	Fri 20/05/22
4	SCB-D.1.1.2	Iterate requirements	23 hrs	69 hrs	Wed 18/05/22	Fri 20/05/22
5	**SCB-D.1.2**	**Generate subsystem requirements**	**16 hrs**	**84 hrs**	**Fri 20/05/22**	**Mon 23/05/22**
6	SCB-D.1.2.1	Generate full requirements discovery tree	9 hrs	27 hrs	Fri 20/05/22	Mon 23/05/22
7	SCB-D.1.2.2	Validate requirements	3 hrs	9 hrs	Mon 23/05/22	Mon 23/05/22
8	**SCB-D.2**	**Subsystem Concept Generation & Trade-Off**	**24 hrs**	**681 hrs**	**Mon 23/05/22**	**Wed 25/05/22**
9	**SCB-D.2.1**	**Generate and select subsystem design option**	**24 hrs**	**279 hrs**	**Mon 23/05/22**	**Wed 25/05/22**
10	SCB-D.2.1.1	Create design option tree	23 hrs	69 hrs	Mon 23/05/22	Wed 25/05/22
11	SCB-D.2.1.2	Eliminate unfeasible and weak concepts	23 hrs	69 hrs	Mon 23/05/22	Wed 25/05/22
12	SCB-D.2.1.3	Choose subsystem design options	23 hrs	69 hrs	Mon 23/05/22	Wed 25/05/22
13	**SCB-D.2.2**	**Initialize trade-off**	**16 hrs**	**138 hrs**	**Tue 24/05/22**	**Wed 25/05/22**
14	SCB-D.2.2.1	Choose selection criteria	15 hrs	45 hrs	Tue 24/05/22	Wed 25/05/22
15	SCB-D.2.2.2	Choose selection criteria weights	15 hrs	45 hrs	Tue 24/05/22	Wed 25/05/22
16	**SCB-D.2.3**	**Execute trade-off**	**8 hrs**	**108 hrs**	**Wed 25/05/22**	**Wed 25/05/22**
17	SCB-D.2.3.1	Create trade-off matrix	7 hrs	21 hrs	Wed 25/05/22	Wed 25/05/22
18	SCB-D.2.3.2	Rate all proposed subsystems	7 hrs	21 hrs	Wed 25/05/22	Wed 25/05/22
19	SCB-D.2.3.3	Choose desired subsystem	7 hrs	21 hrs	Wed 25/05/22	Wed 25/05/22
20	SCB-D.2.3.4	Iterate on trade-off matrix	7 hrs	21 hrs	Wed 25/05/22	Wed 25/05/22
21	**SCB-D.2.4**	**Perform sensitivity analysis**	**8 hrs**	**87 hrs**	**Wed 25/05/22**	**Wed 25/05/22**
22	SCB-D.2.4.1	Perform analysis on parameters trade-off ta	7 hrs	21 hrs	Wed 25/05/22	Wed 25/05/22
23	SCB-D.2.4.2	Perform on relation between mass and cost	7 hrs	21 hrs	Wed 25/05/22	Wed 25/05/22
24	SCB-D.2.4.3	Perform on relation between size and cost	7 hrs	21 hrs	Wed 25/05/22	Wed 25/05/22
25	**SCB-D.3**	**Verification Planning**	**8 hrs**	**177 hrs**	**Wed 25/05/22**	**Wed 25/05/22**
26	**SCB-D.3.1**	**Refine subsystem concept**	**8 hrs**	**87 hrs**	**Wed 25/05/22**	**Wed 25/05/22**
27	SCB-D.3.1.1	Choose components of subsystem	7 hrs	21 hrs	Wed 25/05/22	Wed 25/05/22
28	SCB-D.3.1.2	Decide on subsystem architecture	7 hrs	21 hrs	Wed 25/05/22	Wed 25/05/22
29	SCB-D.3.1.3	Create simple 2D subsystem model	7 hrs	21 hrs	Wed 25/05/22	Wed 25/05/22
30	**SCB-D.3.2**	**Plan subsystem verification**	**8 hrs**	**66 hrs**	**Wed 25/05/22**	**Wed 25/05/22**
31	SCB-D.3.2.1	Decide on verification method	7 hrs	21 hrs	Wed 25/05/22	Wed 25/05/22
32	SCB-D.3.2.2	Plan verification	7 hrs	21 hrs	Wed 25/05/22	Wed 25/05/22
33	**SCB-D.4**	**Model Initialization**	**32 hrs**	**846 hrs**	**Mon 30/05/22**	**Thu 02/06/22**
34	**SCB-D.4.1**	**Create detailed systems models (CAD, FEM, CFD)**	**32 hrs**	**375 hrs**	**Mon 30/05/22**	**Thu 02/06/22**
35	SCB-D.4.1.1	Set up CAD management	31 hrs	93 hrs	Mon 30/05/22	Thu 02/06/22
36	SCB-D.4.1.2	Set up CFD software	31 hrs	93 hrs	Mon 30/05/22	Thu 02/06/22
37	SCB-D.4.1.3	Set up FEM software	31 hrs	93 hrs	Mon 30/05/22	Thu 02/06/22
38	**SCB-D.4.2**	**Execute model verification and validation**	**32 hrs**	**375 hrs**	**Mon 30/05/22**	**Thu 02/06/22**
39	SCB-D.4.2.1	Choose model verification method	31 hrs	93 hrs	Mon 30/05/22	Thu 02/06/22
40	SCB-D.4.2.2	Choose model validation method	31 hrs	93 hrs	Mon 30/05/22	Thu 02/06/22
41	SCB-D.4.2.3	Execute verification and validation	31 hrs	93 hrs	Mon 30/05/22	Thu 02/06/22
42	**SCB-D.5**	**Subsystem Testing and Verification**	**16 hrs**	**507 hrs**	**Thu 02/06/22**	**Fri 03/06/22**
43	**SCB-D.5.1**	**Evaluate subsystem design**	**16 hrs**	**183 hrs**	**Thu 02/06/22**	**Fri 03/06/22**
44	SCB-D.5.1.1	Analyze subsystems using models	15 hrs	45 hrs	Thu 02/06/22	Fri 03/06/22
45	SCB-D.5.1.2	Determine subsystem performance	15 hrs	45 hrs	Thu 02/06/22	Fri 03/06/22
46	SCB-D.5.1.3	Specify subsystem layout	15 hrs	45 hrs	Thu 02/06/22	Fri 03/06/22
47	**SCB-D.5.2**	**Characterize RAMS**	**16 hrs**	**183 hrs**	**Thu 02/06/22**	**Fri 03/06/22**
48	SCB-D.5.2.1	Reliability analysis	15 hrs	45 hrs	Thu 02/06/22	Fri 03/06/22
49	SCB-D.5.2.2	Fault tree analysis	15 hrs	45 hrs	Thu 02/06/22	Fri 03/06/22
50	SCB-D.5.2.3	Safety assessment	15 hrs	45 hrs	Thu 02/06/22	Fri 03/06/22
51	**SCB-D.5.3**	**Verify subsystem design**	**16 hrs**	**93 hrs**	**Thu 02/06/22**	**Fri 03/06/22**
52	SCB-D.5.3.1	Assess requirements compliance	15 hrs	45 hrs	Thu 02/06/22	Fri 03/06/22
53	**SCB-D.6**	**Cost Breakdown**	**8 hrs**	**123 hrs**	**Fri 03/06/22**	**Fri 03/06/22**
54	**SCB-D.6.1**	**Generate cost breakdown**	**8 hrs**	**99 hrs**	**Fri 03/06/22**	**Fri 03/06/22**
55	SCB-D.6.1.1	Identify major mission cost positions	8 hrs	24 hrs	Fri 03/06/22	Fri 03/06/22
56	SCB-D.6.1.2	Generate space segment cost estimations	7 hrs	21 hrs	Fri 03/06/22	Fri 03/06/22
57	SCB-D.6.1.3	Generate ground segment cost estimations	5 hrs	15 hrs	Fri 03/06/22	Fri 03/06/22
58	SCB-D.6.1.4	Generate control segment cost estimations	5 hrs	15 hrs	Fri 03/06/22	Fri 03/06/22
59	**SCB-D.7**	**Subsystem Integration & System Definition**	**20 hrs**	**1,080 hrs**	**Tue 07/06/22**	**Thu 09/06/22**
60	**SCB-D.7.1**	**Integrate subsystems**	**20 hrs**	**240 hrs**	**Tue 07/06/22**	**Thu 09/06/22**
61	SCB-D.7.1.1	Review relationships between subsystems	20 hrs	60 hrs	Tue 07/06/22	Thu 09/06/22
62	SCB-D.7.1.2	Review interfaces between subsystems	20 hrs	60 hrs	Tue 07/06/22	Thu 09/06/22
63	SCB-D.7.1.3	Integrate subsystems	20 hrs	60 hrs	Tue 07/06/22	Thu 09/06/22
64	**SCB-D.7.2**	**Define system layout**	**20 hrs**	**240 hrs**	**Tue 07/06/22**	**Thu 09/06/22**
65	SCB-D.7.2.1	Finalize subsystem interfaces	20 hrs	60 hrs	Tue 07/06/22	Thu 09/06/22
66	SCB-D.7.2.2	Finalize subsystem physical models	20 hrs	60 hrs	Tue 07/06/22	Thu 09/06/22
67	SCB-D.7.2.3	Update system CAD model	20 hrs	60 hrs	Tue 07/06/22	Thu 09/06/22
68	**SCB-D.7.3**	**Generate system diagrams**	**20 hrs**	**240 hrs**	**Tue 07/06/22**	**Thu 09/06/22**
69	SCB-D.7.3.1	Derive systems electrical diagram	20 hrs	60 hrs	Tue 07/06/22	Thu 09/06/22
70	SCB-D.7.3.2	Derive systems data diagram	20 hrs	60 hrs	Tue 07/06/22	Thu 09/06/22
71	SCB-D.7.3.3	Derive systems communications flow	20 hrs	60 hrs	Tue 07/06/22	Thu 09/06/22
72	**SCB-D.7.4**	**Update system characteristics and budgets**	**20 hrs**	**300 hrs**	**Tue 07/06/22**	**Thu 09/06/22**
73	SCB-D.7.4.1	Identify changes in system characteristics	20 hrs	60 hrs	Tue 07/06/22	Thu 09/06/22
74	SCB-D.7.4.2	Apply changes and update characteristics	20 hrs	60 hrs	Tue 07/06/22	Thu 09/06/22
75	SCB-D.7.4.3	Identify changes in system budgets	20 hrs	60 hrs	Tue 07/06/22	Thu 09/06/22
76	SCB-D.7.4.4	Apply changes and update budgets	20 hrs	60 hrs	Tue 07/06/22	Thu 09/06/22
77	**SCB-D.8**	**Model Iteration**	**8 hrs**	**279 hrs**	**Thu 09/06/22**	**Thu 09/06/22**
78	**SCB-D.8.1**	**Update systems models**	**8 hrs**	**87 hrs**	**Thu 09/06/22**	**Thu 09/06/22**
79	SCB-D.8.1.1	Update CAD management	7 hrs	21 hrs	Thu 09/06/22	Thu 09/06/22
80	SCB-D.8.1.2	Update CFD software	7 hrs	21 hrs	Thu 09/06/22	Thu 09/06/22
81	SCB-D.8.1.3	Update FEM software	7 hrs	21 hrs	Thu 09/06/22	Thu 09/06/22
82	**SCB-D.8.2**	**Execute model verification and validation**	**8 hrs**	**168 hrs**	**Thu 09/06/22**	**Thu 09/06/22**
83	SCB-D.8.2.1	Choose model verification method	16 hrs	48 hrs	Wed 08/06/22	Thu 09/06/22
84	SCB-D.8.2.2	Choose model validation method	16 hrs	48 hrs	Wed 08/06/22	Thu 09/06/22
85	SCB-D.8.2.3	Execute verification and validation	16 hrs	48 hrs	Wed 08/06/22	Thu 09/06/22
86	**SCB-D.9**	**System Testing and Verification**	**16 hrs**	**360 hrs**	**Thu 09/06/22**	**Fri 10/06/22**
87	**SCB-D.9.1**	**Evaluate system configuration**	**16 hrs**	**96 hrs**	**Thu 09/06/22**	**Fri 10/06/22**
88	SCB-D.9.1.1	Analyze systems using models	8 hrs	24 hrs	Thu 09/06/22	Thu 09/06/22
89	SCB-D.9.1.2	Determine systems performance	8 hrs	24 hrs	Fri 10/06/22	Fri 10/06/22
90	**SCB-D.9.2**	**Characterize RAMS**	**16 hrs**	**120 hrs**	**Thu 09/06/22**	**Fri 10/06/22**
91	SCB-D.9.2.1	Reliability analysis	8 hrs	24 hrs	Thu 09/06/22	Thu 09/06/22
92	SCB-D.9.2.2	Fault tree analysis	8 hrs	24 hrs	Fri 10/06/22	Fri 10/06/22
93	SCB-D.9.2.3	Safety assessment	8 hrs	24 hrs	Fri 10/06/22	Fri 10/06/22
94	**SCB-D.9.3**	**Verify system configuration**	**16 hrs**	**96 hrs**	**Thu 09/06/22**	**Fri 10/06/22**
95	SCB-D.9.3.1	Assess requirements compliance	16 hrs	48 hrs	Thu 09/06/22	Fri 10/06/22
269	**D.10**	**System Integration & Mission Definition**	**15 hrs**	**157 hrs**	**Fri 10/06/22**	**Mon 13/06/22**
250	**D.10.1**	**Integrate systems**	**16 hrs**	**35 hrs**	**Fri 10/06/22**	**Mon 13/06/22**
251	D.10.1.1	Review relationships between system element	7 hrs	21 hrs	Fri 10/06/22	Fri 10/06/22
252	D.10.1.2	Review interfaces between system elements	7 hrs	7 hrs	Fri 10/06/22	Fri 10/06/22
253	D.10.1.3	Integrate systems	7 hrs	7 hrs	Mon 13/06/22	Mon 13/06/22
254	**D.10.2**	**Define mission layout**	**16 hrs**	**45 hrs**	**Fri 10/06/22**	**Mon 13/06/22**
255	D.10.2.1	Finalize system interface	15 hrs	15 hrs	Fri 10/06/22	Mon 13/06/22
256	D.10.2.2	Finalize system physical model	15 hrs	15 hrs	Fri 10/06/22	Mon 13/06/22
257	D.10.2.3	Update mission CAD model	15 hrs	15 hrs	Fri 10/06/22	Mon 13/06/22
258	**D.10.3**	**Generate mission diagrams**	**16 hrs**	**69 hrs**	**Fri 10/06/22**	**Mon 13/06/22**
259	D.10.3.1	Derive mission electrical diagram	15 hrs	15 hrs	Fri 10/06/22	Mon 13/06/22
260	D.10.3.2	Derive mission data diagram	15 hrs	19 hrs	Fri 10/06/22	Mon 13/06/22
261	D.10.3.3	Derive mission communications flow	15 hrs	15 hrs	Fri 10/06/22	Mon 13/06/22
262	**D.10.4**	**Update mission characteristics and budgets**	**16 hrs**	**28 hrs**	**Fri 10/06/22**	**Mon 13/06/22**
263	D.10.4.1	Identify changes in mission characteristics	7 hrs	7 hrs	Fri 10/06/22	Fri 10/06/22
264	D.10.4.2	Apply changes and update characteristics	7 hrs	7 hrs	Mon 13/06/22	Mon 13/06/22
265	D.10.4.3	Identify changes in mission budgets	7 hrs	7 hrs	Fri 10/06/22	Fri 10/06/22
266	D.10.4.4	Apply changes and update budgets	7 hrs	7 hrs	Mon 13/06/22	Mon 13/06/22
267	**D.11**	**Production Plan**	**16 hrs**	**48 hrs**	**Fri 10/06/22**	**Mon 13/06/22**
268	**D.11.1**	**Plan manufacturing, assembly & integration**	**16 hrs**	**48 hrs**	**Fri 10/06/22**	**Mon 13/06/22**
269	D.11.1.1	Determine manufacturing methods	16 hrs	16 hrs	Fri 10/06/22	Mon 13/06/22
270	D.11.1.2	Determine assembly methods	16 hrs	16 hrs	Fri 10/06/22	Mon 13/06/22
271	D.11.1.3	Determine integration methods	16 hrs	16 hrs	Fri 10/06/22	Mon 13/06/22
272	**D.12**	**Mission Validation & Significance identification**	**16 hrs**	**48 hrs**	**Fri 10/06/22**	**Mon 13/06/22**
273	**D.12.1**	**Validate mission**	**16 hrs**	**16 hrs**	**Fri 10/06/22**	**Mon 13/06/22**
274	D.12.1.1	Validate mission requirements	8 hrs	8 hrs	Fri 10/06/22	Fri 10/06/22
275	D.12.1.2	Validate stakeholder requirements	8 hrs	8 hrs	Mon 13/06/22	Mon 13/06/22
276	**D.12.2**	**Review terrestrial impact**	**16 hrs**	**16 hrs**	**Fri 10/06/22**	**Mon 13/06/22**
277	D.12.2.1	Investigate terrestrial applications	8 hrs	8 hrs	Fri 10/06/22	Fri 10/06/22
278	D.12.2.2	Propose terrestrial use cases	8 hrs	8 hrs	Mon 13/06/22	Mon 13/06/22
279	**D.12.3**	**Identify secondary scientific outcomes**	**16 hrs**	**16 hrs**	**Fri 10/06/22**	**Mon 13/06/22**
280	D.12.3.1	Review literature	8 hrs	4 hrs	Fri 10/06/22	Fri 10/06/22
281	D.12.3.2	Review instruments	8 hrs	4 hrs	Fri 10/06/22	Fri 10/06/22
282	D.12.3.3	Determine secondary scientific outcomes	8 hrs	8 hrs	Mon 13/06/22	Mon 13/06/22
283	**D.13**	**Final Report**	**23 hrs**	**78 hrs**	**Mon 13/06/22**	**Wed 15/06/22**
284	**D.13.1**	**Integrate deliverables into report**	**16 hrs**	**30 hrs**	**Mon 13/06/22**	**Wed 15/06/22**
285	D.13.1.1	Create report structure	8 hrs	8 hrs	Mon 13/06/22	Tue 14/06/22
286	D.13.1.2	Create figures	8 hrs	8 hrs	Mon 13/06/22	Tue 14/06/22
287	D.13.1.3	Write report	8 hrs	8 hrs	Tue 14/06/22	Wed 15/06/22
288	D.13.1.4	Layout report	6 hrs	6 hrs	Tue 14/06/22	Tue 14/06/22
289	**D.13.2**	**Perform quality control**	**16 hrs**	**48 hrs**	**Tue 14/06/22**	**Wed 15/06/22**
290	D.13.2.1	Check content of report	16 hrs	16 hrs	Tue 14/06/22	Wed 15/06/22
291	D.13.2.2	Check language and spelling	16 hrs	16 hrs	Tue 14/06/22	Wed 15/06/22
292	D.13.2.3	Check layout of report	16 hrs	16 hrs	Tue 14/06/22	Wed 15/06/22
293	**D.14**	**Final Review**	**24 hrs**	**70 hrs**	**Wed 15/06/22**	**Tue 21/06/22**
294	**D.14.1**	**Prepare presentation**	**23 hrs**	**70 hrs**	**Thu 16/06/22**	**Tue 21/06/22**
295	D.14.1.1	Define contents of presentation	12 hrs	12 hrs	Wed 15/06/22	Thu 16/06/22
296	D.14.1.2	Structure presentation	8 hrs	16 hrs	Thu 16/06/22	Thu 16/06/22
297	D.14.1.3	Create slides	7 hrs	7 hrs	Fri 17/06/22	Fri 17/06/22
298	D.14.1.4	Perform quality control	7 hrs	7 hrs	Mon 20/06/22	Mon 20/06/22
299	**D.14.1.5**	**Perform presentation**	**15 hrs**	**28 hrs**	**Mon 20/06/22**	**Tue 21/06/22**
300	D.14.1.5.1	Fix time & date	7 hrs	7 hrs	Mon 20/06/22	Mon 20/06/22
301	D.14.1.5.2	Practice presentation	7 hrs	14 hrs	Mon 20/06/22	Mon 20/06/22
302	D.14.1.5.3	Hold presentation	7 hrs	7 hrs	Tue 21/06/22	Tue 21/06/22
303	**D.15**	**Final Feedback**	**16 hrs**	**64 hrs**	**Mon 20/06/22**	**Tue 21/06/22**
304	**D.15.1**	**Review feedback**	**8 hrs**	**32 hrs**	**Mon 20/06/22**	**Tue 21/06/22**
305	D.15.1.1	Read feedback	8 hrs	16 hrs	Mon 20/06/22	Tue 21/06/22
306	D.15.1.2	Identify key feedback	8 hrs	16 hrs	Mon 20/06/22	Tue 21/06/22
307	**D.15.2**	**Implement feedback**	**8 hrs**	**32 hrs**	**Mon 20/06/22**	**Tue 21/06/22**
308	D.15.2.1	Change sections	8 hrs	24 hrs	Mon 20/06/22	Tue 21/06/22
309	D.15.2.2	Review changes	8 hrs	8 hrs	Mon 20/06/22	Tue 21/06/22
310	**E**	**Symposium**	**110 hrs**	**209 hrs**	**Mon 06/06/22**	**Fri 24/06/22**
311	**E.1**	**Symposium Preparation**	**64 hrs**	**87 hrs**	**Mon 06/06/22**	**Wed 15/06/22**
312	**E.1.1**	**Prepare Jury Summary**	**24 hrs**	**66 hrs**	**Mon 06/06/22**	**Wed 08/06/22**
313	E.1.1.1	Determine current & planned project develop	15 hrs	15 hrs	Mon 06/06/22	Tue 07/06/22
314	E.1.1.2	Write about it in the form of a short summary	15 hrs	15 hrs	Mon 06/06/22	Tue 07/06/22
315	E.1.1.3	Select the picture to be included in the report	7 hrs	7 hrs	Wed 08/06/22	Wed 08/06/22
316	E.1.1.4	Deliver the jury summary	7 hrs	7 hrs	Wed 08/06/22	Wed 08/06/22
317	**E.1.2**	**Design Poster**	**24 hrs**	**63 hrs**	**Mon 13/06/22**	**Wed 15/06/22**
318	E.1.2.1	Brainstorm concepts	7 hrs	7 hrs	Mon 13/06/22	Mon 13/06/22
319	E.1.2.2	Select an editor software	7 hrs	7 hrs	Mon 13/06/22	Mon 13/06/22
320	E.1.2.3	Generate content (text + images)	15 hrs	15 hrs	Mon 13/06/22	Tue 14/06/22
321	E.1.2.4	Fix layout	7 hrs	7 hrs	Wed 15/06/22	Wed 15/06/22
322	E.1.2.5	Deliver the design poster	7 hrs	7 hrs	Wed 15/06/22	Wed 15/06/22
323	**E.2**	**Symposium Presentation**	**16 hrs**	**59 hrs**	**Wed 22/06/22**	**Thu 23/06/22**
324	**E.2.1**	**Prepare Presentation**	**8 hrs**	**35 hrs**	**Wed 22/06/22**	**Wed 22/06/22**
325	E.2.1.1	Brainstorm concepts	7 hrs	7 hrs	Wed 22/06/22	Wed 22/06/22
326	E.2.1.2	Generate content (text + images)	7 hrs	7 hrs	Wed 22/06/22	Wed 22/06/22
327	E.2.1.3	Fix layout	7 hrs	7 hrs	Wed 22/06/22	Wed 22/06/22
328	E.2.1.4	Schedule the presenters	7 hrs	7 hrs	Wed 22/06/22	Wed 22/06/22
329	E.2.1.5	Deliver the presentation	7 hrs	7 hrs	Wed 22/06/22	Wed 22/06/22
330	**E.2.2**	**Perform presentation in front of Jury**	**8 hrs**	**24 hrs**	**Thu 23/06/22**	**Thu 23/06/22**
331	E.2.2.1	Rehearse the presentation	8 hrs	8 hrs	Thu 23/06/22	Thu 23/06/22
332	E.2.2.2	Decide the dress code	8 hrs	8 hrs	Thu 23/06/22	Thu 23/06/22
333	E.2.2.3	Perform the presentation	8 hrs	8 hrs	Thu 23/06/22	Thu 23/06/22
334	**E.3**	**Project Summary (Seal Booklet)**	**24 hrs**	**47 hrs**	**Mon 20/06/22**	**Wed 22/06/22**
335	**E.3.1**	**Gather necessary content**	**8 hrs**	**24 hrs**	**Mon 20/06/22**	**Tue 21/06/22**
336	E.3.1.1	Note the main points covered in the final repo	8 hrs	8 hrs	Mon 20/06/22	Tue 21/06/22
337	E.3.1.2	Select the most relevant ones	8 hrs	8 hrs	Mon 20/06/22	Tue 21/06/22
338	E.3.1.3	Decide a structure for the summary	8 hrs	8 hrs	Mon 20/06/22	Tue 21/06/22
339	**E.3.2**	**Write-up content for booklet**	**16 hrs**	**23 hrs**	**Tue 21/06/22**	**Wed 22/06/22**
340	E.3.2.1	Write content of the booklet	8 hrs	8 hrs	Tue 21/06/22	Wed 22/06/22
341	E.3.2.2	Proofread the text	8 hrs	8 hrs	Tue 21/06/22	Wed 22/06/22
342	E.3.2.3	Deliver the booklet	7 hrs	7 hrs	Wed 22/06/22	Wed 22/06/22
343	**E.5**	**Symposium Feedback**	**8 hrs**	**16 hrs**	**Fri 24/06/22**	**Fri 24/06/22**
344	**E.5.2**	**Review Feedback**	**8 hrs**	**16 hrs**	**Fri 24/06/22**	**Fri 24/06/22**
345	E.5.2.1	Receive feedback	8 hrs	8 hrs	Fri 24/06/22	Fri 24/06/22
346	E.5.2.2	Identify key feedback	8 hrs	8 hrs	Fri 24/06/22	Fri 24/06/22
347	**F**	**Concept Exploration**	**3184 hrs**	**0 hrs**	**Fri 26/06/22**	**Wed 03/01/24**
350	**H**	**Risk Reduction / Technology Development**	**4199 hrs**	**0 hrs**	**Mon 01/01/24**	**Fri 02/01/26**
354	**N**	**Detailed Design and Development**	**4986 hrs**	**0 hrs**	**Thu 01/01/26**	**Fri 12/05/28**
356	**I**	**Manufacturing & AIT**	**5056 hrs**	**0 hrs**	**Fri 12/05/28**	**Sat 12/10/30**
361	**J**	**Launch Mission Hardware**	**1,023 hrs**	**0 hrs**	**Sat 12/10/30**	**Wed 14/05/31**
369	**K**	**Transfer to Venus**	**704 hrs**	**0 hrs**	**Wed 14/05/31**	**Fri 12/09/31**
372	**L**	**Mission Operations**	**6896 hrs**	**0 hrs**	**Fri 12/09/31**	**Mon 01/01/33**
374	**M**	**Mission Disposal**	**352 hrs**	**0 hrs**	**Mon 01/01/33**	**Thu 01/03/33**

Figure 2.34: Detailed Gantt Chart Page 2

2.8.2. Project Gantt Chart

The high-level project Gantt chart illustrating the project timeline has been provided in Figure 2.35. A detailed Gantt chart with the breakdown of tasks throughout all phases has been split into Figures 2.33 and 2.34.

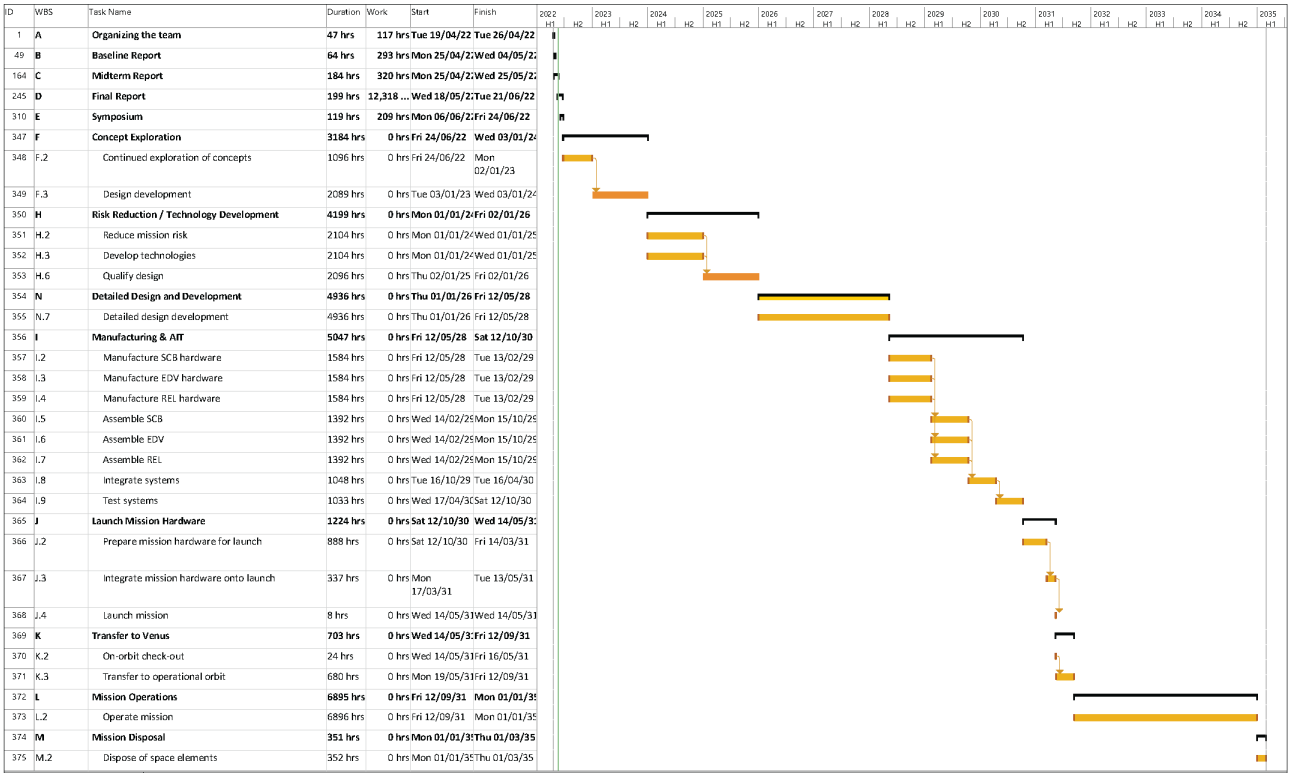

ID	WBS	Task Name	Duration	Work	Start	Finish
1	A	**Organizing the team**	**47 hrs**	**117 hrs**	**Tue 19/04/22**	**Tue 26/04/22**
49	B	**Baseline Report**	**64 hrs**	**293 hrs**	**Mon 25/04/2**	**Wed 04/05/2**
164	C	**Midterm Report**	**184 hrs**	**320 hrs**	**Mon 25/04/2**	**Wed 25/05/2**
245	D	**Final Report**	**199 hrs**	**12,318 ...**	**Wed 18/05/2**	**Tue 21/06/22**
310	E	**Symposium**	**119 hrs**	**209 hrs**	**Mon 06/06/2**	**Fri 24/06/22**
347	F	**Concept Exploration**	**3184 hrs**	**0 hrs**	**Fri 24/06/22**	**Wed 03/01/2**
348	F.2	Continued exploration of concepts	1096 hrs	0 hrs	Fri 24/06/22	Mon 02/01/23
349	F.3	Design development	2089 hrs	0 hrs	Tue 03/01/23	Wed 03/01/2
350	H	**Risk Reduction / Technology Development**	**4199 hrs**	**0 hrs**	**Mon 01/01/2**	**Fri 02/01/26**
351	H.2	Reduce mission risk	2104 hrs	0 hrs	Mon 01/01/24	Wed 01/01/25
352	H.3	Develop technologies	2104 hrs	0 hrs	Mon 01/01/24	Wed 01/01/25
353	H.6	Qualify design	2096 hrs	0 hrs	Thu 02/01/25	Fri 02/01/26
354	N	**Detailed Design and Development**	**4936 hrs**	**0 hrs**	**Thu 01/01/26**	**Fri 12/05/28**
355	N.7	Detailed design development	4936 hrs	0 hrs	Thu 01/01/26	Fri 12/05/28
356	I	**Manufacturing & AIT**	**5047 hrs**	**0 hrs**	**Fri 12/05/28**	**Sat 12/10/30**
357	I.2	Manufacture SCB hardware	1584 hrs	0 hrs	Fri 12/05/28	Tue 13/02/29
358	I.3	Manufacture EDV hardware	1584 hrs	0 hrs	Fri 12/05/28	Tue 13/02/29
359	I.4	Manufacture REL hardware	1584 hrs	0 hrs	Fri 12/05/28	Tue 13/02/29
360	I.5	Assemble SCB	1392 hrs	0 hrs	Wed 14/02/25	Mon 15/10/29
361	I.6	Assemble EDV	1392 hrs	0 hrs	Wed 14/02/25	Mon 15/10/29
362	I.7	Assemble REL	1392 hrs	0 hrs	Wed 14/02/25	Mon 15/10/29
363	I.8	Integrate systems	1048 hrs	0 hrs	Tue 16/10/29	Tue 16/04/30
364	I.9	Test systems	1033 hrs	0 hrs	Wed 17/04/3	Sat 12/10/30
365	J	**Launch Mission Hardware**	**1224 hrs**	**0 hrs**	**Sat 12/10/30**	**Wed 14/05/3**
366	J.2	Prepare mission hardware for launch	888 hrs	0 hrs	Sat 12/10/30	Fri 14/03/31
367	J.3	Integrate mission hardware onto launch	337 hrs	0 hrs	Mon 17/03/31	Tue 13/05/31
368	J.4	Launch mission	8 hrs	0 hrs	Wed 14/05/31	Wed 14/05/31
369	K	**Transfer to Venus**	**703 hrs**	**0 hrs**	**Wed 14/05/3**	**Fri 12/09/31**
370	K.2	On-orbit check-out	24 hrs	0 hrs	Wed 14/05/31	Fri 16/05/31
371	K.3	Transfer to operational orbit	680 hrs	0 hrs	Mon 19/05/31	Fri 12/09/31
372	L	**Mission Operations**	**6895 hrs**	**0 hrs**	**Fri 12/09/31**	**Mon 01/01/3**
373	L.2	Operate mission	6896 hrs	0 hrs	Fri 12/09/31	Mon 01/01/3
374	M	**Mission Disposal**	**351 hrs**	**0 hrs**	**Mon 01/01/3**	**Thu 01/03/35**
375	M.2	Dispose of space elements	352 hrs	0 hrs	Mon 01/01/35	Thu 01/03/35

Figure 2.35: High-Level Project Gantt Chart

2.8.3. Mission Technical Budgets

The systematic allocation of shared technical quantities is critical when developing complex systems. In the following, an overview over the central budgets on mass (Table 2.14), positioning and velocity error (Table 2.15), cost (Table 2.12) and reliability (Table 2.13) is provided. These four budgets are propagated on systems level, since they represent a quantity on which constraints are imposed that pertain to the mission as a whole, and therefore needs to be allocated between mission segments. It is important to note that volume budgets are not allocated on the mission level, as the volume available is more than five times greater than the volume occupied by the mission hardware. Moreover, it is not the volume that drives the designs, but the packaging requirements which is not straightforward to allocate and is done in subsequent design phases. Firstly, the cost budget is presented in Table 2.12. The cost positions for the systems that are part of the space segment are propagated from lower-level analysis and include development and production cost. Operations costs are assigned to the CCC and MIO segments, and are attained using statistical methods.

Table 2.12: The mission-level cost budget of the LOVE mission.

Segment	**Cost [FY2022 €K]**
SCB	192088.99
EDV	78206.94
REL	20006.80
TRV	48907.95
Operations (MIO & CCC)	24260.53
Launch Vehicle	63650.00
Total	**523803.72**
Margin	**20%**
Total with Margin	**628564.46**
Requirement	**630000**
Compliant with Reqs.	**YES**

Table 2.13: The mission-level reliability budget of the LOVE mission.

Segment	**Mission Achieved [1]**
PLD	0.9914
SCB	0.9607
EDV	0.9767
REL	0.9739
TRV	0.995
Launch Vehicle	0.999
Total	**0.901**
Requirement	**0.900**
Compliant with Reqs.	**YES**

It is important to note that the cost exceeds the initial estimate, which is in line with cost estimations made in [49] and with heritage missions. In consultation with the customer, the mission cost constraint is therefore relaxed. Next up, the reliability budget is presented in Table 2.13, assuming 99.9% reliability for the LAV.

The results are derived in Section 2.7. It can be seen that the largest portion of the reliability budget is afforded to the SCB since it is the least well-understood system within the mission. Next up, the mass budget of the mission is shown in Table 2.14.

Table 2.14: The mission-level total mass budget of the LOVE mission.

Segment	Mass [kg]
PLD	41.56
SCB	399.43
EDV	528.38
REL	149.02
TRV	217.27
Total	**1335.67**
Margin	**20%**
Total with Margin	**1602.81**
Requirement	**4020**
Compliant with Reqs.	**YES**

Table 2.15: The mission-level 3σ position and velocity uncertainty with respect to Venus.

Segment	3D Position [m]	Velocity[m/s]
SCB	82725.70	1.047
REL	18900	0.00105
Total	**101625.70**	**1.04805**
Margin	**5%**	**5%**
Total with Margin	**105623.83**	**1.1**
Requirement	**105623.83**	**1.1**
Compliant with Reqs.	**YES**	**YES**

As the table shows, the mission under-utilises the available mass budget given by the launch vehicle significantly. However, since the chosen launch vehicle is more cost-effective than smaller launchers, this result does not prompt a reconsideration of launcher choice. Comparing to reference missions, the results agree with similar mission concepts and past entry vehicles [49]. The next and last budget to be considered is the uncertainty budget for position and velocity of the PLD position. This is done on a mission level, since the relay position must be known in order for it to provide ranging to the SCB (cf. Figure 2.5. The budget for the REL are based on worst-case values found in [23], with a margin of 5% applied. The overall requirement is derived from MIS-REQ-2.16 and 2.17.

The position and velocity of the REL can be determined to a very exact degree, of which the chosen ground stations are a part of, leaving very high margins for the SCB. This is required in order to allow for dead reckoning to be used for position and velocity determination. It is important to note that this only applies to the horizontal position of the SCB, as the vertical position is acquired through other measures.

3
Payload

The payload (PLD) carried on-board the LOVE mission directly functions to fulfill the scientific purpose of this mission. It tackles two main scientific goals set by the mission; ”Higher Atmosphere Sensing” and ”Life Sensing”.

This chapter presents a clear overview of the constituents of the PLD and its main functions relating to the overall mission in Section 3.1. Following that, the PLD requirements are defined and presented in Section 3.3. Section 3.4 provides the final instrument selection. The different mass, volume and cost budgets for the current estimate are then categorised in Section 3.5 before lastly tackling the risk and reliability analysis of the PLD constituents in Section 3.6.

3.1. Payload Functional and Architecture Analysis

The PLD aims to fulfill the actual scientific need determined by the purpose of the mission and thus has several functions to carry out. These functions are provided in Subsection 3.1.1 are used to determine the type and

number of instruments, summarised in Subsection 3.1.2.

3.1.1. Payload Functional Allocation

From a mission level overview of functions, as showed in Section 2.2, the PLD can be specifically linked to that of performing the scientific investigation (F6). This is further elaborated as performing scientific measurements on the subject, Venus (F6.4) and storing the observed data (F6.5) while housed in the SCB.

3.1.2. Payload System Architecture

The functions of the PLD presented in Figure 3.1 are fulfilled by the instruments chosen and discussed further down in Section 3.4.

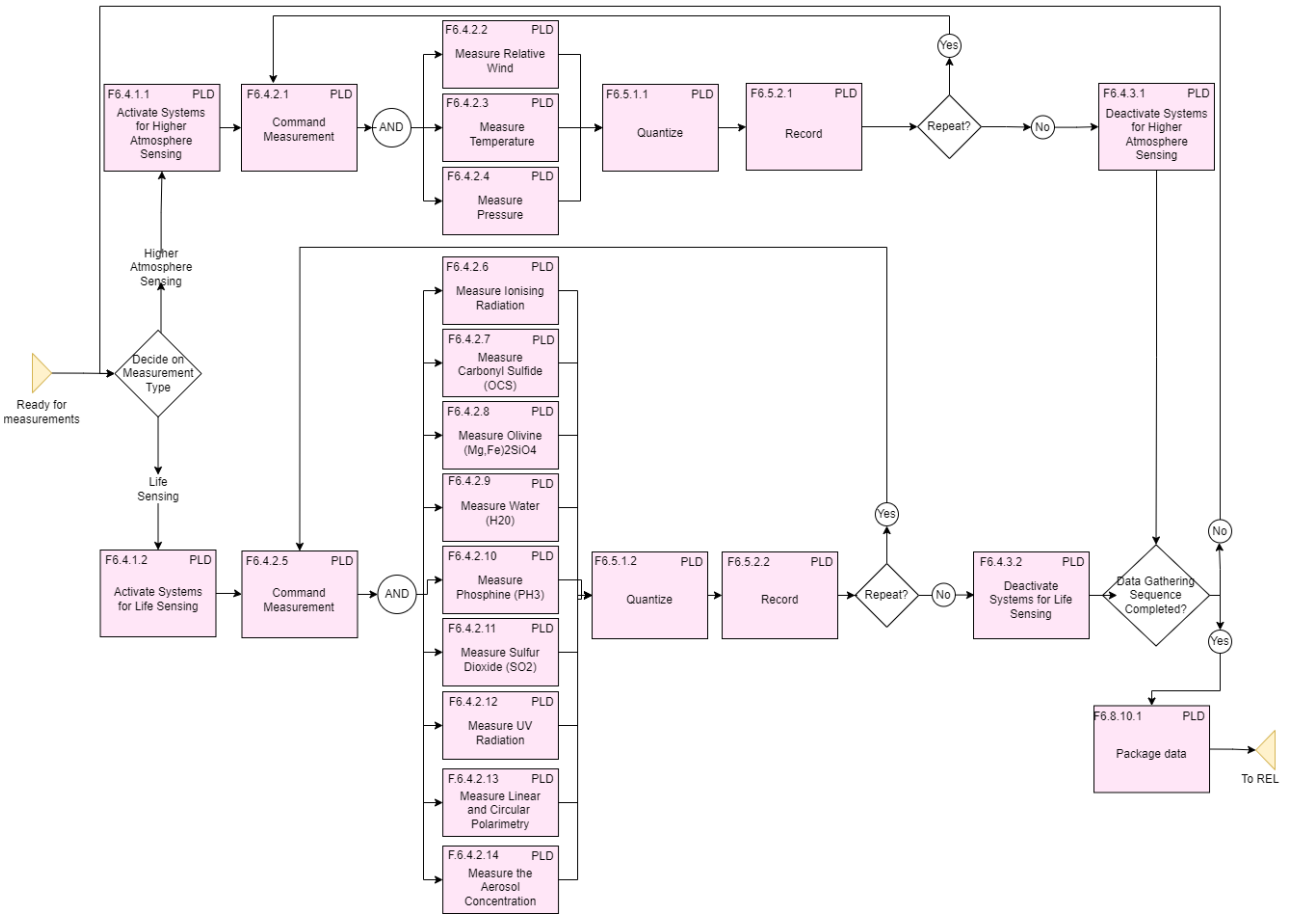

Figure 3.1: The PLD functional flow diagram.

3.2. Payload Measurement Strategy

In order to fulfil the key mission requirements outlined in Section 2.3, a measurement strategy must be devised. This is roughly split into two classes of measurements: Firstly, regular measurements of general environment properties such as temperature and pressure. Secondly, measurement of chemicals, polarization and aerosols occurring every four hours on average.

For wind, temperature, pressure and solar radiation, measurements are taken every 8.6 s to comply with the horizontal spatial resolution requirements of <1 km. For all other measurements, measurements are taken on the down stroke of the path (cf. Subsection 2.4.1 every 2088.3 s, resulting in a set of 12 data sets taken. The measurements done for these data sets are to be taken within 0.1 s of each other. This is done for each measurement cycle, satisfying the requirement related to measurement frequency while also providing an altitude profile of all measurements, adding to the scientific value.

3.3. Payload Requirements Definition

Before selecting the instruments for the PLD, their requirements are flowed down from those defined for the mission. A total of 34 functional requirements for phase F6 are defined, which are elaborated upon under Subsection 3.3.1. Furthermore, a total of 13 non-functional requirements are directly flowed down from the mission requirements, which are discussed in Subsection 3.3.2. Lastly, both non-functional and functional interface requirements are defined, which together come to a total of 12, which is shown in Subsection 3.3.3.

3.3.1. PLD Functional Requirements Phase F6

The PLD functional requirements are largely flown down from phase F6, which represents 'Perform Scientific Investigation'. Furthermore, the F6 functional requirements can be further split up into requirements pertaining to the different scientific stakeholder requirements: investigating the presence of biomarkers (PSC-REQ-1), investigation of habitability (PSC-REQ-2), disproving other sources than microbial life as dominant biomarker producers (PSC-REQ-3) and higher atmospheric investigation (PSC-REQ-5). Various key requirements are identified and are shown in Table 3.1.

Table 3.1: The key PLD system functional requirements.

ID	Description	Rationale
PLD-REQ-2.3	The PLD shall be able to measure atmospheric temperature with an accuracy of at least 1 K in the upper atmosphere.	Directly flown down from top-level mission requirement for atmospheric profiling.
PLD-REQ-2.4	The PLD shall be able to measure atmospheric pressure with an accuracy of at least 1 $mbar$ in the upper atmosphere.	Directly flown down from top-level mission requirement for atmospheric profiling.
PLD-REQ-2.9	The PLD shall be able to measure zonal (East-West) wind speed magnitudes with an accuracy of at least 1 m/s in the upper atmosphere.	Directly flown down from top-level mission requirement for atmospheric profiling.
PLD-REQ-3.2	The PLD shall measure the concentration levels of phosphine with an accuracy of at least 1 ppb.	Directly flown down from top-level mission requirement for biomarker investigations.
PLD-REQ-3.4	The PLD shall measure the concentration levels of ammonia with an accuracy of at least 1 ppm.	Directly flown down from top-level mission requirement for biomarker investigations.
PLD-REQ-3.6	The PLD shall measure the concentration levels of carbonyl sulfide with an accuracy of at least 1 $ppmv$.	Directly flown down from top-level mission requirement for biomarker investigations.
PLD-REQ-3.7	The PLD shall be able to detect circular polarization with an accuracy of at least 10^{-4} $C \cdot m^{-2}$.	Directly flown down from top-level mission requirement for biomarker investigations.
PLD-REQ-4.2	The PLD shall measure the concentration levels of sulfur dioxide with an accuracy of at least 10 ppb.	Directly flown down from top-level mission requirement for habitability investigations.
PLD-REQ-4.4	The PLD shall measure the concentration levels of water with an accuracy of at least 10 ppm.	Directly flown down from top-level mission requirement for habitability investigations.
PLD-REQ-4.6	The PLD shall measure ultraviolet irradiance with an accuracy of at least $1 * 10^{-7}$ $UV : PAR$.	Directly flown down from top-level mission requirement for habitability investigations.
PLD-REQ-4.8	The PLD shall measure the radiation incidence on Venus with an accuracy of at least 0.01 Gy.	Directly flown down from top-level mission requirement for habitability investigations.

Table 3.1: The key PLD system functional requirements.

ID	Description	Rationale
PLD-REQ-4.9	The PLD shall measure the presence of aerosols with an accuracy of at least 150 nm.	Directly flown down from top-level mission requirement for habitability investigations.
PLD-REQ-5.1	The PLD shall detect natural olivine with a minimum particle volume of at least 0.1 mm^3	Directly flown down from top-level mission requirement for investigations around different biomarker producers.

3.3.2. PLD Non-Functional Requirements from Direct Flow-Down

The non-functional requirements are largely flown down directly from the mission requirements. They pertain to the areas of: Cost, debris mitigation, planetary protection, sustainability, production and assembly, national and international standards and launch vehicle compatibility. The key non-functional requirements only include the cost requirement as is shown in Table 3.2.

Table 3.2: The key PLD system non-functional requirements.

ID	Description	Rationale
PLD-REQ-8.1	The PLD cost shall not exceed 96 $M€$.	Derived from PLD cost budget with 20% margin.

3.3.3. PLD Interface Requirements

Lastly, both non-functional and functional interface requirements are defined. These are not flown down from the mission requirements, but pertained to the areas of: Mass, power, volume, data, communication and its mechanical environment. The key requirements of this category are shown in Table 3.3.

Table 3.3: The key PLD system interface requirements.

ID	Description	Rationale
PLD-REQ-0.1	The mass of the PLD shall not exceed 49.87 kg.	Derived from PLD mass budget with 20% margin.
PLD-REQ-0.2	The maximum electrical power draw of the PLD shall not exceed 97.88 W.	Derived from PLD power budget with 10% margin.
PLD-REQ-0.4	The overall volume taken up by PLD shall not exceed 0.17 m^3.	Derived from PLD volume budget with 20% margin.
PLD-REQ-0.6	The PLD shall deliver data to SCB at rates no faster than 391.60 Mb/s.	Derived from PLD data budget with 100% margin.

3.4. Payload Instrument Selection and Configuration

A total of six instruments are ultimately selected to be taken on-board the SCB of the LOVE mission as the scientific payload. These are chosen according to the requirements defined for the PLD, as is described in Section 3.3. Each instrument is discussed individually below:

- **Radiation Assessment Detector (RAD):** measures ionising radiation [15].
- **Tunable Laser Spectrometer (TLS):** measures chemical markers: phosphine, ammonia, carbonyl sulfide, sulfur dioxide, water, carbon monoxide and carbon dioxide [49].
- **Rover Environmental Monitoring Station (REMS):** measures atmospheric properties: pressure, temperature, humidity, wind and UV radiation [30].

- **Venus Spectrometer (VenSpec):** performs mineralogy and measures chemical markers: water, carbonyl sulfide, sulfur dioxide, phosphine, ammonia, semi-heavy water and sulfur monoxide [26].
- **Nephelometer:** measures the composition of aerosols [68].
- **Life Signature Detection Polarimeter (LSDpol):** measures linear and circular polarisation.

3.5. Payload Technical Budgets

The PLD mass, volume, power, data and cost budgets are shown respectively in Tables 3.4, 3.6, 3.7, 3.8 and 3.5. Some of the estimates are made from SMAD[42]. It is to be noted that with and without the margin, the requirements are complied with.

Table 3.4: The PLD mass budget.

Subsystem	Component	Mass [kg]
PLD	RAD	1.5
	TLS	4.5
	REMS	2
	VenSpec	31.36
	Nephelometer (Pioneer)	1.2
	LSDpol	1
Total		**41.56**
Margin		**20%**
Total with margin		**49.872**
Requirement		**50**
Compliant with requirement		**Yes**

Table 3.5: The PLD cost budget.

Subsystem	Component	Cost [FY2022 M€]
PLD	RAD	10
	TLS	10
	REMS	10
	VenSpec	30
	Nephelometer (Pioneer)	10
	LSDpol	10
Total cost		**80**
Margin		**20%**
Total data generated with margin		**96**
Requirement		**96**
Compliant with requirement		**YES**

Table 3.6: The PLD volume budget.

Subsystem	Component	Dimensions [cm]	Volume [cm3]
PLD	RAD	10.3 x 12.2 x 20.4	2563.464
	TLS	26 x 10 x 10	2600.000
	REMS boom	15.108 x 5.616 x 9.377	795.6051
	REMS UVS	5.521 x 6.818 x 1.904	71.670
	REMS ICU	12.009 x 12.000 x 7.968	1148.252
	VenSpec M	59.0 × 21.5 × 20.4	25877.400
	VenSpec H	65.5 x 46.3 x 27.5	83397.875
	VenSpec U	50.0 x 20.0 x 20.0	20000.000
	Nephelometer ESS	3.9 x 7.3 x 12.6	358.722
	Nephelometer OSS	7.8 x 8.7 x 10.9	739.674
	LSDpol	40 x 5	3141.593
Total volume			**140694.257**
Margin			**20%**
Total volume with margin			**168833.110**
Requirement			**170000.000**
Compliant with requirement			**YES**

Table 3.7: The PLD power budget.

Subsystem	Component	Peak Power [W]	Duty Cycle [-]	Energy per 24 hours [Wh]
PLD	RAD	4.2	0.004067460317	0.41
	TLS	26.1	0.004070881226	2.550
	REMS	10.08	1	241.92
	VENSPEC	45.2	0.004065265487	4.410
	Nephelometer	2.4	0.0040625	0.234
	LSDpol	1	0.004083333333	0.098
Total power				**88.980**
Margin				**20%**
Total power with margin				**106.776**
Requirement				**110.000**
Compliant with requirement				**YES**

Table 3.8: The PLD data budget.

Subsystem	Component	Peak Data Generation [kb/s]	Data Generation per 24 hours [kb]
PLD	RAD	500	500
	TLS	752.3148148	752.3148148
	REMS	2031.636011	2031.25
	VenSpec	371.332405	371.332405
	Nephelometer (Pioneer)	144	144
	LSDpol	192000	18800
Total peak data generation [kb/s]			**195799.2832**
Margin			**100%**
Total data generated with margin [kb/s]			**391598.5665**
Requirement [kb/s]			**391600**
Compliant with requirement			**YES**

3.6. Payload Reliability and Risk

The reliability and risk analysis of the PLD takes the approach of considering the importance of a measurement, potential redundancies and various risks that affect the range of internal instrument reliability. In this case, many risks and their respective mitigation and contingency plans are already presented in the previous report [2]. At that stage, the risk analysis has remained to be qualitative. Currently, those strategies have been implemented in a qualitative form to provide a quantitative analysis of the PLD reliability, which is documented in Subsection 3.6.1

3.6.1. Payload Reliability and Availability Analysis

Table 3.9 shows the final reliability values for the instruments selected for the PLD subsystem. Depending on the number and type of instruments as specified in Section 3.4, the overlaps in what these instruments measure and how many requirements they are able to satisfy as from Section 3.3 determine the reliability allocated to the aforementioned instruments. As an example, the TLS and VenSpec have some overlap in the chemical markers they are supposed to measure. This proves to be a form of redundancy. So, considering the high importance of the measurement of these chemical markers (which demands high reliability), given that there is some form of redundancy, the reliability of measurement of these chemical markers go up. This flows back into the instrument reliability which is quantitatively reflected here.

Table 3.9: The final PLD reliability values.

Instrument	Reliability [-]
RAD	0.950
TLS	0.975
REMS	0.975
VenSpec	0.975
Nephelometer (Pioneer)	0.950
LSDpol	0.950
TOTAL	**0.991**

Table 3.10: The PLD technical risk.

Technical Risk Results		
Failure Classes	**(-)**	**(%)**
Due to minor anomalies/degradations	0.007720475687	0.7720475687
Due to major anomalies/degradations	0.1707106903	17.07106903
Due to total failures	0.009796991003	0.9796991003
Total Mission Loss	**0.188228157**	**18.8228157**
Total Mission Achieved	**0.811771843**	**81.1771843**

4
Spacecraft Bus

This chapter presents the detailed design of the spacecraft bus (SCB) of the LOVE mission. Its starting point is a conceptual design of a pumped gas balloon consisting of a zero pressure balloon, which contains a smaller super pressure balloon [2]. It allows for altitude control by either pumping gas from the zero pressure into the super pressure balloon to decrease buoyancy and go down, or by venting gas in the other direction to go upwards. The ratio between the radii of the super pressure and zero pressure balloon is taken from literature and set at 1:2 [46]. Furthermore, the maximum altitude of 62 km dictates the size of the zero pressure balloon and the minimum altitude of 50 km dictates the required amount of the to-be selected gas.

Before going into the detailed design, Section 4.1 presents the SCB functional and architecture analysis, secondly Section 4.2 presents the SCB requirements definition and Section 4.3 goes into its performance analysis. After that, Section 4.4 goes into a more high-level design overview of the spacecraft bus, Section 4.5 presents its technical budgets and Section 4.6 goes into the reliability and risk associated with the SCB mission segment. From Section 4.7 onwards, each section goes into the detailed design of the individual subsystems of the SCB, starting with the Transmission and Command (TNC). Section 4.8 goes into the Onboard Data Handling (OBD), Section 4.9 discusses the lifting system (LFT), Section 4.10 is dedicated to the Position and Attitude Control (PAC), Section 4.11 presents the Location and Attitude Determination (LAD), Section 4.12 shows the decisions made on the Electrical Power System (EPS), Section 4.13 goes into the SCB Mechanisms (MEC), second to last Section 4.14 discusses the structure (STR) and lastly, the thermal management (THE) is presented in Section 4.15.

4.1. Spacecraft Bus Functional and Architecture Analysis

The SCB has several functions it needs to fulfill to complete the mission. These functions are used to determine the components that are needed in the SCB and what function they have. This leads to the total architecture of the system, which is summarised in Subsection 4.1.2. The relations between the subsystems are then summarised in an N2 chart in Subsection 4.1.3.

4.1.1. Spacecraft Bus Functional Allocation

In Section 2.2 the functions of the LOVE mission are presented. A number of these are specifically for the SCB. The SCB first becomes functional in the sixth phase of the mission which is performing the scientific investigation (F6). In the final phase of the mission, discarding of all mission constituents (F7), the SCB also has functions to fulfill.

The first function is to deploy its systems (F6.1), this includes the antenna, solar panels and payload. The SCB also needs to perform the initial positioning (F6.2), this entails achieving the correct latitude, longitude, altitude and attitude. Following this, the SCB has to position itself to be able to perform the measurements (F6.3). Once these measurements have been performed, this data needs to be stored (F6.5), which includes processing the data and packaging it. The SCB also needs to support the payload operations (F6.6), by providing electrical power, supporting the structure and providing thermal control. The final function of the SCB in this phase is communicating between the SCB and the REL (F6.8).

The next phase is to discard of all mission constituents. First, the SCB needs to maintain the SCB systems (F7.3) by providing electrical power, supporting the structure, and providing thermal control. This needs to be done when the mission is extended. The final function of the SCB is to decommission the SCB (F7.5), this is done by reducing the lift until the SCB burns up in the atmosphere.

4.1.2. Spacecraft Bus System Architecture

A block diagram demonstrating the SCB system architecture can be seen in Figure 4.1. From this, one can assign functions of the SCB to the different subsystems, provided as follows:

1. Transmission and Command (F6.8) in Section 4.7
2. Onboard Data Handling (F6.5) in Section 4.8
3. Lifting System (F6.2 & F6.3) in Section 4.9
4. Position and Attitude Control (F6.2 & F6.3) in Section 4.10
5. Location and Attitude Determination (F6.2 & F6.3) in Section 4.11
6. Electrical Power System (F6.6 & F7.3) in Section 4.12
7. Mechanisms (F6.1) in Section 4.13
8. Structure (F6.6 & F7.3) in Section 4.14
9. Thermal Management (F6.6 & F7.3) in Section 4.15

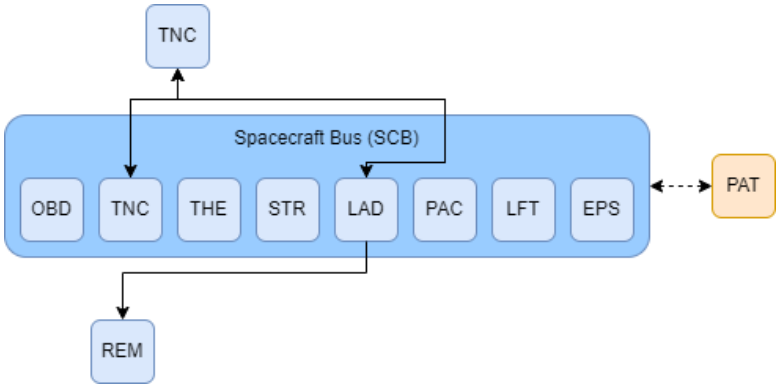

Figure 4.1: The SCB system architecture.

4.1.3. Spacecraft Bus System N2 Chart

The N2 chart of the SCB is presented in Table 4.1. This table shows all the outputs of the subsystems in its rows and the columns represent the inputs for the subsystem. This chart is used to get an overview of the subsystems of the SCB and how they are related.

Table 4.1: The N2 chart of the SCB.

SCB-OBD	Commands to SCB, Data from SCB, Housekeeping data	Commanding of temperature control		Required position, Required attitude			Required power	
Housekeeping data	SCB-TNC			Updated location			Required power	(Pointing of antenna)
Housekeeping data		SCB-THE					Required power	
			SCB-STR					
Housekeeping data		Relative position to the sun, Altitude		SCB-LAD	Position, Attitude		Required power	
Housekeeping data, position and attitude					SCB-PAC	Lift commands	Required power	
Housekeeping data						SCB-LFT	Required power	
Power, Housekeeping data	Power	Power		Power	Power	Power	SCB-EPS	Power
							Required power	SCB-MEC

4.2. Spacecraft Bus Requirements Definition

Before designing the SCB, the requirements are flowed down from those defined for the mission. A total of 14 functional requirements for phase F6 are defined, which are elaborated upon under Subsection 4.2.1. A total of 5 functional requirements for phase F7 are defined, which are elaborated upon under Subsection 4.2.2. Furthermore, a total of 14 non-functional requirements are directly flowed down from the mission requirements,

which are discussed in Subsection 4.2.3. Lastly, both non-functional and functional interface requirements are defined, which together came to a total of 6, as shown in Subsection 4.2.4.

4.2.1. SCB Functional Requirements Phase F6

These SCB functional requirements are flown down from phase F6, which represents 'Perform Scientific Investigation'. Some key requirements are identified and are shown in Table 4.2.

Table 4.2: The key SCB system functional requirements F6.

ID	Description	Rationale
SCB-REQ-4.1	The SCB shall deploy the PLD.	Derived from F6.1.3.
SCB-REQ-4.3	The SCB shall have a starting vertical attitude of 0° with a maximum deviation of 5°.	Derived from F6.2.4, dictates the SCB to be perfectly pointing down for the VenSpec measurements. Originally there was a need for a specific East-West attitude, but that's no longer needed due to the eggshell antennas.
SCB-REQ-4.7	The SCB shall command the PLD to turn on the scientific instruments.	Derived from F6.4.1.
SCB-REQ-4.8	The SCB shall collect scientific data as dictated by the scientific requirements.	Derived from F6.4.2.
SCB-REQ-4.14	The SCB shall maintain structural integrity.	Derived from F6.6.3.

4.2.2. SCB Functional Requirements Phase F7

These SCB functional requirements are flown down from phase F7, which represents 'Discard of all mission constituents'. Various key requirements are identified and are shown in Table 4.3.

Table 4.3: The key SCB system functional requirements F7.

ID	Description	Rationale
SCB-REQ-5.1	The SCB shall receive the command to decommissioning from the REL.	Derived from F7.8.
SCB-REQ-5.2	The SCB shall execute the command to decommission.	Derived from F7.8.
SCB-REQ-5.4	The SCB shall transmit the end of health tone to the REL.	Derived from F7.9.

4.2.3. SCB Non-Functional Requirements from Direct Flow-Down

The non-functional requirements are largely flown down directly from the mission requirements. They pertain to the areas of: cost, debris mitigation, planetary protection, sustainability, production and assembly, national and international standards and launch vehicle compatibility. The key non-functional requirements only include the cost requirement, as is shown in Table 4.4.

Table 4.4: The key SCB system non-functional requirements.

ID	Description	Rationale
SCB-REQ-6.1	The SCB cost shall not exceed 192 $M€$.	Based on the mission cost budget.
SCB-REQ-6.12	The SCB to be selected shall be existing or foreseeable.	Based on the mission timeline.
SCB-REQ-6.14	The SCB shall be ready for launch in 2031	Segment needs to be ready for launch in time.

4.2.4. SCB Interface Requirements

Lastly, both non-functional and functional interface requirements are defined. These are not flown down from the mission requirements, but pertain to the areas of: mass, power, volume, data, communication and its me-

chanical environment. The key requirements of this category are shown in Table 4.5.

Table 4.5: The key SCB system interface functional and non-functional requirements.

ID	Description	Rationale
SCB-REQ-7.7	The SCB shall withstand the Venusian atmosphere for 200 terrestrial days.	Derived from the mission duration.
SCB-REQ-8.1	The SCB shall receive commands from REL.	Derived from the REL communication part of F6.

4.3. Spacecraft Bus Performance Analysis

In this section the performance of the SCB is discussed. The performance is defined as the ability to control the SCB and follow the path specified in PAT. First, the deployment of the SCB from the entry and descent vehicle (EDV) is described in Subsection 4.3.1. Next, the general performance of the SCB during nominal operations is discussed in Subsection 4.3.2 and Subsection 4.3.3. The first of these sections describes how the SCB performs in terms of altitude, and the latter describes the ground track performance, including drifting from the equator.

4.3.1. Spacecraft Bus Entry and Deployment Analysis

The deployment sequence has been carefully designed to ensure that the SCB ends up at the correct altitude, without ever exceeding the lower altitude limit of 50 km. The largest part of the entry and deployment sequence is discussed in Chapter 5, since the EDV handles the majority of the deployment steps. This chapter analyses all the steps that the SCB specifically has to perform and gives an overview of the altitudes, velocities and forces.

Timeline

At t = 0 s the vehicle hits the upper part of the Venusian atmosphere at 11.37 km/s. After experiencing a period of high g loads with a peak of 35 g, the vehicle reaches the transonic regime and deploys respectively the drogue at t = 195 s and then the main parachute at t = 212 s as shown in figure 4.2. During this period the SCB is operational and communicates with the EDV to ensure all instruments are performing nominally. At t = 222 s the heatshield is dropped, exposing the SCB to the Venusian atmosphere for the first time. Five seconds later the EDV starts lowering the SCB using three ropes, and the balloon unfolds. This takes 60 s and from this point onwards, the deployment tasks shift largely to the SCB.

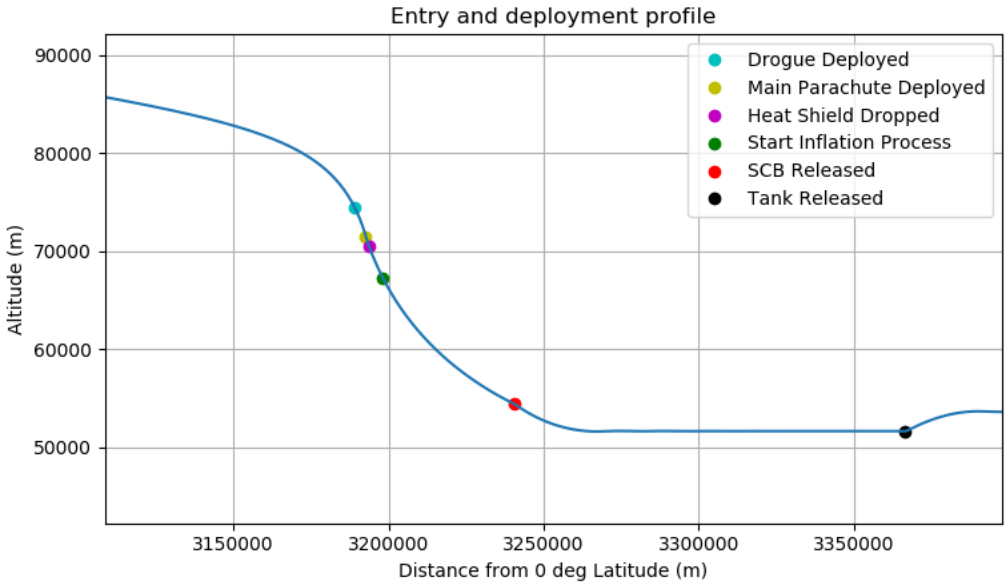

Figure 4.2: The profile over the entry with the position of key steps labeled.

As soon as the balloon has fully unfolded, which occurs at t = 287 s, its inflation process begins. First the ropes that are used to lower the SCB are detached using pyrotechnics, and a structural element running through the

balloon starts taking the loads. Secondly the valve to the hydrogen tank opens and starts filling the super pressure balloon. This balloon is filled first, due to it being able to handle a pressure difference with the environment of 8400 Pa. After it has been filled to the required pressure using the pressure sensors in the balloon module, the hydrogen is directed to the zero-pressure balloon. The hydrogen tank now empties itself until its pressure becomes too low to support the mass flow, after which the valve is closed. At t = 895 s and at an altitude of 54.44 km, determined by the pressure sensor in the EDV, the EDV releases the balloon which then falls down and stabilises at an altitude of 51.65 km.

At this altitude the tank valve is disconnected from the balloon module and the structural tank elements connected to the SCB are released at the same time. This causes a load transfer to the ropes connecting the balloon module to the SCB. After dropping the tank, the SCB shoots upwards and returns to a stable condition at 53.65 km. Here the spools holding the ropes unwind, lowering the SCB to a distance of 12 m from the balloon module. Now it is able to deploy its antennas and the boom holding the REMS instrument. After regaining contact with the REL, it is able to start the operations phase.

Balloon Folding
The initial folding strategy of the balloon is done by pressure packing the material into a circular slab. From the CAD model it follows that the optimum diameter of the folded slab of balloon material is approximately 1.3 m and this packing method yields a pack density of approximately 800 kg/m^3 [44]. Hence the balloon can ultimately be packed into a slab which is only 20.1 mm thick. This result is validated by comparing the volume of the slab with the volume of the actual balloon material. The slab volume is approximately twice the volume of the balloon material, thus validating the possibility of packing it within the defined slab.

Verification and Validation
There are several altitudes in the deployment sequence of the balloon that can be used to verify that the model is valid. The initial gas distribution is used to specify the altitude that the SCB stabilises at while the tank is still attached. If the altitude at which the model determines it should drop the tank matches this specified value, then that part of the model is valid. The same can be done for the reverse of the gas distribution. In the time that the gas tank is dropped and the SCB reaches its new equilibrium altitude, there is no change in the gas distribution. Therefore the reverse of the gas distribution code can be used to determine what this equilibrium altitude must be. This validates the second half of the balloon deployment model.

4.3.2. Spacecraft Bus Altitude Profile Performance Analysis
The limits of the altitude that the SCB is designed for are no lower than 50 km and no higher than 62 km. A design margin of 0.5 km has been added to both of these altitudes. This is done to ensure that if there are problems with the PAC subsystem of the SCB, the SCB is not damaged, and also functions as a safety factor for the balloon sizing.

In this model, the SCB has a horizontal velocity equal to the average horizontal wind on Venus. The path specified is an equatorial path. The winds of Venus and their effect are explained in more detail in Subsection 4.3.3. For the altitude performance, vertical wind gusts of 3 m/s are considered to be the maximum gusts the SCB experiences.

In Figure 4.3 the controlled motion of the balloon over several periods is shown. This is the path that the balloon must follow during operations as specified in the requirements. These velocities are the velocities of the SCB in the radial direction of Venus. The required ascent speed is 3.5 m/s and the required descent speed is 0.5 m/s.

However, due to a problem with the control loop for the altitude pattern of the SCB, the SCB does not actually achieve these velocities constantly for the entire descent or ascent. The current control loop compares the current velocity to the target velocity and either gives the command to increase it's velocity, decrease it's velocity or change direction. The change in direction command is given when the SCB reaches the maximum or minimum altitude region. In Figure 4.3 the descent velocity is around 0.6 m/s on average and the ascent velocity is 2.78 m/s on average. The SCB should be able to reach the 3.5 m/s required ascent velocity. This is reached at the beginning of the ascent manoeuvre but the control loop model slows down the movement.

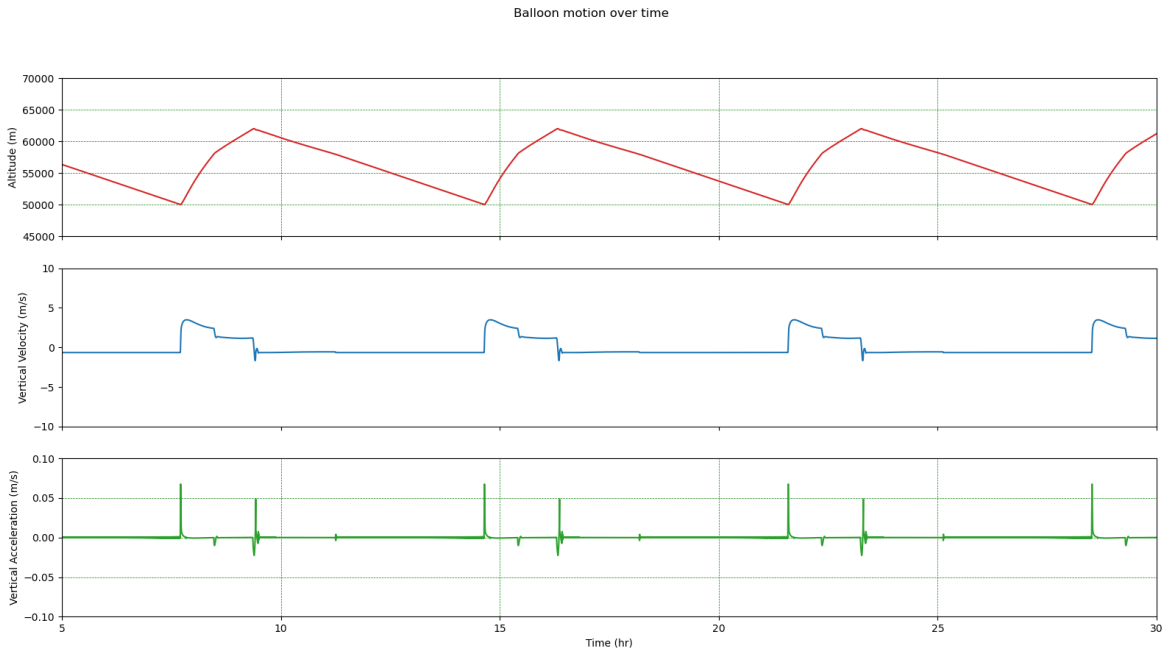

Figure 4.3: The motion of the balloon over time (hr) during operations.

At 58 km there is a small nod in the slope of the path. This was found to be due to an anomaly in the atmospheric model. 58 km was one of the altitudes that the altitude depending gradient of both the temperature and the pressure changes. This is especially visible during ascent of the SCB as the vent size stays the same but the volume of the balloon and thus the lift depends on the density of the atmosphere. This disrupts the motion of the SCB.

The altitude of the balloon can be validated by cross checking the gas distribution of the balloon system with the altitude. This is done by taking the altitude of the balloon at five random intervals per period, and using a simple calculation to determine the amount of gas that must be in the super pressure balloon at that time. Using this validation strategy, the model for the balloon motion has been validated.

4.3.3. Spacecraft Bus Ground Track Performance Analysis

According to mission requirement MIS-REQ-2.2, it is required for the mission to take its measurements within a latitude range of -5 to +5 °. Furthermore, measurements are to be taken over the ntire longitudinal range of Venus; 0-360 ° as dictated by mission requirement MIS-REQ-2.1. As previously discussed in Subsection 4.3.2, this results in a desired equatorial path for the SCB, where it oscillates and takes measurements in an altitude range of 50 to 62 km. Being a pumped hydrogen balloon, the SCB only has active control in the vertical direction, hence its movements in both the latitudinal as well as the longitudinal direction are completely dependent on the Venusian winds.

Venusian Wind Categorisation

The Venusian winds can be categorised in three categories: vertical, zonal and meridional winds. The vertical winds are mostly small random fluctuations in the order of a few meters per second as discussed in Subsection 4.3.2.

The zonal winds blow in an East to West direction, which is the same as the planetary rotation [88]. They are the largest in magnitude of all Venusian winds and thus the main driving force behind the SCB path around the planet. In the 50-62 km altitude range, the zonal wind magnitudes range from approximately 60-90 m/s at 0 ° latitude (as shown in Figure 4.4) and increase to approximately 70-100 m/s at 45 ° latitude on either side of the equator (as shown in Figure 4.5). The model used for the plots in Figures 4.4 and 4.5 is generated according to data from the Pioneer probes [43].

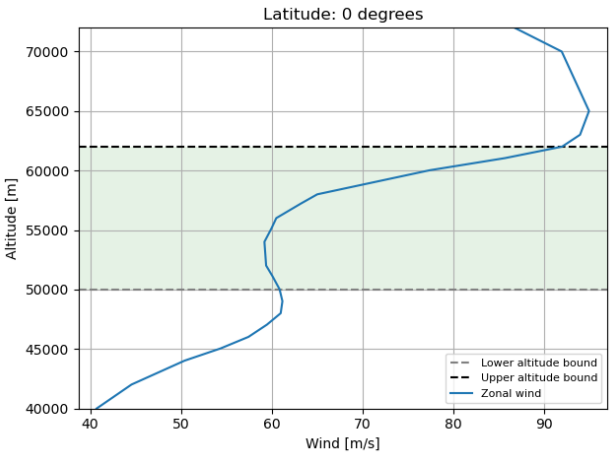

Figure 4.4: The zonal wind speeds at 0 ° latitude on Venus.

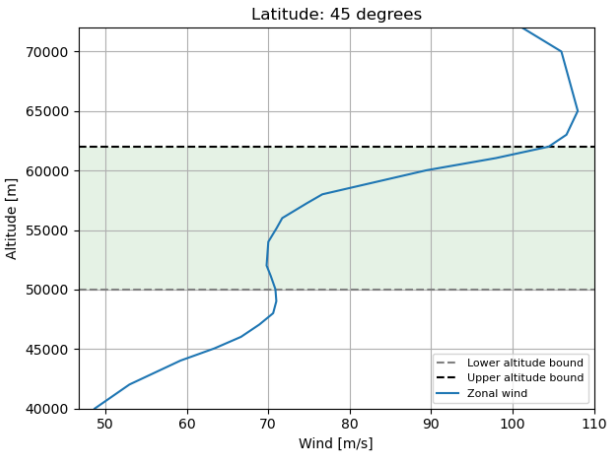

Figure 4.5: The zonal wind speeds at 45 ° latitude on Venus.

The meridional winds blow in the North to South as well as South to North direction. These winds are driven by the Hadley cell circulation present in the Venusian atmosphere, as shown schematically in Figure 4.6. The exact atmospheric dynamics and responsible mechanisms behind these Hadley cells are still only partially understood, but a rough model can be made which models their magnitude and direction on both the day- and nightside of Venus.

The meridional winds have been modelled according to data from the Pioneer probes [43] and are shown for 0 and 45 ° of latitude respectively in Figures 4.7 and 4.8. Here the negative values (which are within the red area for the altitude range) represent poleward winds, and positive values (which are within the green area for the altitude range) represent equatorward winds. This distinction cannot be made for exactly 0 ° latitude, hence Figure 4.7 represents meridional winds within ±1 ° of latitude. It can be seen in Figure 4.8 that the magnitudes of the meridional winds steeply increase as you move further from the equator. Furthermore the winds differ over the day- and nightside of Venus, effectively reversing itself.

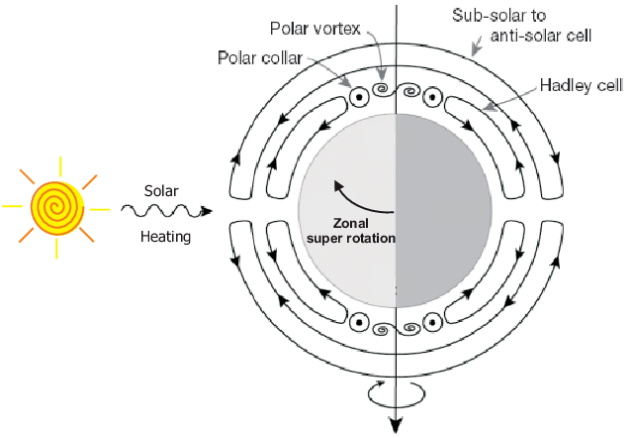

Figure 4.6: The Hadley cells within the Venusian atmosphere [66].

Both the zonal and meridional wind models are verified by comparing the plots with different sources of literature (e.g. [47, 56, 88]). It is apparent however, that the Pioneer probes are the only semi-extensive source of Venusian wind data. Hence it is expected that the models are rough in comparison to the actual Venusian winds.

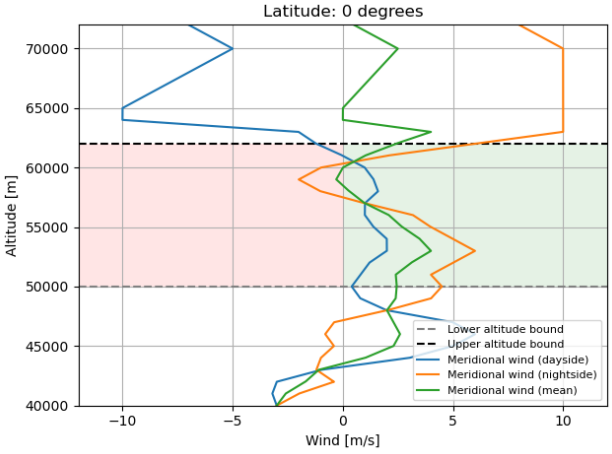

Figure 4.7: The meridional winds at 0 ° latitude.

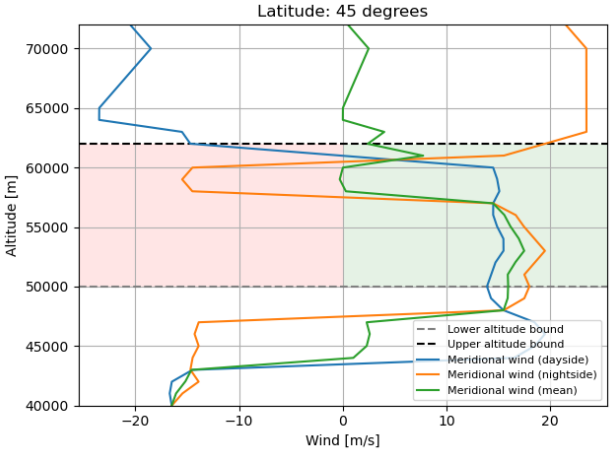

Figure 4.8: The meridional winds at 45 ° latitude.

Spacecraft Drifting

For modelling the actual SCB ground track due to the Venusian winds, two large assumptions are made:

1. The SCB always travels with the same velocities as the wind at its current position.
2. Within the models, 20-180 ° longitude assumes the dayside values, 200-360 ° longitude assumes the night side values and both 0-20 and 180-200 ° in longitude assumes mean values for the wind.

For the zonal winds this implies the SCB is consistently blown around the equator with velocities between 60 and 90 m/s. However, this also implies that the SCB might drift away from the equator due to the meridional winds. Using the wind model of Figures 4.4, 4.5, 4.7 and 4.8, a model is created which calculates the drifting in operations during a set amount of circumnavigations. This model is shown for approximately 1.1 orbits in Figure 4.9.

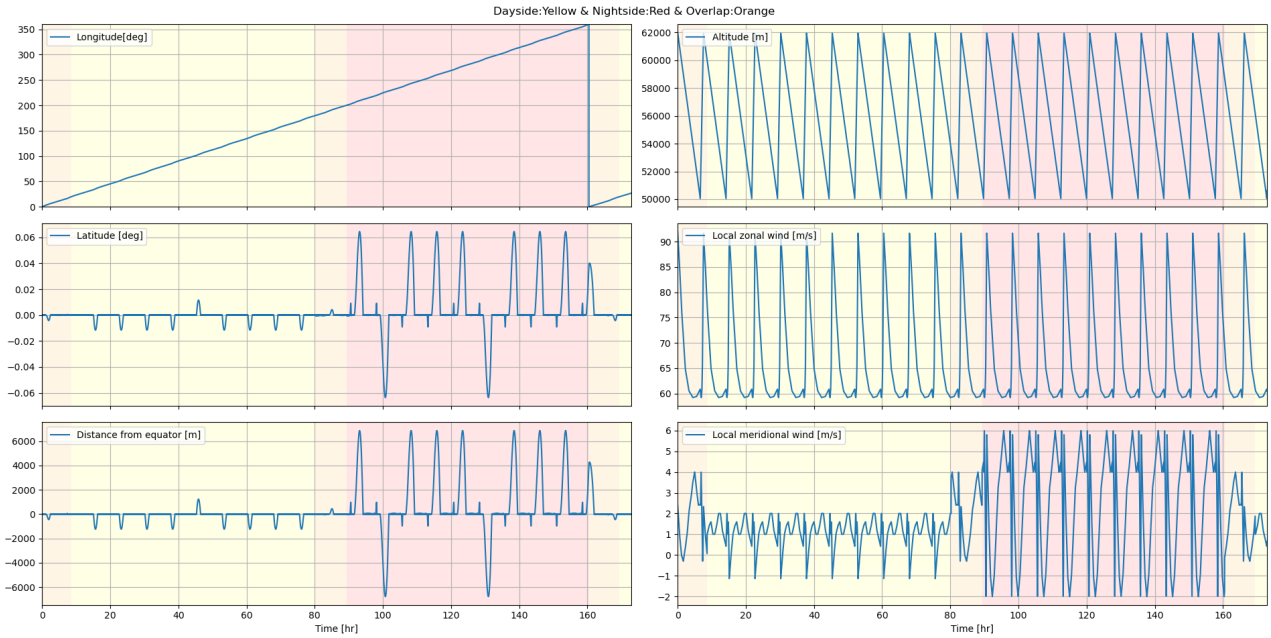

Figure 4.9: the modelled drifting during 1.1 orbit of operations (with starting conditions of 0 ° latitude, 0 ° longitude and 62 km altitude).

Figure 4.9 shows that the SCB indeed drifts from the equator repetitively, with magnitudes up to ±0.06 ° latitude or approximately 6 km from the equator. These fluctuations fit well within the requirements and as the SCB keeps travelling it automatically drifts back to the equatorial path. It can thus be concluded that, with the current available meridional wind data, drifting can be neglected.

However, as aforementioned, current meridional wind data is rough and likely to be inaccurate. Therefore, in case of unpredicted gusts of large magnitude, the driftback procedure is also simulated. This procedure can be performed in two manners: either the SCB keeps following its dictated path and relies on the modelled equatorward wind to drift it back, or the SCB goes to an altitude of 53 km and stays there until it once again reaches a latitude of 0 °. The reason why 53 km is the optimum altitude for driftback follows from the meridional wind model, as shown in Figures 4.7 and 4.8. It can be seen for both the day- and nightside that the equatorward wind with the largest magnitude is present at this altitude and that there is no known risk of getting caught in poleward winds.

Taking an assumed drift of 15 ° latitude with initial conditions of 0 ° longitude and a starting altitude of 62 km yields a driftback in approximately 140 hrs for following the defined path (as shown in Figure 4.10), and approximately 100 hrs for going to the optimum altitude (as shown in Figure 4.11). While the optimum altitude driftback is 1.4 times as fast as the path driftback, it does result in a loss of data, since measurements are not performed over the complete altitude range. Which of the two options, or a combination of both, is chosen for driftback is thus dependent on the exact conditions in which it is necessary.

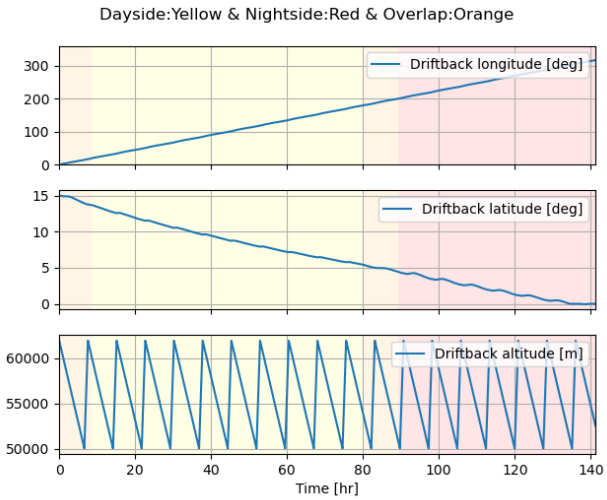

Figure 4.10: The driftback from 15 ° latitude whilst following the defined path.

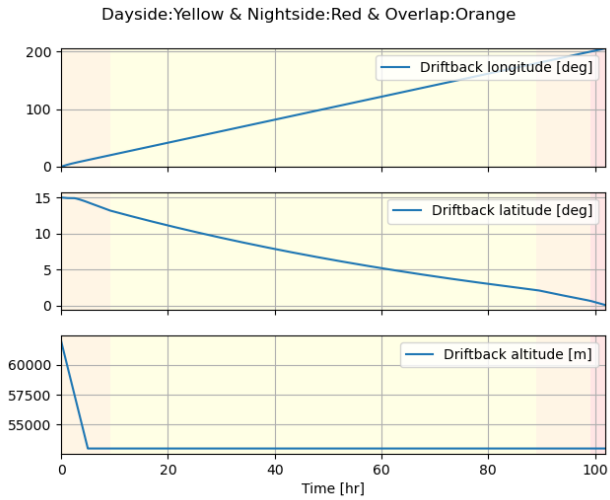

Figure 4.11: The driftback from 15 ° latitude whilst going to the optimum altitude of 53 km.

4.4. Spacecraft Bus Design Overview

In this section, a general overview of the SCB design is presented. A detailed description of the segments of this is given in the relevant sections. In Subsection 4.4.1 a description of the design is given. Following this section, the material and production characteristics of the SCB are discussed in Subsection 4.4.2.

4.4.1. Spacecraft Bus Design Description

As determined in the midterm report [2], the chosen SCB is a pumped gas balloon SCB. The gas chosen for this design is hydrogen. This concept entails that there is a gondola that is held up by a balloon system consisting of a super pressure balloon within a zero pressure balloon. The balloon module contains a pump and venting system, which is part of the SCB-PAC. This balloon module is described in more detail in Section 4.9 and Section 4.10. The total design of the SCB is shown in Figure 4.15

The gondola is a hexagonal structure with the payload and batteries attached to its sides. On the top part of this structure, there is space for the solar arrays and the antenna. The inside of the structure provides room for the spherical gas tank that is used to fill the balloon system during deployment. There is a release mechanism that releases the gas tank once there is no use for it anymore. The gondola also has one downward deployable boom, this is used to position a part of the payload that requires it to be placed at a distance from the SCB. The structure is shown in Figure 4.12 and Figure 4.13

The final part of the SCB design is the structure attached to the bottom of the balloon. This structure links the gondola to the balloon with 3 wires. This structure also contains the gas pump and the reserve gas tank. The structure is shown in Figure 4.14.

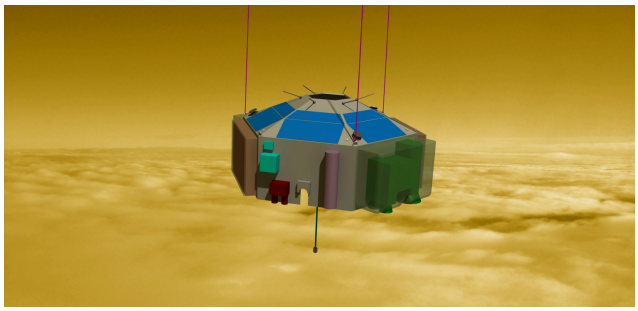

Figure 4.12: The SCB gondola design.

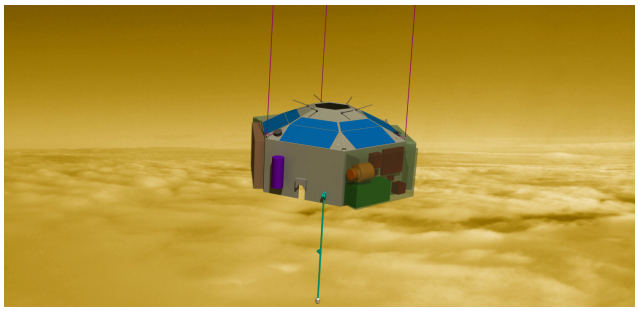

Figure 4.13: The SCB gondola design.

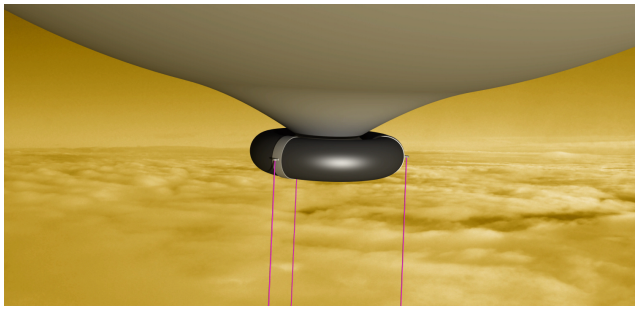

Figure 4.14: The design of the reserve tank.

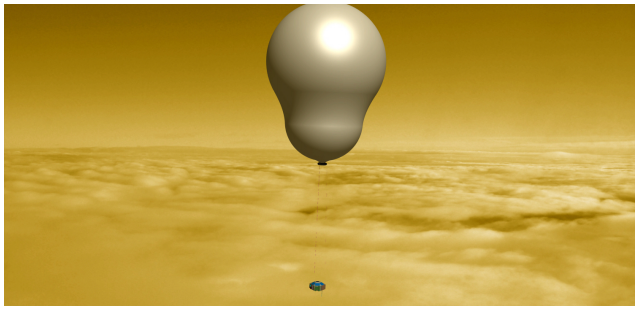

Figure 4.15: The full SCB design of the gondola and the balloon.

4.4.2. Spacecraft Bus Materials and Production Characteristics

In the following sections of this report, the detailed design of all of the components of the SCB is described. In these sections the material choice and if possible the production characteristics are described. This section aims to give an overview of the most important material choices and production characteristics.

The material selected for the super pressure balloon is Vectran Type NT, and the material selected for the zero pressure balloon is Kapton Type 250FN029. These two balloon components have different conditions and loads they need to withstand, therefore the material selection differs. The ropes connecting the balloon module to the gondola is also made of Vectran.

Another important material choice is the material to be used for both of the gas tanks. For this, gas tanks for space use from an external supplier are selected. The tanks are composite overwrapped pressure vessels with a polymer lining. These tanks are purchased from an external supplier, thus no production method needs to be considered.

Finally, the gondola structure is made of a sandwich structure composed of an aluminium honeycomb and aluminium face sheet. This is determined to be the lightest material that is suitable for the conditions that the structure needs to withstand.

4.5. Spacecraft Bus Technical Budgets

The resource allocation of a mission is an important aspect to track. In this section the budgets for the SCB are presented. In these budgets, margins are added. The results of these budget are summarised in the mission technical budgets.

4.5.1. SCB Mass Budget

The mass budget for the SCB is given in Table 4.6. In this table the mass of all subsystems and their components are given. The mass is summed up and a 20% design margin is added.

Table 4.6: The SCB mass budget.

Subsystem:	Component	Mass [kg]:
SCB-OBD	RAD750 6U	1.22
	Flash memory	-
SCB-TNC	LGA	0.60
	IRIS	0.88
	SSPA	0.13
	LNA	0.23
SCB-THE	Thermal covers	5.50
	Heat pipes	0.50
	Insulation	0.34
SCB-STR	Gondola	16.03
	Ropes	1.25
	Balloon module	7.00
SCB-LAD	LN200s	0.75

	6x Sun sensors	0.30
SCB-PAC	Pump system and valves	28.60
SCB-LFT	Zero-pressure balloon material	49.82
	Super-pressure balloon material	27.19
	Main tank hydrogen	14.63
	Reserve tank hydrogen	1.15
	Main tank structure	77.41
	Reserve tank structure	22.46
SCB-EPS	Batteries	66.95
	Solar panels	2.08
SCB-MEC	All mechanisms combined	1.00
PLD	RAD	1.50
	TLS	4.50
	REMS	2.00
	VenSpec	31.36
	Nephelometer	1.20
	LSDpol	1.00
Total		**367.56**
Margin		**20%**
Total with Margin		**441.07**
Requirement		**441.07**
Compliant with Reqs.		**YES**

4.5.2. SCB Volume Budget

The volume of all components of the SCB is given in Table 4.7. For each of the components of the SCB, the subsystem that it is part of is given. Also, the dimensions as well as the volume it takes up are given.

Table 4.7: The SCB volume budget.

Subsystem	**Component**	**Dimensions [cm]**	**Volume [cm^3]**
SCB-TNC	IRIS V2 Transponder	10.4 x 11.85 x 6.5	801.06
SCB-TNC	IRIS V2 SSPA	8.75 x 4.3 x 2.3	86.5375
SCB-TNC	IRIS V2 LNA	7.55 x 4.3 x 1.3	42.2045
SCB-EPS	Battery	144 * 9.3 x 8.6 x 4.1	47220.192
SCB-EPS	PCDU	6.30 x 6.30 x 6.30	250.047
SCB-EPS	Solar arrays	100 x 74 x 0.1	740
SCB-OBD	Single-board computer	23.3 x 22.0 x 3.0	1537.8
SCB-LAD	LN200s	8.89 x 8.89 x 8.51	672.563171
SCB-LAD	Coarse sun (6x)	2.0 x 1.0 x 0.57	1.14
SCB-OBD	W25N512GVxIG/IT	0.8 x 0.6 x 0.075	0.036
PLD	Total payload	-	137552.6641
TOTAL VOLUME			188904.2443
MARGIN			20%
TOTAL WITH MARGIN			226685.0932

4.5.3. SCB Power Budget

The power budget is provided in Table 4.8. It includes the maximum power consumption at peak power, as well as the average power consumption over a time period of 24 hrs.

Table 4.8: The power budget of the SCB.

Subsystem	Component	Peak Power [W]	Energy per 24 hours [Wh]
TNC	IRIS V2 Transponder	4.75	32.78
LAC	Hydrogen pump	57.35	1122
LAD	Sensors	12	288
OBD	W25N512GVxIG/IT Flash memory	0.09	2.16
PLD	RAD	4.2	0.41
	TLS	26.1	2.55
	REMS	10.08	241.92
	Venspec	45.2	4.41
	Nephelometer	2.4	0.234
	LSDpol	1	0.098
Total		163.17	1694.56
Margin		**20%**	**20%**
Total with Margin		179.49	1864.02
Requirement		179.49	1864.02
Compliant with Reqs		YES	YES

4.5.4. SCB Data Budget

Table 4.9: The data volumes per component, where the data volume refers to the average amount of data generated per 24 hours.

The data budget is given in Table 4.9. The data volume is provided for all relevant components of the SCB. The subsystem that the component is part of is also listed. All the housekeeping data is included as the Processor data budget, which is estimated from [13]. The data from instruments is obtained using the communications model.

Subsystem	Component	Data volume [kbit]
PLD	RAD	13
	TLS	53
	REMS	3716
	VenSpec	195675
	Nephelometer	6
	LSDpol	33022
SCB-OBD	Processor	2560
Total		**235045**
Margin		**50%**
Total with Margin		**352567.5**
Requirement		**352567.5**
Compliant with Reqs		**YES**

4.5.5. SCB 3σ Position and Velocity Uncertainty Relative to Venus

The position and velocity error propagated from the mission-level budget is shown below in Table 6.8. Note that the 3D uncertainty on mission level is propagated to latitudinal and longitudinal uncertainty, whereas the altitude uncertainty is treated separately as it does not rely on ranging, but uses barometric measurements instead.

Table 4.10: The SCB-level 3σ position and velocity uncertainty.

Segment	Latitude and Longitude Position [m]	Velocity[m/s]
SCB-LAD	60786.38	0.996
SCB-TNC	18000	0.001
Total	**78786.38**	**0.9961**
Margin	**5%**	**5%**
Total with Margin	**82725.7**	**1.046**
Requirement	**82725.7**	**1.047**
Compliant with Reqs.	**YES**	**YES**

As can be seen, most of the budget is allocated to the SCB-LAD, which determines the position of the SCB

if no ranging is available based on accelerometer data. This is a relatively inaccurate process, hence the large budget allocated to it. For the allocation of uncertainty to SCB-TNC, the same accuracy as for the REL position is assumed.

4.5.6. SCB Reliability Budget

An important resource for the mission is the reliability of all segments. The reliability of the SCB has been determined using the same method that is described in Section 2.7. The results for the reliability are presented in Table 4.11.

Table 4.11: The reliability budget of the SCB.

Subsystem	**Mission Achieved [1]**
LAD	0.9966
EPS	0.9960
LFT	0.9949
MEC	0.9999
OBD	0.9997
PAC	1
STR	0.9867
THE	0.9968
TNC	0.9894
Total	0.9599
Requirement	0.9599
Compliant with Reqs	YES

4.5.7. SCB Cost Estimation

Since the detailed design of the SCB does not specify all exact parts of the mission a statistical approach has to be used to produce a cost estimation at this stage. The chosen method for the SCB is the SMAD [42] cost estimation for spacecraft weighing less than 500 kg. This method gives cost estimating relations for the subsystems of the SCB based on the mass.

These values do not give an accurate cost estimation for our mission yet. SMAD[42] provides a number of factors that increase the cost of the SCB. In the table the average, minimum and maxim value of the factor that should be applied are given. Based on this, the appropriate values are determined and compiled, which leads to the conclusion that a margin of 149 % must be applied to the total cost.

Table 4.12: The SCB cost estimation per subsystem in FY2022 €K.

Subsystem	**Cost [FY2022 €K]**
Structure	7836.3
Thermal	2198.1
Attitude determination & control system	7676.5
Electrical power supply	52041.6
Propulsion (Gas tank)	16020.6
Telemetry, Tracking & Command	2398.0
Command and Data Handling	3115.6
Integration, Assembly & Test	25982.2
Program	42805.3
Total	**160074.16**
Margin	**20%**
Total with Margin	**192088.99**
Requirement	**192088.99**
Compliant:	**YES**

The next factor that must be taken into account in the cost estimation is the TRL. For the pumped helium concept, a TRL of 5 is given by JPL [33]. This implies that the cost must be multiplied by a factor 1.3 according to SMAD [42]. Finally, the cost must be converted to $FY2022Euros$. This is done by applying 22.37% inflation and

converting it from dollars to euros. This leads to the cost estimation given in Table 4.12. The total cost includes the program cost estimated for the SCB.

4.6. Spacecraft Reliability and Risk

In this section the reliability and the risks of the SCB are discussed. First the reliability for the SCB is analysed. In the following subsection the risk map for the SCB is presented together with the mitigation strategies applied.

4.6.1. Spacecraft Reliability Analysis

The total reliability of the SCB is presented in Table 4.13. This table shows an overview of the technical risks due to minor, major anomalies/ degradation's and total failure. These values are generated by the method described in Section 2.7.

Table 4.13: The technical risk of the SCB.

Technical Risk Results		
Failure Classes	(-)	(%)
Due to minor anomalies/degradations	0.0033	0.33
Due to major anomalies/degradations	0.024	2.4
Due to total failures	0.013	1.3
Total Mission Loss	0.040	4.0
Total Mission Achieved	0.96	96

4.6.2. Spacecraft Risk Map

The total mission reliability of the SCB is 95.99%. This is after mitigation has been applied, the reliability of the SCB before mitigation is 94.17%. In Figure 4.16 the risk map of the SCB is presented.

In the risk map, 1-3 represents the first three risks: tank release mechanism (1), boom deployment mechanism (2) and the lowering mechanism (3). For these 3 risks, the same mitigation strategy is applied. A redundant system is added to all of these mechanisms.

In the risk map 4-10 represents the final seven risks considered. These risks concern the gondola(4), balloon module (5), ropes of the gondola (6), ropes inside the balloon (7), ropes used in the lowering mechanism (8), main gas tank (9) and the reserve tank (10). For these seven risks, the mitigation strategy chosen is to perform a more in depth analysis of these components, in order to reduce the risk of failure.

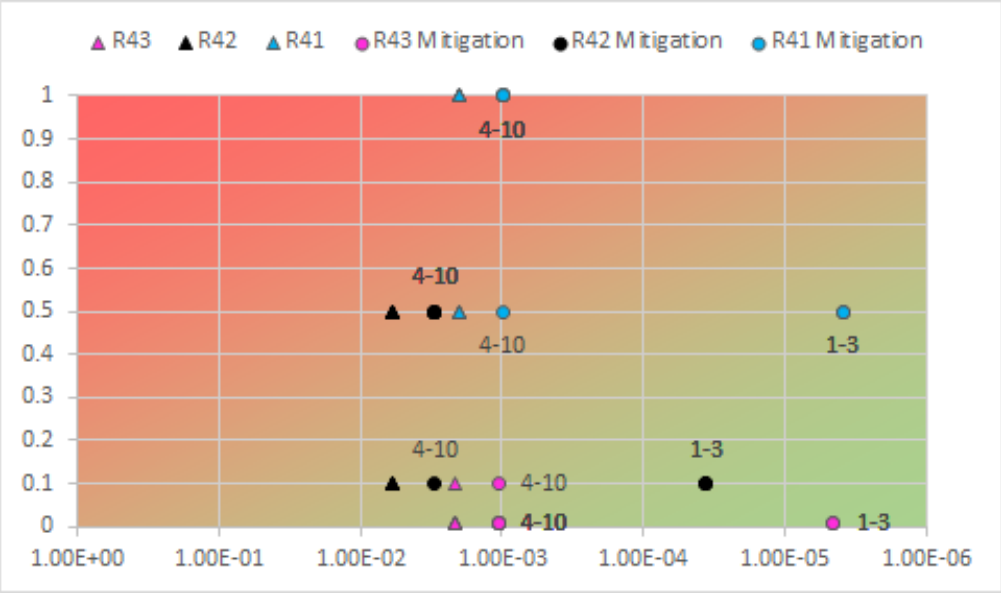

Figure 4.16: A risk map of the SCB.

4.7. Spacecraft Bus Transmission and Command Subsystem

The Transmission and Command subsystem (TNC) is the subsystem that the SCB uses to communicate with the RELs, to transmit data as to be able to fulfill its mission. This subsystem also handles housekeeping data and commands received from the REL. This section contains the architecture, sizing and final design of the SCB-TNC.

4.7.1. SCB-TNC Functional and Architecture Analysis

Before delving into the components, the architecture of this subsystem must be explored. The following text explains the functions carried out by the SCB-TNC subsystem, along with explaining the inner workings of the subsystem itself.

SCB-TNC Functional Allocation

The SCB-TNC must be able to communicate with the REL, where 'communicating' includes receiving commands (F6.8.3), transmitting (F6.8.4) and receiving ranging signals (F6.8.7), transmitting ranging data (F6.8.8), transmitting scientific data (F6.8.10) and transmitting housekeeping data (F6.8.12). Furthermore, the SCB-TNC must also be able to receive a decommissioning command (F7.5.1) and transmit a health tone during the decommissioning phase of the mission (F7.5.4).

SCB-TNC Subsystem Architecture

The SCB-TNC subsystem is composed of the following elements:

- 6 Monopole Low Gain Antennas
- 1 Transponder

This can be visualized in the communications flow diagram in Figure 2.29, which shows the subsystem in context with respect to the rest of the SCB.

Within this subsystem, the low gain antennas transmit and receive all information from either one of the RELs in the UHF band. Each individual antenna is a monopole, but by having 6 of them arranged in a specific geometry an isotropic radiation pattern can be achieved. The transponder is then able to receive and transmit signals through the antennas, also in the UHF band.

SCB-TNC Hardware Block Diagram

The following figure is a block diagram that displays in detail the interfaces between the transponder and the antennas.

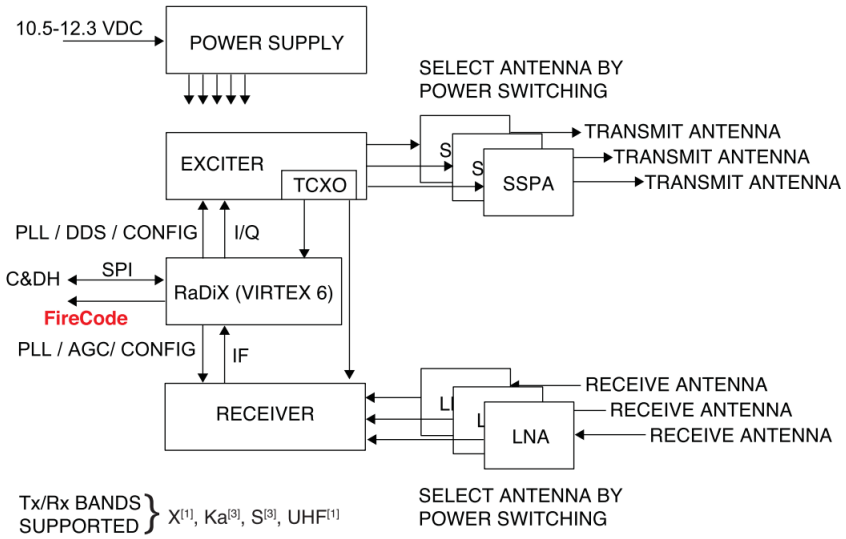

Figure 4.17: The IRIS V2 Transponder block diagram [57].

It must be noted that the SCB-TNC subsystem must receive power from the SCB-EPS in order to be able to stay on-line and properly function, and that all the data it receives and transmits has to go through the on board data

handling subsystem, the SCB-OBD. Furthermore, components of the SCB-TNC subsystem are provided with structural stability by the structure of the SCB.

4.7.2. SCB-TNC Key Requirements

The following key requirements for the SCB-TNC are identified, based on the analysis presented above, and its allocated budgets:

Table 4.14: The key SCB-TNC subsystem requirements, driving requirements are marked with [!].

ID	Description	Rationale
SCB-TNC-REQ-1.5	[!]The SCB-TNC shall receive commands from REL.	Derived from F6.8.3.
SCB-TNC-REQ-1.9	[!]The SCB-TNC shall transmit scientific data to REL.	Derived from F6.8.10.
SCB-TNC-REQ-1.10	[!]The SCB-TNC shall transmit housekeeping data to REL.	Derived from F6.8.12.

SCB-TNC Verification and Validation

During the first preliminary sizing of the SCB-TNC, the worst case distances (and attenuation) between SCB and RELs was assumed, although in later analysis the actual distances and attenuations are used. For the attenuation values, a constant attenuation per kilometer value was assumed, thus the total attenuation was calculated depending on the distance between the SCB and the REL systems. It is vital to ensure results obtained through the developed model are valid, to guarantee a correct sizing and selection of components. As such, the model used to select the SCB's antenna was verified through manual calculations to ensure its results are accurate.

As part of the verification and validation process, the interference between the SCB-mounted antennas and the balloon was briefly investigated. The material used in the balloon was found not to interfere with the antennas' radiation pattern. Moreover the size of the tank above the spacecraft allows the UHF signals to diffract around it, due to the UHF signal's wavelength - thus the radiation pattern remains unaffected.

4.7.3. SCB-TNC Final Design Overview and Evaluation

This subsection discusses the procedure to select the components that are part of the SCB-TNC, which includes the antenna and the transponder elements.

SCB-TNC Selection Antenna

The antenna selected for the SCB-TNC is based on the 'ANT-100' Monopole Antenna [72], which transmits in the UHF band. This antenna is selected due to its simplicity, low cost and flexibility, since it can be placed anywhere within the SCB, which allows for an optimal isotropic radiation pattern. The radio-frequency (RF) power of this antenna is 3.5 W, and using preliminary figures it is determined that communicating between the SCB and the RELs at the required bitrate ensures a suitable link margin. Further analysis is carried out later on, where the bitrate between the SCB and the RELs is plotted over time, in order to verify that the average bitrate is in fact sufficient. This is done by simulating the data generation on the SCB as well as simulating data storage on the SCB over time. This can be seen in Figure 4.18.

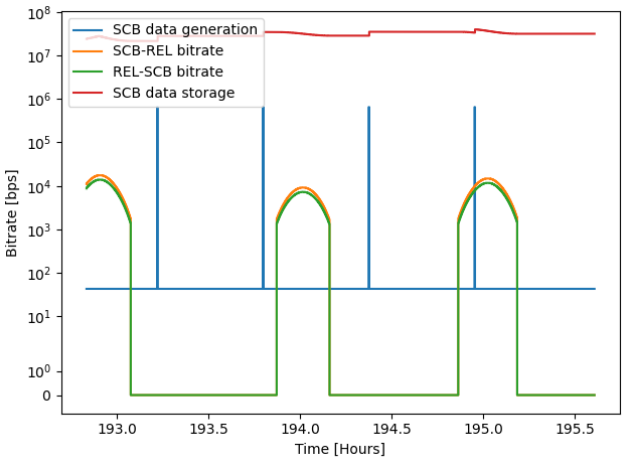

Figure 4.18: The uplink and downlink bitrates between both RELs and SCB as well as the data generated by the SCB and its data storage, at approximately 193 hours into the mission.

SCB-TNC Selection Transponder
The selection of the spacecraft's transponder follows from the selection of the antennas. The transponder selected is the IRIS V2 Transponder, which has been used in past missions [39] and is able to support UHF band communications. Its block diagram can be seen in Figure 4.17.

SCB-TNC Sensitivity Analysis
During the development of the code used to size the antennas, various sensitivity analyses are done to ensure the code's output behaves as expected with respective input changes. In order to test this, several inputs are changed at a time, including variables such as the power of the antenna, the system noise temperature and the atmospheric losses. The average bitrate is used to assess the effects of the input changes.

An example of this is changing the RF power of the antenna. Nominally, the low gain antenna that is selected consumes 3.5 W of power. On average, this guarantees a bitrate of 3.03 $kbps$. Increasing the power of the antenna is expected to increase the average achievable bitrate. This is tested by increasing the power to 4 W, which in turn increases the average bitrate to 3.46 $kbps$, as expected. Similar results are achieved by changing other inputs.

SCB-TNC Final Design Parameters
The final design parameters for the SCB-TNC subsystem are summarised in Table 4.15. The IRIS V2 also includes a Solid-State Power Amplifier (SSPA) and a Low Noise Amplifier, however for for the rest of the report these are all referred to IRIS V2 Transponder', as to be concise.

Table 4.15: Summary of the SCB-TNC component properties, where the IRIS V2 Transponder includes the SSPA and the LNA.

Component	Mass (kg)	Volume (cm^3)	Power (W)	Voltage (V)	Cost (FY2022 $k€$)	Sources
ANT-100 UHF/VHF Monopole Antenna (x6)	0.6	-	35	5	880.20	[72, 24, 42]
IRIS V2 Transponder (x1)	1.1	929.80		12 - 28		[57, 42]

Some of the values presented for the antennas are estimated using EnduroSat's UHF Antenna III [24]. For the transponder, the cost can not be found and as such it is estimated using the new SMAD [42]. In Table 4.16 the properties of the low gain antenna are listed, along with information about the communication link between the SCB and the RELs.

Table 4.16: Properties of the ANT-100 Monopole Antenna.

Component	Uplink Frequency (MHz)	Downlink Frequency (GHz)	RF Power (W)	Power (W)	Gain (dB)	EIRP (dBm)
ANT-100 UHF/VHF Monopole Antennas	390	438	3.5	4.75	0.0	33.44

The BPSK modulation scheme is chosen for communications due to its high spectral efficiency [42]. Moreover, a loss between the transponder and the antenna of 2 dB is assumed. For a more detailed link budget, refer to Subsection 6.7.4.

4.8. Spacecraft Bus Onboard Data Handling Subsystem
The SCB must be able to process and distribute any and all received commands, as well as transmit any generated data onboard. All of this is carried out by the Onboard Data Handling Subsystem (OBD). This section deals with the SCB-OBD, and how the SCB deals with generated data, as well as with transmitted data.

4.8.1. SCB-OBD Functional and Architecture Analysis
In the following paragraphs, both functions that must be carried out by the SCB-OBD and its architecture are analysed.

SCB-OBD Functional Allocation
The SCB-OBD handles the last two phases of the mission, these being the operational phase and the end of life phase. Specifically, this subsystem has to process (F6.5.2), package (F6.5.3) and store the incoming data (F6.5.1), process any commands and send the data to their respective subsystems (F6.9.6). At end of life, the SCB-OBD must be able to execute the decommissioning command in order to end the mission (F7.5.2).

SCB-OBD Subsystems Architecture

The SCB-OBD is composed of the following elements:

- 1 Processor
- 1 Data Storage Unit

The processor is in charge of managing the data flows, whether that is into the SCB or out of the SCB, and packages data. The processor must also send data into the data storage unit, whose purpose is to hold on to this data until the processor determines it can transfer data to the RELs again. All data flows regarding the SCB-OBD are shown in Figure 2.29, where the architecture is also displayed.

SCB-OBD Software Block Diagram

Figure 4.19 contains a block diagram that shows the way the SCB-OBD manages the generated data.

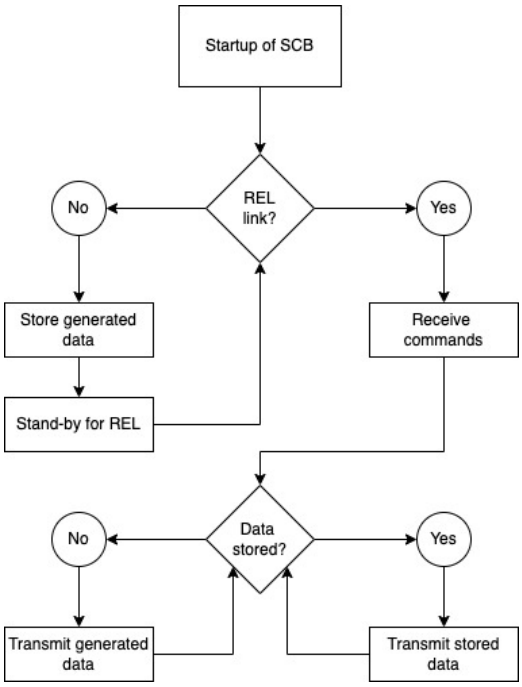

Figure 4.19: The software block diagram for the SCB-OBD, showing the data managing process.

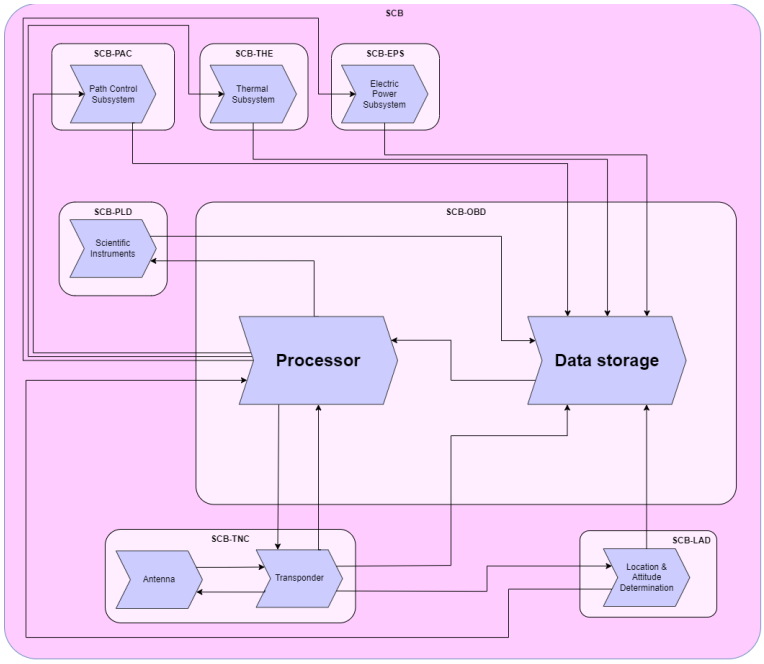

Figure 4.20: The block diagram for the SCB-OBD, showing all connections between the processor, the data storage unit and the rest of the SCB's components.

SCB-OBD Hardware Block Diagram

Figure 4.20 displays a block diagram which contains the various hardware connections between the SCB-OBD and other SCB subsystems.

4.8.2. SCB-OBD Key Requirements

The following key requirements for the SCB-OBD are identified, based on the analysis presented above, and its allocated budgets:

Table 4.17: The key SCB-OBD subsystem requirements, driving requirements are marked with [!].

ID	Description	Rationale
SCB-OBD-REQ-4.1	[!]The SCB-OBD shall be able to process data at a rate of at least 1.3Mbps.	Derived from F6.5.2.
SCB-OBD-REQ-4.2	[!]The SCB-OBD shall have a capacity of no less than 11 Mbytes.	Derived from F6.5.1.

4.8.3. SCB-OBD Trade-off

Several elements of the SCB-OBD subsystem have gone through a trade-off, shown in Figure 4.21. The first one is the processing location, which can either be done on the SCB or on ground. It is decided to process data onboard, since processing it on ground is impractical for the link budget. The second element is the processing approach, which is decided to be processing in software, since performing processing in hardware does not allow for processing changes over time, thus it is not as flexible as processing data in software. The third and final element is the processing partition, which is chosen to be processing between the SCB and the PLD, since no processing between the SCB and the PLD implies the addition of separate processing for the PLD.

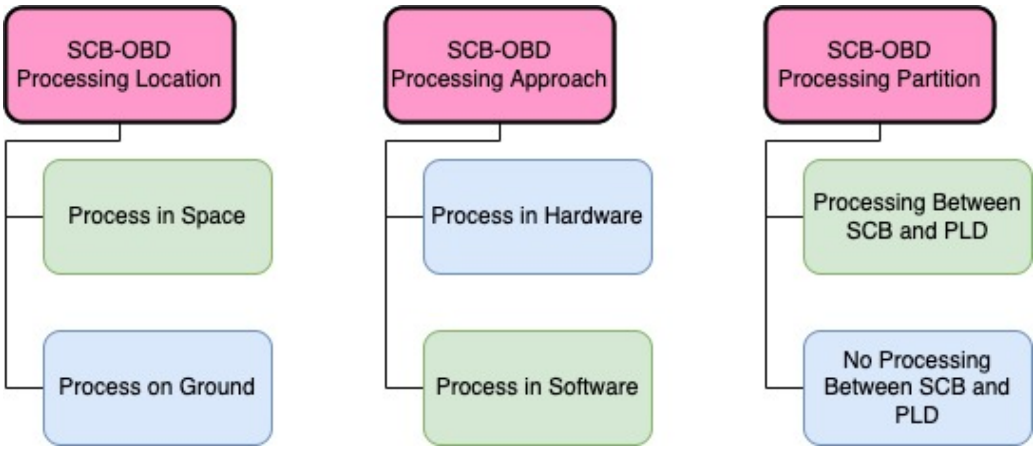

Figure 4.21: The design options tree of the SCB-OBD.

4.8.4. SCB-OBD Sizing

The SCB-OBD subsystem has two major elements to be sized. The first one is the OBD data storage unit, and the second one being the processor itself. This section briefly describes how these two components are sized.

SCB-OBD Sizing OBD Storage

The sizing of the data storage unit for the SCB is directly derived from the model of the communications link between the SCB and the RELs, as well as between the RELs and the ground. A simplified graph generated from this model can be seen in Figure 4.18. Using this model for the entirety of the mission, it is determined that the maximum data storage that the spacecraft needs at any tinme is no more than 7 $MBytes$. Furthermore, margins are applied based on ECSS standards [75], which states that a margin of 50 % for the memory must be used, which sets the required data storage at approximately 11 $Mbytes$.

In order to verify these results, a second version of the model is written using a different calculation method to calculate data storage, which results in the same values as the ones obtained using the original code.

SCB-OBD Sizing OBD Processor

To size the processor, the maximum generated data rate is obtained from the aforementioned model. From the model, the maximum data rate over the entire mission is about 651 $kbps$, and thus the processor must be able to process data at a minimum rate of 651 $kbps$. According to standards [75], a margin of 100 % has to be set for processing speeds, which sets the required data rate to approximately 1.3 $Mbps$.

Model Limitations, Verification and Validation

The communications model made to simulate communications between systems uses a time-step of 10 seconds, thus when simulating the periods of some scientific instruments are rounded off to the nearest 10 seconds. Furthermore it was assumed that all data is first stored in the data storage unit, then it is transmitted once the processor is able to verify a communications link between the SCB and the RELs. The communications model made in order to size the components of the onboard data handling subsystem for the SCB was verified as to ensure its results are in accordance to reality. This was done by manually calculating the data storages at random points during the mission and comparing them to the output of the model.

4.8.5. SCB-OBD Final Design Overview and Evaluation

The final design parameters for the SCB-OBD are summarised in this section.

SCB-OBD Component Selection
With reference to the previously calculated numbers for maximum data storage, the W25N512GVxIG/IT Flash storage [95] is selected, which has a maximum data storage of 64 MB. Regarding the processor, the RAD750 6U [84] is selected, which contains interfaces that are able to support the data rate that is required.

SCB-OBD Sensitivity Analysis
Similar to the sensitivity analysis done in Figure 4.7.3, input parameters are changed in the model, in order to observe the output's response and verify the functionality of the code.

As an example, the bitrate of the RAD instrument is increased tenfold, in order to test the sensitivity of the model. With the original RAD bitrate, the maximum required data storage is exactly 6376640 $bytes$, but with the new bitrate the maximum required data storage is 6385798 $bytes$, which is to be expected.

SCB-OBD Final Design Parameters
A summary of the properties of the selected components is presented in Table 4.18.

Table 4.18: A summary of the properties of the SCB-OBD components.

Component	Mass (kg)	Volume (cm^3)	Power (W)	Voltage (V)	Cost (FY2022 $k€$)	Sources
RAD750 6U	1.22	1537.8	14	3.3	682.90	[84, 42]
W25N512GVxIG/IT	-	0.036	0.09	3		[95, 42]

It is worthy to note that some properties of these components are estimated using the new SMAD [42]. Other component-specific properties can be found in Subsection 4.8.5.

4.9. Spacecraft Bus Lifting System
The SCB-LFT is determined to be a gas pumped balloon concept. The components providing the lift are the super pressure balloon, zero pressure balloon and the lifting gas. In this section the detailed design of these components is performed. In Subsection 4.9.1 the functions and the architecture of the lifting subsystem are described together with a hardware block diagram. Following this, the sizing and trade-offs for the lifting system are done in Subsection 4.9.3. Finally, in Subsection 4.4.1 an overview of the final design is given, including the material selection and the sensitivity analysis.

4.9.1. SCB-LFT Functional and Architecture Analysis
In this subsection, the functions of the SCB-LFT are used to determine the architecture of the subsystem. Fist the functions are presented, then the architecture is described.

SCB-LFT Functional Allocation
The SCB-LFT has a number of functions. When the SCB has been released from the EDV and has dropped the hydrogen tank, the correct altitude needs to be obtained (F6.3.1). The SCB is able to do this by pumping or venting the hydrogen gas in the balloon module. The second function is to maintain this correct altitude specified by the path (F6.3.2). This is done through a simple control loop with the valves and pump which is optimised in a further stage of the design.

SCB-LFT Systems Architecture
As previously described, the SCB-LFT must provide enough lift to support the SCB during operations. It must also have control over its altitude, this is done by changing the amount of lift produced by the balloon.

The lifting system consists of a super pressure balloon, zero pressure balloon and a lifting gas. This concept allows the SCB to reach a certain altitude depending on the gas distribution between the super pressure and zero pressure balloon. With this capability it is able to perform all functions specified in Subsection 4.9.1.

4.9.2. SCB-LFT Key Requirements
The following key requirements for the SCB-LFT are identified, based on the analysis presented above, and its allocated budgets. The value of these forces are determined using the lift necessary to float at the maximum altitude (62 km).

Table 4.19: The key SCB-LFT subsystem requirements, driving requirements are marked with [!].

ID	Description	Rationale
SCB-LFT-REQ-1.1	[!]The SCB-LFT shall provide no less than 3088 N of lift at 50 km altitude.	The amount of lift needed to hold up the SCB at 50 km
SCB-LFT-REQ-2.1	[!]The SCB-LFT shall provide no less than 3088 N lift at 62 km altitude.	The amount of lift needed to hold up the SCB at 62 km

4.9.3. SCB-LFT Sizing and Trade-off

The lift concept chosen in the previous design phase is the pumped helium concept. As discussed in the previous section, the helium has been replaced with hydrogen for this design. The concept remains the same for most aspects, this means that there are not many design choices that still have to be made through trade-offs. Most of the design is done through sizing for performance.

SCB-LFT Gas trade-off

For the gas selection within the pumped gas balloon, there are two logical options between which a qualitative trade-off is performed: Hydrogen and Helium. They are scored on six criteria as shown in Table 4.20: mass, sustainability, leakage, cost, danger level and confidence/TRL. Ultimately, hydrogen is selected as the lifting gas for the LOVE mission. In comparison to Helium, hydrogen excels in four out of six scoring criteria. Furthermore, the high danger level can be compensated for by taking sufficient safety precautions. Besides that, hydrogen does have flight heritage on Earth, it simply requires additional analysis to guarantee its compatibility with ballooning in the Venusian atmosphere.

Table 4.20: The lifting gas trade-off between hydrogen and helium.

Criterion		Hydrogen		Helium		Source:
Type:	**Weight:**	**Description:**	**Score:**	**Description:**	**Score:**	
Mass	**40%**	Light (2.02 g/mol)	3	Heavy (4 g/mol)	1	[4, 3]
Sustainability	**5%**	Unlimited availability	3	Limited availability (very resource-intensive)	1	[94]
Leakage	**20%**	Slow leakage (diatomic molecule)	2	Fast leakage (monatomic molecule)	1	[5]
Cost	**10%**	Cost (0.112 $\$/m^3$)	3	Expensive (7.57 $\$/m^3$)	1	[92]
Safety	**5%**	Hazardous, extremely flammable	0	Not hazardous	3	[4, 3]
Confidence/ TRL	**20%**	Low	1	High (Flight heritage on Venus)	3	[60]
Total	**100%**	**2.25**		**1.5**		

SCB-LFT Sizing Super Pressure and Zero Pressure Balloon

In the midterm report [2] the sizing method for the super pressure and zero pressure balloon is described in detail. The same principle for the balloon sizing is used in the detailed design phase. The zero pressure balloon is sized for the maximum altitude that is required for the mission with a 500 m margin. The super pressure balloon is sized for a surplus pressure of 1 kPa when the balloon is experiencing a 3 m/s downward wind gust. The volume needed for these two balloons was 131 m^3 for the super pressure balloon and 919 m^3 for the zero pressure balloon (this excludes the volume of the super pressure balloon within the zero pressure balloon). This lead to a super pressure balloon with a radius of 3.15 m and a zero pressure balloon of 6.3 m radius. The balloon is fully inflated when it is at the maximum altitude of 62 km. When it is below this altitude, the balloon is not fully inflated and not a perfect spherical shape.

The results of this sizing are validated by adjusting the model to fit the description of the Venus Flagship Mission[49] concerning the gas content and the desired altitude range. The model must then produce a balloon

system with the same dimensions as specified in the flagship mission report. This is indeed true, therefore the model for the sizing of the super pressure and zero pressure is considered valid.

For the detailed design, a thickness sizing for the balloon is performed, which then (with the density of the selected material and known dimensions) results in a value for the masses of the balloons. Firstly, the super pressure balloon is sized for withstanding the high pressure of the hydrogen inside it. This pressure p is calculated with Equation 4.1 through the amount of moles of hydrogen present in the balloon n_{gas}, the temperature T and volume V.

$$p = \frac{n_{gas} \cdot R \cdot T}{V} \tag{4.1}$$

$$t = \frac{p \cdot r}{2 \cdot \sigma} \tag{4.2}$$

Calculating the pressure within the balloon at every altitude, with a safety margin of 500 m on either side of the altitude range, yields the maximum possible pressure p in the super pressure balloon. Combining this maximum pressure with the radius of the sized balloon r and the tensile strength of the material σ, assuming an ideal balloon, then yields the material thickness t through Equation 4.2 [76].

$$m_{leakage_{op}} = \mu \cdot t \cdot A \cdot p \tag{4.3}$$

Since the zero pressure balloon does not have to withstand high internal pressures, its thickness is chosen according to the nominal thickness of the selected material. This thickness selection is a trade-off between material mass, which can be calculated straightforwardly, and hydrogen leakage during operations. This leakage $m_{leakage_{op}}$ was computed through Equation 4.3 with the permeability of the material μ for a predefined thickness, mission duration t, inner surface area of the balloon through which leakage occurs A and inner pressure p. Actual results of the thickness, mass and leakage in operations sizing for the balloons follow under Subsection 4.9.4.

SCB-LFT Sizing Main Hydrogen Tank

The total amount of hydrogen that follows from the balloon sizing is carried within the main hydrogen tank. For this tank, two main trade-offs have to be performed: one for the shape and one for the material. For the shape, a spherical tank is selected. A spherical tank is conventional and thus has a high TRL. Furthermore, a sphere is the most space-efficient for the packing within the EDV and it is the simplest to attach and later-on detach from the SCB gondola.

For the main tank production, an external supplier, Steelhead composites, is selected which offers two types of hydrogen tanks: Composite overwrapped pressure vessels of type III (metal lined) and of type IV (polymer lined) [81]. These tanks are all functional within the necessary temperature range, have flight heritage and can store hydrogen with 350 $bars$ of pressure. Between the two tank types, metal lined tanks excel slightly in most performance characteristics, but are generally around twice as heavy. Hence the type IV polymer lined tank is selected.

For sizing the tank, an average thickness is taken from the off-the-shelf 350 bar type IV tanks [82], which results in being approximately 21.89 mm. Furthermore, the areal density of the material used for these tanks is derived in the same manner which results in it being approximately 2.02E-5 kg/mm^2. Rewriting the ideal gas law (shown in Equation 4.1) for the volume then yields the geometric properties for the main tank through basic computation. By calculating the surface area of the tank, its mass is derived to be approximately 77.41 kg. This calculation is performed in an iteration with the amount of hydrogen in the main tank $m_{hydrogen_{maintank}}$. This amount is a sum of the hydrogen required for the mission $m_{hydrogen_{mission}}$, the hydrogen lost in transfer $m_{leakage_{transfer}}$ and the hydrogen left in the tank after the balloon filling process $m_{leakage_{filling}}$ as shown in Equation 4.4.

$$m_{hydrogen_{maintank}} = m_{hydrogen_{mission}} + m_{leakage_{transfer}} + m_{leakage_{filling}} \tag{4.4}$$

The amount of hydrogen necessary for the mission has been computed previously to be 14.63 kg. During the transfer, some hydrogen is lost as it leaks through the tank. Using the permeability of the type IV tank of $\mu = 2 \cdot 1.00784 \cdot 4E-8 kg/ms$ [81], inner tank surface area A, transfer time $t_{transfer}$ and tank thickness t_{tank} as shown in Equation 4.5 yields the amount of lost hydrogen in transfer. Secondly, the leftover hydrogen in the tank after filling the zero pressure balloon must be taken into account. No pump is connected to the main tank, hence the hydrogen no longer leaves the tank once it reaches the same pressure as the atmosphere. The amount

of leftover hydrogen can be calculated through applying the ideal gas law at the tank drop altitude. This results in a combined loss of 0.18 kg, thus a total necessary amount of hydrogen to be carried in the tank of 14.81 kg.

$$m_{leakage_{transfer}} = \frac{\mu \cdot A \cdot t_{transfer}}{t_{tank}} \tag{4.5}$$

SCB-LFT Sizing Reserve Hydrogen Tank
The reserve hydrogen tank carries the reserve hydrogen taken on-board to compensate for the hydrogen leakage from the balloon during operations. This tank is selected to be toroidal, since this is the only acceptable tank shape for the packing of the SCB within the EDV. It is sized with the same thickness, material and internal pressure as the main tank. Using the necessary volume of the tank and the CAD model, the dimensions of the inner and outer diameter of the toroid are found and implemented within the balloon sizing model.

Model Limitations, Verification and Validation
The sizing of the balloon module was validated by comparing it to the Venus Flagship Mission[49]. This was done by changing the gas to helium and using the same payload weight. The model for the sizing of the tanks was validated by doing hand calculations to check the results.

4.9.4. SCB-LFT Final Design Overview and Evaluation

In this subsection the final design of the the SCB-LFT is presented and discussed. First the material selection is done, followed by a sensitivity analysis of the design. In the final part, all the design choices and sizing are summarised.

SCB-LFT Materials Selection Super Pressure and Zero Pressure Balloon
For the material selection of both the super- and the zero pressure balloon, different selection criteria are taken into account. Both balloons have to function as a hydrogen barrier and remain intact through handling and deployment, hence they need to have a low permeability and resistance to pinhole growth. Furthermore, the zero pressure balloon has to function without degradation in the Venusian environment, this entails the need for sulfuric acid and solar heating resistance. As the super pressure balloon is placed within the zero pressure balloon, its reaction to the atmospheric properties is of lesser importance. However, the super pressure balloon requires the use of a stronger material as it has to sustain much higher loads due to the highly pressurized hydrogen content than the zero pressure balloon.

For the super pressure balloon material, Vectran type NT is selected. Vectran is a high-performance fiber with long-term high strength characteristics [45]. The fibres are available off-the-shelf and by covering them in a type 150 textile processing finish, they can be weaved into a high-strength fabric with low permeability [93]. Using the previously described sizing methods from Subsection 4.9.3, the super pressure balloon material is determined to have a thickness of approximately 155.5 μm and a mass of approximately 27.19 kg. This model is validated by comparing it to the design of a long duration Venus balloon from literature for which the fabric (also made from Vectran) is designed to be 170 μm in thickness, which lies close to the calculated value for the LOVE mission [34].

For the zero pressure balloon material, Kapton Type 250FN029 was selected. It is an off-the-shelf bilaminate material by Dupont de Nemours Inc. [20]. The main structure of the balloon follows from a Kapton HN polyimide film with a nominal thickness of 50.8 μm [18]. This material is tough and has a high thermal durability. In order to boost its total acidic resistance and better the permeability characteristics, the Kapton HN film is covered in a FEP fluorocarbon resin with a nominal thickness of 12.7 μm [18]. The FEP film also has good long-term thermal characteristics. Ultimately this then results in a zero pressure balloon material mass of approximately 49.82 kg.

$$\mu_{combined} = \frac{1}{\frac{1}{\mu_1} + \frac{1}{\mu_2}} \tag{4.6}$$

Bilaminate materials have, in their essence, better permeability characteristics than a single layer of a single material type. The combined permeability of the Kapton HN and FEP films can be calculated through Equation 4.6 [77]. Here the permeability of the materials is already calculated for their respective thicknesses resulting in 19000 $mL/m^2 24hMPa$ for 50.8 μm of Kapton HN and 24630 $mL/m^2 24hMPa$ for 12.7 μm of

the FEP film (using the permeability per mil from [19]), ultimately that results in a total permeability of 10726 $mL/m^2 24hMPa$ for the Kapton Type 250FN029. Then using the method previously presented in Subsection 4.9.3, the hydrogen leakage ends up at approximately 1.15 kg in operations. This hydrogen has to be taken on-board in a reserve tank.

SCB-LFT Sensitivity Analysis
The sizing of the SCB-LFT is done in an iterative loop. Therefore, to consider the validity of the results, a sensitivity analysis must be performed. In this case it is done by varying the empty mass of the SCB, the gas choice, the reserve tank configuration and the material selection and checking that the mass iteration converges. The results of these iterations are not documented, but the model converges for each change made. Therefore, the results of this sizing are considered robust.

SCB-LFT Final Design Parameters
The final design of the SCB-LFT is a hydrogen pumped balloon design with a super pressure and zero pressure balloon. The zero pressure balloon has a radius of 6.31 m and the super pressure has a radius of 3.15 m. The total mass of the zero pressure balloon material is 49.82 kg and the total mass of the super pressure material is 27.19 kg. The balloon design can be seen in Figure 4.15.

The final design of the hydrogen tank is a spherical tank with a diameter of 1.10 m and a volume of 0.625 m^3. The tank transports 14.63 kg of hydrogen and an extra 0.2 kg to compensate the tank leakage during transfer. The reserve tank is a toroidal tank with an inner radius of 0.088 m and an outside radius of 0.320 m. The tank provides the balloon module with an extra 1.15 kg of hydrogen. The design of the tanks can be seen in Figure 4.22.

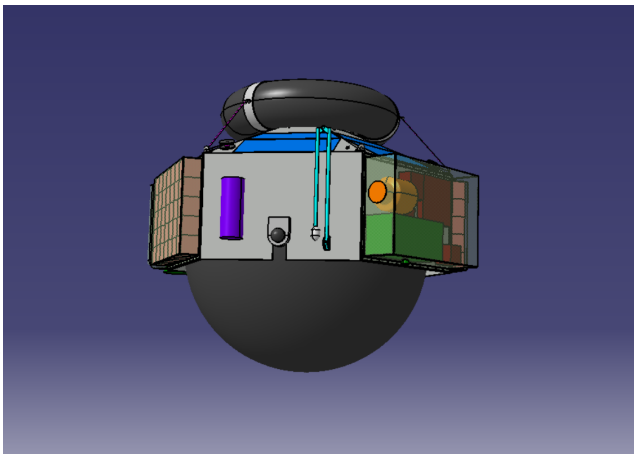

Figure 4.22: The design of the hydrogen tanks of the SCB.

4.10. Spacecraft Bus Position and Attitude Control System

The SCB needs to be able to follow the path specified in PAT, therefore it is necessary to have control over the SCB. In this section the SCB-PAC is designed and discussed. An important note is that the SCB does not have any form of control over its attitude, since this is not necessary for this mission. There are no requirements for the payload or the communications on the attitude, thus no control for the attitude has been designed. The SCB is able to control its altitude and thus its position. First, in Subsection 4.10.1 the functions and architecture of the subsystem are discussed. Next, the key requirements for the SCB-PAC are discussed in Subsection 4.10.2. Following this, the components of the SCB-PAC are sized in Subsection 4.10.3. To conclude, the final design is given in Subsection 4.10.4.

4.10.1. SCB-PAC Functional and Architecture Analysis

In this subsection, the functions are used to determine the architecture of the SCB-PAC. First, the relevant functions of the functional flow diagram in Section 2.2 are given. Next, the resulting architecture of the SCB-PAC are given.

SCB-PAC Functional Allocation
The first three functions of the SCB-PAC are needed for the initial positioning of the SCB after its deployment. The SCB-PAC needs to make the SCB reach the correct altitude (F6.2.1), latitude (F6.2.2) and longitude (F6.2.3). After this, the PAC must control the SCB to follow the path and thus maintain the specified altitude (F6.3.1) and latitude (F6.3.2). Finally, the SCB-PAC is used during the decommissioning phase of the mission. The SCB-PAC must reduce the lift (F7.5.3) such that the SCB can burn up in the lower altitudes of the atmosphere.

SCB-PAC Systems Architecture
The SCB-PAC consists of valves and pumps that move around the hydrogen in the system. These pumps and valves must be sized to provide the correct ascent and descent velocities to follow the path. With this architecture, the SCB is able to control its altitude. According to the functions, the SCB must also be able to control its latitude and longitude. For this there are no new hardware components that need introducing to the subsystem. This is done using the winds of Venus, as explained before in Subsection 4.3.3.

4.10.2. SCB-PAC Key Requirements
The following key requirements for the SCB-PAC are identified, based on the analysis presented above, and its allocated budgets:

Table 4.21: The key SCB-PAC subsystem requirements, driving requirements are marked with [!].

ID	Description	Rationale
SCB-PAC-REQ-1.1	[!]The SCB-PAC shall give the SCB a starting altitude of 62 km.	Derived from F6.2.1, shall likely be either 50km or 62km depending on whether it is initiated at the bottom or top of the path.
SCB-PAC-REQ-1.5	The SCB-PAC shall obtain the correct altitude along the PAT with an accuracy of at least 100 m.	Derived from F6.3.1. (part of "The SCB shall position itself for measurements along PAT.") with taking into account MIS-REQ-2.7 of having to take measurements with a height resolution of 100 m.
SCB-PAC-REQ-1.6	The SCB-PAC shall give the SCB a starting latitude of 0 degrees.	Derived from F6.2.2.

4.10.3. SCB-PAC Sizing
There are two components of the SCB-PAC that need to be sized: The valve and the gas pump. The valve size determines the rate at which the hydrogen can be moved from the super pressure balloon too the zero pressure balloon, and thus influences the ascent rate. The pump influences the rate at which gas can be moved from the zero pressure balloon to the super pressure balloon.

Firstly, the vent is sized. The path specifies that the SCB must be able to ascend with 3.5 m/s, thus the vent must be sized such that this requirement can be met. A simple relation for the mass flow in kg/s and the characteristics of the vent is given in Equation 4.7[33]. In this relation the C_d value is assumed to be 0.035 according to literature for hydrogen vents[87]. This relation also uses the difference in pressure between the super pressure balloon and the atmospheric pressure, which is equal to the pressure in the zero pressure balloon. This relation, combined with trying out various values for the diameter of the valve in the model for the upward motion, has led to the conclusion that a valve with a 20 mm diameter is chosen. This value is checked with literature and it is determined that this size for a vent is within a valid range.

$$\dot{m}_{vent} = C_D \cdot \frac{\pi}{4} \cdot d^2 \cdot \sqrt{2(P_{sp} - P_{atm})} \tag{4.7}$$

Next, the pump is considered. The path specifies that the SCB must be able to descent with 0.5 m/s, thus the pump must be chosen so that this requirement can be met. Extensive literature research is done for the sizing of a gas tank that can meet these requirements, however, there are no options that currently meet them. Therefore, it is decided to develop a pump that can meet these requirements. The pump that is to be developed must have a pump rate of 200 L of hydrogen per minute. This is what is assumed to be possible for helium in a prototype study by JPL[33].

For this stage of the design, an estimate of the mass and power is needed. For the power required to operate the pump, the power specified for the pump of the Venus Flagship Mission[49] is scaled according to the amount of moles of gas that the pump needs to move around. This results in a pump power of 57.35 W. The mass of

the pump is estimated to be 28.6 kg. This is based on an estimate for other pump weights found, after which a 30 % uncertainty margin is applied.

Model Limitations, Verification and Validation
The valve sizing and pump sizing was compared to literature[33][49] and therefore these values are considered valid. A limitation of the model of the control system is the error in the control loop discussed in Subsection 4.3.2.

4.10.4. SCB-PAC Final Design Overview and Evaluation

In this section, the final design of the SCB-PAC is presented. First, the sensitivity of the results is discussed. After this, a final overview of the design is presented, including a figure of the performance of the pump and vent during operations.

SCB-PAC Sensitivity Analysis
The sensitivity of the results has to be evaluated to determine how valid this SCB-PAC sizing is. The vent sizing can be evaluated, which is done by trying out several diameters for different altitudes and checking that the performance still matches the requirement. However, due to the uncertainty of the exact design of the pump, no sensitivity analysis can be performed yet. This must be done in the next design phase, once a more exact design is determined.

SCB-PAC Final Design Parameters and Evaluation
The final design of the SCB-PAC is a pump of 28.6 kg that requires 57.35 W to pump 200 L hydrogen gas per minute. The vent has a diameter of 20 mm.

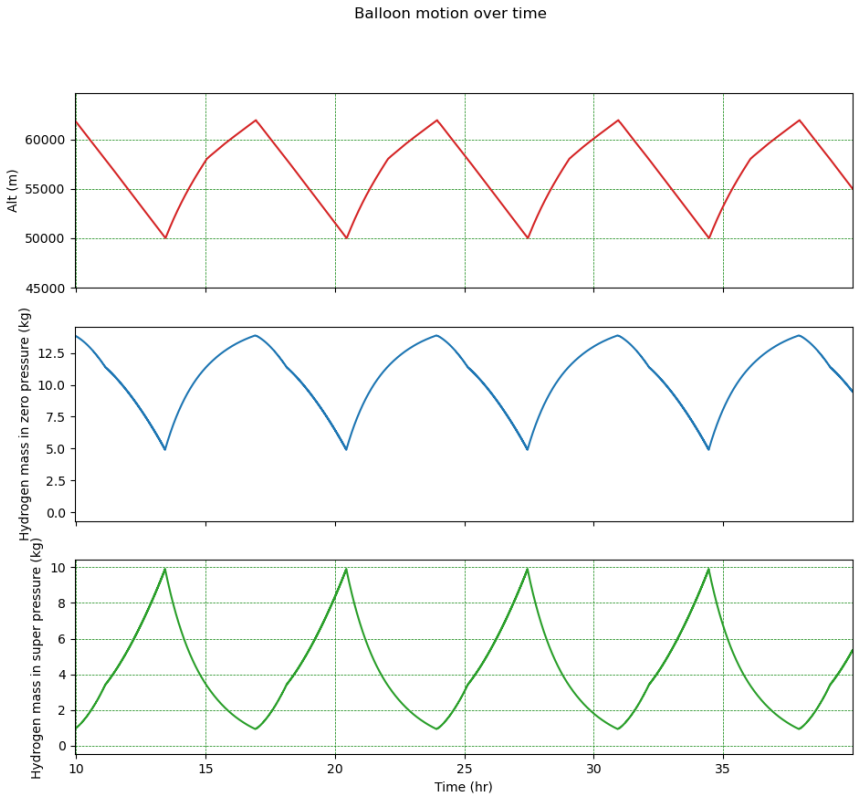

Figure 4.23: The altitude profile and the hydrogen mass of the zero and super pressure balloon over time.

Now that the valve and the pump have been sized, the characteristics of the SCB-PAC can be applied to the controlled motion of the balloon. This motion is shown in Figure 4.23. The first graph shows the altitude of the SCB above the surface of Venus in meters over time in hours. The next two graphs show the content of the zero pressure balloon and super pressure balloon over time. The content of the balloon is the amount of hydrogen

gas in kilograms. In the figure, the increasing amount of hydrogen in the zero pressure balloon represent the SCB-PAC making the SCB increase its altitude. It is the opposite for when the content of the super pressure balloon is increased.

4.11. Spacecraft Bus Location and Attitude Determination System

In order for the SCB to determine its location, a location and attitude determination subsystem must be present. The goal of this subsystem is to obtain position and velocity data to aid in the operation of the spacecraft and provide context to the science data. Furthermore, its measurements are integral to the determination of the wind speed. First, the functions and architecture of the SCB-LAD are discussed in Subsection 4.11.1. Then, the key requirements to the SCB-LAD are presented in Subsection 4.11.2. Subsequently, the results of the performance analysis are shown in Subsection 4.11.3 and the final design is treated in Subsection 4.11.4.

4.11.1. SCB-LAD Functional and Architecture Analysis

In order to begin the design of the SCB-LAD, the functions to be performed must be identified and allocated to individual components.

SCB-LAD Functional Allocation

The main functions that the SCB-LAD has to fulfil are F6.6.4: determining the position, attitude and velocity of the SCB.

SCB-LAD Systems Architecture

The SCB-LAD systems architecture consists of the following components:

- 1 Inertial Measurement Unit (IMU)
- 6 Sun Sensors

The SCB-LAD-IMU is used to measure the rotational rates of the SCB, as well as the direction and magnitude of the acceleration vector acting on the SCB. The sun sensors provide the azimuth and elevation angle of the sun, with the goal of providing additional information on the direction in which the SCB is pointing, since this cannot be easily ascertained. It is also used in conjunction with the rotational rate and acceleration vector data to determine pitch and roll. Furthermore, the position of the SCB is calculated through dead reckoning from the acceleration data, and is regularly updated using ranging data from the REL-TNC. Moreover, the SCB-LAD takes in atmospheric density data which is made available by the PLD-REM subsystem to get exact altitude data based on atmospheric models.

SCB-LAD Hardware and Software Block Diagram

Figure 4.24 shows the hardware block diagram of the SCB-LAD. Figure 4.25 shows the software block diagram of the SCB-LAD.

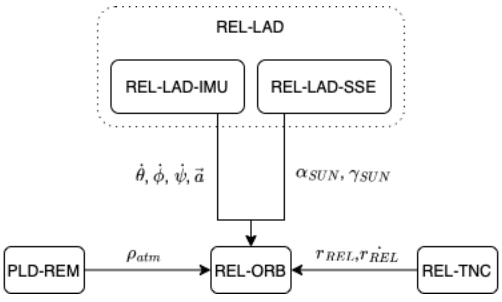

Figure 4.24: The hardware block diagram of the SCB-LAD.

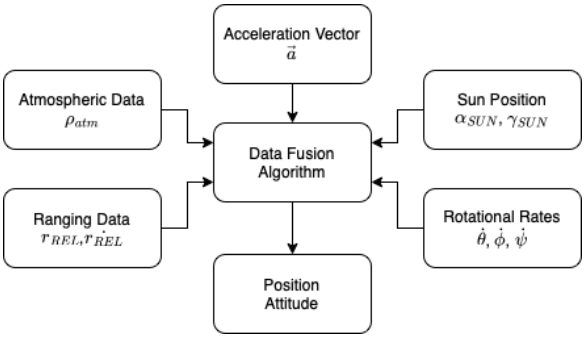

Figure 4.25: The software block diagram of the SCB-LAD.

It can be seen that the sensor data is fed into a data fusion algorithm which estimates the position and attitude of the SCB based on the input data.

4.11.2. SCB-LAD Key Requirements

The following key requirements for the SCB-LAD are identified, based on the analysis presented above, and its allocated budgets. Note that for the purposes of requirements derivation, the SCB-LAD is considered to only consist of the SCB-LAD-IMU and the SSE-LAD-IMU.

Table 4.22: The key SCB-LAD subsystem requirements, driving requirements are marked with [!].

ID	Description	Rationale
SCB-LAD-REQ-1.1	[!]The SCB-LAD shall be able to determine SCB attitude with a 1σ uncertainty of 5 deg.	Derived from F6.2.4, dictates the SCB to be vertical for the Venspec measurements.
SCB-LAD-REQ-2.1	[!] The SCB-LAD shall measure SCB velocity with a 1σ uncertainty of better than 0.996 m/s	Required to be able to perform wind measurements, see mission velocity error allocation.
SCB-LAD-REQ-2.2	The SCB-LAD shall measure SCB position with a 1σ uncertainty of better than 84785.43 m	Required to be able to perform all measurements , see mission velocity error allocation.
SCB-LAD-REQ-2.3	[!] The SCB-LAD shall measure SCB vertical position with a 1σ uncertainty of better than ±0 m	Required to be able to all measurements.

4.11.3. SCB-LAD Performance Analysis

The main aspect of the LAD that is sized as part of the design analysis is the bias stability of the IMU. This is important, since the IMU and its acceleration data are the only way of determining the SCB position during communications eclipse until the contact with the REL can be reestablished. Other design parameters of the IMU to be considered are the noise and scale factor of the system. Please note that the sizing is based on analytical calculations The following assumption is introduced:

1. The error resulting from bias is a constant acceleration over time.
2. The signal-to-noise ratio needs to be better than 5 for all measurements.
3. The drag of the the SCB is equal to a sphere with the diameter of the superpressure balloon.

The main consideration for the bias instability is the fact that this error is integrated twice, the first time to get the velocity and the second time to get the position:

$$err_v = a_{bias} * t_{eclipse} \tag{4.8}$$

For constant a_{bias}, which is the sum of noise, scale factor and bias instability and with err_v being the velocity error, and $t_{eclipse}$ being the eclipse time. It then follows that:

$$err_p = \frac{err_v * t_{eclipse}}{2} \tag{4.9}$$

Considering a maximum eclipse time of 2920 s, a maximum allowed velocity error of 0.966 m/s and a maximum position error of 84785.43 m, it turns out that the velocity error is critical in terms of the bias. It results that the total bias acceleration shall be no more than $3.31 * 10^{-4}$ m/s^2. This result represents the worst case, as likely the bias is not constant for some aspects of the bias, such as the noise.

Next up, the altitude performance is investigated. The PLD-REM used to get the pressure/density data has an accuracy of 10 Pa. Looking at the the pressure gradient at 62.5 km, which is -2.8 Pa/m, this results in an altitude accuracy of 3.575 m. It is important to note that changes in the atmosphere and uncertainties in the atmosphere are not to be taken into account here, however, since the required uncertainty is only 50 m, this results in a high margin to account for lack of knowledge of the atmosphere.

Lastly, the sensitivity of the system to gusts is investigated. The driving requirement is a sensitivity of 0.1 m/s, meaning that the system needs to be able to detect the acceleration caused by a gust. The instantaneous acceleration caused by a 0.1 m/s instantaneous change in wind velocity is $2.88 * 10^{-4}$ m/s^2, using assumption 3. With a noise of $1.47 * 10^{-5}$ m/s^2, the SNR is 19.6.

Model Limitations, Verification and Validation

While the model used is purely based on analytical calculations, validation is still required. For the purpose of this analysis, the model is considered valid if it gives a conservative performance estimation of the SCB-LAD performance. Therefore, if the analyses are to be considered valid, it must be shown that they represent worst-case or at least conservative estimations.

Regarding the IMU performance analysis, the model assumes constant bias in one direction, which is the worst case as it leads to straightforward addition of the bias over time. In reality, due to SCB rotation and the fact that noise follows a normal distribution instead of having a constant value, the uncertainty is less. For the analysis of altitude performance, the upper altitude represents the part with the lowest pressure gradient - once again, this is indeed the worst case. For sensitivity, the assumption that is introduced regarding drag is indeed conservative, as the balloon is indeed larger and the gondola also contributes to drag.

4.11.4. SCB-LAD Final Design Overview and Evaluation

Now, the detailed design of the SCB-LAD is presented with focus on the components chosen, a sensitivity analysis and a presentation of the final design parameters.

SCB-LAD Component Selection

For the selection of the SCB-IMU and SCB-SSE, the main factors that are considered are the performance and flight heritage. For the IMU, the Northrop-Grumman LN200S is chosen due to its high precision and extensive flight heritage on planetary missions [32]. The sun sensor selected is the Tensor Tech CSS100.

SCB-LAD Sensitivity Analysis

Now, the sensitivity of the SCB-LAD design to design changes, namely a change in the critical performance requirement - maximum velocity error. As calculated in [2], the bias acceleration of the LN200S is $9.189 * 10^{-5}$, meaning that the sizing of the IMU is robust down to a required velocity error of 0.268 m/s. Furthermore, the sun sensors have an accuracy of $\pm 0.5°$, leaving a 10x margin to the requirement. Therefore, the robustness of the design is considered to be high.

SCB-LAD Final Design Parameters and Evaluation

Finally, the final design parameters of the SCB-LAD are shown in Table 4.23:

Table 4.23: A summary of the properties of the SCB-LAD components.

Component	Mass [kg]	Power [W]	Energy [Wh]	Bias [m/s^2]/ Accuracy [deg]	Sources
LN200S	0.748	12	288	$9.189 * 10^{-5} m/s^2$	[32]
CSS100	0.004	0.0066	0.156	±0.5 deg	[89]

4.12. Spacecraft Bus Electrical Power System

The spacecraft is equipped with various instruments, each of which requires electrical power to operate. Next to that, the SCB that supports these instruments includes various subsystems that require electrical power. Therefore the SCB is equipped with an EPS, of which the designing and sizing is documented in the following sections.

4.12.1. SCB-EPS Functional and Architecture Analysis

The architecture of the SCB-EPS consists of different parts, that each have their own role. However, the design of the SCB-EPS ultimately has to be able to fulfill the functions of the SCB-EPS. With the functions in mind, the design of the architecture of the SCB-EPS can be described.

SCB-EPS Functional Allocation

During the operational phase on Venus, the SCB-EPS has a couple of functions to fulfill. First of all, the SCB-EPS must generate electrical power (F6.6.1). Next to that, the SCB-EPS must store electrical power (F6.6.1). Lastly, the SCB-EPS must distribute electrical power to all the subsystems and components that require it (F6.6.1).

SCB-EPS Systems Architecture

The SCB-REL consists of a combination of a solar array (SAR) and a secondary battery (BAT), as well as a power control and distribution unit (PCD). The SAR is split up into multiple body mounted solar panels on the top of the spacecraft, that together make up the required solar panel area. The battery consists of multiple connected battery modules that are placed on the sides of the spacecraft. The SAR provides a power generation for the spacecraft when sunlight is received. In support, the battery stores excess power generated and provides power during eclipse conditions as well as peak power conditions.

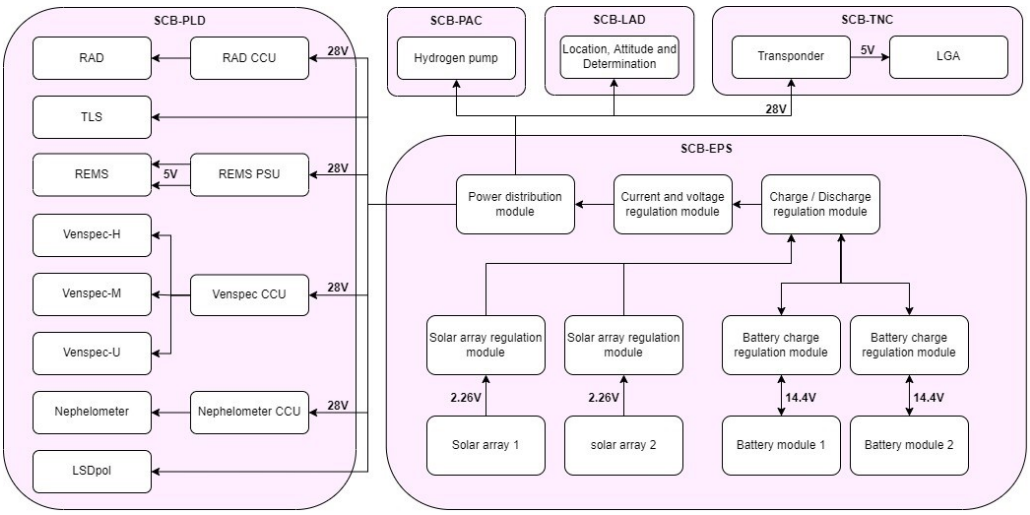

Figure 4.26: The hardware block diagram of the SCB-EPS.

SCB-EPS Hardware Block Diagram

The architecture of the SCB-EPS described in Subsection 4.12.1 can be represented in a block diagram of the hardware used and their interrelations, which is shown in Figure 4.26. The arrows represent the flow of electrical power within the SCB-EPS as well as to other subsystems. For specific power flows the voltage is specified, indicating that a certain output voltage or input voltage is required.

4.12.2. SCB-EPS Key Requirements

The following key requirements for the SCB-EPS are identified, based on the analysis presented above, and its allocated budgets:

Table 4.24: The key SCB-EPS subsystem requirements, driving requirements are marked with [!].

ID	Description	Rationale
SCB-EPS-REQ-4.1	[!]The SCB-EPS shall provide an average power of at least 84.5 W for the duration of the operational phase.	Derived from the power consumption of the SCB.
SCB-EPS-REQ-4.2	[!]The SCB-EPS shall provide a peak power of at least 177 W during the operational phase.	Derived from the power consumption of the SCB.

4.12.3. SCB-EPS Sizing and Trade-off

The design of the SCB-EPS starts with a trade-off on the various design options. After this, several final concepts are left for consideration. These concepts are sized on the power generation, as well as power storage, such that the results can be considered for a final trade-off and a decision on the design is made. This sizing is initially done with estimated values to determine the results of the trade-off. After the design choice is made and components are selected, the sizing model is updated with accurate values to determine the final design parameters. In Figure 4.27 the design options tree is shown for all the concepts considered. The concepts that are considered unfeasible or are not chosen are marked with red crosses and blue colours respectively. The concepts marked in green are the concepts that are sized and considered in the final trade-off.

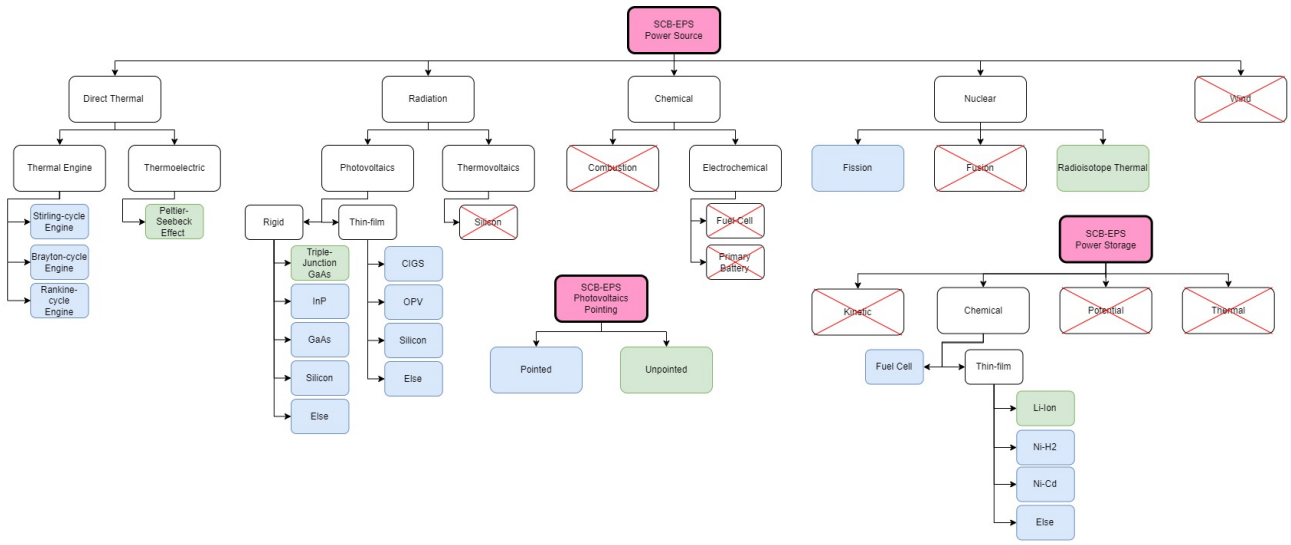

Figure 4.27: The design options tree of the SCB-EPS.

SCB-EPS Sizing EPS Power Generation

A simplified model is made to size the output power of each of the four power generation methods: Solar panels (SCB-EPS-CON-1), a thermoelectric generator (SCB-EPS-CON-2), a radioisotope thermal generator (SCB-EPS-CON-3) or solar panels combined with a thermoelectric generator (SCB-EPS-CON-4). All models are based on the path generated for the SCB, which consists of cycles of increasing and decreasing altitude, as well as its longitudinal location on Venus. The power generation is modelled for the worst case path, and is shown for one orbit around Venus in Figure 4.12.3. Due to the scattering of solar radiation in the Venusian atmosphere, the model of the solar power neglects the incidence angle of the sun on the solar panel, but models the solar flux based on the length of the path through the atmosphere [11]. All models are verified using various unit tests and comparison to hand calculations and are validated by generating graphs and comparisons to literature.

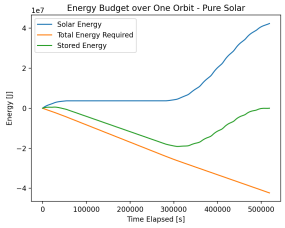

Figure 4.28: SCB-EPS-CON-1 energy budget.

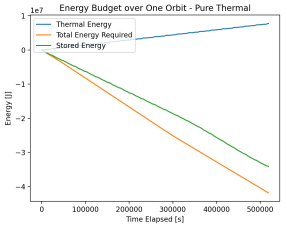

Figure 4.29: SCB-EPS-CON-2 energy budget.

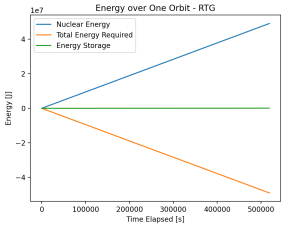

Figure 4.30: SCB-EPS-CON-3 energy budget.

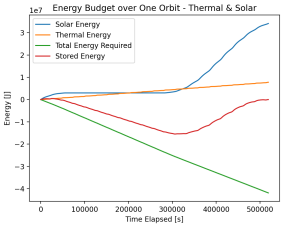

Figure 4.31: SCB-EPS-CON-4 energy budget.

SCB-EPS Sizing EPS Storage

The sizing of the SCB-EPS storage is done within the same models as the power generation sizing, and the results can also be seen in Figure 4.12.3. The model of the battery is the same for each of the four different power generation methods. It determines the charge or discharge of the battery based on the power excess or deficit between the generation and consumption of power. By cumulating this, the energy storage is determined. The model is verified using unit tests and simplified hand calculations and is validated by creating and inspecting graphs.

SCB-EPS Trade-off Results

The final scoring for the figures of merit of each concept are shown in Table 4.25. Within the table, if applicable, the most notable reasons for the scores are provided such as to give a small and concise insight in the trade-off process.

Table 4.25: The final trade-off results of the SCB-EPS.

	Risk: (30%)	Performance: (35%)	Schedule (10%)	Cost: (20%)	Sustainability: (5%)
SCB-EPS-CON-1	High TRL, simple system	Long eclipse duration drives the battery mass	No significant scheduling implications	Competitive pricing, low cost for small spacecraft	No significant effects
SCB-EPS-CON-2		Power requirements can not be met with limited surface area			
SCB-EPS-CON-3	High impact risks	Low mass, high power generation	No significant scheduling implications	Relatively high cost for small spacecraft	No significant effects
SCB-EPS-CON-4	Added complexity	Batteries smaller but still significant	No significant scheduling implications	Added costs due to complexity	No significant effects

Model Limitations, Verification and Validation

The model used in this section is limited to the atmosphere of Venus, and can be used for accurate initial estimates. However, for precise calculations it must be updated with more accurate calculations of solar flux. Nonetheless, it has been validated and verified using literature, hand calculations and unit tests.

4.12.4. SCB-EPS Final Design Overview and Evaluation

With the trade-off and the sizing finished, the final design of the SCB-EPS can be presented. The individual components selected for each part are documented first, then the sensitivity analysis performed and its results are described and the final design parameters are presented.

SCB-EPS Component Selection

The SCB-EPS consists of three major parts, the SAR for power generation, the batteries for power storage, and the PCD for the distribution of power. For each of these parts, the component and its most important characteristics are given below.

Table 4.26: The SCB-EPS-SAR specifications.

Part	Component	Efficiency @28° C [%]	Voltage [V]	Documentation
SAR	Triple junction GaAs	26.8	2.26	[59] [58]

Table 4.27: The SCB-EPS-BAT specifications.

Part	Component	Specific energy density [Wh/kg]	Volumetric energy density [Wh/L]	Documentation
BAT	GomSpace BPX 4S-2P	150	228.7	[59] [31]

Table 4.28: The SCB-EPS-PCD specifications.

Part	Component	Mass [kg]	Volume [L]	Peak output [W]	Output voltages [V]	Documentation
PCD	Pumpkin EPSM 1	0.300	0.25	160	3.3-50	[59]

SCB-EPS Sensitivity Analysis

To determine how stable this design is, the most important input variables have been increased and decreased in the model. The results of these changes are documented in Table 4.29. It can be seen that the change in altitude mostly has an effect on the solar array size. This is due to the change in solar radiation. To allow for further design changes, a margin of 10% has been applied to the power consumption input before sizing. Next to that, the batteries as well as the solar panels can be scaled up to allow for larger power budgets or lower altitudes.

Table 4.29: The sensitivity analysis results of the SCB-EPS.

Parameter changed	Change	SAR area (%)	SAR mass (%)	BAT capacity (%)	BAT mass (%)
Output power	+10%	+10.81	+10.10	+10.00	+10.01
Output power	-10%	-9.46	-10.10	-10.00	-9.99
Altitude	+10%	-13.51	-13.94	+0.12	+0.12
Altitude	-10%	+17.57	+16.35	-0.05	-0.04

SCB-EPS Final Design Parameters and Evaluation

The most important final design parameters of the SCB-EPS are presented in Table 4.30. The mass and volume include the total mass of all components used in the SCB-EPS. For the determination volume of the SAR, a thickness of 1mm is used, which is based on the solar cell thickness, as well as the thickness of additional layers such as thermal insulation, structural rigidity, radiation protection and paint.

Table 4.30: The final design parameters of the SCB-EPS.

Total Mass [kg]	Volume [L]	Solar array size [m^2]	Battery capacity [Wh]	Average power output [W]
69.3	48.2	0.74	8033	84.5

4.13. Spacecraft Bus Mechanisms

The SCB requires multiple mechanisms in order to deploy all the relevant components. Some of these operations need to be done during deployment, while others need to happen during SCB operations. In this section the functions and the architecture are analysed in Subsection 4.13.1, followed by an overview of the final design in Subsection 4.13.2.

4.13.1. SCB-MEC Functional and Architecture Analysis

There are 5 different mechanical systems in the SCB, consisting of 15 different elements. The following sections first explain the design choices made, after which the actual implementation on the SCB are shown using images from the CAD design.

SCB-MEC Functional Allocation

The 5 mechanisms of the SCB are:

- 6 deployable antennas
- 1 boom for the REMS instrument
- 3 spools containing a rope that is connected to the balloon module
- 2 tank release mechanisms
- 3 EDV rope connection points

This counts up to the earlier mentioned 15 elements. The designs of the mechanisms are as follows: The antennas are deployed by making use of torsional springs. While being retracted, the antenna is held down by the balloon module above. Once the SCB is lowered it automatically extends.

The boom uses 2 electromotors to power its 2 rotational joints. Once deployed the system locks in place, but has the option to unlock and re-orientate if necessary.

Each spool has a clamping mechanism limiting the speed the spool can unwind at. During deployment the IMU controls this mechanism to ensure all 3 are deployed at the same speed. This mechanism also holds the SCB weight during deployment, before the SCB is lowered relative to the EDV.

The tank release mechanism is deployed by use of 2 pyrotechnics per side. These separate the structure holding the tank. The EDV rope is also released by use of 2 pyrotechnics at the connection points.

SCB-MEC Systems Architecture

Figure 4.32 shows the geometry of the 5 different mechanisms from left to right in the same order as the list above. The top row corresponds to the geometry before deployment, and the lower corresponds to that after deployment.

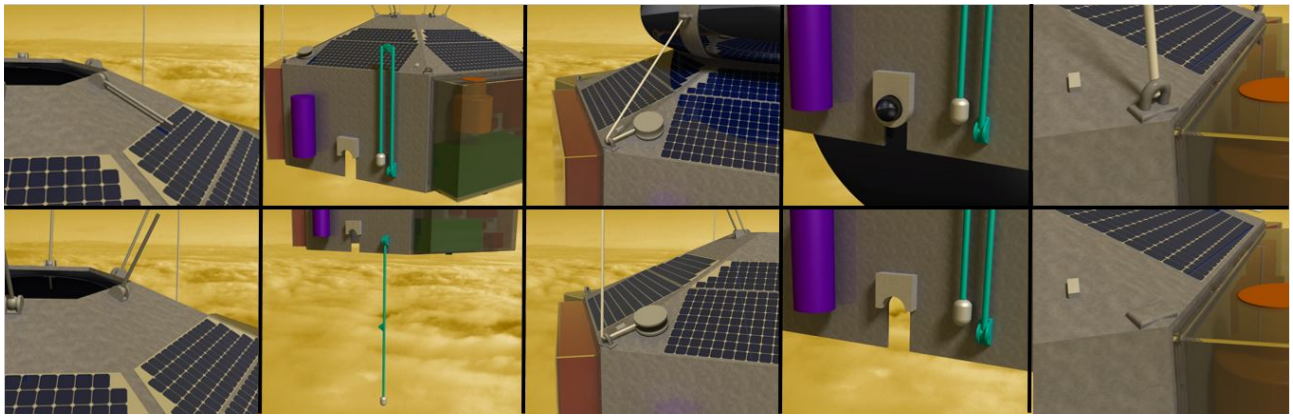

Figure 4.32: The mechanisms before (top) and after (bottom) deployment.

The following key requirements for the SCB-MEC are identified, based on the analysis presented above, and its allocated budgets:

Table 4.31: The key SCB-MEC subsystem requirements, driving requirements are marked with [!].

ID	Description	Rationale
SCB-MEC-REQ-1.1	[!]The SCB-MEC shall be able to lower the SCB relative to the balloon module	Required for stability purposes and antenna deloyment
SCB-MEC-REQ-1.2	[!] The SCB-MEC shall be able to release the Tank	Required for sufficient altitude performance
SCB-MEC-REQ-1.3	[!]The SCB-MEC shall be able to release the EDV lowering ropes	Required to be able to detach from the EDV.
SCB-MEC-REQ-2.1	The SCB-MEC shall be able to deploy the boom	Required for correct functioning of REMS module

4.13.2. SCB-MEC Final Design Overview and Evaluation

The final design consists of mechanisms which have an extensive heritage in spaceflight and have been proven successful and reliable in previous comparable missions. Pyrotechnics specifically have been proven to be extremely reliable and accurate. The most complex and expensive mechanism consists of the motors for the boom joints, however these do not need to be very accurate and do not need to survive for the full mission span.

4.14. Spacecraft Bus Structure

The subsystems of the SCB are linked by the SCB-STR, which carries the loads, while offering support and protection to other parts of the vehicle. In this section the main functions and architecture are discussed, followed by the sizing procedure and lastly, the final design is presented and evaluated.

4.14.1. SCB-STR Functional and Architecture Analysis

In this section, the functions performed by the SCB-STR are presented, along with the general architecture.

SCB-STR Functional Allocation

From Section 2.2, it can be derived that the main function to be performed by the SCB-STR is ”Maintain structural integrity of the SCB”, as shown for instance by function F6.6.3.1. In order to achieve this, the structure needs to be able to withstand all loads that it is exposed to during the entire mission duration, apart from end of life decommissioning.

SCB-STR Configuration

At this stage of the design process the analysis of the structure of the SCB is limited to the main structural components. Looking at figures 4.12 to 4.15, it can be noticed that the layout calls for a balloon module attached directly underneath the balloon, and a gondola which hangs below it using three ropes. Moreover, during the deployment phase, function F5.4.2 calls for the SCB to be slowly lowered and deployed from the EDV, after which the balloon gets inflated. To create enough space to complete the inflation, the ropes that lower the SCB need to be cut, meaning a different rope has to take up the weight of the SCB. This rope runs inside the balloons, from top to bottom of the zero pressure balloon.

From these functions, the main structural components are identified to be: The gondola’s structure, the balloon module’s structure, the three lowering ropes for the gondola, and the rope that runs vertically through the balloons. The three ropes used to lower the SCB from the EDV follow the same sizing process as the others, but are considered part of the EDV-MEC and are therefore treated in Section 5.12. Figure 4.33 shows a schematic of the components mentioned in this section.

4.14.2. SCB-STR Key Requirements

The following key requirements for the SCB-STR are identified, based on the analysis presented above, and its allocated budgets:

Table 4.32: The key SCB-STR subsystem requirements, driving requirements are marked with [!].

ID	Description	Rationale
SCB-STR-REQ-1.3	[!] The SCB STR shall be able to withstand an acceleration of 50 g	Based on entry loads.
SCB-STR-REQ-1.7	[!] The SCB STR shall not have an overall volume in its folded/undeployed state within the EDV that exceeds 0.19 m^3.	Based on volume budget.
SCB-STR-REQ-1.12	The SCB STR shall provide a structural support to all other subsystems during the entire operations of the SCB	-

4.14.3. SCB-STR Structural Analysis and Sizing

In this section the structural analysis and sizing of the components that are mentioned in Subsection 4.14.1 is treated.

Gondola

The basic concept for the structure of the gondola is determined to be a hexagon composed of multiple vertical panels, as shown in Section 4.4. This is due to packaging requirements inside the EDV, as the main hydrogen

tanks and SCB's subsystems heavily constrain the space, and therefore also the shapes available for the gondola's structure. Because of this, the main dimensions are set and the structural analysis performed looks mainly into the thickness of the panels and the material choice.

For this preliminary analysis, it is decided to take a worst-case scenario approach. Due to time and resource limitations, each panel is analysed individually, hence without taking the stiffening effect of adjacent panels into account, nor that of the triangular upper section of the gondola. All panels are loaded with other subsystems and components on the outer face, but they are all lighter than the batteries, meaning that the main loading case for the panels is a bending scenario where the base is approximated to be clamped, and each panel has to hold half of the total weight of SCB batteries, which are distributed across two different panels. The critical condition for the structure is during atmospheric entry, where it experiences up to 50 g of deceleration, while resting on the internal structure of the EDV. Because the main hydrogen tank rests on top of the internal structure of the EDV, its weight is not taken into account in the structural analysis. Figure 4.34 shows the loading scenario used for sizing for one of the two panels that carry the batteries.

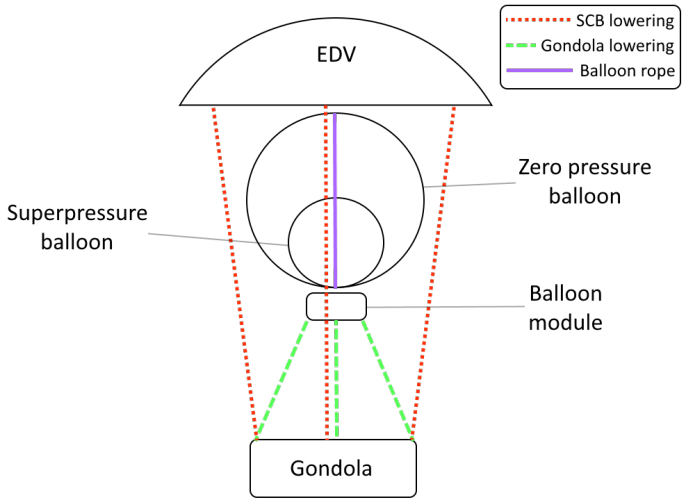

Figure 4.33: Schematic of the three rope groups used in the SCB structural design.

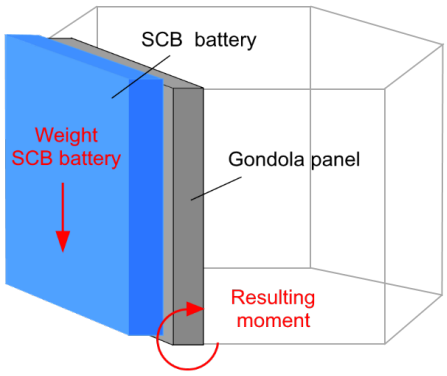

Figure 4.34: Schematic of the moment created in a panel of the gondola by the weight of the batteries.

A python program is made to calculate the required panel thickness, given the width and height of the panels and the geometry and weight of the batteries. The analysis is performed for a series of materials, namely titanium, stainless steel, aluminium, carbon fiber reinforced polymer and a sandwich structure composed of an aluminium honeycomb and aluminium face sheets. It is found that the carbon fiber and sandwich structures are the lightest overall, and the latter is chosen for the second phase of the sizing process due to its simplicity and the fact that it uses a unique material.

In the following phase, the thickness of the aluminium sheets and the spacing between them has been optimised, while ensuring that the normal stress through the metal sheets is within acceptable ranges. For simplicity the triangular panels on the top of the gondola are assumed to have the same thickness and spacing as the side panels. The final design includes a 1.25 design safety factor, and a 1.1 factor to account for the weight of parts used to link the panels together and attach the instruments and other components to it.

Since aluminium has a bad chemical compatibility with sulfuric acid, all the panels are anodized with a layer of coating.

Balloon Module

Due to time and resource constrains it has not been possible to perform an accurate analysis of the balloon module. Furthermore, this component constitutes the interface between the balloon and the gondola, hence an analysis of the exact design is deemed too advanced for this stage of the design. Although, a generic structure is made for the CAD model and paths are provided for all the known loads. Ultimately. the weight of the balloon module is assumed to be 7 kg, a rather conservative estimate considering its volume is less than half the one of the gondola and the structure is much more compact than the hexagonal shape of the gondola.

Ropes
For simplicity, the ropes are all sized using the same material, namely vectran [93], a high-performance liquid crystal polymer fiber. Vectran is chosen because of its remarkable strength, low permeability, UV, chemical, and cut resistance, and favorable thermal properties, other than a satisfactory chemical match with sulfuric acid. A model is made to estimate the thickness and therefore the mass of all the rope groups based on the number of ropes and the loads they have to carry. Margin factors are used to account for the worsening of the performance due to sulfuric acid, UV radiation, and temperature range, along with a 1.25 design safety factor.

Model Limitations, Verification and Validation
One of the main assumptions the SCB-STR structural model makes is that material properties and model geometry is linear. Given the high stiffness of the sandwich structure used for the gondola and vectran for the ropesV, deformations are small and loading stays within the elastic region. Furthermore, a safety margin was applied. Hence, this assumption is acceptable. To verify the model, hand calculations are performed for the equations as well as face validity of the results. Validation of the model could be performed using a commercial finite element method solver; however, as the equations used to size the structure are accepted across the engineering industry, it is fair to say that the results are realistic.

4.14.4. SCB-STR Final Design Overview and Evaluation
In this section the final design for the structure of the SCB is presented.

SCB-STR Sensitivity Analysis
The sensitivity performed on the inputs shows as expected that the mass grows proportional to changes in the inputs, and the conservative approach used, especially for the gondola's structure, allows sufficient margin for later changes in the design.

SCB-STR Final Design Parameters and Evaluation
The final design of the gondola consists of an hexagon made of six aluminium sandwich panels 46.8 mm wide and 69.7 mm high. The metal sheets are each 0.55 mm thick and the honeycomb structure is 15 mm thick. The total mass, including the triangular panels on the top of the gondola and the various factors previously described, is 16.03 kg.

The temporary design for the balloon module consists of a mass of 7 kg and a volume of 0.023 m^3. The final design for the ropes consists of a balloon rope 1.7 mm thick with a mass of 41 g, while the three ropes used for lowering of the gondola are each 0.8 mm thick and have a mass of 15 g. All ropes are made of vectran [93]. The volume of the ropes is in the order of 4 cm^3.
The results for the ropes and for the gondola panels are verified by hand calculations.

4.15. Spacecraft Bus Thermal Management System
The SCB thermal management system is the subsystem responsible for keeping the other SCB subsystems within their defined temperature ranges. This sections covers the functions and architecture of the REL-SCB, as well as the thermal analysis and sizing of the components that lie therein.

4.15.1. SCB-THE Functional and Architecture Analysis
The functions of the SCB-THE are described below, after which the architecture is outlined. Lastly, an overview of the hardware used in the REL-THE and how they are interfaced with other subsystems is presented.

SCB-THE Functional Allocation
The main functions of the SCB thermal system are to maintain the payload within their operating and non-operating temperature ranges during the operational phase (F6.6.2) and the SCB during the operational phase (F6.9.2), as well as decommissioning (F7.3.2). This involves monitoring the temperature of the different subsystems, identifying those whose temperatures fall outside of the operating range, and adjusting the temperature to be within the bounds.

SCB-THE Systems Architecture

The SCB-THE comprises of three components: the insulation (INS), cover (COV), and heat pipe (PIP). The INS is responsible for insulating the SCB internals from the environment, the COV is responsible for emitting dissipated heat to the environment, and the PIP is responsible for providing a heat transfer path between the internals and the COV.

SCB-THE Hardware Block Diagram and Configuration

Figure 4.35 shows the hardware block diagram for the SCB-THE. $\dot{Q}_i$ represents the heat transfer for different elements. Heat is absorbed from and emitted to the environment by the COV; the INS receives this heat and reduces the heat transfer to the PIP, which acts as heat transport for the dissipated heat from the SCB to the environment.

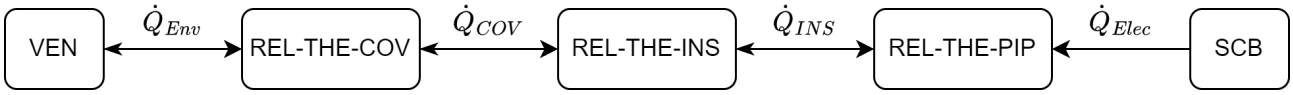

Figure 4.35: The SCB-THE block diagram.

4.15.2. SCB-THE Key Requirements

The following key requirements for the SCB-THE are identified, based on the analysis presented above, and its allocated budgets:

Table 4.33: The key SCB-THE subsystem requirements, driving requirements are marked with [!].

ID	Description	Rationale
SCB-THE-REQ-1.1	The THE shall monitor the temperature of the SCB during the entire mission.	Derived from F6.9.2.
SCB-THE-REQ-2.2	[!] The THE shall maintain the SCB subsystems within their operational temperature range of 273.15 K - 313.15 K during the entire mission.	Derived from F6.9.2.
SCB-THE-REQ-2.3	[!] The THE shall maintain the SCB subsystems within their non-operational temperature range of 253.15 K - 313.15 K during the entire mission.	Derived from F6.9.2.

4.15.3. SCB-THE Trade-off Studies

The design options for the SCB-THE can be seen in Figure 4.36. Electrical heating has been dismissed, since the subsystems do not get cold enough to merit heating. Furthermore, active loops and passive control are not needed, since the thermal balance can be achieved with passive heat transfer, which is shown in Subsection 4.15.4. For those that are feasible but not selected, the extremely low thermal conductivity of MLI is not needed for the temperatures on Venus and thermal conductance lies inferior to heat pipes in total heat transfer capabilities.

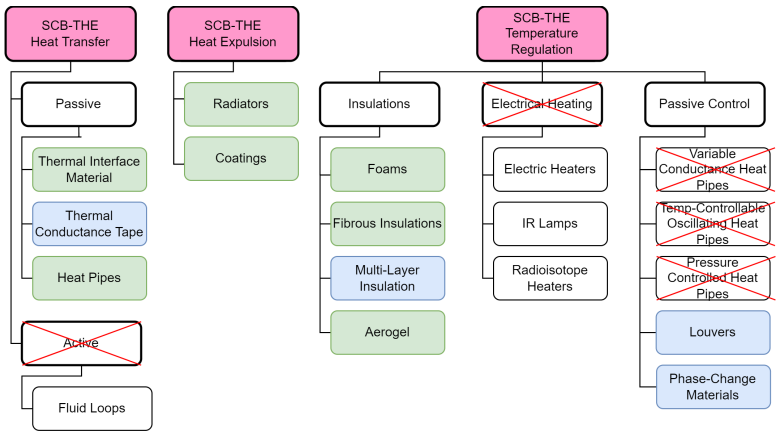

Figure 4.36: Design option trees for the SCB-THE.

4.15.4. Spacecraft Bus Thermal Analysis

The operating and non-operating temperatures ranges of the components within the SCB must first be identified, where the battery limits both the lower and upper bounds. The non-operating temperature range is 253.15-313.15 K, with the battery again limiting both bounds. From this, the operational environment of the SCB must be considered.

Solar radiation from the Sun, albedo radiation reflected from the Venusian surface, infrared energy radiated by Venus, and dissipated heat from the internal components comprise the sources of heat that are being absorbed by the REL. Consequently, heat is radiated away from the REL to the atmosphere. Note, due to the presence of the Venusian atmosphere, convective heat transfer also occurs. Thermal equilibrium occurs between the heat being absorbed and emitted, shown in Equation 4.10, where the heat absorbed and heat emitted can be calculated using Equation 4.11 and Equation 4.12, respectively. These equations are obtained from [17].

$$\dot{Q}_{absorbed} + \Sigma P_{dissipated} = \dot{Q}_{emitted} \tag{4.10}$$

$$\dot{Q}_{absorbed} = \dot{Q}_s + \dot{Q}_a + \dot{Q}_{IR} = \alpha_s \cdot J_s \cdot A_s + \alpha_s \cdot a \cdot J_s \cdot F \cdot A_a + \alpha_{IR} \cdot \sigma \cdot T_{IR}^4 \cdot A_{IR} \tag{4.11}$$

$$\dot{Q}_{emitted} = \epsilon_{IR} \cdot \sigma \cdot A_r \cdot (T_{REL} - T_{Env})^4 + h_c \cdot (T_{REL} - T_{Env}) \cdot A_h \tag{4.12}$$

In these equations, the subscripts are used for the solar radiation (s), albedo (a), infrared radiation (IR), radiation (r), and convection (h). Note that the absorptivity in the IR range (α_{IR}) can be set equal to the emissivity in the IR range (ϵ_{IR}) according to Kirchhoff.

According to [41], "convection is so strong that the skin temperature rapidly saturates at the local atmospheric temperature". Hence, for this analysis, the effect of solar radiation, albedo, and planet flux is disregarded but is still accounted for by using low absorptivity materials. The convective heat transfer coefficient can be approximated for horizontal plates with Equation 4.13 and the Rayleigh number can be calculated using Equation 4.14, from [52].

$$h_c = \frac{0.27k}{L} Ra_L^{1/4} \tag{4.13}$$

$$Ra_L = \frac{\rho g \beta}{\eta \alpha} (T - T_{Env}) D^3 \tag{4.14}$$

These parameters are a function of the atmospheric properties (density, pressure, temperature) and thus vary over the SCB path. The following references are used to calculate certain CO_2 properties: dynamic viscosity [37]; thermal conductivity [53]; specific heat [91]. The variation in the convective heat transfer over the path can be seen in Figure 4.37. These results are validated against convective heat transfer measurements for Mars, which also possesses a CO2-rich atmosphere [78]. The thermal balance now reduces to Equation 4.15.

$$\Sigma P_{dissipated} = h_c \cdot (T_{REL} - T_{Env}) \cdot A_h \tag{4.15}$$

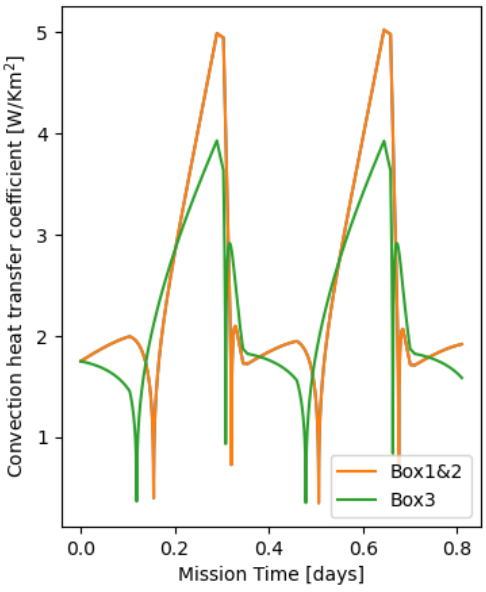

Figure 4.37: The variation in h_c over the mission time.

The power dissipated can be determined based on the electrical power consumed and the efficiency of the components. For the components for which no source values are found, an efficiency of 80% is assumed. Since the BAT and PCD do not necessarily consume power, the dissipated power is calculated based on the efficiency of these components to deliver the overall input power to the electronics. Since box 1 and box 2 contain the batteries, and box 3 contains the rest of the electronics, the power dissipated is different. The COV is used to interface with the Venusian atmosphere. Due to the cyclic nature of the path, the Venusian temperature range lies beyond the temperature range of the SCB, meaning that heat is both absorbed from and emitted to the environment over time. The SCB-THE can be adapted to make the most of the environment if more heating is

required, the next step is to decrease the COV area and add insulation; if more cooling is required, increase the COV area and remove insulation. In the case insulations are used, the heat transfer through the insulation can be calculated using Equation 4.16. This is iterated a few times to obtain the results in Figure 4.38. These results are logical, since the effect of the added insulation is that it decreases the amplitude of the cyclic temperature and shifts the range slightly upwards, as can be seen for box 3. Although box 3 lies within its temperature margins without insulations, the added use reduces the range, making it better both thermally and structurally. Boxes 1 and 2 do not need insulation, since their cyclic amplitude is relatively insignificant.

$$\dot{Q}_{MLI} = \frac{A_{MLI} \cdot k_{eff} \cdot (T_{MLI} - T_{REL})}{t_{MLI}} \tag{4.16}$$

To achieve the cooling needed for box 3, a double layer is used for the COV. On top of the assumed 1 mm thick main cover, there is an extra layer spaced from the main cover with a thickness of 0.5 mm. Furthermore, for box 3, an effective thermal conductivity of $7 * 10^{-3} W/(mK)$ is selected which falls within foams and fibrous insulations [21]. Furthermore, an insulation thickness of 0.5 mm *is obtained. For a fibrous insulation density of 100 kg/m^3 [21], this leads to an insulation mass of 0.338 kg. For boxes 1 and 2, no extra thermal solutions are needed to be employed from the main cover.

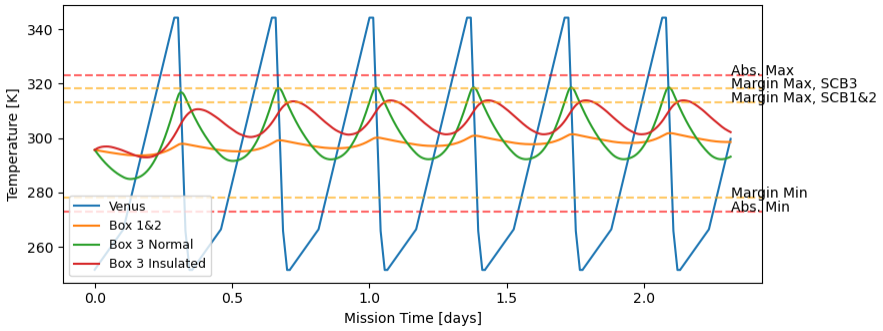

Figure 4.38: The SCB thermal range for boxes 1 & 2 (batteries), and box 3 (electronics) over the mission duration.

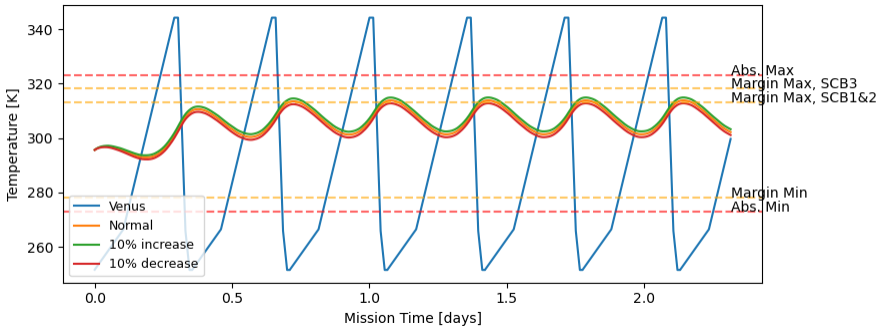

Figure 4.39: The sensitivity of internal temperature to increase/decrease of electric power consumption by 10% over mission duration.

Model Limitations, Verification and Validation

One of the main assumptions the SCB-THE thermal model makes is that heat transfer through convection is assumed to dominate over other thermal factors. In reality, these other factors have an effect on the resulting thermal balance, although for the level of analysis being performed here it is acceptable. This should be verified in the following iteration. To verify the model, hand calculations are performed for the equations as well as face validity of the results. Validation of the convective heat transfer was performed with respect to data provided for Mars, which is reasonable given the similarity in atmospheric composition.

4.15.5. SCB-THE Final Design Overview and Evaluation

With the thermal analysis and the sizing finished, the final design of the REL-THE can be presented. The sensitivity analysis performed and its results are described below, and the final design parameters are presented thereafter.

SCB-THE Sensitivity Analysis
A sensitivity analysis has been performed on the thermal analysis and sizing of the SCB-THE. For the SCB-THE, the main variables that are susceptible to change are the path parameters and the power dissipation of the electrical system, which comes from the design of other subsystems. For the change in path altitude, the convective heat transfer coefficient changes, and hence the heat transfer from the environment changes. It is difficult to determine the exact correlation of this change due to the parametric nature of the variables used to calculate h_c. However, it can be noted that if the path is spent longer times at lower altitudes, the SCB heats up beyond thermal temperature margins, but likely remains within the absolute bounds. For the change in power dissipation, the effect of an increase / decrease by 10% on the thermal balance can be seen in Figure 4.39. These changes have little effect on the thermal balance of the SCB.

SCB-THE Final Design Parameters and Evaluation
The final design parameters of the REL-THE are given in Table 4.34.

Table 4.34: The final design parameters of the SCB-THE.

Component	Size [m^3]	Mass [kg]	Source
INS	0.002	0.338	-
COV	TBD	0.086	From Section 4.14
PIP	-	0.500	Assumed

5
Entry and Descent Vehicle

The detailed design of the Entry and Descent Vehicle (EDV) is undertaken in this chapter. The EDV houses the SCB and its components and has to protect it from the moment it is released from the TRV into the Venusian atmosphere and then deploys the SCB into its specified altitude.

The functions and the constituents of the EDV following from the mission level are further elaborated in Section 5.1. This is followed by the categorisation of the requirements defined for this subsystem in Section 5.2. Then, a trajectory and deployment analysis is given for the EDV in Section 5.3 before considering the stability analysis in Section 5.4. Following that, Section 5.5 considers the entire vehicle design overview. Then the technical budgets derived for mass, volume and cost for the EDV are presented in Section 5.6, before the reliability and risk analysis in Section 5.7. Following this, the chapter delves into detailed design of the numerous subsystems of the EDV, starting with the Transmission and Command (TNC) in Section 5.8. Section 5.9 goes into the Onboard Data Handling (OBD), Section 5.10 goes into the Parachutes (PAR), Section 5.11 goes into the Electrical Power System (EPS). The mechanisms (MEC), structures (STR) and thermal (THE) designs are finally discussed in Section 5.12, Section 5.13 and Section 5.14 concluding the chapter.

5.1. Entry and Descent Vehicle Functional and Architecture Analysis
The EDV must fulfill several functions to ensure mission success. These functions are used to determine the subsystems, and subsequently the components that are needed in the EDV to perform these tasks, outlined in Subsection 5.1.1. This leads to the total architecture of the system, which is summarised in Subsection 5.1.2. The relations between the subsystems are then summarised in the functional N2 chart provided in Subsection 5.1.3.

5.1.1. EDV Functional Allocation
During transfer the EDV is attached to the TRV, which carries all the responsibilities during that period. Once reaching Venus, the EDV is responsible for entering the atmosphere safely (F5.1). While doing that it must store telemetry data (F5.2) and communicate that data to the REL (F5.3). When the conditions during entry are

correct it starts the deployment of the EDV-MEC systems (F5.4). Once that is complete the EDV must start deploying the SCB (F5.5). When the SCB is ready for flight under its own power, the EDV must release it and dispose of itself (F5.6).

5.1.2. EDV System Architecture

A block diagram demonstrating the EDV system architecture can be seen in Figure 5.1. From this, one can assign functions of the EDV to the different subsystems, provided as follows: 81

1. OBD: Command system and handle data - F5.2.1, F5.3.3, F5.4.1, F5.5.1
2. TNC: Communicate with REL/SCB - F5.3.1, F5.3.2, F5.3.4, F5.3.5, F5.3.6, F5.3.7
3. ADC: Determine and control attitude - F5.5.1
4. EPS: Supply electric energy - F5.4.7
5. MEC: Deploy mechanisms - F5.4.2, F5.4.3
6. STR: Maintain structural integrity - F5.4.6, F5.5.2, F5.6.1
7. THE: Control temperature - F5.4.4

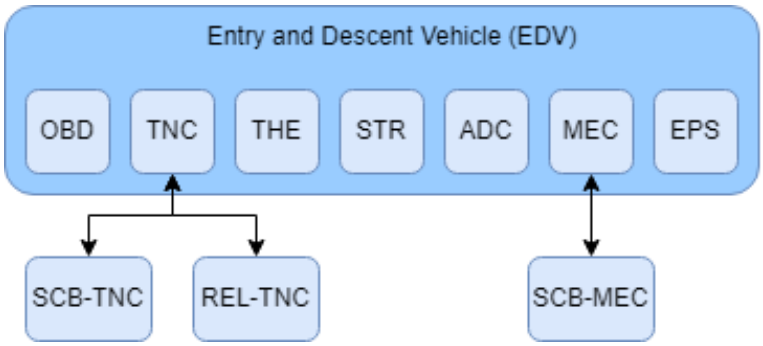

Figure 5.1: EDV system architecture.

5.1.3. EDV System N2 Chart

The N2 chart of the EDV is presented in Table 5.1. This table shows all the outputs of the subsystems in its rows and the columns represent the inputs for the subsystem. This chart is used to get an overview of the subsystems of the EDV and how they are related.

EDV-OBD	House keeping data, Commands	Commands	Commands	x	x	Commanding of SCB deployment / heat shield separation	Commanding of parachute deployment
Housekeeping data, commands	EDV-TNC		Antenna pointing	x	x	x	x
Housekeeping data, commands	Power	EDV-EPS	Power			Power	Power
House keeping data, velocity and altitude	Distance to REL		EDV-ADC	x	x	Attitude	Attitude
Housekeeping data				EDV-THE			
Housekeeping data					EDV-STR		
Deployment status						EDV-MEC	
Deployment status							EDV-PAR

Table 5.1: The functional N2 chart of the EDV.

5.2. Entry and Descent Vehicle Requirements Definition

To be able to design the EDV it is necessary to have good system and subsystem requirements. These can be flowed down from the functional and architectural analysis. This is done through the intermediate step of

creating a requirements breakdown tree. Driving requirements are marked with '[!]'.The requirements displayed in the following table do not represent all the 32 system requirements derived for the EDV.

Table 5.2: The key EDV system requirements, driving requirements are marked with [!].

ID	Description	Rationale
EDV-REQ-1.1	[!] The EDV shall survive structural launch loads of 50 g.	Derived from F5.4.
EDV-REQ-2.2	The EDV shall be deployable by the TRV.	Derived from F4.6.
EDV-REQ-2.3	The EDV shall be placed in a trajectory within the equatorial plane with a maximum drift of 4° in latitude.	Derived from F4.6.
EDV-REQ-3.1	[!] The EDV shall follow the TRA-EDV.	Derived from F5.3.
EDV-REQ-3.2	[!] The EDV shall release the SCB at 54.44 km.	Derived from F5.6.
EDV-REQ-3.3	The EDV shall constrain the temperature range of the SCB between 250 and 373 K.	Derived from F5.3.
EDV-REQ-3.4	The EDV shall confirm the correct SCB deployment conditions are reached.	Derived from F5.4.
EDV-REQ-3.5	[!] The EDV shall release SCB into PAT.	The SCB needs to be deployed in its specified path.
EDV-REQ-4.1	The EDV shall establish connection link with REL.	Derived from F5.2.
EDV-REQ-4.3	The EDV shall transmit housekeeping data to the REL.	Derived from F5.2.
EDV-REQ-5.2	[!] The EDV's mass shall not exceed 550 kg.	- Failure to comply with this requirements might make it impossible to launch with the selected launcher.
EDV-REQ-5.3	[!] The reliability of the EDV shall be at least 0.95.	The EDV needs to contribute to the reliability of the mission in a way that ensure the overall mission reliability objective.
EDV-REQ-6.1	The EDV cost shall not exceed 70 $millionEUR$.	Flows from stakeholder cost requirements.
EDV-REQ-6.2	The EDV shall not leave any debris in the Venus' orbit.	Flows from stakeholder sustainability requirements.
EDV-REQ-6.12	The EDV shall be ready for launch in 2031.	Segment needs to be ready for launch in time.

As is visible in the above table, the EDV requirements are focused on delivering the SCB to the correct altitude and fully functioning.

5.3. Entry and Descent Vehicle Trajectory and Deployment Analysis

In the section, first the entry trajectory is analysed, followed by the descent trajectory and finally the deployment. Also the verification and validation of the code are explained.

5.3.1. Entry Trajectory

1140 $seconds$ or exactly 19 min before hitting the upper parts of the Venusian atmosphere, the EDV is spun up and released by the TRV. The TRV releases the EDV into a hyperbolic orbit past Venus of which the periapsis sits 78 km above the surface. It is vital that the final orbit does not deviate too far from the expected one, since the margins between bouncing off the atmosphere or experiencing too high g loads are very thin. If the orbit

is off by 15 km in the direction away from the planet, the EDV does not enter and never returns. If it is off by 15 km towards the planet, the G-forces exceed the maximum G's for the structure and the spacecraft is lost. This responsibility lays with the TRV and is thus not further worked out in this report. Finally, the TRV uses its thrusters to lower its own periapsis. This is done to ensure disposal of the vehicle and ensure a collision with the EDV is impossible.

After the 19 min cruise phase the EDV hits the upper atmosphere (250 km) with a velocity of 11.37 km/s and at an angle of 10.375 °. The trade-off during entry consists of finding a balance between maximum G-forces and total heating. This is because the use of an ablative heatshield makes the total heating more critical than the peak heating. This specific orbit has been chosen since it keeps the G-force manageable (36 g), while the total heating is also kept in check. Besides that, this periapsis altitude offers some leeway in case the TRV fails to place the EDV in exactly the correct orbit. This EDV path is shown from release up to entry in the figure below.

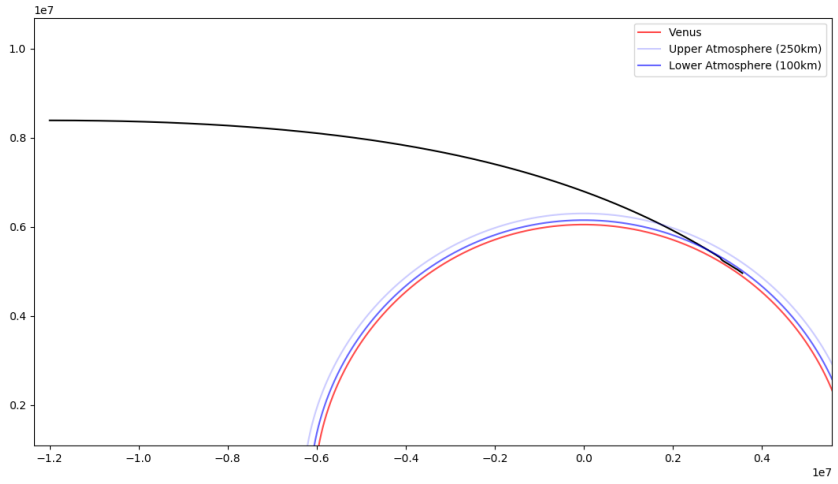

Figure 5.2: EDV path from deployment to entry.

5.3.2. Descent Force and Thermal Loads

The EDV does not experience significant thermal loads or G-loads until it goes below an altitude of 140 km. After crossing this limit, it slowly starts heating up without decelerating. Once it goes lower than 114 km the EDV also starts losing velocity due to drag. This delay continues throughout the entire entry with the peak G-loads happening 10 s after the peak Q-loads. This process is visible in the figure below, where the x-axis refers to the time since TRV deployment. A slight jump can be seen at 1550 s, this is due to a misalignment between the upper and lower atmosphere density model and can be neglected. Also visible in the G-force is, in this order, the deployment of the drogue, the deployment of the main parachute and the dropping of the heatshield. Figure 4.2 in the previous chapter also shows the path during this period.

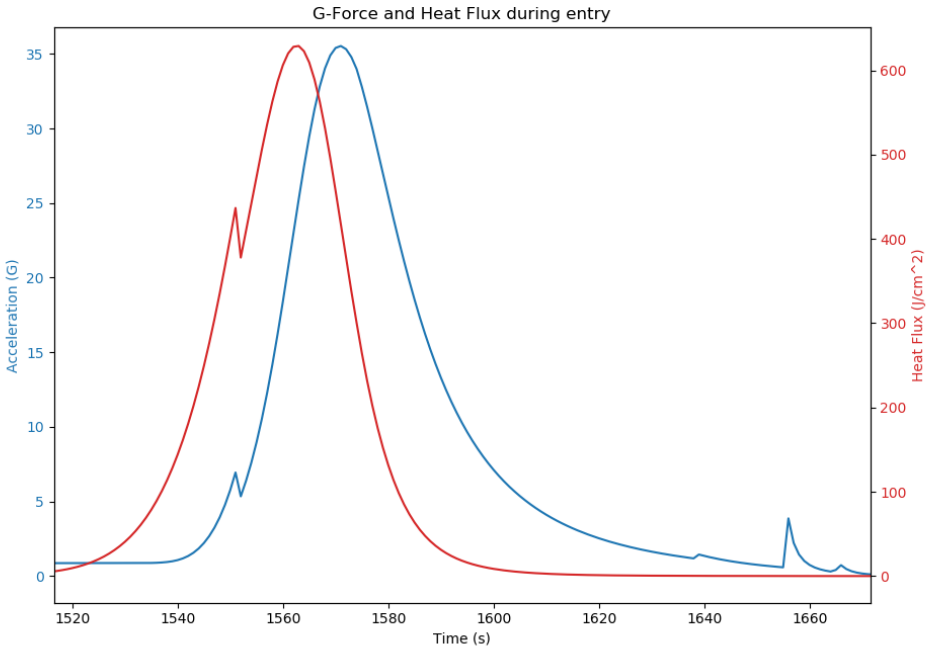

Figure 5.3: G-forces and heat flux.

5.3.3. Deployment Steps

After the velocity of the EDV has reduced to within the supersonic regime and the G-force has dropped below 2 g, an accelerator sends a signal to the mortar to fire the drogue parachute. This drogue parachute mostly helps for vehicle stability during the period of transonic velocity and does not provide a very large drag. This deployment starts a timer which triggers the following deployments. At 20 s the main parachute deploys which slows the EDV down considerably. At 30 s the heatshield is released as well. Finally at 32 s the lowering of the SCB starts, which takes 60 s to complete. After this the SCB commands the further deployment steps, except for the SCB release. This happens at an altitude of 54.44 km which is determined by a pressure sensor in the EDV IMU. This final deployment step happens 895 s or roughly 15 min after first hitting the atmosphere. It also symbolises the last operation of the EDV, which slowly keeps falling down until the heat or pressure ends its operation.

5.3.4. Model Limitations, Verification and Validation

To ensure the results of the trajectory and force analysis code are correct, it is verified by comparison to previous Venus entry missions. By modifying the vehicle parameters to equal those of the Vega 2 missions, the peak heating, total heating and peak G-forces are verified.

5.4. Entry and Descent Vehicle Stability Analysis

The EDV experiences strong aerodynamic forces during entry and therefore maintaining it in a correct and stable attitude is of great importance for a correct deployment sequence. It is decided during trade-off that the EDV does not have a dedicated system of its own for this purpose. Nevertheless the matter of stability needs to be addressed, this is done in this section, starting with an overview of the main functions to be performed by the ADC, a background on the preliminary trade-offs performed, and finally the chosen concept and justification.

5.4.1. EDV Stability Functional Analysis

The need for an attitude stabilization on the EDV comes indirectly from function F5.3.6.1 in Section 2.2, which says the EDV-STR shall maintain the integrity of the EDV during entry. Since the heat shield is placed only on one side of the EDV, the correct attitude is vital to the survivability of the vehicle. Therefore the main function to be performed by the EDV-ADC is that of maintaining the initial attitude of the vehicle during the entry sequence.

5.4.2. EDV-ADC Trade-off

During the mission concept trade-off of the EDV, two main solutions are found for the EDV-ADC: Using a RCS, or building an EDV that is aerodynamically stable and follows a ballistic entry. The latter is chosen mainly due to a better performance in terms of risk, which is valued higher than performance, the only area where the RCS performed better. This decision is the starting point for the stability design of the EDV, the detailed trade-off procedure can be found in previous work [2].

5.4.3. EDV-ADC Final Design Overview and Evaluation

Most previous missions that have flown to Venus used a sphere-cone shape and a spherical afterbody for their entry vehicle. The half-angle is usually around 40 to 55 °, and is set to 50 for the EDV of the LOVE mission, to follow these stable proven designs. To ensure aerodynamic stability, the center of gravity is placed as low as possible during entry. This is achieved by placing the main tank along the symmetric axis of the EDV, as close as possible to the heat shield.

It is decided to not include any attitude determination and control subsystem in the EDV for a series of reasons. Firstly the SCB does not have a specific location on the planet where it needs to land, the only requirement is to fall within 5 degrees latitude from the equator, therefore a high accuracy during landing is not required. Moreover, as explained in the previous section, the correct positioning of the center of gravity already ensures an aerodynamically stable entry vehicle. Finally, to improve the stability during flight and minimise the effect of inaccuracies during the detachment from the TRV, it is decided to spin stabilise the EDV and, since the latter does not need a propulsion or an attitude control subsystem, the TRV is given the role of spinning both vehicles before detachment. Adding a dedicated subsystem to the EDV increases the overall mass of both vehicles while, giving this role to the TRV only requires more propellant mass and allows to use an ADC that is already present and necessary for corrections during interplanetary flight and Venus entry.

To confirm that the EDV can actually be set on an accurate enough trajectory by the TRV and fall through the atmosphere by itself, the entry point is varied in a range of about 20 km. The EDV showed acceptable G-forces, peak heating and total heating, and this range is therefore deemed large enough for an accurate entry insertion with the TRV. The spin stabilisation requires the moment of inertia around the main axis of the sphere-cone shape to be the largest of all axis. This is confirmed through the CAD model, with a moment of inertia about 1.5 times larger than the next one.

5.5. Entry and Descent Vehicle Design Overview

The EDV is a vehicle that must be able to survive in extreme conditions. It must be able to withstand up to 50 g of acceleration while being heated to 3460 K. It must also keep the SCB protected and needs to house to parachutes. Finally, it must also store the balloon and communicate with the REL. All these requirements drive the design of the EDV and lead to the design shown in section 5.5.1. Furthermore, the chosen materials are also covered.

5.5.1. EDV Design Description

Below, in figure 5.4, the entire EDV can be seen with and without the SCB inside. As specified earlier, the EDV uses a 50 ° sphere-cone heat shield design. In the back the aeroshell protrudes to create space for the balloon module, packed balloon and the parachute bay. The yellow structure can be divided in an upper and lower section. The lower section is defined as the part that drops with the heat shield when it is released. Furthermore, the enclosed bay at the top of the EDV is called the parachute bay, which houses the parachutes among other things. Hanging below the parachute bay is the balloon bag, in which the balloon is folded.

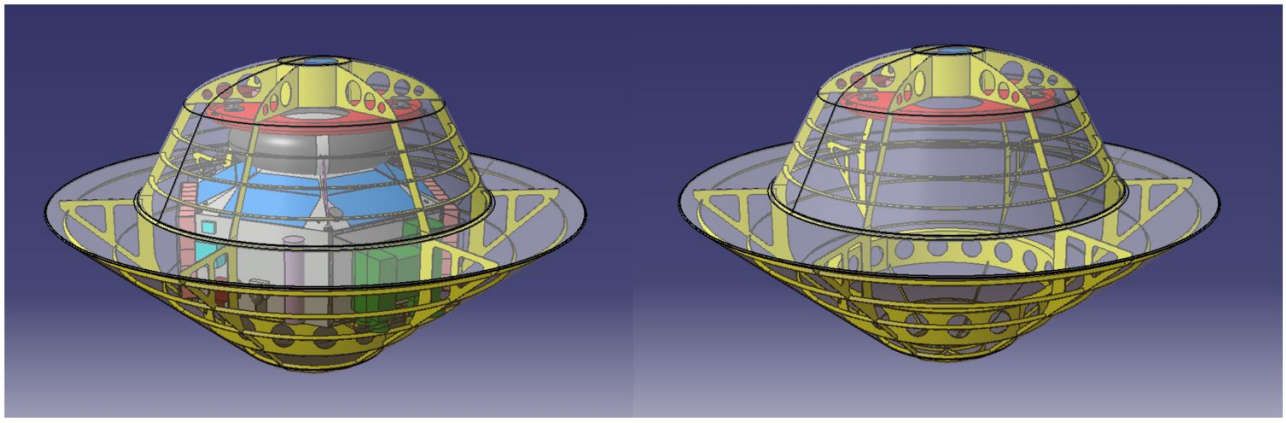

Figure 5.4: See-through EDV with and without SCB.

In figure 5.5 the lower and upper SCB structure can be seen. The entire structure is made out of aluminium-6061 due to its high strength to weight ratio and good heat resistance. The hydrogen tank is located at the bottom of the lower structure. Multiple structural elements are positioned there to transfer the deceleration loads to the tank. Above that is a large ring. This ring supports the SCB during the high load period. Finally the triangular structural elements, together with the circular stringers, transfer the forces on the heat shield to the rest of the structure.

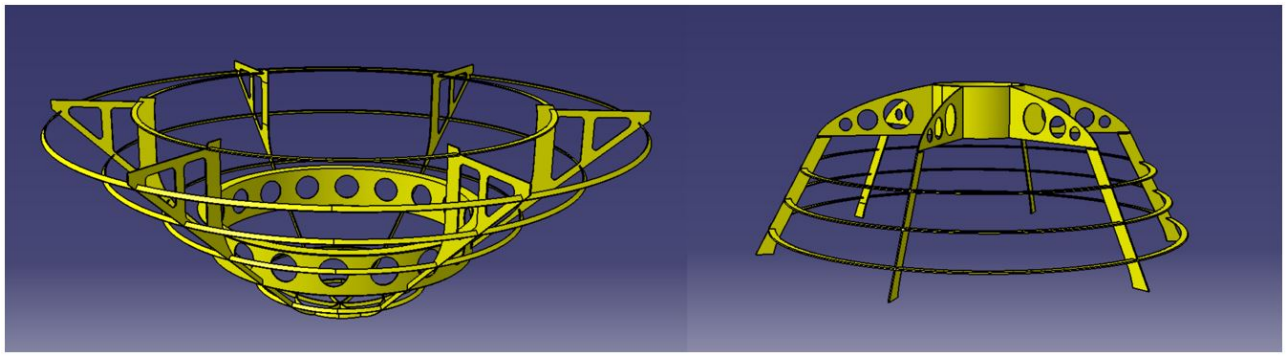

Figure 5.5: Lower and upper SCB structure.

The vertical beam elements in the upper structure are compression loaded during entry and require all three circular stiffeners to prevent them from buckling. The spar-like elements in the parachute bay distribute the force of parachute deployment to the rest of the structure.

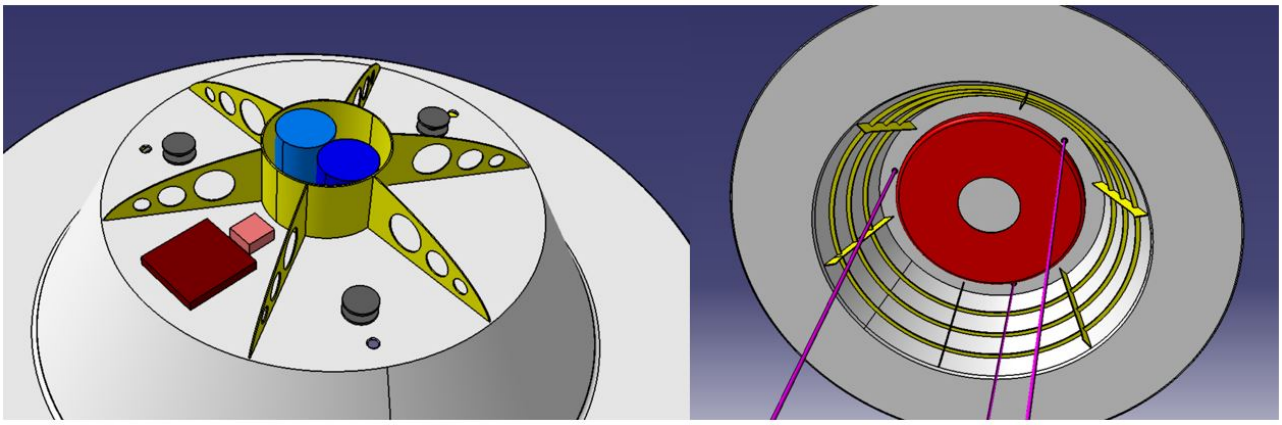

Figure 5.6: Parachute bay layout and the balloon bag.

In figure 5.6 the parachute bay layout is shown on the left side and the balloon bag is shown on the right. The parachute bay consists of the main parachute (dark blue), the drogue (light blue), the three spools for lowering

the SCB, the battery (pink) and finally the CPU and IMU (red). On the right side the balloon bag (red) can be seen as well as the pink ropes that lower the SCB.

Finally in figure 5.7 the outer EDV layers are shown, consisting of the heat shield and the aeroshell. The colours are true to the final design, chosen to minimise heating due to radiation during entry. The aeroshell is made of a 5 mm aluminium-6061, covered with a 2 mm coating of foam and then a very thin mylar-aluminium blanket. The heatshield also consists of 5 mm aluminium-6061 with a 62 mm cover of PICA heatshield material.

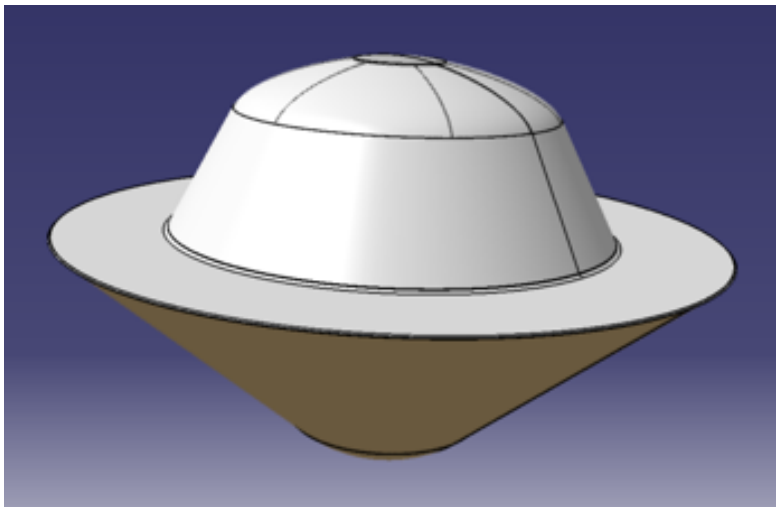

Figure 5.7: Heatshield and aeroshell.

5.6. Entry and Descent Vehicle Technical Budgets

The following tables; Table 5.3, Table 5.4 and Table 5.5 each show the technical budget for the EDV's mass, volume and cost respectively. Some of these estimations are made from SMAD[42] and it is to be noted that without the margin, all the initial requirements are complied with.

Table 5.3: The EDV mass budget.

Segment	**Mass [kg]**
EDV-ADC	0.00
EDV-EPS	0.50
EDV-MEC	3.00
EDV-OBD	0.10
EDV-PAR	1.35
EDV-STR	291.87
EDV-THE	142.00
EDV-TNC	1.50
EDV-PAR	367.50
Freefall mass	135.32
Total mass (kg)	**440.32**
Margin	**20%**
With 20% margin	**528.38**
Requirement	**550.00**
Compliant with requirement	**Yes**

Table 5.4: The EDV volume budget.

Subsystem	**Volume [m3]**
EDV-EPS	3.28E-04
EDV-ADC	0.00E+00
EDV-MEC	2.42E+02
EDV-OBD	2.42E-04
EDV-PAR	9.09E-04
EDV-STR	1.08E-01
EDV-THE	3.81E-02
EDV-TNC	9.29E-04
TOTAL VOLUME	**242.18**
Margin	**20%**
With 20% margin	**290.62**
Requirement	**300.00**
Compliant with requirement	**Yes**

Table 5.5: The EDV Cost Budget

Subsystem	Cost [FY2022 €k]
EDV-EPS	20.63
EDV-ADC	52379.93
EDV-MEC	
EDV-PAR	
EDV-STR	
EDV-THE	
EDV-OBD	628.28
Program	**12143.61**
TOTAL COST	**65172.45**
Margin	**20%**
With 20% margin	**78206.94**
Requirement	**70000.00**
Compliant with requirement	**No**

5.7. Entry and Descent Vehicle Reliability and Risk

This section describes the reliability and risk analysis for the EDV in Sections 5.7.1 and 5.7.2 respectively.

5.7.1. EDV Reliability Analysis

The total reliability of the EDV is provided in Table 5.6, similar to the preceding sections and derived from the method described in Section 2.7.

Table 5.6: EDV Reliability table.

Subsystem	Reliability [-]
EDV-ADC	1.00000
EDV-EPS	0.99998
EDV-MEC	0.99149
EDV-OBD	0.99966
EDV-PAR	0.99393
EDV-STR	0.99676
EDV-THE	0.99486
EDV-TNC	0.99996
TOTAL	**0.976838**
Prior to mitigation	**91.907%**

5.7.2. EDV Risk Map

As seen on Table 5.6, the reliability of the EDV prior to mitigation is 91.9% and afterwards has gone up to 97.7%. The risk map for the EDV showing the shifts caused by mitigation strategies is displayed in Figure 5.8.

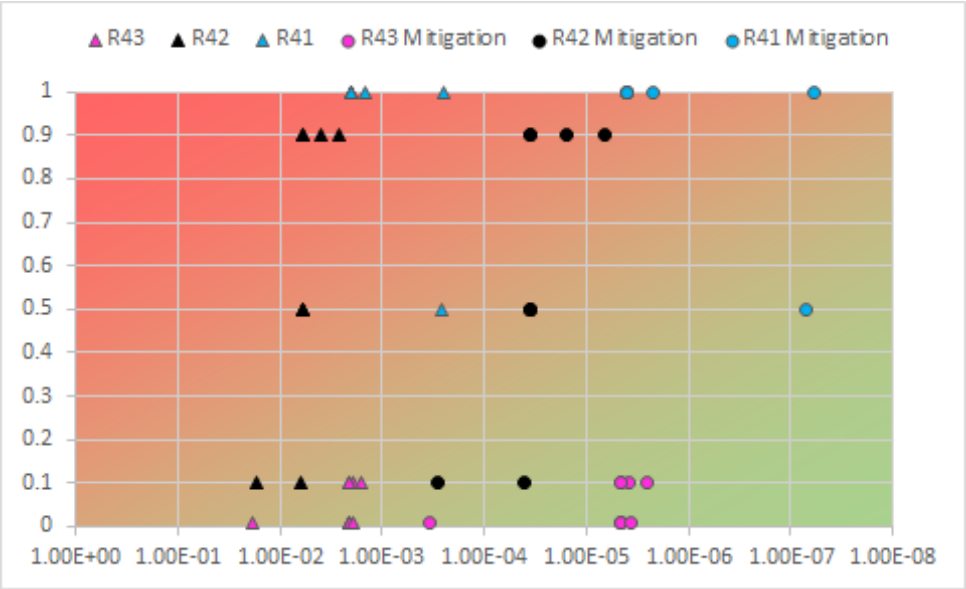

Figure 5.8: EDV Risk Map

The risks represented in the figure include the minor degradation, major degradation and total failure of all the different components in the EDV. The components with the largest probability of failures, represented by the triangles, are identified to be within the mechanisms; heat shield, lowering of the SCB, wire-cutting and EDV detachment. Using redundancy in design, accounting for margins and choosing highly reliable material options, the probability of these failures are largely reduced as shown by the circles.

5.8. Entry and Descent Vehicle Transmission and Command Subsystem

This section covers the architecture, sizing and selection of the EDV-TNC.

5.8.1. EDV-TNC Functional and Architecture Analysis

Before presenting the selected elements for the EDV-TNC, the architecture of the subsystem is discussed.

EDV-TNC Functional Allocation

The EDV-TNC's functions consist of establishing a connection between the EDV and the REL (F5.3.1), sending housekeeping data to the REL during descent (F5.3.2) and receiving any commands from the REL (F5.3.5), during phase 5 of the mission (Entry to Venus' atmosphere).

EDV-TNC Subsystems Architecture

The architecture for this subsystem is similar to that of the SCB-TNC architecture, since it contains 4 monopole low gain antennas and a transponder. The antennas are used by the transponder to establish a connection and receive/send data. Only 4 monopole antennas are included (unlike in the SCB), since 4 antennas are enough to establish an isotropic radiation pattern.

EDV-TNC Hardware Block Diagram

Due to its similarities to the SCB-TNC, the block diagram for this subsystem is essentially the same as the one displayed in Figure 4.17.

5.8.2. EDV-TNC Key Requirements

The following key requirements for the EDV-TNC are identified, based on the analysis presented above, and its allocated budgets:

Table 5.7: The key EDV-TNC subsystem requirements, driving requirements are marked with [!].

ID	Description	Rationale
EDV-REQ-4.2	[!]The EDV-TNC shall transmit sensor data to the REL.	Derived from F5.3.2.
EDV-REQ-4.3	[!]The EDV-TNC shall receive commands from the REL	Derived from F5.3.5.
EDV-REQ-4.6	The EDV-TNC shall transmit housekeeping data to the REL	Derived from F5.3.2.

5.8.3. EDV-TNC Trade-off

A trade-off is done for the transmission strategy of the EDV, whether to transmit directly to the CCC (ground), to both the CCC and the REL or only to the REL, which can be seen in Figure 5.9.

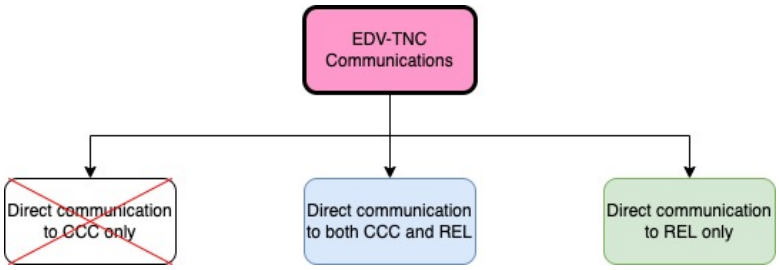

Figure 5.9: EDV-TNC Design Options Tree.

It is determined that the best option for the mission is to directly communicate to the REL only, since transmitting to the CCC as well implies having some sort of pointing mechanism, which adds an extra layer of complexity to an already difficult task, which is entering the Venusian atmosphere.

5.8.4. EDV-TNC Sizing

The sizing of the antennas and the transponder are shown in the following subsubsections.

EDV-TNC Sizing Antenna

The antenna is sized by estimating the worst case scenarios during entry and descent, which consider 2 REL positions and 2 EDV positions (just before entry and just after entry). Using a reference number from the Curiosity mission [48], an estimated link margin is obtained. It is assumed that a UHF communications band is used. From this sizing it is determined that an isotropic antenna that is able to transmit with 3.5 W of RF power is enough to establish a link between the EDV and the REL with a high enough bitrate (approximately 8 $kbps$).

EDV-TNC Sizing TNC Transponder

The sizing of the transponder heavily depends on the sizing of the antenna. Therefore, the transponder must be able to transmit in UHF, with an electrical power of at least 4.75 W which is what the antenna consumes.

Model Limitations, Verification and Validation

The model used to select the EDV-TNC components contained a set of assumptions which limit the accuracy of the model. First it was assumed that the communications link between the EDV and the REL would remain operational for the entirety of the descent period, however the conditions endured by the EDV system during re-entry may interfere with this link (which is why the EDV-TNC incorporates a data storage unit, to ensure all data is recorded). During the model creation, only a limited number of cases are considered - the 'worst-case' scenarios - where the distances between the EDV and the RELs was the largest. To verify the model of the link between the EDV-TNC and the REL system, the calculations done are verified manually by hand.

5.8.5. EDV-TNC Final Design Overview and Evaluation

This subsection briefly presents the final design of the EDV-TNC, including the selected components.

EDV-TNC Component Selection
It is found that the antennas used for the SCB-TNC are also compliant with the requirements for the EDV-TNC, thus the same antennas are selected, but only 4 (ANT-100 UHF Monopole Antennas). The transponder is also selected this way, such that the selected transponder is the IRIS V2 Transponder, similar to in the SCB-TNC.

EDV-TNC Sensitivity Analysis
A sensitivity analysis is carried out on the set of calculations that is used to verify the link margin, however it is not included in this document due to its trivial nature.

EDV-TNC Final Design Parameters
In Table 5.8 some of the properties of the selected components are listed. For more details on the antenna used, refer to Table 4.16.

Table 5.8: A summary of the properties of the TNC components for the EDV, where the 'IRIS V2 Transponder' also includes the SSPA and the LNA.

Component	Mass (kg)	Volume (cm^3)	Power (W)	Voltage (V)	Cost (FY2022 kEUR)	Sources
ANT-100 UHF/VHF Monopole Antenna (x4)	0.4	-	35	5	880.20	[72, 24, 42]
IRIS V2 Transponder (x1)	1.1	929.80		12 - 28		[57, 42]

The power is given as a single number, since the transponder takes in a fixed power and distributes it to the antennas.

5.9. Entry and Descent Vehicle Onboard Data Handling Subsystem
During descent, the EDV generates housekeeping data to inform the CCC of its status, and in case of failure, to know what went wrong. During this section, the architecture and components of the EDV-OBD are presented.

5.9.1. EDV-OBD Functional and Architecture Analysis
This subsection covers a brief explanation of the functions the EDV-OBD carries out, as well as an overview of its architecture.

EDV-OBD Functional Allocation
The EDV-OBD must receive, package, and send all the housekeeping data to the EDV-TNC for transmission (F5.2.1), during entry and descent. Once the descent is complete, the EDV-OBD must also confirm correct deployment conditions (F5.5.1) using data provided by the EDV's own sensors.

EDV-OBD Subsystems Architecture
The EDV-OBD contains a processor and a data storage unit. The former manages the generated data, processes it and packages it to be transmitted. The latter stores all the generated data to have an onboard backup, in case there are any losses during descent.

EDV-OBD Software Block Diagram
The software block diagram for the EDV-OBD closely follows the structure of the SCB-OBD software block diagram in Figure 4.19, thus it is not shown again.

EDV-OBD Hardware Block Diagram
Figure 5.10 shows the hardware block diagram for the EDV-OBD, depicting the connections between the OBD components and other EDV subsystems.

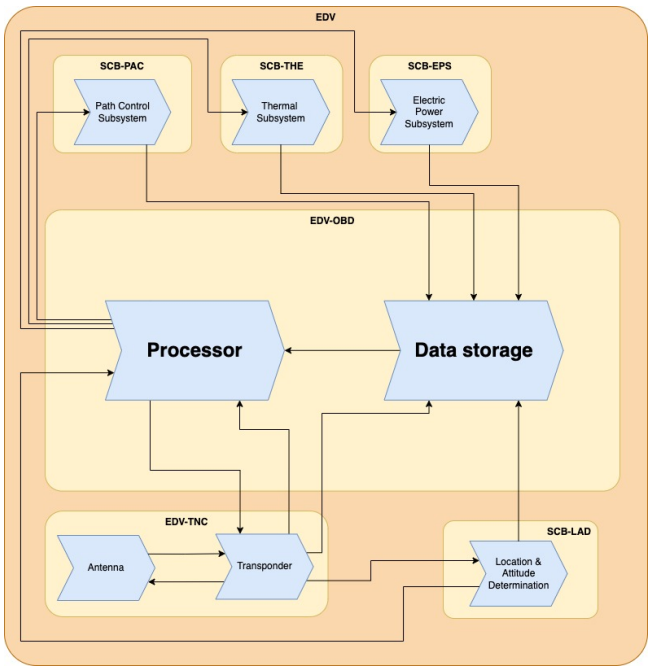

Figure 5.10: Block diagram for the EDV-OBD.

5.9.2. EDV-OBD Key Requirements

The following key requirements for the EDV-OBD are identified, based on the analysis presented above, and its allocated budgets:

Table 5.9: The key EDV-OBD subsystem requirements, driving requirements are marked with [!].

ID	Description	Rationale
EDV-OBD-REQ-1.1	[!]The EDV-OBD shall transmit signals to the REL for the duration of descent.	Derived from F5.2.1.
EDV-OBD-REQ-1.2	[!]The EDV-OBD shall send signals to the REL after descent.	Derived from F5.5.1.

5.9.3. EDV-OBD Trade-off

The trade-off for the EDV-OBD closely follows the SCB-OBD trade-off (in Figure 4.21), where for both trade-offs, the processing location and the processing approach are the same. However, unlike the SCB, it is chosen that for the EDV there is no processing between the EDV and the payload (the sensors in this case), since there is no need for processing for the data that is going to be generated by these sensors.

5.9.4. EDV-OBD Sizing

The EDV-OBD has two main components which have to be sized: The data storage unit and the processor. Both of these sizings are covered in this subsection.

EDV-OBD Sizing OBD Storage

The data storage is sized according to the maximum amount of data that is produced for the entirety of the descent, which is obtained using reference numbers from the Curiosity mission [48]. Thus the total required data storage is 0.9 $Mbytes$. Taking into account margins from ECSS [75], the total data storage must be no less than 1.35 $Mbytes$.

EDV-OBD Sizing OBD Processor

The sizing of the EDV-OBD-CPU is done according to the bitrate the processor must support. It is roughly estimated that the amount of data the processor has to take in is no more than 9 $kbps$. Taking a 100% margin as specified by ECSS [75], the total amount of data the CPU must be able to process is 18 $kbps$.

Model Limitations, Verification and Validation
This model is limited by the assumptions made in the EDV-TNC section Subsection 5.8.4, as a disturbance in the communications link between the EDV and the REL can affect the sizing of the EDV-OBD. Since the sizing of the OBD system was done according to reference data [48], verification and validation could not be carried out for the calculations done.

5.9.5. EDV-OBD Final Design Overview and Evaluation
This subsection compiles the various elements which make up the final design of the EDV-OBD.

EDV-OBD Component Selection
Taking into account the prior sizing, the data storage selected is the W25N512GVxIG/IT Flash storage [95] which is the same device used in the SCB-OBD. For the processor, the Texas Instruments MSP430 [40] is selected, since its communication interface's bitrate is higher than the bitrate produced by the EDV. Furthermore this processor has a low energy consumption.

EDV-OBD Sensitivity Analysis
No sensitivity analysis is done for the OBD, since the sizing is of a trivial nature.

EDV-OBD Final Design Parameters
Some of the general properties of the previously mentioned components are compiled in Table 5.10.

Table 5.10: A summary of the properties of the OBD components for the EDV.

Component	Mass (kg)	Volume (cm^3)	Power (W)	Voltage (V)	Cost (FY2022 kEUR)	Sources
TI MSP430	0.1	242.13	0.072	3.6	597.41	[40, 42]
W25N512GVxIG/IT	-	0.036	0.09	3		[95, 42]

Some of the values presented in this table are estimated from SMAD [42].

5.10. Entry and Descent Vehicle Parachute System
The EDV-PAR is used to slow the EDV from supersonic to subsonic velocities ahead of deployment of the SCB. In the following section, the EDV-PAR is designed. First, functions are assigned in Subsection 5.10.1. Then, the key requirements are presented in Subsection 5.10.2, the EDV-PAR is sized in Subsection 5.10.4 and the final design is discussed in Subsection 5.10.5.

5.10.1. EDV-PAR Functional and Architecture Analysis
Now, the functions of the EDV-PAR are allocated and the architecture is defined.
The main purpose of the EDV-PAR begins with the entry to the Venusian atmosphere (F5) as from Section 2.2. The two components in this subsystem, the drogue and the main chute, shall be ejected at their specified dynamic pressures and velocities while remaining structurally intact. This serves the purpose of reaching the desired deployment conditions for the SCB (F5.3.3).

5.10.2. EDV-PAR Key Requirements
The following key requirements for the EDV-PAR are identified, based on the analysis presented above, and its allocated budgets:

Table 5.11: The key EDV-PAR subsystem requirements, driving requirements are marked with [!].

ID	Description	Rationale
EDV-PAR-REQ-1.1	[!]The parachutes shall survive structural launch loads of 10 g.	Derived from F3.
EDV-PAR-REQ-1.2	[!]The parachutes shall survive a vibrational frequency of 25 Hz.	Derived from F3.

Table 5.11: The key EDV-PAR subsystem requirements, driving requirements are marked with [!].

ID	Description	Rationale
EDV-PAR-REQ-2.1	[!]The parachutes shall stay at a minimum temperature of 223.15 K.	Derived from F4.
EDV-PAR-REQ-3.1	[!]The drogue chute shall be ejected at a dynamic pressure of 1082 Pa.	Derived from F5. .
EDV-PAR-REQ-3.2	[!]The terminal velocity of the EDV after drogue deployment shall be 170 m/s.	Derived from F5.
EDV-PAR-REQ-3.3	[!]The drogue chute shall stay structurally intact at a dynamic pressure of 1082 Pa.	Derived from F5.
EDV-PAR-REQ-3.4	[!]The drogue chute shall pull out the main chute at a dynamic pressure of 713 Pa.	Derived from F5.
EDV-PAR-REQ-3.6	[!] The terminal velocity of the EDV after main chute deployment shall be 70 m/s.	Derived from F5.
EDV-PAR-REQ-3.7	[!]The main chute shall stay structurally intact at a dynamic pressure of 713 Pa.	Derived from F5.

5.10.3. EDV-PAR Trade-off

The first consideration for the EDV-PAR component is the number of deceleration stages. After a preliminary calculation that matches previous interplanetary missions of this level, it is found that having only one stage/one parachute results in too high shock loads for the EDV. For a smoother deceleration, the design choice of having a drogue parachute for the initial descent followed by the main parachute is made.

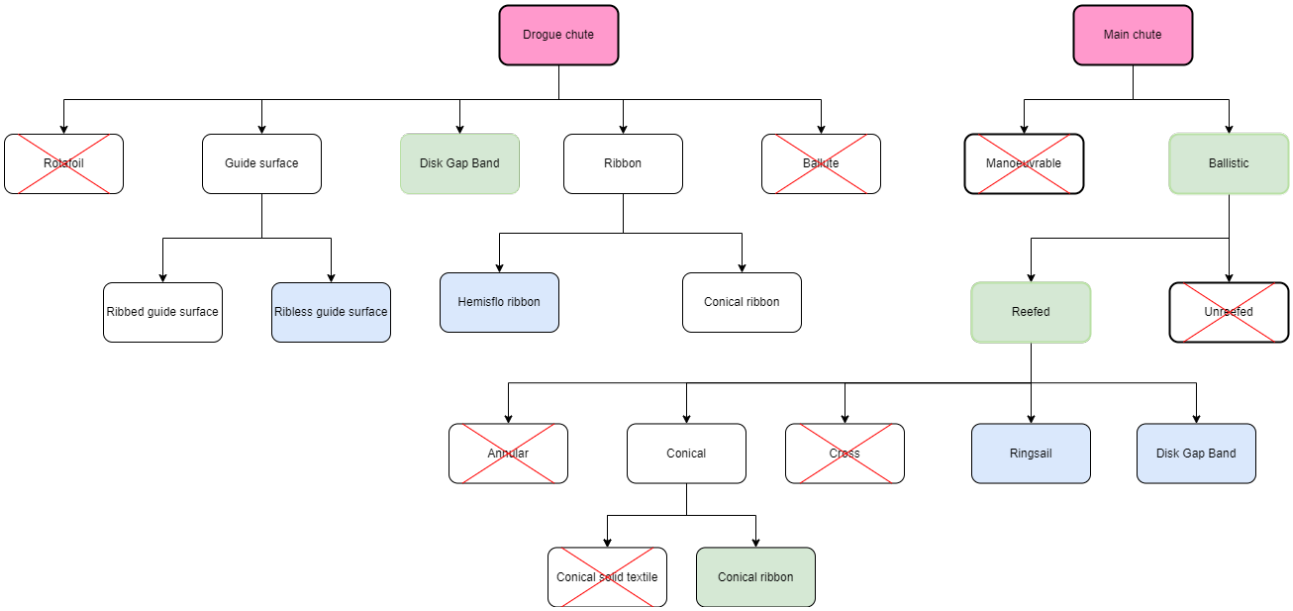

Figure 5.11: The Design option trees for the main and drogue parachute.

Considering that the entry is direct and ballistic, it is mandatory to have a parachute ejection by a mortar or drogue gun. For the dynamic pressures expected at entry, the choice is made to have the drogue parachute be ejected by a mortar. After mortar ejection and depending on the type of drogue parachute oscillation, the main parachute can be deployed by the drogue which is the weight and space saving option, compared to having another mortar or separate ejection mechanism. Thus, a variety of options for the drogue and main are considered for the best pairing. Figure 5.11 shows that the final choices are the disk-gap-band (DGB) and a conical ribbon for the drogue and main respectively. While the DGB allows for trading between stability and drag up until production, both the DGB and conical ribbon parachute types offer high stability and have a lot of favorable

heritage data for high density atmosphere profiles. The main is reefed to allow for longer inflation times to have lower peak forces and longer descent times.

5.10.4. EDV-PAR Sizing

The EDV-PAR sizing takes into account the main driving factor, the terminal velocity. This is followed by a sensitivity analysis and a presentation of the final parameters.

EDV-PAR Sizing for Terminal Velocity

The first consideration for sizing the parachutes is the desired altitude for the beginning and end of the balloon inflation as well as the time for this. This sets the terminal velocity that the main parachute needs to settle into. Since this is during the second (subsonic) stage of descent, the starting velocity comes from defining the subsonic regimen which in this case is Mach 0.8 . Subsequently, for the drogue parachute, its settling terminal velocity reaches Mach 0.8 and the starting velocity is derived from the entry conditions at Mach 1.4, since its function is to bring the EDV from the supersonic to subsonic regimen.

$$C_D S_0 = \frac{m_{EDV}}{q} \tag{5.1}$$

$$D_0 = \sqrt{\frac{4 * S_0}{\pi}} \tag{5.2}$$

$$F_{peak} = \frac{1}{2} q_{max} S_0 C_X X_1 \tag{5.3}$$

$$F_D = q C_D S_0 \tag{5.4}$$

Model Limitations, Verification and Validation

The model for the parachute sizing follows from the the assumptions and models created for the atmospheric properties in Chapter 4 and the general entry model and is therefore limited by them as well. Tables and charts from the parachute sizing heritage literature confirm the sizing for this mission as it has been similar for velocities and dynamic loads of this scale [44].

5.10.5. EDV-PAR Final Design Overview and Evaluation

EDV-PAR Sensitivity Analysis

A sensitivity analysis is performed to check the changes in the peak shock loads experienced by the EDV when the desired terminal velocity is changed. For both the main and the drogue parachutes, this change is proportional to the inputs, as expected. A conservative estimate is used to size both the chutes for the purpose of redundancy, as well as ensuring a smooth descent.

EDV-PAR Final Design Parameters

The EDV-PAR is made of two components, the drogue and the main parachute are each sized according to the terminal velocity they need to settle on. The minimum diameters are sized according to the initial shock load they face from ejection and opening loads. A conservative approach is taken to provide a high descent rate resulting in diameters of 1.6 m and 6.4 m for the drogue and main parachute respectively, while their surface areas are 4 m^2 and 64 m^2. The resulting total volume is 660 m^3 using parachute sizing estimations[44] and go up to 920 m^3 when the drogue is packed into the mortar. Finally, using the packing density, the total mass of the EDV-PAR is calculated to be 0.475 kg. In order to comply with the temperature and structural integrity requirements, the drogue and the main are made of strong and high temperature withstanding materials namely, Nomex and Dacron respectively[44]. The total mass and volume contribution of the parachutes are extremely small but have been used to size the mechanism and for the full integration of the EDV parameters resulting in the technical budgets from Section 5.6.

5.11. Entry and Descent Vehicle Electrical Power System

The EDV, while relying mostly on passive systems, still requires a small amount of electrical power to fully function. This EPS system is not critical, but is still designed to improve the operations of the entry and descent.

5.11.1. EDV-EPS Functional and Architecture Analysis

The architecture of the EDV-EPS is heavily dependent on the functions it has to perform. In the next sections, first the functions of the EDV-EPS are explained, after which the architecture and the hardware is defined.

EDV-EPS Functional Allocation
For a full functioning of the EDV, the EDV-OBD shall create housekeeping data, which is sent to the REL by the EDV-TNC. Both of these subsystems require small amounts of power for a limited period, which must be provided and distributed by the EDV-EPS. Therefore, according to Section 2.2, the EDV must generate electrical power (F5.4.7), and the EDV must distribute the electrical power to the subsystems that require it (F5.4.7).

EDV-EPS Systems Architecture
The EDV-EPS consists of a single battery that contains enough capacity to provide electrical power for the duration of the entry and descent. Besides the battery, a PCD is included to distribute this power.

EDV-EPS Hardware Block Diagram
Similarly to the SCB-EPS described in Subsection 4.12.1, the hardware of the EDV-EPS is shown in Figure 5.12.

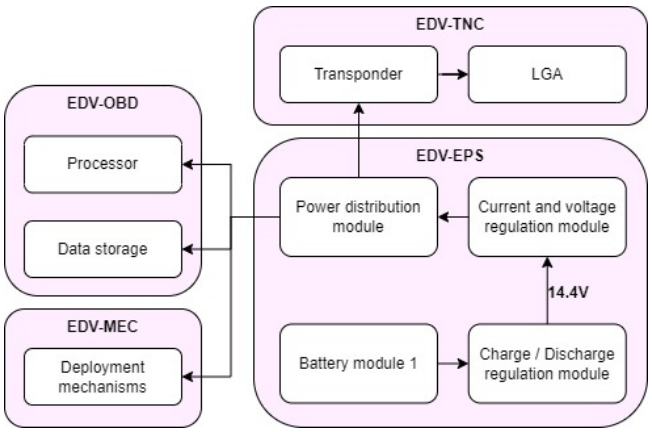

Figure 5.12: The hardware block diagram of the EDV-EPS

5.11.2. EDV-EPS Key Requirements
The following key requirements for the EDV-EPS are identified, based on the analysis presented above, and its allocated budgets:

Table 5.12: Key EDV-EPS subsystem requirements, driving requirements are marked with [!]

ID	Description	Rationale
EDV-EPS-REQ-4.1	[!]The EDV-EPS shall provide an average power of at least 6 W for the duration of the entry and descent phase.	Derived from the power consumption of the EDV.
EDV-EPS-REQ-4.2	[!]The EDV-EPS shall provide a peak power of at least 6 W during the entry and descent phase.	Derived from the power consumption of the EDV.

5.11.3. EDV-EPS Sizing and Trade-off
The design options tree for the EDV-EPS is shown in Figure 5.13. Due to the relatively short duration of the entry and descent compared to the entire mission timeline, a single primary battery suffices and is the only concept left after the trade-off.

EDV-EPS Sizing EPS Storage
To size the EDV-EPS-STO, a single simple calculation is made that consists of the power usage of the EDV-OBD and the EDV-TNC, the duration that the EDV requires electrical power and the characteristics of the electrical components. These values and the final battery size are documented in Table 5.13. This results in a battery capacity of 8 Wh.

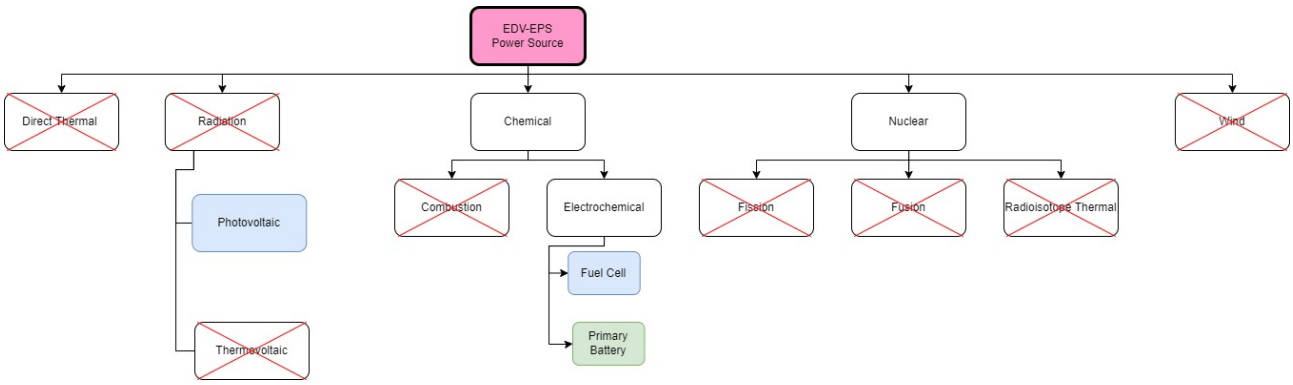

Figure 5.13: Design options tree for the EDV-EPS

Table 5.13: Values used for the sizing of the EDV-EPS

TNC power [W]	4.75	**Duration [s]**	2610	**Battery efficiency [-]**	0.9
OBD power [W]	0.162	**PCD efficiency [-]**	0.9	**Depth of discharge [-]**	0.6

However, in the case of the EDV-EPS, the driving parameter of the size of the battery is not the capacity, but the 5 W discharge power requirement and the minimum battery component size.

Model Limitations, Verification and Validation
The model used in this section is consists of a simple, linear calculation, which is valid for any primary battery system. It has been validated and verified using literature comparisons.

5.11.4. EDV-EPS Final Design Overview and Evaluation
The final overview of the EDV-EPS consists of the component selection, a sensitivity analysis and the final design parameters.

EDV-EPS Component Selection
For reasons related to production schedule, manufacturing and material costs and the design schedule, similar components to the ones that are included in the SCB-EPS have been chosen for the EDV-EPS. The BAT has been provided in Table 4.27 and the PCD has been provided in Table 4.28.

EDV-EPS Sensitivity Analysis
Due to the linearity of the calculations for the size of the battery, any change in power consumption results in an equal change in battery capacity required. However, since the battery size is driven by the required battery discharge power and not the capacity, a change in duration of the entry and descent does not change the battery size. Besides that, a 10% power margin has been applied.

EDV-EPS Final Design Parameters and Evaluation
The final design parameters of the EDV-EPS are given in Table 5.14. It can be seen that compared to the size and mass of the total EDV, the EDV-EPS has a minute contribution.

Table 5.14: Final design parameters of the EDV-EPS

BAT mass [kg]	0.5	**PCD mass [kg]**	0.3
BAT volume [L]	0.33	**PCD volume [kg]**	0.25

5.12. Entry and Descent Vehicle Mechanisms
To safely deliver the SCB into the Venusian atmosphere, a series of mechanisms must be triggered reliably and at the correct moment. In this section, the EDV-MEC functions and architecture are analysed in 5.12.1, followed by an overview of the final design in 5.12.3.

5.12.1. EDV-MEC Functional and Architecture Analysis

There are six different mechanical systems in the EDV, consisting of eight different elements. The following sections first explain the design choices made, after which the actual implementation on the EDV is shown using images from the CAD design.

EDV-MEC Functional Allocation

The 6 mechanisms of the EDV are:

- 1 parachute cover ejection mechanism
- 1 mortar
- 1 drogue connection hook
- 1 heat shield separation mechanism
- 3 spools containing a rope to lower the SCB
- 1 balloon hook

The designs of the mechanisms are as follows: The parachute cover ejection mechanism consists of two pyrotechnic charges which separate it from the EDV.

The mortar uses one large pyrotechnic charge to shoot the drogue chute out the open hole in the aeroshell. The drogue chute is connected to the drogue connection hook

The drogue connection hook transfers the forces from the drogue to the EDV. Once it is time to deploy the main parachute it again uses two pyrotechnic charges to release the drogue and allow it to pull the main parachute out.

The heat shield separation mechanism consists of eight pyrotechnic charges that fire at the desired moment.

The spools use the same friction based lowering system as on the SCB, however they also contain a torsional spring. This is so that once the rope is detached at the SCB, it retreats back into the EDV.

Finally the balloon hook is severed using another pyrotechnic device.

EDV-MEC Systems Architecture

The following image shows the geometry of the six different mechanisms from left to right, in the same order as the list above. The top row corresponds to the geometry before deployment and the lower after deployment.

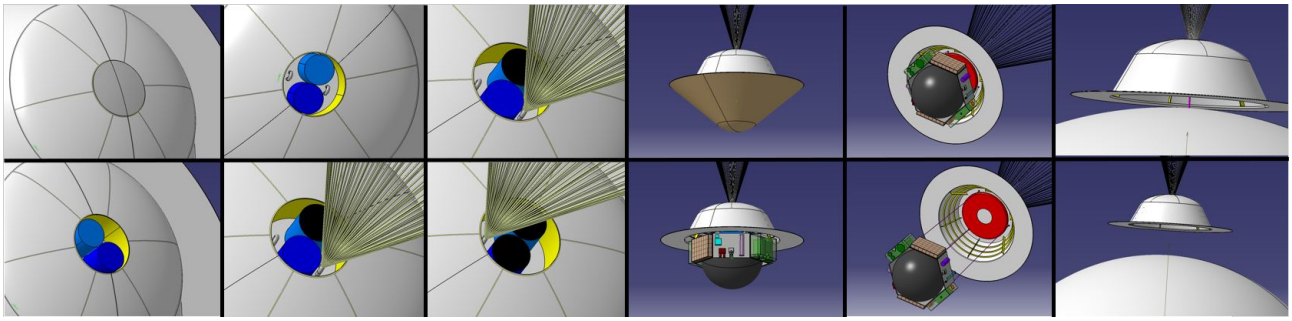

Figure 5.14: The different mechanisms before and after deployment.

5.12.2. EDV-MEC Key Requirements

The following key requirements for the EDV-MEC are identified, based on the analysis presented above, and its allocated budgets:

Table 5.15: The key EDV-MEC subsystem requirements, driving requirements are marked with [!].

ID	Description	Rationale
EDV-MEC-REQ-3.1	[!] The EDV MEC shall deploy after OBD confirmation of correct SCB deployment conditions".	Derived from EDV-REQ-3.4.

Continued on next page

Table 5.15 – continued from previous page

ID	Description	Rationale
EDV-MEC-REQ-3.2	[!] The EDV MEC shall release the heat shield at an altitude of 70.49 km.	Required to deploy the SCB.
EDV-MEC-REQ-3.4	The EDV MEC shall lower the SCB at an altitude of 67.21 km.	Required to deploy the SCB.
EDV-MEC-REQ-3.5	The EDV MEC shall release SCB at an altitude of 54.44 km.	Required to deploy the SCB.
SCB-LAD-REQ-3.1	The EDV MEC cost shall not exceed 1 $millionEUR$.	To reach the system bugdet limit.
EDV-REQ-5.2	The EDV MEC mass shall not exceed 20 kg.	To meet the system mass limit.

5.12.3. EDV-MEC Final Design Overview and Evaluation

Even more than the SCB, the EDV is largely reliant on the correct functioning of pyrotechnics. As explained earlier, pyrotechnics are considered very reliable and are therefore the perfect choice for these mechanisms.

5.13. Entry and Descent Vehicle Structure

The structure of the EDV has to protect the internal components of the EDV, including the SCB during entry and throughout descent. This section provides the methodology by which the detailed design for this structure is performed. Starting with the functional analysis, identifying requirements, and moving on to sizing. The section concludes with the final numbers associated with the EDV-STR.

5.13.1. EDV-STR Functional and Architecture Analysis

The functional and architectural analysis of the EDV-STR first takes a look at all the functions the EDV-STR has to carry out. How it fits into the bigger picture of the mission and the components used to achieve this are listed in the architecture.

EDV-STR Functional Allocation

The EDV-STR's key functions consist of allowing the EDV's contents to survive entry loads (F5.3.1) and provide structural integrity for the entirety of entry until SCB deployment (F5.3.6).

EDV Configuration

The EDV-STR architecture consists of the following:

- Back-shell thin conical shell
- Front-shell thin conical shell
- Internal stringer structure
- Rings for the stringer structure

5.13.2. EDV-STR Key Requirements

The following key requirements for the EDV-STR are identified, based on the analysis presented above, and its allocated budgets:

Table 5.16: The key EDV-STR subsystem requirements, driving requirements are marked with [!].

ID	Description	Rationale
EDV-STR-REQ-2.1	[!]The EDV-STR shall withstand transfer loads of 5 g during the entirety of transfer burns.	Derived from F4.
EDV-STR-REQ-3.4	[!]The EDV-STR shall withstand a maximum temperature of 473.15 K.	Derived from F5.

Continued on next page

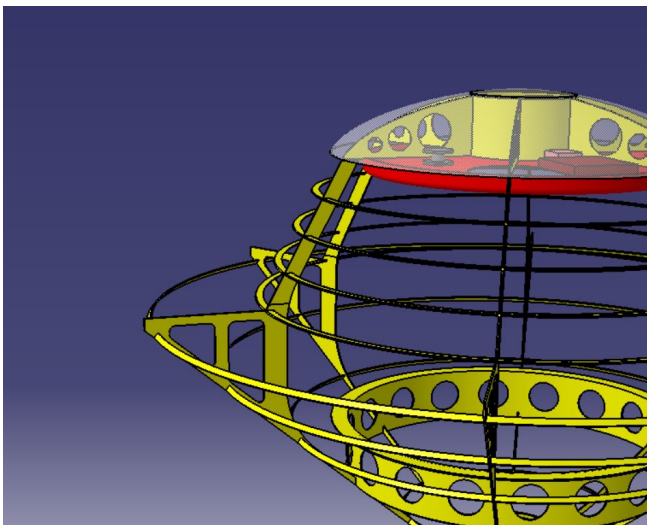

Figure 5.15: EDV structure

Table 5.16 – continued from previous page

ID	Description	Rationale
EDV-STR-REQ-3.4	[!]The EDV-STR shall withstand axial forces due to entry loads of 50 g.	Derived from F5.

5.13.3. EDV-STR Structural Analysis and Sizing

Following the requirements derived as discussed in Section 5.2, the main structural analyses for the EDV are the buckling and stringer face stress analyses. First, these analyses are performed to size the thickness, spacing and any relevant parameters. These parameters are then iterated until the buckling and stress requirements are passed, in addition to being the most cost and mass effective result. Equation 5.5 shows the relationship between the critical axial load on a cone and the cone thickness t, where α represents the cone angle, γ represents the correlation factor accounting for discrepancies from actual loads on cones to the theory, v and E the Poisson's ratio and elastic module of the material respectively. This is applied following the fact that the maximum axial load on the thin conical shell structure cannot exceed the critical allowable buckling load.

$$P_{cr} = \gamma \frac{2\pi E t^2 \cos^2 \alpha}{\sqrt{3(1-v^2)}} \tag{5.5}$$

In the case of the EDV, two conical shells are placed; one on the inside of the top half of the EDV "backshell", and another one below it right behind the front heat shield. The backshell's cone is right below the housing of all the EDV internal components, including the parachutes, as well as the SCB balloon. Thus, during the entry phase where the highest loads faced are up to 50 g , it can be assumed that the worst case for loading on this structure is an axial load on the cone that includes the mass of all the items housed above it at 50 g. For the bottom shell, the loading case is not the same, since much of the SCB components' load is undertaken by the SCB fuel tank.

In order to size the stringers, a good starting point is to follow the assumption that these can be modelled as cantilever beams, rigidly attached on one side, with a point force acting on the opposite side (at the geometric angle the backshell, and subsequently the cone, follows). This is seen in figure 5.15.

$$\sigma = \frac{Mc}{I} \tag{5.6}$$

$$P = \frac{P_{applied}}{n} \tag{5.7}$$

$$\sigma_{max} = \frac{M_A h}{I2} = \frac{6M_A}{bh^2} = \frac{6P}{bh^2}(L\sin\alpha - \frac{h}{2}\cos\alpha) = \frac{6P}{bh^2}(\frac{L\sin\alpha}{n_{ring}} - \frac{h}{2}\cos\alpha) \tag{5.8}$$

To analyse the worst loading case on these stringers, the maximum applied stress due to the compressing load from the top can be considered. Following the model of the beam, this maximum stress acts at the maximum applied moment, the furthest point from the applied load or the base of the stringer. Equation 5.8 shows the relationship between the maximum applied stress (σ) on a stringer, and the base (b) and height (h) of a stringer; L is the length of the stringer while α remains to be the cone angle. This relationship is a combination and development of the general stress equation in Equation 5.6 and the sizing for the load over a number of stringers in Equation 5.7. When switching to analysing it per stringer, the bending moment M over the moment of inertia I would just produce the highest stress when taking into account the furthest point where there is a maximum bending moment M_A as mentioned before. The only problem in this analysis is that due to the long length of this stringer required for the height of the EDV, the number of stringers required becomes too many to fit the material and mass budget for the EDV. Thus, rings are added to this structure which act to divide the stringers where they intersect, lowering the total length of the stringer to consider the applied moment for, as indicated by n_{ring}, the number of rings. Finally, the parameters b, h and n_{ring} are iterated alongside the number of stringers n, from Equation 5.7 until the material, cost and mass budget in addition to the load requirements are satisfied.

Model Limitations, Verification and Validation
The use of a finite-element-modelling software would have made for a much more detailed and accurate structural analysis. However, in the scope and timeline for this project, a very basic model was created using the equations from the preceding section with many assumptions. However, these assumptions follow from structural analysis literature specific for space launch vehicles such as taking the stringers to be end-fixed beams and sizing only for the axial load which is also the driving load for the minimum allowable parameters[10].

5.13.4. EDV-STR Final Design Overview and Evaluation
Finally, the material, sensitivity analysis performed and the finalised structural component parameters are presented in the following, concluding the discussion on the detailed structural design of the EDV.

EDV-STR Materials Selection
The elastic modulus, E, and the Poisson's ratio, v, are the determining variables for the material selection for the EDV-STR. Aluminum-6061, aluminium honeycomb, and beryllium alloys are all considered and after a few iterations for the minimal mass, volume and cost providing option, aluminium-6061 is chosen to be the structural material for all components of the EDV-STR.

EDV-STR Sensitivity Analysis
The sensitivity analysis performed for the structural analysis consists of varying the loads to observe the change in the thickness or dimension of the cone and stringers respectively. The changes in thickness are small and scaled appropriately to the input. Due to this being a structural analysis without a FEM analysis, a very conservative approach regarding margins are taken anyway to ensure a structural rigidity that passes the requirements.

EDV-STR Final Design Parameters and Evaluation
The axial loading on the conical shell results in the sizing of this shell thickness to be 5 mm. The stringers, which are sized to withstand the compression loads as well as the maximum stresses (due to bending moments), result in having a thickness of 5 mm as well as a width of 50 mm for a total number of 6 stringer structures. The supporting rings are not load bearing/transferring but aid in reducing the vertical distance of the moments affecting the stringer structures, and are sized to have a thickness of 5 mm. Altogether, this results in a total volume of 108100 cm^3, and subsequently a mass of 292 kg. This is all integrated in the technical budgets of the EDV in Section 5.6.

5.14. Entry and Descent Vehicle Thermal Management System
Going from the coldness of interplanetary flight to the heat generated due to friction in the atmosphere, the EDV encounters arguably the most extreme thermal environments of the entire mission. The role of the EDV-THE is ensuring that the components and the SCB are shielded from these temperatures. In this section, the main

functions and architecture of the subsystem are discussed, followed by the sizing procedure. Lastly, the results are presented and evaluated.

5.14.1. EDV-THE Functional and Architecture Analysis

In this section the functions performed by the EDV-THE are analysed, along with its architecture.

EDV-THE Functional Allocation

From the functional analysis in Section 2.2, it can be seen in function F5.4.4.1 that the EDV-THE has to protect the inner components and payload from the entry temperatures. On top of this, the EDV has to do the same in space, in the window between being released by the TRV and entering the Venusian atmosphere, where the outside instead is significantly colder than during entry.

EDV-THE Systems Architecture

The two very different thermal scenarios also concern different areas of the EDV: the high temperatures experienced during entry are found mainly at the bottom of the vehicle, while the cold temperatures concern its entirety.

EDV-THE Hardware Block Diagram

The hardware block diagram shown in Figure 5.16 provides an overview of the main hardware components of the EDV-THE and their thermal relations. All thermal relations are reported in the figure, including those not analysed in the sizing process. Blue indicates components of the EDV-THE, while green indicates the other components of the EDV.

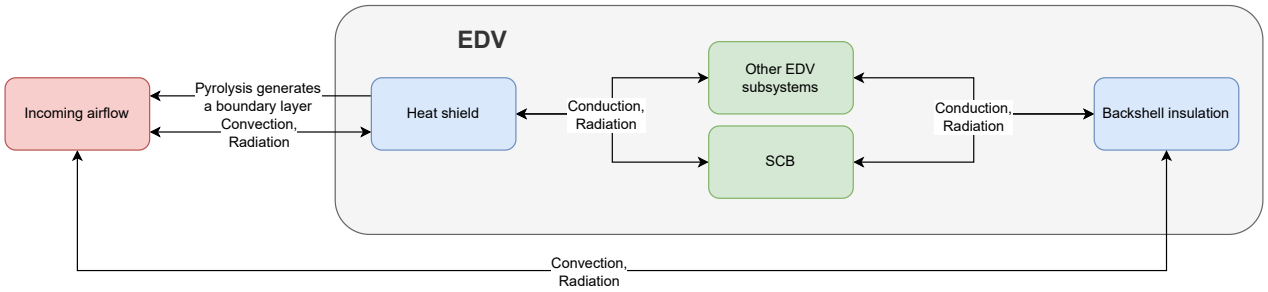

Figure 5.16: A hardware block diagram of the EDV-THE.

5.14.2. EDV-THE Key Requirements

The following key requirements for the EDV-THE are identified, based on the analysis presented above, and its allocated budgets. Not all requirements can be reported due to space limitations.

Table 5.17: The key EDV-THE subsystem requirements, driving requirements are marked with [!].

ID	Description	Rationale
EDV-THE-REQ-1.1	[!] The EDV-THE shall guarantee that the SCB stays below a temperature of 313 K.	Derived from function F5.4.1.1.
EDV-THE-REQ-1.2	[!] The EDV-THE shall guarantee that the SCB stays above a temperature of 273 K.	Derived from function F5.4.1.1.

5.14.3. EDV Thermal Analysis and Sizing

Because the thermal loads vary so greatly in different areas, different strategies are applied to the front, (which is intended as the side that is in the direction of flight, and sometimes referred to as the bottom), as well as the back of the EDV. The front is protected by a heat shield, the only feasible method of dealing with such high temperatures, while the backshell uses a different type of insulation.

Heat Shield

For the heat shield design, it is decided to use an ablative one. This is because it performs very well in terms of weight for single use, is a very well established and proven technology, and has been used extensively on previous missions.

As previously mentioned in Section 5.3, a Python program is made to simulate the entry trajectory of the EDV. This program calculates the heat flux using Chapman's equation Equation 5.9. The formula uses coefficients of Mars, but is still accurate enough for Venus due to the composition of the two planets being very similar, with a carbon dioxide concentration respectively of 95% and 96%. In this formula, c_1 is a coefficient determined by the planet, and is set to 1.9027 for Mars and hence, for Venus. ρ is the density of the air at the current altitude, V is the velocity with respect to the airflow, and R_N is the radius of the nose of the sphere-cone, which is 0.41 m for the EDV of the LOVE mission. m is determined by the type of atmosphere, which is 3.04 for Mars, and n by the type of flow, which is assumed to be laminar in this case and therefore equal to 0.5. The hot wall correction term is not included, since it has a negligible effect for fluxes above 100 W/cm^2 [90], which is the case for this design.

$$q_c = c_1 \frac{\rho^{1-n} V^m}{R_N^m} \tag{5.9}$$

$$T_{max} = \sqrt[4]{\frac{q_{max}}{\sigma \varepsilon}} \tag{5.10}$$

After computing the heat flux, the heat shield can be sized. Modelling the thermodynamics involved with an ablative heat shield is rather difficult, since there is no simple approximation for the reduction in convective heat due to the gas layer created by the pyrolysis of the ablative layer. For this reason, a conservative first order approximation is taken, which assumes that the heat absorbed by the heat shield is balanced by the heat radiated out, virtually ignoring any conduction and convection. The equilibrium temperature is calculated with Equation 5.10 and uses the peak heat flux experienced during entry. Knowing the temperature reached by the heat shield, the heat capacity of the material and the total heat absorbed during entry, the mass can be calculated with Equation 5.11. To know the heat capacity, the material first has to be chosen. A quick trade-off is performed and as an initial estimate, a phenolic impregnated carbon ablator (PICA) is chosen for the TPS design, since it is one of the most established materials in the industry and has a good overall performance. This information also provides the emissivity of 0.84 used in Equation 5.10. The data of PICA-15 is used to linearise and estimate the heat capacity[65] for the temperature ranges experienced by the heat shield. The total heat absorbed is obtained by integrating the heat flux over the descent into the Venusian atmosphere, as shown in Equation 5.12, where S_{edv} is the surface of the EDV covered by the heat shield.

$$m = \frac{Q_{tot}}{C_{abl} \Delta T} \tag{5.11}$$

$$Q_{tot} = S_{edv} \int_{t_0}^{t_{end}} q_c dt \tag{5.12}$$

From the mass of the heat shield, the volume can easily be calculated, taking a conservative estimate of 227 kg/m^3, which is on the high end for the PICA material.

Backshell Insulation

From heritage data and the relationship between the aeroshell's geometric properties and the thermal loads, it is safe to assume that the thermal loads acting on the backshell of the EDV structure are much lower in comparison to the front. For a nose angle of 45 °, the "shoulder" thermal loads that act over the backshell surface go down to only 5% of that of the front heatshield loads[49]. Thus, the first step is to derive the highest surface temperature acting on the back surface. The point of analysing thermal control in this case is to ensure that the internal temperature of all components in the EDV stay within their operational ranges. Thus, once the maximum outside surface temperature is obtained, it is compared to the internal desired temperature needed for thermal control. Then, it is possible to determine the type and size of thermal control and the sizing of it. In this case, the temperature gradient is not too high and the time of entry as compared to mission life time is significantly minuscule. Therefore, active thermal control systems, which are more expensive in terms of mass and cost, are immediately disregarded. Within passive thermal control, there are multiple types, ranging from paints, tapes

and multi-layer-insulation (MLI), to louvres, radiators and heat pipes. Again, the low thermal gradient and short entry time mean that high mass and volume items, such as louvres, radiators and heat pipes can be disregarded [12].

$$\frac{Q}{A} = k_{eff}\frac{T_H - T_C}{t} \tag{5.13}$$

As for the remaining passive thermal control options, a simple heat flux calculation from Equation 5.13 [86] can be used to see what material type, set by thermal conductivity k_{eff}[9] and thickness t, provides the most efficient and reasonable heat flow Q in $Watts$ through the material surface area A. The flow is from the outer surface, where the temperature is T_H, to the internal surface, where the desired temperature is T_C. The heat flow through the material does not directly follow from the heat load experienced, but is rather the desired heat flow through time that the EDV structure has to handle. This is sized as a range of heat flows through the aluminium internal structure, with varying temperature gradients. The lowest temperature gradient is the least damaging to the structure and internal components, and results in the minimum non-zero heat flow. Finally, this heat flux can be used to obtain the thickness for different insulation materials. As an additional note, the thermal control analysis is performed from the point of detachment from the TRV. The requirements imposed on the TRV ensure that the EDV's internal components stay within the desired temperature range until the EDV detachment. After the detachment, both the thermal flux case for the short duration of the EDV just outside the Venusian atmosphere, as well as the case during entry are considered. However, the latter turned out to be the higher load, and thus the driving factor for thermal control sizing.

Model Limitations, Verification and Validation

The model used for the sizing of the heat shield is an extremely simplified version of the true thermodynamic problem. Its limitations come from the fact that the ablation itself is not modelled and hence all the incoming heat flow is absorbed and radiated by the material of the heat shield. This means also that the progressive reduction in thickness is not taken into account. Moreover the temperature change of the heat shield in Equation 5.11 is assumed to start at 0K, which is a very conservative approach. Other parameters can also be improved but have lower impacts on the design. Lastly the approach used for validation is that of comparing the fraction of the EDV mass allocated for the TPS system with past missions, the results of which are shown in Subsection 5.14.4. As for the backshell insulation, for the duration of entry, the thermal aspects apart from convection and radiation from outer space are calculated to be insignificant and thus are ignored. Heritage data and literature regarding shoulder heating surrounding entry vehicles of similar geometric properties were used to validate the numbers obtained for the backshell sizing and material [49].

5.14.4. EDV-THE Final Design Overview and Evaluation

Following the steps described in Subsection 5.14.3, the total mass and dimensions are derived for the heat shield and the backshell insulation. These results are presented and discussed in the following sections.

EDV-THE Sensitivity Analysis

The thermal analysis of the heat shield is heavily dependent on the input values. Because of the direct descent from transfer trajectory, the entry velocity of 11.4 km/s is the main driving factor, along with the entry angle of 9.2 °. Many equations, such as those for drag or heat flux, are dependent on a certain power of the velocity and therefore are quite sensitive to changes in these parameters. It is already shown in Section 5.4 that the entry point has an allowable range of 20 km, and therefore there is sufficient margin on the current design. From a qualitative point of view the design choices made are valid. However, with any change in entry velocity, point or angle the heat shield design has to be iterated. Nevertheless, despite these considerations, the current design includes many conservative numbers, and therefore a more accurate analysis can lead to a lighter and thinner heat shield design.

For the backshell insulation, the model considers the desirable heat flow from the outer surface through the insulation, and then through the aluminium structure to the internal part of the EDV. The temperature gradient through the aluminium surface produces the largest difference in the allowable heat flux, which consequently affects the type and size of the insulation required. This is due to the high conductivity of aluminium. The temperature gradient through the aluminum surface has been made 5 times smaller than the thermal loads that

the structure can actually handle. The resulting thickness for the insulation however, still remains to be very small and proves sufficient.

EDV-THE Final Design Parameters and Evaluation
The final design of the EDV-THE calls for an ablative heat shield on the cone section of the EDV. The heat shield is 6.4 cm thick and has a radius of 1.4 m. The material chosen is a common phenolic impregnated carbon ablator, which yields a total weight of 116.8 kg. This represents 14.4% of the total EDV weight, quite close to the 13.2% suggested by literature [29], hence the results can be considered validated. The difference can be explained by the conservative approach taken when choosing most parameters for the heat shield design, as well as by the fact that the ablation of the heat shield is currently not modelled in the sizing.

The final design of the thermal control of the backshell is simply padding the entirety of the internal thin conical shell with a foam insulation (isocyanate and polyol)[36] on the outer side. With a thermal conductivity, k_{eff} of 0.01 W/mK, this foam proves to be sufficient to withstand 10,215,658 W of heat flux through the material with a temperature gradient of 5.0 K, with just a thickness of 2 mm, including a sufficient margin. With close to no mass or volume addition, a thin 4-layer mylar aluminium blanket of 0.02 mm can be added on the outside. This acts as a protective layer from space in the short duration that the EDV is outside of the Venusian atmosphere. Although the designed insulation is already sufficient to ensure that the EDV stays within the specified temperature range.

6
Relay Satellites

This chapter presents the detailed design of the relay satellite (REL) of the LOVE mission. The design builds upon the selected dual REL configuration, for use as a communication and navigation aid for the SCB. Prior to the detailed design of the REL, Section 6.1 presents the REL functional and architecture analysis, then Section 6.2 presents the definition of the REL requirements, and the pointing strategy employed by the REL is discussed in Section 6.3. Following that, an overview of the REL design is presented in Section 6.4, the technical budgets are given in Section 6.5, and the reliability and risk of the REL is investigated in Section 6.6. After this, the detailed design of each of the subsystems of the REL is performed: TNC in Section 6.7, OBD in Section 6.8, ADC in Section 6.9, PRP in Section 6.10, EPS in Section 6.11, MEC in Section 6.12, STR in Section 6.13, and THE in Section 6.14.

6.1. Relay Functional and Architecture Analysis

The REL must fulfill numerous functions to ensure mission success. These functions are used to determine the subsystems, and subsequently the components that are needed in the REL to perform these tasks, outlined in Subsection 6.1.1. This leads to the total architecture of the system, which is summarised in Subsection 6.1.2. The relations between the subsystems are then summarised in the functional N2 chart provided in Subsection 6.1.3.

6.1.1. Relay Functional Allocation

In the transfer phase to Venus, the REL is responsible for travelling to Venus (F4.3) and inserting itself into the defined orbit (F4.4). During the entry of the EDV into the Venusian atmosphere, the REL must communicate with the EDV (F5.2). When performing the scientific investigation, the REL must communicate with the CCC (F6.7) as well as with the SCB (F6.8). It must also be able to support its own operations (F6.9). Finally, in the decommissioning phase, the REL must relay the decommissioning command to the SCB (F7.2), verify that the SCB has decommissioned (F7.6), whilst supporting its own operations (F7.4). It must then perform its final function by deorbiting (F7.7) and burning up in the atmosphere.

6.1.2. Relay System Architecture

A block diagram demonstrating the REL system architecture can be seen in Figure 6.1. From this, one can assign functions of the REL to the different subsystems, provided as follows:

1. TNC: Communicate with CCC/EDV/SCB - F4.3.1, F4.4.1, F5.2, F6.7, F6.8, F7.2, F7.6, F7.7
2. OBD: Command system and handle data - F4.3.4, F4.4.5, F6.9.6, F7.4.6, F7.7.4
3. ADC: Determine and control attitude - F4.3.3, F4.4.3, F6.9.3, F7.4.3, F7.7.5
4. PRP: Perform trajectory manoeuvres - F4.4.3, F7.7.6
5. EPS: Supply electric energy - F4.3.2, F4.4.2, F6.9.1, F7.4.1
6. MEC: Deploy mechanisms - F4.1.1
7. STR: Maintain structural integrity - F4.3.2, F4.4.2, F6.9.5, F7.4.5
8. THE: Control temperature - F4.3.2, F4.4.2, F6.9.2, F7.4.2

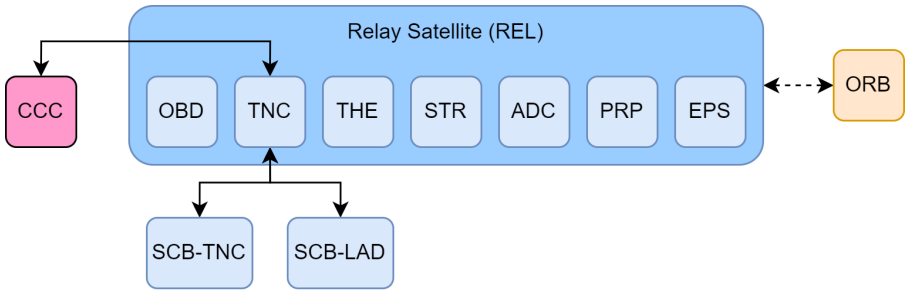

Figure 6.1: The REL system architecture.

6.1.3. Relay System N2 Chart

The N2 chart of the REL is presented in Table 6.1. This table shows all the outputs of the subsystems in its rows, and the columns represent the inputs for the subsystem. This chart is used to get an overview of the subsystems of the REL and how they are related.

Table 6.1: The functional N2 chart of the REL.

REL-EPS	Power	Power		Power	Power, Housekeeping data	Power	Power, pointing of solar panels
Position of Sun, Required power, Pointing solar panels	REL-ADC	Relative position of Sun and Venus		Propulsion Commands	Housekeeping data (Sensors data), Attitude Data, Position & Velocity		
Required power	Required attitude	REL-THE			Housekeeping data		
			REL-STR		Housekeeping data		
Required power	Housekeeping data			REL-PRP	Engine status		
Required power	Required attitude	Commanding of temperature control		Propulsion commands	REL-OBD	Housekeeping data, Commands to SCB, Data from SCB	
	Ranging data				Commands to REL, Commands to SCB, Data from SCB	REL-TNC	Pointing of antenna
Required power							REL-MEC

6.2. Relay Requirements Definition

In order to begin designing the REL in further detail, the results from the functional and architectural analysis must be flowed down to form system and subsystem requirements. This is done through the intermediate step of creating a requirements breakdown tree. The presentation of the key requirements and driving requirements are analogous to the method presented in Section 2.3 and these requirements are given in Table 6.2. Driving requirements are marked with '[!]'. It is important to realize that the requirements displayed in the following table do not represent the 65 system requirements and 208 subsystem requirements derived for the REL.

Table 6.2: Key REL system requirements, driving requirements are marked with [!].

ID	Description	Rationale
REL-REQ-1.5	The REL shall receive commands from the CCC during the transfer phase.	Derived from F4.8.

Continued on next page

Table 6.2 – continued from previous page

ID	Description	Rationale
REL-REQ-2.8	The REL shall receive commands from the CCC during the entry phase.	Derived from F5.2.
REL-REQ-3.3	The REL shall transmit commands to the SCB.	Derived from F6.7.
REL-REQ-3.4	[!] The REL shall transmit scientific data to the CCC.	Derived from F6.7.
REL-REQ-3.7	[!] The REL shall receive commands from the CCC during the operational phase.	Derived from F6.7.
REL-REQ-3.8	The REL shall receive scientific data from the SCB	Derived from F6.7.
REL-REQ-3.10	[!] The REL shall have a minimum data rate of $2.8kbps$.	Need to transmit data produced by payload.
REL-REQ-3.11	The REL shall transmit on a frequency band of $8.400 - 8.450GHz$.	Need to select band to transmit on.
REL-REQ-3.12	The REL shall receive a frequency band of $7.145 - 7.190GHz$.	Need to select band to receive on.
REL-REQ-3.13	[!] The REL shall process a maximum daily data volume of $370.6Mbits/day$.	Need to transmit data produced by payload.
REL-REQ-3.14	[!] The REL shall transmit signals with a signal-to-noise margin of at least $3dB$.	Signal must be strong enough to be distinguished.
REL-REQ-3.15	[!] The REL shall receive signals with a signal-to-noise margin of at least $3dB$.	Signal must be strong enough to be distinguished.
REL-REQ-3.16	[!] The REL shall have a gap time with the SCB of no more than $48.67min$.	Navigation data must be updated periodically to calibrate internal instruments.
REL-REQ-3.18	The REL shall transmit ranging signals to the SCB.	Derived from F6.8.
REL-REQ-4.1	The REL shall transmit the command to decommission the SCB to the SCB.	Derived from F7.8
REL-REQ-5.1	[!] The REL cost shall not exceed $20.01MEUR$.	Flows from stakeholder cost requirements.
REL-REQ-6.1	[!] The mass of the REL shall not exceed $149.02kg$.	REL has to have a constraint on the mass due to the nature of space missions.

It can be seen that the REL is mainly responsible for providing relay communication and navigation aid for the SCB, with most of the requirements being derived from those main functions.

6.3. Relay Pointing Strategy

In the following section, the pointing strategy of the REL is presented. This is crucial to further analysis and sizing of REL subsystems such as REL-TNC, REL-EPS and REL-THE. In order to be able to define a pointing strategy, a spacecraft coordinate system has to be defined. This spacecraft coordinate system is shown in Figure 6.2:

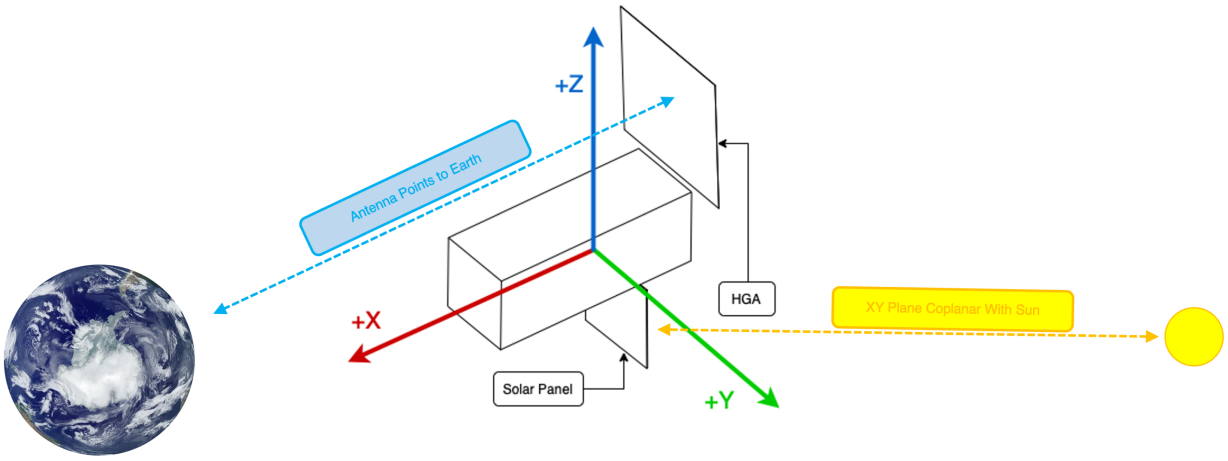

Figure 6.2: REL coordinate system showing positive X aligned with HGA antenna, and the pointing problem

IT can be seen that the positive x-axis is aligned with the HGA of the REL, the positive z-axis is pointing towards the body panel of the REL holding the HGA and the y-axis forms a right-handed coordinate system.

The pointing strategy of the REL is now determined based on the following criteria:

- Maximize communication time with Earth.
- Provide permanently shaded body panels for effective heat dissipation.
- Provide efficient power harvesting of solar panels with either no pointing or one-axis pointing.

With these criteria in mind, the z-axis of the spacecraft is defined to be orthogonal to the REL-Earth-Sun plane. This enables continuously shaded body panels and allows for continuous illumination of the solar panels. Depending on whether the solar panels are pointed or not, the x-axis is either continuously pointed at Earth in case of the unpointed solar panel, or the spacecraft is alternately pointed at Earth and pointed such that the Sun is aligned with the solar panel axis in case Earth is not visible. Figure 6.3 shows the evolution of the unit vector in the z-axis of the relay coordinate system.

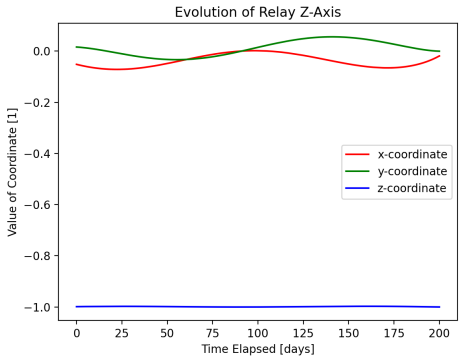

Figure 6.3: REL pointing over mission duration.

It can be seen that the attitude of the REL remains nearly constant over much of the mission duration, showing that this pointing strategy is relatively benign in terms of slew requirements. However, attitude changes for manoeuvres are not considered in this analysis, but due to the relatively low time taken up by these events, the model of SCB pointing is still deemed valid for the purpose of link, thermal and power analysis.

6.4. Relay Design Overview

In this section, a general overview of the REL design is presented. A detailed description of the segments of this is given in the relevant sections. In Section 6.4, a description of the design is given. Following this section, the material and production characteristics of the REL is investigated in Subsection 6.4.2.

6.4.1. Relay Design Description

From the midterm report [2], a dual REL configuration was selected to relay communications to and from the SCB and CCC, and to provide navigation aid for the SCB. To do so, the REL has a HGA that communicates on the X-band frequency range with the CCC and multiple LGAs that communicate on the UHF-band frequency range with the SCB. The bulk of the REL volume is dominated by the PRP subsystem which contains the propellant and engine necessary to insert itself into orbit around Venus. The electronics are mounted above the propellant tanks within a protective cover. The solar array is mounted underneath the REL on its own pointing mechanism. A final overview of the REL can be found in Figure 6.4.

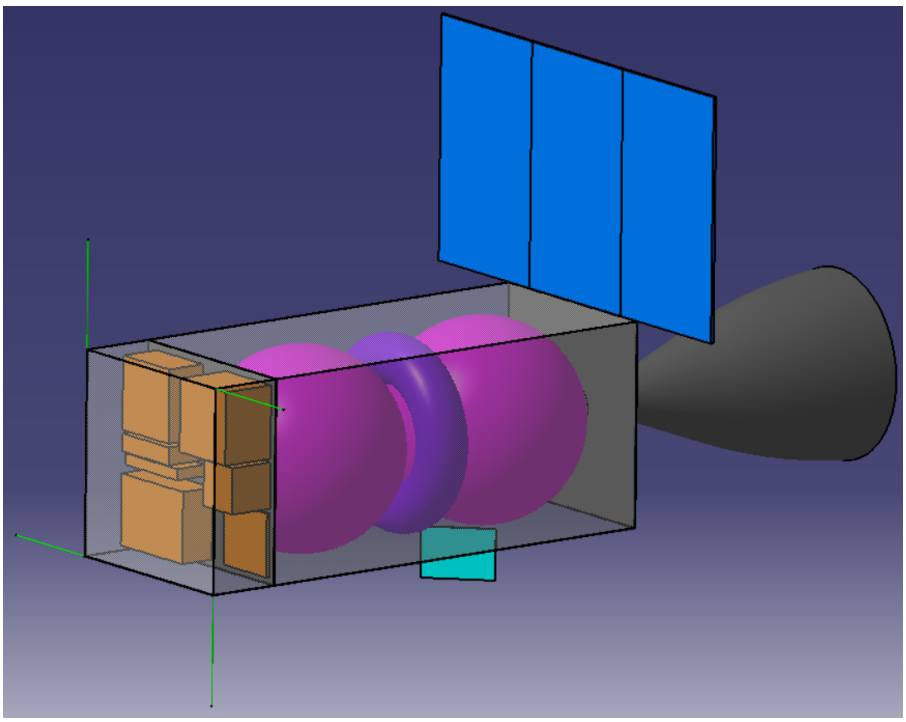

Figure 6.4: See-through REL CAD design.

6.4.2. Relay Materials and Production Characteristics

In the following sections of this report, the detailed design of all the subsystems of the REL is described. In these sections the material choice and if possible the production characteristics are described. The materials that are considered in the design the REL have been provided in Table 6.3. Stainless steel 304 was dismissed due to its high density.

Table 6.3: Mechanical properties of common aerospace materials.

Material	Unit	Ti6Al4V	AlBeMet	Al6061	CFRP
Density	kg/m3	4430	2070	2700	1700
E	GPa	71	197	69	220
Yield Stress	MPa	828	198	241	1400
Poisson Ratio	-	0.31	0.17	0.33	0.28
Specific Heat	J/(kg K)	526.3	1465	900	1100
Thermal Conductivity	W/(m K)	6.7	210	239	200
Solar Absorptance	-	0.75	0.16	0.09	0.83
Thermal Emittance	-	0.6	0.15	0.03	0.91
Source	-	[55]	[51]	[54]	[14]

6.5. Relay Technical Budgets

The resource allocation of a mission is an important aspect to track. In this section the budgets for the REL is presented. In these budgets, margins are added. The results of these budget are summarised in the mission technical budgets.

6.5.1. REL Mass Budget

The mass budget for the REL is given in Table 4.6. In this table the mass of all subsystems and their components are given. The mass is summed up and a 20% design margin is added.

Table 6.4: REL mass budget.

Subsystem:	Component	Mass [kg]:

REL-OBD	TI MSP430 6U	0.10
	Flash memory	-
REL-TNC	LGA	0.40
	HGA	1
	IRIS V2 Transponder	0.88
	IRIS V2 SSPA	0.13
	IRIS V2 LNA	0.23
REL-THE	MLI	1.81
	RTR	0.09
	PIP	0.50
REL-STR	TUB	1.48
	COV	0.36
REL-EPS	BAT	0.50
	SOA	0.32
	PCD	0.30
REL-MEC	All mechanisms combined	0.50
REL-ADC	XACT-50	1.23
REL-PRP	BPT	1.02
	CGT	1.67
	ENG	3.60
Total		**15.97**
Margin		**20%**
Total with Margin		**19.16**
Requirement		**19.16**
Compliant with Reqs.		**YES**

6.5.2. REL Volume Budget

The volume of all components of the REL is given in Table 6.5. For each of the components of the REL, the subsystem that it is part of is also given. Besides that, the dimensions as well as the volume it takes up are given.

Table 6.5: REL volume budget.

Subsystem	**Component**	**Dimensions [cm]**	**Volume [cm^3]**
REL-TNC	IRIS	10.4 x 11.85 x 6.5	801.06
REL-TNC	SSPA	8.75 x 4.3 x 2.3	86.5375
REL-TNC	LNA	7.55 x 4.3 x 1.3	42.2045
REL-TNC	HGA	59.7 x 33.5 x 0.417	833.97915
REL-EPS	BAT	13.5 x 9.8 x 4.9	648.27
REL-EPS	PCD	6.30 x 6.30 x 6.30	250.047
REL-EPS	SOA	10 x 7 x 0.1	7
REL-OBD	CPU	8.66 x 9.32 x 3.00	242.1336
REL-OBD	ROM	0.8 x 0.6 x 0.075	0.036
REL-ADC	XACT-50	10 x 10 x 7.54	754
REL-PRP	BPT	R=17.32	43450
REL-PRP	CGT	R=13.35, r=3.78	3770
REL-PRP	ENG	50 x 24.8 x 24.8	30752
TOTAL VOLUME			81637.26775
MARGIN			20%
TOTAL WITH MARGIN			97964.7213
Requirement			**97964.7213**
Compliant with Reqs.			**YES**

6.5.3. REL Power Budget

The power budget is provided in Table 6.6. It includes the maximum power consumption at peak power, as well as the average power consumption over a time period of $24hrs$.

Table 6.6: Power budget of the REL.

Subsystem	Component	Peak Power [W]	Energy per 24 hours [Wh]
REL-TNC	IRIS	35	840
REL-OBD	MEM	0.09	2.16
REL-OBD	CPU	0.07	1.73
REL-EPS	BAT	n/a	n/a
REL-EPS	PCD	n/a	n/a
REL-PRP	ENG	35	-
REL-ADC	STK	1	18.00
REL-ADC	RWL	27	36.00
Total		98.16	897.89
Margin		**20%**	**20%**
Total with Margin		107.98	987.68
Requirement		107.98	987.68
Compliant with Reqs		YES	YES

6.5.4. REL Data Budget

The data budget is given in Table 6.7. The data volume is provided for all relevant components of the REL. The subsystem that the component is part of is also listed. All the housekeeping data is included as the Processor data budget, which is estimated from [13]. The data from instruments was obtained using the communications model.

Table 6.7: REL data volumes per component, where the data volume refers to the average amount of data generated per 24 hours.

Subsystem	Component	Data volume [kbit]
REL-TNC	Transmitter	244530
REL-OBD	Processor	2560
Total		**247090**
Margin		**50%**
Total with Margin		**370635**
Requirement		**370635**
Compliant with Reqs		**YES**

6.5.5. REL Reliability Budget

An important resource for the mission is the reliability of all segments. The reliability of the REL has been determined using the same method that was described in the mission risk in Section 2.7. The results for the reliability are presented in Table 6.9.

6.5.6. REL 3σ Position and Velocity Uncertainty

Table 6.8: The REL-level 3σ position and velocity error.

Segment	Latitude and Longitude Position [m]	Velocity[m/s]
REL-TNC	18000	0.001
Total	**18000**	**0.001**
Margin	**5%**	**5%**
Total with Margin	**18900**	**0.00105**
Requirement	**18900**	**0.00105**
Compliant with Reqs.	**YES**	**YES**

6.5.7. REL Cost Estimation

Since the detailed design of the REL does not specify all exact parts of the mission, a statistical approach has to be used to produce a cost estimation at this stage. The chosen method for the REL is the SMAD[42] cost estimation for spacecraft weighing less than 500 kg, as described in Subsection 4.5.7. The TRL of the REL has been assumed been assumed to be 8, given the use of the many flight proven components. The breakdown of the cost estimation for the REL has been provided in Table 6.10.

Table 6.9: The reliability budget of the REL.

Subsystem	Mission Achieved [1]
REL-STR	0.9981
REL-THE	0.9931
REL-ADC	0.9998
REL-EPS	0.9960
REL-PRP	0.9869
REL-TNC	1.0000
REL-OBD	0.9997
REL-MEC	0.9999
Total	0.9740
Requirement	0.9740
Compliant with Reqs	YES

Table 6.10: The REL cost estimation per subsystem in FY2022 €K.

Subsystem	Cost [FY2022 €K]
REL-STR	452.5
REL-THE	358.9
REL-ADC	1851.3
REL-EPS	1379.5
REL-PRP	216.0
REL-TNC	720.9
REL-OBD	695.8
Program	5756.2
	16005.4
Margin	**20%**
Total with Margin	**20006.8**
Requirement	**20006.8**
Compliant:	**YES**

6.6. Relay Reliability and Risk

In this section the reliability and the risks of the REL are discussed. First the reliability for the REL is analysed. In the following subsection the risk map for the REL is presented together with the mitigation strategies applied.

6.6.1. Relay Reliability Analysis

The total reliability of the REL has been provided previously in Table 6.9. The reliability of each subsystem is derived from the method described in Section 2.7.

6.6.2. Relay Risk Map

It should be noted that the total reliability outlined in Table 6.9 is the reliability after risk mitigation. Prior to mitigation, the reliability of the REL has been 97.05%, compared to 97.40% after. The risk map for the REL showing the shifts caused by mitigation strategies is displayed in Figure 6.5. The risks represented in the figure include the minor degradation, major degradation and total failure of the different components of the REL. The components with the largest probability of failures, represented by the triangles, are identified to be within the mechanisms: The separation mechanism from the LAV, and the deployment mechanisms for the SOA, HGA, and LGA. Using redundancy in the design, the probability of these failures is reduced to obtain a more reliable

design, as shown by the circles.

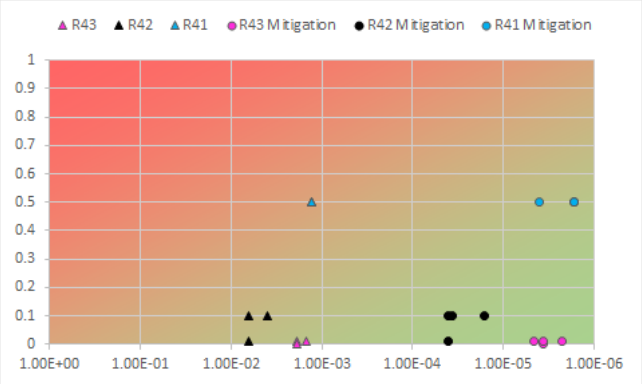

Figure 6.5: The REL risk map.

6.7. Relay Transmission and Command Subsystem

The REL-TNC is a subsystem used to transfer all the data obtained by the SCB and relay it to the ground stations (CCC), as well as receiving commands from CCC and relaying them to the SCB. This section covers in detail the functions that are accomplished along the entirety of the mission by the REL-TNC subsystem, as well as its architecture and the components that make up this subsystem.

6.7.1. REL-TNC Functional and Architecture Analysis

First, an analysis of the functions carried out by the REL-TNC is presented, followed by an analysis of its architecture.

REL-TNC Functional Allocation

During the transfer to Venus (phase 4 of the mission) the REL-TNC must receive commands from the CCC and send housekeeping data back (F4.3.1, F4.4.1, F4.5.1).

Once the EDV starts entry into the Venusian atmosphere, the REL-TNC must establish a connection with the EDV (F5.3.1), receive EDV data (F5.3.2), send data back to the CCC (F5.3.4), receive commands from CCC (F5.3.5), and send commands back to the EDV (F5.3.7).

In the operational phase of the mission, the REL system has to communicate with the SCB (F6.8.1). This includes tasks such as transmitting commands to SCB (F6.8.2), receiving scientific data (F6.8.11), transmitting and receiving ranging signals to the SCB (F6.8.6, F6.8.5), receiving ranging data from the SCB (F6.8.9), and receiving housekeeping data from the SCB (F6.8.13). Moreover, the REL has to communicate simultaneously with CCC (F6.7.1), which includes receiving commands from CCC (F6.7.3), transmitting and receiving ranging signals from CCC (F6.7.6, F6.7.5), receiving ranging data from the CCC (F6.7.9), transmitting scientific data to the CCC (F6.7.10) and transmitting housekeeping data to CCC (F6.7.12).

Finally, during the decommissioning phase of the mission the REL-TNC must receive decommissioning commands from the CCC and relay them to the SCB (F7.2.3). It must also end the health tone from the SCB (F7.6.1), and transmit the SCB health status (F7.6.3). The last function of the REL-TNC subsystem is to receive the decommissioning command for the REL (F7.7.3).

REL-TNC Subsystems Architecture

The architecture of the REL-TNC subsystem consists of the following:

- 4 Monopole Low Gain Antennas
- 1 High Gain Antenna
- 1 Transponder

Where the 4 low gain antennas handle communications between either the EDV or later on also the SCB, and the high gain antenna communicates back to the CCC. The former is done in the UHF band, while the latter is done in the X-band.

REL-TNC Hardware Block Diagram
A more detailed block diagram of the transponder can be found in Figure 4.17.

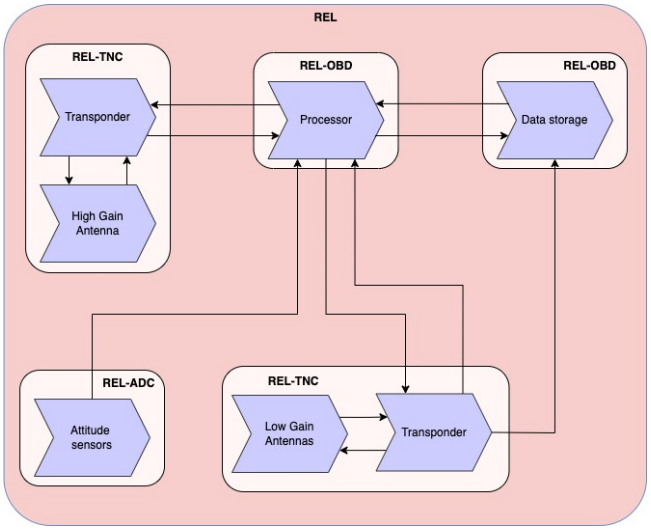

Figure 6.6: Block diagram of the hardware used in the REL-TNC, including other components of the REL system.

6.7.2. REL-TNC Key Requirements
The following key requirements for the REL-TNC are identified, based on the analysis presented above, and its allocated budgets:

Table 6.11: Key REL-TNC subsystem requirements, driving requirements are marked with [!].

ID	Description	Rationale
REL-TNC-REQ-2.4	[!]The REL-TNC shall transmit to the CCC in a frequency range of $8.400 - 8.450GHz$.	Derived from F6.7.6.
REL-TNC-REQ-2.2	[!]The REL-TNC shall receive from the CCC in a frequency range of $7.145 - 7.190GHz$.	Derived from F6.7.3.
REL-TNC-REQ-2.6	[!]The REL-TNC shall transmit data to the CCC at a speed of no less than $2.8kbps$.	Derived from the communications model.

6.7.3. REL-TNC Sizing
In the REL-TNC, 3 elements have to be sized, these being the low gain antenna, the high gain antenna, and the transponder. This subsection contains the sizing procedures for all three.

REL-TNC Sizing Antenna
For the low gain antenna sizing, since the main purpose of this component is to communicate with the SCB-TNC, the sizing procedure from the SCB-TNC was used. This consisted of determining whether a $3.5W$ set of UHF antennas can communicate with the desired bitrate and obtain the desired link margin ($3dB$). These results have been calculated manually, and verified using code.

The high gain antenna is sized similarly, where the highest distance between Earth and Venus and an estimation of the expected bitrate are first used, assuming an RF power of $5W$, and assuming the frequency band is be the X-band. This results in a suitable link margin, which has later been verified through code with more accurate numbers.

REL-TNC Sizing Transponder
Similar to other subsystems in this mission, the transponder sizing has come as a result of the antenna sizing. Since it is decided that both the UHF band and the X-band are used during communications, a compatible transponder must be chosen, with enough input power to feed both sets of antennas.

Model Limitations, Verification and Validation

Preliminary design assumed worst-case distances and conservative data estimation. However, the communications model was used for further analysis and thus the already-mentioned assumptions apply. This communications model (which was used to simulate the communications link between the RELs and the SCB, as well as the communications link between the RELs and the CCCs) was verified through manual calculations at random times in the mission. Furthermore, the code was also verified using a similar code which used a different approach when calculating the available bitrates between systems.

6.7.4. REL-TNC Final Design Overview and Evaluation

This subsection contains the selection of the 3 main components of the REL-TNC subsystem, as well as a summary of their basic properties.

REL-TNC Component Selection

First, the low gain antenna is selected. This selection follows from the antenna selection on the SCB-TNC, in which 6 ANT-100's are selected. For the REL-TNC, 4 ANT-100's are selected instead, since this is the minimum set of antennas required to guarantee an isotropic radiation pattern. This allows for the REL to point towards Earth while also being able to communicate with the SCB.

Next follows the selection of the high gain antenna, which results in the X-band High Gain Antenna from the MarCo mission [38] being selected. This antenna is able to emit the required RF power at the required frequency band, and has also been used before, thus it is determined to be an appropriate choice for the high gain antenna.

Finally, the selection of the transponder, which is chosen to be the IRIS V2 Transponder (also used in the SCB and the EDV), since it is able to support antennas for both the X-band and the UHF bands.

REL-TNC Sensitivity Analysis

As part of the verification process, the model used to calculate the possible bitrate between Earth and the REL is put through a sensitivity analysis, where inputs are changed in order to observe if the output changes accordingly.

An example of this is changing the high gain antenna RF power by reducing it from its original $5W$ down to $3W$. For the REL-1, the original average bitrate throughout the mission is approximately $4.3kbps$. After changing the RF power of the high gain antenna, the average bitrate went down to $2.6kbps$, which is what is expected. Furthermore, other inputs such as altitude and instrument data rate are changed to further evaluate the behaviour of the output.

REL-TNC Final Design Parameters

Table 6.12 summarises the main properties of the REL-TNC.

Table 6.12: Summary of the properties of the REL-TNC components, where the 'IRIS V2 Transponder' also includes the SSPA and the LNA.

Component	Mass (kg)	Volume (cm^3)	Power (W)	Voltage (V)	Cost (USD)	Sources
ANT-100 UHF/VHF Monopole Antenna (x4)	0.4	-	35	5	677,211	[72, 24, 42]
X-Band High Gain Antenna (x1)	1	833.98		-		[38, 42]
IRIS V2 Transponder (x1)	1.1	929.80		12 - 28		[57, 42]

The power is depicted for the entire REL-TNC, since the transponder takes in this power ($35W$) and distributes it to either antenna. The cost is estimated using the new SMAD [42]. For more information on the low gain antenna, refer to Table 4.16. Table 6.13 contains more information on the high gain antennas for both the 1st and the 2nd relay.

Table 6.13: The properties of the high gain antennas for REL-1 and REL-2.

Component	Uplink Frequency (GHz)	Downlink Frequency (GHz)	RF Power	Power (W)	Gain (dB)
REL1 High Gain Antenna	7.17	8.425	5	30	29.2
REL2 High Gain Antenna	7.27	8.525	5	30	29.2

The reason REL-1 and REL-2 have different uplink and downlink frequencies is to be able to use 'Multiple Spacecraft Per Aperture' (MSPA) [25], which allows for a single ground station to receive data from two different spacecraft at the same time, as long as the link between each spacecraft and the ground station is at a different frequency. Moreover, the electrical power consumed per high gain antenna is an approximation derived from the IRIS Transponder.

In Table 6.14 a summary of the link budget can be found, for both REL-SCB communications and REL-CCC communications. Some numbers in this table are assumed, such as the system noise temperature or the phase modulation index.[50]. Other values (such as the atmospheric attenuation and the path loss) are not included as they greatly vary during the mission.

Table 6.14: Link budgets for communications between the SCB and the RELS, as well as the RELs and CCC.

Parameter	REL-SCB	SCB-REL	REL1-CCC	REL2-CCC
Carrier Frequency (MHz)	438	390	8425	8525
Phase Modulation Index (rad)	1.2			
Tx power (W)	3.5		5	
Tx passive loss (dB)	2		2	
Tx antenna gain (dB)	0		29.2	
Tx EIRP (dB)	33.44		64.19	
System noise temperature (K)	250		50	
Rx system loss (dB)	5		1	

6.8. Relay Onboard Data Handling Subsystem

During the lifespan of the mission, the REL is in charge of transmitting information back and forth between the SCB and the CCC. The OBD manages all the data that is sent and received, how it is processed and whether or not it is stored. This section discusses in detail the different aspects of the SCB-OBD.

6.8.1. REL-OBD Functional and Architecture Analysis

In the course of this next subsection, the functions and the architecture of the REL-OBD are described.

REL-OBD Functional Allocation

During the travel to venus (in phase 4 of the mission), the REL-OBD must use available data to prepare for Venusian orbit insertion (F4.3.4), and after insertion it must reconfigure the REL to prepare for the operational phase of the mission (F4.4.5). During the EDV's descent to Venus, the REL-OBD must process all the incoming and outgoing data between the EDV and the REL (F5.3.3), as well as the CCC and the REL (F5.3.6). Once in the operational phase, the REL must process all commands received from CCC as well as process all the data received from the SCB (F6.9.6). Finally, during the decommissioning phase of the mission, the REL-OBD must process any extra commands from CCC (F7.4.6), determine the SCB status once it has been ordered to decommission (F7.6.2) and execute the decommissioning command for the REL (F7.7.4).

REL-OBD Subsystems Architecture

The REL-OBD is composed of a processor and a data storage unit. The former is in charge of processing and distributing all incoming data as well as sending out commands, while the latter stores incoming data until it can be transmitted.

REL-OBD Software Block Diagram

Figure 6.7 contains a block diagram that shows the way in which data is handled by the REL-OBD.

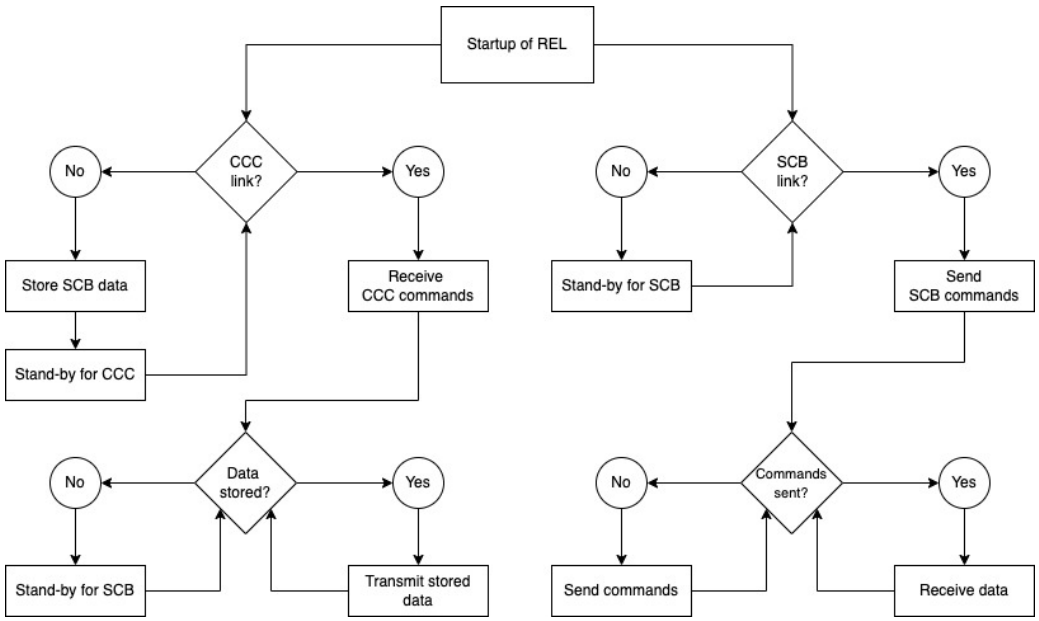

Figure 6.7: The software block diagram for the REL-OBD, showing the data managing process for both REL-CCC communications and REL-SCB communications.

REL-OBD Hardware Block Diagram

Since the REL-TNC and the REL-OBD are heavily intertwined, a hardware block diagram is made for both of these subsystems combined, which can be found in Figure 6.6.

6.8.2. REL-OBD Key Requirements

The following key requirements for the REL-OBD are identified, based on the analysis presented above, and its allocated budgets:

Table 6.15: The key REL-OBD subsystem requirements, driving requirements are marked with [!].

ID	Description	Rationale
REL-OBD-REQ-2.1	[!]The REL-OBD shall process incoming data until EOL.	Derived from F6.9.6.
REL-OBD-REQ-1.4	[!]The REL-OBD shall be able to process at a data rate of no less than $192 kbps$.	Derived from the communications model.
REL-OBD-REQ-2.4	[!]The REL-OBD shall be able to store no less than $50 MB$ of data.	Derived from the communications model.

6.8.3. REL-OBD Trade-off

The trade-off for this subsystem closely resembles the trade-off for the SCB-OBD shown in Figure 4.21, where the only difference lies in 'Processing Partition'. In the SCB-OBD it is decided to have processing between the SCB and the PLD, in the REL-OBD there is no processing between the REL and the PLD, since there is no actual payload. The other branches of the design option tree remain the same.

6.8.4. REL-OBD Sizing

This subsection deals with the sizing of the previously introduced components: The processor and the data storage unit. This is done with the help of the SCB-REL-CCC communications model first mentioned in Chapter 4.

REL-OBD-STO - Sizing OBD Storage

Since this mission uses two identical RELs, the sizing is done for both RELs simultaneously. Although at a first glance it might seem both RELs have the same maximum data storage, it turns out that, due to their different

trajectories, the maximum data storage differs slightly. A sample of the results from the communications model with respect to the data storage sizing can be seen in Figure 6.8.

The sizing of the REL data storage units is done by finding the maximum data storage needed for the entirety of the mission. According to the model, REL-1 and REL-2 do not need any more data storage than 33 and $32 Mbytes$ respectively at all times. However, following literature [75] a margin of 50% is taken for both data storage units bringing the maximum up to $50 Mbytes$ and $48 MBytes$ for REL-1 and REL-2.

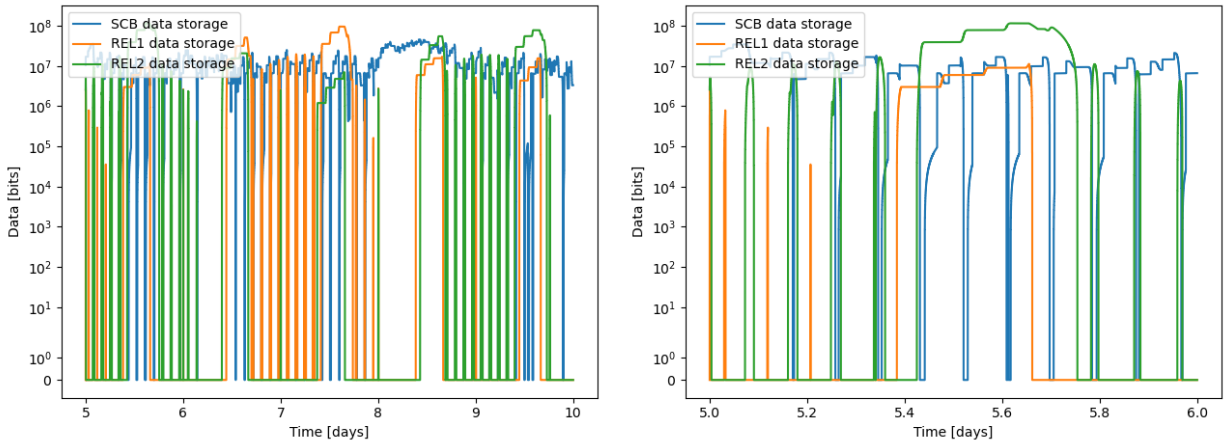

(a) The SCB, REL-1 and REL-2 data storage from day 5 to day 10 of the mission.

(b) The SCB, REL-1 and REL-2 data storage from day 5 to day 6 of the mission.

Figure 6.8: The results from the communications model presenting the data storage over time.

REL-OBD Sizing Processor

The sizing for the REL-OBD processor resembles the sizing for previous processors for other subsystems, where the maximum achievable data rate of the system is used. Based on the aforementioned model, the maximum transmitted bitrate between the SCB and both RELs is obtained, which is approximately 72 $kbps$. Moreover, assuming a worst-case-scenario by taking the maximum bitrate between both RELs and the CCC, the maximum bitrate through the RELs is approximately 96 $kbps$. Applying a 100% margin [75] means that the processor to be chosen must at least be able to process data at a rate of 192 $kbps$.

Model Limitations, Verification and Validation

Since the sizing of the EDV-OBD was done using the communications model, both the assumptions the verification and validation procedures that are carried out are those listed in Subsection 4.8.4. These include comparing the model output to calculations done by hand, and comparing it to outputs of a similar model with a different calculation method. Furthermore, it is assumed that all incoming data is first stored in the data storage unit before being transmitted once the processor decides to.

6.8.5. REL-OBD Final Design Overview and Evaluation

In this subsection the final design of the REL-OBD is shown.

REL-OBD Component Selection

For the data storage unit selection, the W25N512GVxIG/IT Flash storage [95] is selected, since its total storage is above what is required for the REL-OBD. This is also the same data storage unit used for both the SCB-OBD and the EDV-OBD. For the processor selection, the Texas Instruments MSP430 [40] is selected as its communication interface's bitrate is high enough to support the incoming data. This is the same processor that is used in the EDV-OBD.

REL-OBD Sensitivity Analysis

Various sensitivity analyses are performed for the entire model during the SCB-OBD sizing in Subsection 4.8.5, thus it is not treated any further.

REL-OBD Final Design Parameters

Table 6.16 summarises the general properties of the selected components.

Table 6.16: A summary of the properties of the OBD components for both RELs.

Component	Mass (kg)	Volume (cm^3)	Power (W)	Voltage (V)	Cost (USD)	Sources
TI MSP430	0.1	242.13	0.072	3.6	628,282	[40, 42]
W25N512GVxIG/IT	-	0.036	0.09	3		[95, 42]

6.9. Relay Attitude Determination and Control System

Like with any satellite, the Attitude Determination and Control System (ADC) is of crucial importance to the success of the mission, due to the lack of any meaningfull atmosphere to resist unauthorised attitude adjustments. Without a mechanism to keep the REL updated on its orientation and keep it pointed at either the CCC or the SCB, the collected data can not be transmitted back to the CCC, rendering the whole mission inoperable.

6.9.1. REL-ADC Functional and Architecture Analysis

To communicate with the CCC and transmit the scientific data obtained by the SCB back to Earth, the REL must be kept within certain limits. The REL-ADC is designed identically for both RELs, since they have the same requirements and disturbances.

REL-ADC Functional Allocation

The functions that this subsystem has to perform are as follows: the REL-ADC must determine the REL's orientation and the REL-ADC must keep its antennas pointed at either the Earth or the SCB, depending on the phase of the mission.

REL-ADC Systems Architecture

The REL-ADC's architecture consists of two separate parts: First, the Xact-50 reaction wheels assembly to rotate and orient the REL, and second, the RCS thrusters, which are used after every orbit to dump momentum. These thrusters are fed from the same pressurant tank that backfills the main propellant tanks. The high pressure in this tank suggest that a pressure regulator valve might need to be inserted in the pipework between the tank and the thrusters. However, this is left for further and more detailed design reports.

REL-ADC Hardware Block Diagram

The REL-ADC only interacts with three other subsystems, which is shown below in Figure 6.9: The REL-EPS, since certain segments of the REL-ADC need power, the REL-OBD, to receive commands and provide updates, and the REL-PRP, which supplies the gas for the RCS thrusters.

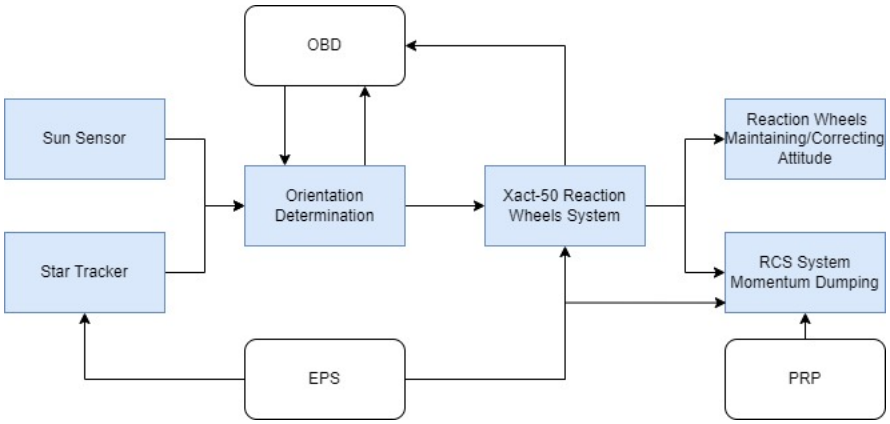

Figure 6.9: REL-ADC hardware block diagram.

6.9.2. REL-ADC Key Requirements

The following key requirements for the REL-ADC are identified, based on the analysis presented above, and its allocated budgets:

Table 6.17: The key REL-ADC subsystem requirements, driving requirements are marked with [!].

ID	Description	Rationale
REL-ADC-REQ-1.2	[!] The ADC shall determine the attitude of the REL in all three axis.	Required to facilitate accurate pointing.
REL-ADC-REQ-1.4	[!] The ADC shall be able to point the REL to the required attitude with a speed of $0.5°/s$.	Required to compensate any encountered drift.
REL-ADC-REQ-1.5	[!] The ADC shall be able to point the REL to the required attitude with an accuracy of $1.75°$.	Derived from the selected earth-pointing antenna.

6.9.3. REL-ADC Analysis, Trade-off and Design Selection

Before the REL-ADCS components can be selected, the demands on the system need to be quantified:

REL-ADC Torque

There are four main potential sources of attitude disturbances: magnetic torque, gravitational torque, solar radiation and atmospheric drag. Magnetic torque can be neglected, since Venus does not have a magnetosphere such as the Earth. Similarly, after initial calculations, the orbital altitude of 1700 km results in an incredibly small atmospheric drag, thus this is neglected too. Consequently, the two sources of disturbance that need to be calculated to select and size the REL-ADC are gravitational disturbances and solar radiation pressure on the REL's solar array, which is done according to the two formulas below [42]:

$$T_s = \frac{\Phi}{c} A_S (1 + q*)(cp_S - cm) cos\phi \qquad (6.1) \qquad\qquad T_g = \frac{3\mu}{2R^3} |I_z - I_y| sin(2\zeta) \qquad (6.2)$$

This results in the following values: solar radiation can cause up to $1.2 * 10^{-6} Nm$ of max torque; gravitational drag can cause up to $2.1 * 10^{-7} Nm$ of max torque. It thus becomes clear that the maximum torque of the solar radiation is significantly larger than the torque generated by Venus's gravitational field. Since these values represent the upper limit on torque, the value of the solar radiation is selected for the design of the REL-ADC as a worst-case scenario. This is to account both for all the other much smaller experienced rotational forces, as well as to provide margin for the REL-ADC, which is critical for the operation of the RELs.

REL-ADC Pointing accuracy

Another requirement that the REL-ADC needs to fulfill is the acceptable pointing accuracy of the REL-TNC. Since the antenna pointing at the SCB is almost omnidirectional, no rotation angle requirements are attached to it. The antenna pointing towards Earth however, needs to do so with an accuracy of at least 1.75 °, as was derived in [2]. Since the antenna does not pivot but is fixed in place to the REL, the REL itself needs to provide this pointing accuracy when data transfer to Earth takes place.

REL-ADC Slew rate

Finally, it is desired that the REL can correct the expected/documented 1.4 ° of offset generated by the Falcon 9 decoupling mechanism within a few seconds. This slew rate is also sufficient to keep the REL pointed at either Earth or the SCB over the time durations needed for tracking and data transfer to occur.

REL-ADC Trade-off

To select which combination of determination and control options are required, table 19.8 and table 19.9 from the new SMAD [42] are used. From these tables, it is evident that reaction wheels with momentum storage can meet both the torque, accuracy and slew rate requirements, for 3-axis stabilisation.

6.9.4. REL-ADC Sizing

REL-ADC Sizing for Momentum Storage

From the torque load derived in Subsection 6.9.3, the needed momentum storage can be computed. Since the mission is deemed too long to store all the momentum accumulated over the 200 days of operations, it is decided to size / select the reaction wheels to handle the accumulated momentum for one full orbit and to consequently

de-spin the spacecraft using thrusters to ”drain” the wheels every orbit. The maximum needed torque to keep the REL steady is given at $1.2 * 10^{-6}\ Nm$, which, once multiplied with the orbital period, results in the need to store up to 0.009 Nms of momentum after one orbit, depending on the orbital period (less when eclipse times are taken into account).

REL-ADC Component Selection
After a look through commercially available off-the-shelf reactions wheels, the Xact-50 attitude control system from the Blue Canyon Technical company is decided to best fit the requirements. This component meets both the slew rate, momentum storage and angle pointing accuracy requirements, but it also comes with attitude determination sensors, star trackers as well as a sun sensor [8]. Furthermore, the system has flight heritage in the MarCo mission.
To dump the accumulated momentum stored by the Xact-50 system, RCS thrusters are used. RCS cold gas thrusters have been selected to perform the momentum dumping, as the small size of the relay and the wide range of cold gas RCS thrusters allows for the required thrust precision and control. To provide some specifics, two equations from [42] are used:

$$F = \frac{h}{L * t} \tag{6.3}$$

$$m = \frac{Ft}{g * ISP} \tag{6.4}$$

Where F is the force required of the RCS thrusters to dump the amount of stored momentum (h) with a motion arm (L), which is half the width of the relay, over a given time (t) which is selected at 1 second. The required force is found to be 0.05 N. Then the propellant mass (m) can be found by multiplying the force found with the time and dividing this by the exhaust velocity of the RCS system, which is assumed to be 9.81 times an ISP of 70 s. This value of m multiplied by the number of orbits the REL performs over the course of 200 $days$ (roughly 2304 with an orbital period of 125 $mins$) results in the total amount of nitrogen RCS gas that the REL needs to carry, in this case 0.174 kg.

Model Limitations, Verification and Validation
No code is used to derive these equations and results. Instead they are obtained directly from [42] and are purely algebraic. Hence no Verification and Validation is performed, besides from performing sanity checks on the resulting values, which they all pass.

6.9.5. REL-ADC Final Design Overview and Evaluation
The REL-ADC consists of a sun sensor + star tracker for orientation, Xact-50 for reaction control and momentum storage (as well as containing the aforementioned sensors), and six 0.05 N RCS thrusters to dump the accumulated momentum quickly once every orbit, and provide added control authority if circumstances demand it.

REL-ADC Sensitivity Analysis
The ADC is very conservatively designed, both to give it a substantial margin to deal with any unexpected situations and changing mission needs, but also because it is very difficult to accurately predict the exact disturbance forces that the REL encounters due to the very limited number of Venus orbiters sent to the planet so far. If the pointing and slew requirements change, it most likely does not have any significant impact. If they are increased to the point that a new reaction wheel assembly or bigger RCS thrusters are needed, a redesign and resizing is needed (since the ADC does have a decent impact on the mass budget), but this is not considered likely, given how conservative all the performed calculations are.

REL-ADC Final Design Parameters
Table 6.18 summarizes the general properties of the selected components.

Table 6.18: A summary of the properties of the ADC components for both RELs.

Component	Mass (kg)	Size (cm^3)	Cost (USD)	Source
Xact-50	1.23	754	1851,355	[8]
RCS system	1.67	2980		[42]

6.10. Relay Propulsion System

Due to the desired circular orbit, a large propulsion system is needed for the REL to complete its objectives. After decoupling from the upper stage of the Falcon 9 booster, the RELs need to perform a burn to arrive at Venus shortly before the EDV, before performing one of the largest orbital insertion burns ever performed by an interplanetary spacecraft. This section goes into a detailed analysis of the propulsion system, its requirements and its components.

6.10.1. REL-PRP Functional and Architecture Analysis

To reach its intended orbit after separating from the booster's upper stage, the REL needs a propulsion subsystem. As a result, this mission is unusual, but not unprecedented in terms of its delta-V budget, which is the main design driver of both the REL-PRP, as well as the overall RELs dimensions. Though there is technically a small difference in the delta-V's of the two RELs, it is not considered sufficient to justify designing different PRP subsystems for them.

REL-PRP Functional Allocation

The REL-PRP must provide the delta-V for both RELs to reach their desired orbits, must perform en-route corrections to make them arrive at different times, and it must be able to de-orbit the RELs at the end of the mission.

REL-PRP Systems Architecture

The architecture of the REL-PRP is both straightforward and absolutely defining for the architecture of the entire REL: a large bipropellant engine, supplied with fuel and oxidiser via pipes, with pressure rather than pumps pushing the propellant into the engine's combustion chamber. Meanwhile the tanks themselves are backfilled from a highly pressurised pressurant tank filled with nitrogen.

REL-PRP Hardware Block Diagram

As mentioned in Subsection 6.10.1, the REL-PRP consists of only four large components and a series of pipes, valves and sensors which are not displayed to maintain clarity. The only interactions with other subsystems occur where the engine requires power for start-up, and the information provided to the REL-OBD, which is displayed in Figure 6.10.

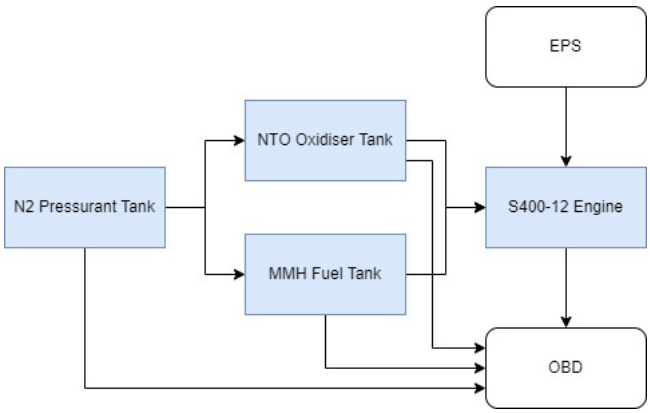

Figure 6.10: REL propulsion subsystem hardware block diagram.

6.10.2. REL-PRP Key Requirements

The key requirements for the REL-PRP have been identified, based on the analysis presented above, and its allocated budgets. These have been provided in Table 6.19.

Table 6.19: The key REL-PRP subsystem requirements, driving requirements are marked with [!].

ID	Description	Rationale
REL-PRP-REQ-1.1	[!]The REL-PRP shall provide at least 4 km/s of delta-V.	Derived from orbital mechanics, dictated by the final orbit.
REL-PRP-REQ-1.6	[!] The REL-PRP shall have a thrust of at least 282 N.	Required to limit the gravitational losses.

6.10.3. REL-PRP Trade-off

Before the propulsion system can be designed in detail, its nature and limits need to be determined. This is done by first generating the design option tree displayed below in Figure 6.11, before pruning to just one option in the subsequent sections.

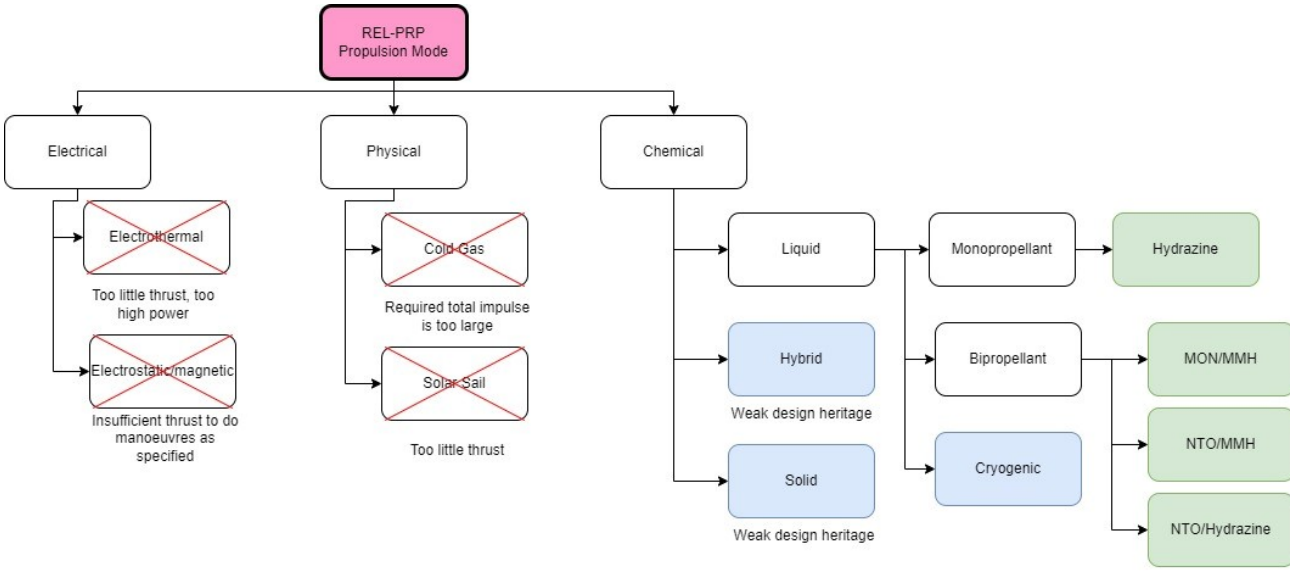

Figure 6.11: The REL-PRP design options tree.

Propulsion Type Selection

The high delta-V requirement eliminates any propulsion system with an ISP below 250, while the need to get into orbit quickly enough to track the EDV on descent prevents any low-thrust electrical propulsion systems from being considered. Also, the difficulty with thermal control eliminates cryogenic fuels as an option. This leaves various bi-propellant chemical engines as the main contenders.

6.10.4. Propellant Selection

In order to prune further, the temperature ranges of the respective fuel and oxidiser options are compared to the expected internal temperature range that the REL experiences. In order for the REL-PRP to be effective, both fuel and oxidiser have to remain liquid before entering the combustion chamber. This results in the selection of the NTO/MMH combination; Nitrogen Tetroxide as the oxider and Methyl Hydrazine as the fuel. Both of these substances are found to have acceptable melting & boiling points, as well as adequate combined performance in terms of ISP, restart cycles and thrust levels.

6.10.5. REL-PRP Sizing

REL-PRP Delta V Budget

In order to design or select the REL-PRP, the main thing that needs to be determined is the total amount of delta-V that the REL needs to posses in order to satisfy its mission requirements. For the midterm, a rough estimate is made to determine the delta-V needed to get to a low Venusian orbit when starting from an earth escape trajectory. However, for the final design, a more in-depth analysis needs to be performed.

Utilising the lecture slides from AE2230-I (adapted for a Venus-bound mission), a code is made to model a fast(er) trajectory to calculate the total delta-V needed to arrive at Venus several days in advance of the EDV, which takes approximately 147 $days$ according to cosmic train schedule (link / ref) utilising a standard hohmann transfer. Setting the final orbit at 1701 km above the surface of Venus, a total delta-V of around 3084 m/s is needed to arrive just over one day before the EDV enters, and around 3087 m/s to arrive a little over two days earlier. Far faster transfers are possible with adding only a few dozen or hundred m/s, but this is considered unnecessary.

Since this model is important, and all further REL-PRP characteristics flow from it, verification and validation need to be performed. For verification, repeated intermediate results (such as the semi-major axis, the relative

velocities and angles when arriving at Venus, and the individual delta-V values) are checked at various escape velocities. This shows that as the velocity while escaping Earth increases, the total delta-V increases as well (since the REL needs to slow down more upon arriving at Venus compared to a normal Hohmann transfer). Since all of this is consistent with the real world, the code is considered to be verified. For validation, delta-V maps of the solar system are consulted. As the results agree with literature, the code is considered valid.

Next, the orbital maintenance due to atmospheric drag is modelled, and is found to be no more than 0.5 m/s over the lifetime of the mission due to the high altitude, and is therefore considered negligible. Two further assumptions are made due to insufficient or unpredictable information:

1. No large orbital inclination burns need to be done by the REL after arriving in Venus orbit.
2. No inclination change during interplanetary transfer.

Now, the de-orbit burn needs to be quantified. After studying the atmospheric parameters of Venus, it is decided that the periapses should be lowered to 150 km above the surface to facilitate a rapid orbital degradation, causing the RELs to burn up shortly after the end of the mission. This requires a delta-V of around 374 m/s. (again using equations from the slides of in this case lecture 3 of AE2230-I)

Adding the acquired delta-V's together gives an initial budget of: 3087 + 374 = 3461 m/s. However, in order to compensate for the earlier assumptions, a considerable margin of over 15% is added to the final number to account for any other small or unexpected burns, while also providing a buffer against any potential dry mass growths or giving the REL the option to substantially change its orbit's shape, altitude and inclination, if the need arises. Consequently, a total delta-V budget of 4 km/s is considered adequate

REL-PRP Sizing Propellant Tanks
The calculations needed for the main propellant tanks are relatively easy with the following assumptions:

1. I_{sp} is 292 seconds
2. Mixture ratio is 1.65

This results in the following values:

Around 45.611 kg of propellant is needed assuming a dry mass of 15 kg and an ISP of 292 (derived from the rocket equation). selecting a mixture ratio of 1.65 results in 17.211 kg MMH and 28.4 kg NTO. This leads to a Volume of 0.0197 m^3 MMH and 0.0198 m^3 NTO for the two tanks with their densities known. Combining the two volumes and applying a 1.1 factor to account for the pipes, valves and tank walls leads to the propellant system to have a total volume of 0.04345 m^3.

REL-PRP Sizing Pressurant Tanks
It is deemed easier to use a pressurant gas to keep the propellant at the needed pressures for the engine's combustion chamber. To limit complications, N2/nitrogen is selected for the pressurant system of the propellant tanks, since it is already the RCS gas. Again utilising the new SMAD [42], the two equations below and an N2 density table are used to design and size the pressurisation system.

$$V_{total} = \frac{M_{gas} R_{gas} T}{P} = V_P + V_{Pres} \qquad (6.5) \qquad\qquad M_{gas} = \frac{P V_P}{R_{gas} T - P/\rho} \qquad (6.6)$$

V_{pres}, the volume of the pressurant tank, is the desired output. To calculate this, the mass of the pressurant gas needs to be derived first. All other variables; $Rgas$, T (the minimum temperature at the end of the mission), P (the end-of-life pressure), V_p (the volume of the propellant tanks, here rounded to 0.04 m^3) and ρ (the density of the pressurant gas at maximum pressure and temperature) are known values.

These equations produce a result of 676 g pressurant needed, which results in a pressurant tank volume of 0.00238 m^3. However, this does not take into account the loss of pressurant nitrogen mass due to it also being used for the RCS thrusters. Using the same density as used earlier, another 0.0006 m^3 must be accounted for to hold the 174 g of RCS fuel, since a tank pressure of 10 bar must be maintained at EOL. Combined, they therefore must have a (highly) pressurised volume of 0.00249 m^3. Applying the same 1.1 factor used in Item 6.10.5 to account for the size of the tank walls, valves and pressure lines, the pressurant system thus has a volume of around 0.00298 m^3.

REL-PRP Sizing Thrust
It is decided that, in order to select the minimum thrust that the selected engine has to provide, gravitational losses have to be approximated to find an acceptable burn time limit for the orbital insertion around Venus. In order to leave a 1.1 factor between total delta-V used and the delta-V budget, 193 m/s is the maximum amount of gravitational losses that are considered acceptable. Utilising a short code, it is found that this entails a minimum thrust of 282 N and a transfer time of 400 s, assuming an ISP of 292. Five assumptions are used to generate this code, which is not expanded on for the sake of brevity, but they are found to be both reasonable and conservative, and consequently are used to generate the result mentioned above. Hence engines within the range of 250-500 N of thrust are considered.

Model Limitations, Verification and Validation
The Verification and Validation used for the code that the delta-V budget is generated from is described locally in Subsection 6.10.5. The code used for the thrust sizing in Equation 6.10.5 is considered Verified and Validated if the assumptions used to create it are proven to be reasonable but conservative, which they are. All other calculations are either derived from algebraic formulas from the orbital mechanics course, or obtained from [42]. As both of these are considered reliable sources of information, no further Verification and Validation is performed there.

6.10.6. REL-PRP Final Design Overview and Evaluation
With the propellant and its tanks defined, the only component that needs to be specified is the main thruster, done with the information gathered in Equation 6.10.5. After this is done, a sensitivity analysis is performed, before the final relevant design parameters are presented.

REL-PRP Component Selection
For the main engine, after comparing various off-the-shelve and commercially available components, the model S400-12 of the 400 N bipropellant apogee motor from orbital propulsion centre, a member of arianegroup, is selected. A picture, taken from [83] is displayed in Figure 6.12.

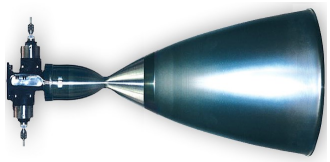

Figure 6.12: The S400-12 Thruster on the REL-PRP.

REL-PRP Sensitivity Analysis
This engine has a higher mass than what has originally been accounted for, but it also has a higher ISP than what has been used for the original propellant tank sizing. A quick rocket equation calculation confirms that the delta-V requirement is met with the new ISP so long as the dry mass of the REL does not exceed 17.56 kg. Even with the heavier engine, it is not expected that this is the case.

The delta-V requirements have been made as conservatively as possible, but if the original dry mass of 15 kg is still assumed valid, then the new total delta-V of the REL is around 4325 m/s, so there is room for expanding the orbital requirements of the REL in that case. Anything above this requires the redesign and most likely resizing of the entire REL, and is therefore considered highly undesirable.

REL-PRP Final Design Parameters
Table 6.20 summarises the general properties of the selected components.

Table 6.20: A summary of the properties of the components of the PRP for both RELs.

Component	Mass (kg)	Size (cm^3)	Cost (USD)	Source
S400-12	3.6	30.752	215,994	[83]
propellant tanks	1.02	40.000		[42]

6.11. REL Electrical Power System
The REL electrical power system is a crucial subsystem in any REL satellite, for many other subsystems require electrical power to perform their functions. Since almost every spacecraft sent into orbits around the Earth or other planets in solar system have been equipped with an EPS, the experience on designing this subsystem is high and much of the design process has been widely investigated before. Yet, each mission is unique and requires their own custom made EPS, which is documented in this section.

6.11.1. REL-EPS Functional and Architecture Analysis

In order to perform all of its tasks, the REL needs electrical power to be supplied to several subsystems. This electrical power must be generated, stored and distributed by the REL-EPS. Due to their similar functions and designs, the REL-EPS is designed identically for both RELs. After the design is made, the sizing is done separately for both RELs, using the same methods and model, but with their unique inputs.

REL-EPS Functional Allocation

The functions of the REL-EPS are similar for the operational phase and the transfer phase, hence, each of the mentioned functions applies to both phases. The REL-EPS must generate electrical power (F6.9.1) & (F4.3.2.1), the REL-EPS must store this electrical power (F6.9.1) & (F4.3.2.1), and the REL-EPS must distribute this power to the subsystems that require it (F6.9.1) & (F4.3.2.1).

REL-EPS Systems Architecture

The architecture of the REL-EPS follows a traditional spacecraft EPS layout, consisting of a solar array that generates the primary power and a secondary battery that stores the electrical power such that it can provide power during eclipse conditions. The solar array uses a mechanism, combined with the attitude strategy of the REL, to ensure that the incidence angle of the sun on to the solar array is always 0 °. This mechanism consists of a one axis rotation of maximum 180 °. The secondary battery consists of two blocks of multiple connected identical Li-ion batteries that are used together to provide the power storage and discharge current and voltage required. Within the REL-EPS, a power distribution module is included, as well as voltage and current regulators and a battery charge & discharge regulator.

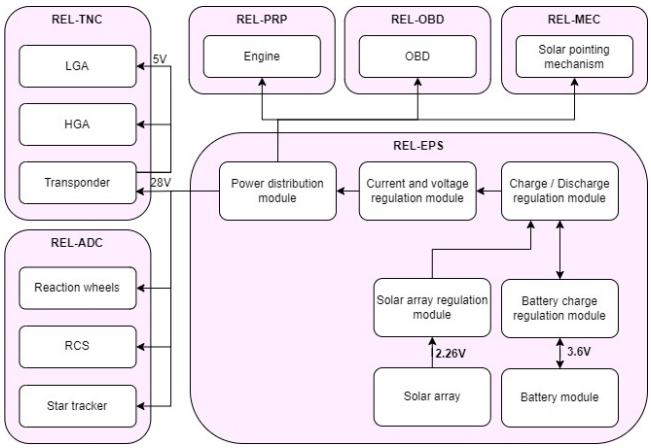

Figure 6.13: The hardware block diagram of the REL-EPS.

REL-EPS Hardware Block Diagram

In Subsection 6.11.1 the architecture, and thus partly the hardware, of the REL-EPS is described. The individual parts of the EPS are connected to each other in order to fulfill a unified function. The way these individual parts are related to each other, as well as to other subsystems outside of the REL-EPS is presented in Figure 6.13. In the respective block diagram certain voltages are indicated between power flows. This indicates that either the power is generated in a certain voltage, or a power consumer requires the input power to be in a specific voltage. In the case that no voltage is specified this means that there are no specific requirements or these requirements are unavailable.

6.11.2. REL-EPS Key Requirements

The following key requirements for the REL-EPS are identified, based on the analysis presented above, and its allocated budgets:

Table 6.21: Key REL-EPS subsystem requirements, driving requirements are marked with [!].

ID	Description	Rationale
REL-EPS-REQ-4.1	[!]The REL-EPS shall provide an average power of at least 28.44 W for the duration of the operational phase.	Derived from the power consumption of the REL.
REL-EPS-REQ-4.2	[!]The REL-EPS shall provide a peak power of at least 49.64 W during the operational phase.	Derived from the power consumption of the SCB.

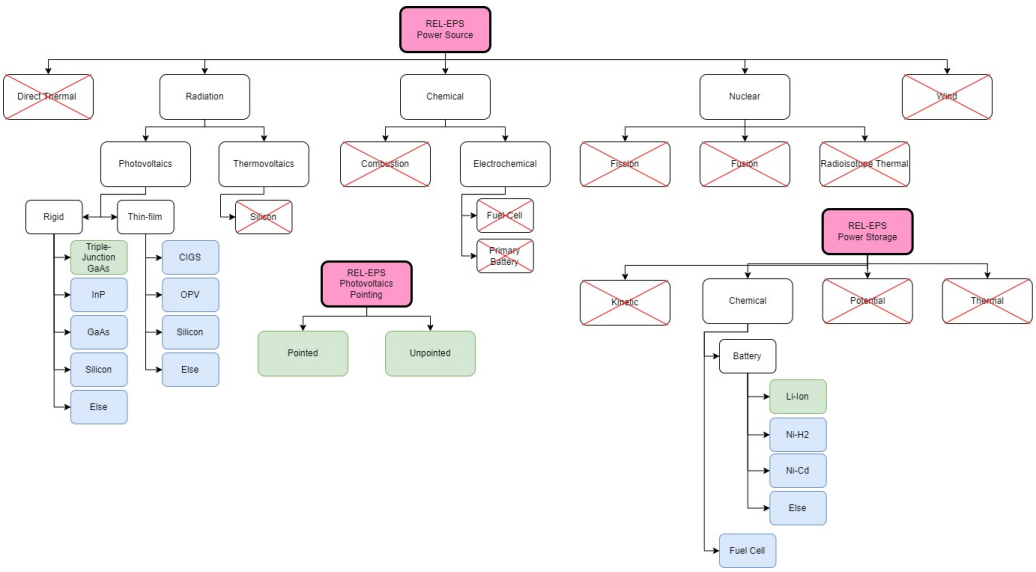

Figure 6.14: The design option tree of the trade-off for the REL-EPS.

6.11.3. REL-EPS Sizing and Trade-off

For the REL-EPS to be accurately defined, several parts need to be chosen and sized. As stated in Subsection 6.11.1, the REL-EPS consists of a solar panel and a secondary battery. To come to this decision, a trade-off on several options has been performed. After this trade-off, these parts are sized with respect to mass, the solar panel area, and the battery capacity. With the sizing completed, a final trade-off can be performed such that the REL-EPS subsystem is completely defined. The concepts considered for the initial trade-off are presented in the design options tree shown in Figure 6.14 In this design options tree the not chosen and unfeasible concepts have been indicated by blue boxes and red crosses respectively. The concepts that are coloured in green are the concepts that are considered for a final trade-off and are used for the sizing of the REL-EPS. It can be seen that the final trade-off for the REL-EPS is made on whether a pointing mechanism is included to decrease the incidence angle on the solar panel. REL-EPS-CON-1 is further used to describe the case of a pointed solar array, and REL-EPS-CON-2 refers to an unpointed solar array.

REL-EPS-STO Sizing EPS Storage

For the sizing of the EPS storage, as well as the EPS power generation, one single model is used that combines both aspects and provides results on both aspects. The model first determines the power consumption of all subsystems on the REL over the course of the complete operational phase. For this, the results of other models are used to size the other subsystems and their power usage. Subsequently, the solar power received on the solar panel is calculated using the angle between the REL and the sun over the complete mission duration, as well as the solar flux modelled by the thermal subsystem, which also includes the eclipse conditions. The next step is to model how much the battery is charged or discharged at all times and iterating this together with the solar panel area to come to an optimised solution for the lowest mass. These results are then used to check whether the REL-EPS can also provide sufficient power during the transfer phase. This relies mainly on the size of the solar panels, due to the eclipse conditions being nonexistent during transfer. The final results of the sizing of the REL-EPS with respect to the battery are shown in Table 6.22. The table includes both the results for the concept of pointed solar panels, as well as an unpointed solar panel. For the trade-off, both concepts are sized for REL-1. After the design choice has been made, the REL-EPS is sized for both REL-1 as well as REL-2. The model has been verified using unit tests and producing and inspecting various graphs for all arrays used. Validation consists of comparing to initial sizing models used, as well as comparison to hand calculations for simple cases, and comparison to literature estimates.

Table 6.22: Sizing parameters of the REL-EPS storage.

Concept	Battery capacity [Wh]	Battery mass [kg]	Battery volume [L]	Peak discharge [W]
REL-EPS-CON-1	35.74	0.238	0.156	49.64
REL-EPS-CON-2	35.74	0.238	0.156	49.64

REL-EPS Sizing Power Generation

The sizing of the solar panel uses the same model as the sizing of the battery described in Figure 6.11.3. The results of the model and the iterations for both concepts for REL-1 are described in Table 6.23.

Table 6.23: Sizing parameters of the REL-EPS power generation.

Concept	SAR area [m^2]	SAR mass [kg]	Peak solar power [W]	Average solar power [W]
REL-EPS-CON-1	0.16	0.733	126.55	78.90
REL-EPS-CON-2	0.07	0.321	55.38	44.67

REL-EPS Trade-off Results

The results of the final figures of merit for the trade-off done between REL-EPS-CON-1 and REL-EPS-CON-2 are shown in Table 6.24.

Table 6.24: The final trade-off results of the REL-EPS.

	Risk: (30%)	Performance: (35%)	Schedule (10%)	Cost: (20%)	Sustain-ability: (5%)
REL-EPS-CON-1	High TRL and low risk system	0.07 m^2 Solar array	No significant changes	Snowball effect of smaller solar array	No effects
REL-EPS-CON-2	Risk of not receiving sunlight	0.16 m^2 Solar array	No significant changes	Snowball effect of larger solar	No effects

From these final results a clear conclusion follows, in which REL-EPS-CON-1, using pointed solar panels, is taken as the winner of the trade-off and thus the final design for the REL-EPS.

Model Limitations, Verification and Validation

The model used in this section is limited to the orbit around Venus, and can be used for accurate initial estimates. However, for precise calculations it must be updated with more accurate iteration strategies and constants and values. Nonetheless, it has been validated and verified using literature, hand calculations and unit tests.

6.11.4. REL-EPS Final Design Overview and Evaluation

With the trade-off and the sizing finished, the final design of the REL-EPS can be presented. The individual components selected for each part are documented in Subsection 6.11.4, the sensitivity analysis performed and its results are described in Subsection 6.11.4, and the final design parameters are presented in Table 6.11.4.

REL-EPS Component Selection

The REL-EPS consists of three major contributing parts: The power generation, the power storage, and the power distribution. For each of these parts, the SOA has been provided in Table 4.26, the BAT in Table 4.27, and the PCD in Table 4.28.

REL-EPS Sensitivity Analysis
A sensitivity analysis has been performed on the sizing of the REL-EPS. For the REL-EPS, the variable that can is susceptible to change is the power consumption, which comes from the design of other subsystems. Therefore, this parameter has been altered in the model to determine the changes in results. These results are documented in Table 6.25.

Table 6.25: Sensitivity analysis results of the REL-EPS.

Parameter changed	Change in parameter	SAR area (%)	SAR mass (%)	Battery capacity (%)	Battery mass (%)
Power consumption	+10%	+14.29	+14.29	+9.91	+9.91
Power consumption	-10%	-14.29	-14.29	-9.79	-9.79

These results show that the REL-EPS sizes almost linearly with the change in power consumption. This is considered to be not a problem, since a margin of 10% is already used on the power consumption before sizing the REL-EPS.

REL-EPS Final Design Parameters and Evaluation
The final design parameters of the REL-EPS are given for both satellites in Table 6.26

Table 6.26: Final design parameters of the REL-EPS.

	Total Mass [kg]	Volume [L]	Solar array size [m^2]	Battery capacity [Wh]	Average power output [W]
REL-1	1.12	0.91	0.07	35.74	28.44
REL-2	1.12	0.91	0.07	36.84	28.39

6.12. REL Mechanisms
The REL-MEC subsystem is often overlooked in the design of satellites, but must nonetheless be included to ensure that the mission can succeed. However, due to the modest size of the subsystem and its contribution to the REL, the detail of the documentation is kept to a minimum.

6.12.1. REL-MEC Functional and Architecture Analysis
The REL-MEC can provide crucial pointing assists to other subsystems where the REL-ADC can fall short or conflicts with other subsystems. Besides that, it can ensure a smaller launch and transfer volume with the help of deployment mechanisms. These functions are described in Subsection 6.12.1. The architecture needed for these functions follow in Subsection 6.12.1. Due to the pointing strategy used by the relay, as described in Section 6.3, little additional mechanisms are required to ensure the correct attitudes of all subsystems.

REL-MEC Functional Allocation
The first part of the REL-MEC is to provide one-time deployment mechanisms to external parts of the REL such that a tighter transfer packing is allowed. The functions that this includes are: The REL-MEC must deploy the REL-EPS-SAR, the REL-MEC must deploy the REL-TNC-LGA, and the REL-MEC must deploy the REL-TNC-HGA. The second part takes the full duration of the operational phase and consists of one function: The REL-MEC must point the REL-EPS-SAR to the sun whenever the sun is visible.

REL-MEC Systems Architecture
The architecture of the REL-MEC consists of four separate simple mechanisms, three of which are folding mechanisms, one of which is a rotation mechanism. To deploy the REL-TNC-LGA, as well as the REL-EPS-SAR, each component folds 90° outwards in one axis, after which it locks and is ready for operation. For the

deployment of the REL-TNC-HGA, the part first folds 90 ° outwards in one axis, after which the two outside panels fold 180 ° outwards to create a flat, tri-part area. The mechanism of the REL-EPS-SAR that ensures its continuous pointing towards the sun consists of a single, one axis, rotation device which rotates the connecting rod between the SAR and the REL structure a maximum of 180 °.

6.12.2. REL-MEC Final Design Overview and Evaluation

Due to the modest size of this subsystem and its small contribution to the total REL mass and volume, the REL-MEC is not worked out in as much detail as some other subsystems. This is one of the reasons why no specific components have been selected for each part. Besides that, it is not very trivial to find specific commercially available components for these functions, since the design parameters are very unique and specific and often the components are designed for each case rather than chosen. Nonetheless, estimations and literature are used to get an estimate of the mass of the mechanisms which hass been calculated to be 0.5 kg.

6.13. Relay Structure

The REL-STR consists of the REL-STR-TUB and REL-STR-COV. The REL-STR-TUB is the primary load structure of the REL, and is responsible for housing the propellant tanks and providing a mounting platform for the REL subsystems. The REL-STR-COV serves to protect the REL electronics from the space environment. REL-STR is also responsible for designing and sizing the propellant tanks to withstand the pressure levels specified in Section 6.10.

6.13.1. REL-STR Functional and Architecture Analysis

The functions of the REL-STR are described hereafter, after which the configuration is outlined.

REL-STR Functional Allocation

The main functions of the REL-STR are to maintain the structural integrity of the REL to provide a platform for the REL subsystems to operate upon during the transfer phase (F4.3.2 & F4.4.2), operational phase (F6.9.5), and decommissioning (F7.4.5). This involves monitoring the temperature of the different subsystems, identifying those whose temperatures fall outside of the operating range, and adjusting the temperature to within the bounds.

Relay Configuration

The structural configuration of the REL can be seen in Figure 6.15. Note, during launch (which is the critical loading case) the HGA, LGA and SOA are stowed. The deployed configuration is shown.

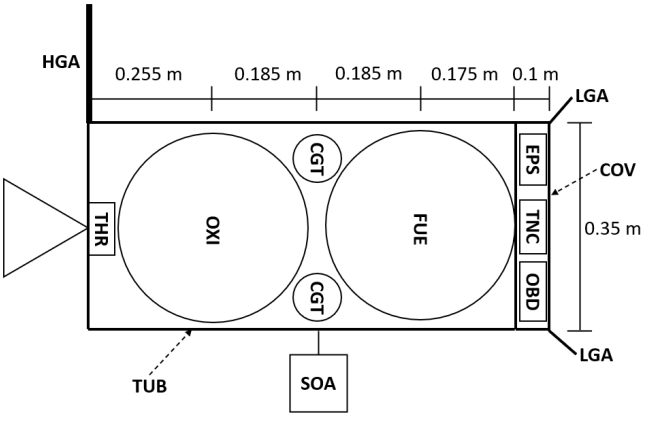

Figure 6.15: The (deployed) structural configuration of the REL.

6.13.2. REL-STR Key Requirements

The following key requirements for the REL-STR are identified, based on the analysis presented above, and its allocated budgets:

Table 6.27: The key REL-STR subsystem requirements, driving requirements are marked with [!].

ID	Description	Rationale
REL-STR-REQ-1.1	The STR shall maintain structural integrity of REL during the entire mission.	Derived from F6.9.5.
REL-THE-REQ-1.2	The STR shall protect the REL subsystems from deep space environment during the entire mission.	Derived from F6.9.5.
REL-STR-REQ-3.9	[!] The STR shall withstand a maximum axial load factor of 8.5 g generated by the LAV.	Derived from F3.2.
REL-STR-REQ-3.10	[!]The STR shall withstand a maximum lateral load factor of 3 g generated by the LAV.	Derived from F3.2.

6.13.3. REL-STR Structural Analysis and Sizing

From Section 6.10, the total volume of the propellant tanks amounts to 0.04345 m^3. For the shape, spherical tanks have been selected for ease of manufacturing and uniform load distribution, over cylindrical tanks. Each propellant tank needs to store 0.02173 m^3, resulting in a radius of 173.24 mm. For a stored pressure of 1 MPa, as mentioned in Section 6.10, the minimum thickness of the tanks can be calculated using Equation 6.7. A safety factor of 1.5 is assumed.

$$t_{TNK} = SF_{TNK} \frac{P_{TNK} \cdot r_{TNK}}{2 \cdot \sigma_y} \tag{6.7}$$

In [73], it is specified that a minimum thickness of 0.8 mm is used for the propellant tanks of satellites. For each of the materials, the calculated thickness lies below this; hence, the material with the lowest density is selected. This gives an aluminium propellant tank with a thickness of 0.8 mm and a mass of 0.511 kg, each for the fuel and oxidizer tanks.

For the pressurant tank, the total volume amounts to 0.00377 m^3. Since the propellant tanks are aligned vertically, it is preferable that the pressurant tank is stored between the propellant tanks for packaging. Assuming that the propellant tanks are spaced apart by 20 mm, it is determined that the maximum radius of the pressurant tank is 48.89 mm. For a spherical tank shape, numerous tanks must be used to fit within the constraints. In fact, a minimum of 8 spherical tanks, each with a radius of 48.29 mm need to be used to achieve the total volume. The total circular path length available around the tanks is 792.35 mm. If each of these tanks are mounted one after the other, nearly all of the space is taken up at 772.64 mm of path length. This leaves little room for the valves, pressure lines, electrical harness, etc.

While being more difficult to manufacture, a more volume-efficient shape is to use a toroidal pressurant tank. It can be seen in Figure 6.16 that a torus has a major radius R and a minor radius r. It has the constraints that the combination of the major radius, minor radius, and wall thickness must not exceed the tangent axis of the propellant tanks and must not interference with the propellant tanks.

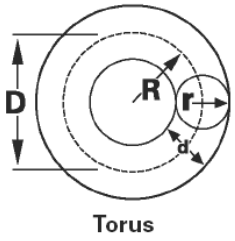

Figure 6.16: Torus parameters.

The stresses inside a toroidal pressure vessel can be approximated by those in a cylindrical pressure vessel. There exists two principal stresses for the latter: longitudinal stress and hoop stress. The hoop stress is twice as large compared to the longitudinal stress and is hence the limiting design factor. For a stored pressure of 27.6 MPa, the minimum thickness of the pressurant tank can be calculated using Equation 6.8. A safety factor of 1.5 is assumed.

$$t_{CGT} = SF_{CGT} \frac{P_{CGT} \cdot r_{CGT}}{\sigma_y} \tag{6.8}$$

This yields the results provided in Table 6.28. While CFRP yields a much lighter design, there are concerns over the manufacturability of a composite toroidal fuel tank. Thus, Ti6Al4V is selected to be conservative. This gives a CGT mass of 1.671 kg.

Now that the REL-PRO-TNK and REL-PRO-CGT have been sized, the TUB and COV can be designed. The TUB is the primary load structure of the REL and must sustain loadings of up to 8.5 g during launch on the Falcon 9 [80]. As specified in Section 6.4, a box structure is selected for the layout. The main failure mode for thin plates is buckling. Crippling, or buckling of individual plates is considered but it is not the critical failure mode.

Since the tanks and electronics are mounted at different locations along the x-axis, there is a variation of loading along the length of the TUB. The highest loading occurs near the bottom, which can be seen in Figure 6.17. Thus, the minimum thickness of the TUB can be determined for this section using Equation 6.9. A safety factor of 1.25 is assumed. Note, the constant C is a function of element width and height. Ultimately, CFRP gives the most lightweight structure at 1.476 kg for a thickness of 0.8 mm, which is shown in Table 6.29. Extending this thickness to the COV, the mass can be determined to be 0.357 kg, yielding an overall REL-STR mass of 1.833 kg.

$$\sigma_{cr} = C\frac{\pi^2 E}{12(1-\nu^2)}\left(\frac{t}{b}\right)^2 \tag{6.9}$$

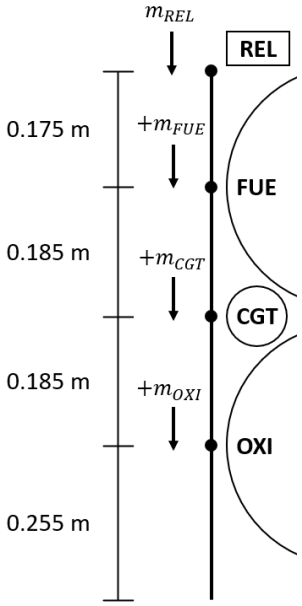

Figure 6.17: Distribution of loading over REL-STR-TUB.

Table 6.28: The REL pressurant tank dimensions and mass.

Material	R (mm)	r (mm)	t (mm)	Mass (kg)
Ti6Al4V	133.500	37.839	1.892	1.671
AlBeMet	126.500	38.872	8.128	3.266
Al6061	128.000	38.643	6.638	3.500
CFRP	134.500	37.698	1.115	0.379

Table 6.29: REL-TUB mass for different materials.

Material	t (mm)	Mass (kg)
Ti6Al4V	1.150	5.528
AlBeMet	0.825	1.853
Al6061	1.150	3.369
CFRP	0.800	1.476

Model Limitations, Verification and Validation

One of the main assumptions the REL-STR structural model makes is that material properties and model geometry is linear. Given the high stiffness of CFRP used for the TUB and COV, deformations are small and loading stays within the elastic region. Furthermore, a safety margin was applied. Hence, this assumption is acceptable. To verify the model, hand calculations are performed for the equations as well as face validity of the results. Validation of the model could be performed using a commercial finite element method solver; however, as the equations used to size the structure are accepted across the engineering industry, it is fair to say that the results are realistic.

6.13.4. REL-STR Final Design Overview and Evaluation

With the thermal analysis and the sizing finished, the final design of the REL-THE can be presented. The sensitivity analysis performed and its results are described in Subsection 6.13.4, after which the final design parameters are presented.

REL-STR Sensitivity Analysis

A sensitivity analysis has been performed on the structural analysis and sizing of the REL-STR. For the REL-STR, the main variables that are susceptible to change are the subsystem masses and the volume of the propellant, which comes from the design of other subsystems. For the change in subsystem masses, the load exerted on the lowest structural element changes. The mass can increase by up to 50% before the TUB can no longer support the buckling loads. For the change in the volume of the propellant, this changes the element width b. This changes the critical buckling stress by the inverse square, whilst also changing the constant C.

REL-STR Final Design Parameters and Evaluation

The final design parameters of the REL-STR are given in Table 6.30.

Table 6.30: Final design parameters of the REL-STR.

Component	Dimensions	Mass [kg]	Cost [$kEUR$]
TUB	0.35 x 0.35 x 0.90 cm (t=0.8 mm) & 2x(0.35 x 0.35 x 0.08 cm)	1.476	452.5
COV	0.35 x 0.35 x 0.08 cm & 2x(0.35 x 0.10 x 0.08 cm)	0.357	
BPT	R=17.32 cm, t=0.08 cm	1.022	
CGT	R=13.35 cm, r=3.78 cm, t=0.18 cm	1.671	

6.14. Relay Thermal Management System

The REL-THE is the subsystem responsible for keeping the other REL subsystems within their defined temperature ranges. This sections covers the functions and architecture of the REL-THE, as well as the thermal analysis and sizing of the components that lie therein.

6.14.1. REL-THE Functional and Architecture Analysis

The functions of the REL-THE are described hereafter, after which the architecture is outlined. Lastly, an overview of the hardware used in the REL-THE and how they are interfaced with other subsystems is presented.

REL-THE Functional Allocation

The main functions of the REL-THE are to maintain the subsystems within their operating and non-operating temperature ranges during transfer phase (F4.3.2 & F4.4.2), operational phase (F6.9.2), and decommissioning (F7.4.2). This involves monitoring the temperature of the different subsystems, identifying those whose temperature falls outside of the operating range, and adjusting the temperature to within the bounds.

REL-THE Systems Architecture

The REL-THE comprises of three components: MLI, RTR, and PIP. The MLI is responsible for insulating the REL internals from the environment, the RTR is responsible for radiating dissipated heat to the environment, and the PIP is responsible for providing a heat transfer path between the internals and the RTR.

REL-THE Hardware Block Diagram and Configuration

Figure 6.18 shows the hardware block diagram for the REL-THE. $\dot{Q}_i$ represents the heat transfer for different elements. Heat is absorbed by the MLI from the environment; the PIP receives this heat as well as the dissipated heat from the electronics and transfers it to the RTR, which is subsequently emitted back to the environment.

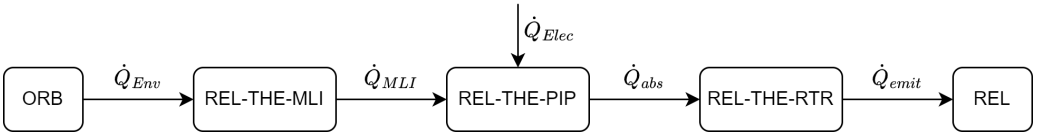

Figure 6.18: The block diagram of the REL-THE.

6.14.2. REL-THE Key Requirements

The following key requirements for the REL-THE are identified, based on the analysis presented above, and its allocated budgets:

Table 6.31: The key REL-THE subsystem requirements, driving requirements are marked with [!].

ID	Description	Rationale
REL-THE-REQ-1.1	The REL-THE shall monitor the temperature of the REL during the entire mission.	Derived from F6.9.2.
REL-THE-REQ-2.2	[!] The REL-THE shall maintain the REL subsystems within their operational temperature range of 273.15 K - 294.15 K during the entire mission.	Derived from F6.9.2.

Continued on next page

Table 6.31 – continued from previous page

ID	Description	Rationale
REL-THE-REQ-2.3	[!] The REL-THE shall maintain the REL subsystems within their non-operational temperature range of 264.15 K - 294.15 K during the entire mission.	Derived from F6.9.2.

6.14.3. Relay Thermal Analysis and Sizing

The operating and non-operating temperatures ranges of the components within the REL must first be identified. The operational temperature range is 273.15-294.15 K, where the battery limits the lower bound and the pressurant limits the upper bound. The non-operating temperature range is 264.15-294.15 K, with the pressurant limiting both bounds. From this, the operational environment of the REL must be considered.

Solar radiation from the Sun, albedo radiation reflected from the Venusian surface, infrared energy radiated by Venus, and dissipated heat from the internal components comprise the sources of heat that are being absorbed by the REL. Consequently, heat is radiated away from the REL to the space environment since it is very cold (3.7 K). Equation 4.10, Equation 4.11 and Equation 4.12 can be used to calculated the thermal balance. Note, since space is a vacuum, there is no heat flow to the REL by convection or conduction, therefore these are removed from consideration.
Due to the pointing strategy, the REL experiences different lighting conditions throughout its mission, both from solar flux, and albedo and planet flux. This results in the change of projected area over time, which can be calculated using Equation 6.10 and Equation 6.11.

$$A_s = A_{front,rear}|\cos\theta_s| + A_{side}\sin\theta_s \tag{6.10}$$

$$A_{a,IR} = A_{rear}|\cos\theta_{a,IR}|\sin\phi a, IR + A_{side}(\sin\theta_{a,IR}|\cos\phi_{a,IR}| + \sin\theta_{a,IR}\sin\phi_{a,IR} + |\cos\theta_{a,IR}\cos\phi_{a,IR}|) \tag{6.11}$$

Using these equations as well as Equation 4.11, the heat absorbed by the REL can be determined for the different thermal factors. It was determined that the absorbed heat is in excess of 1000 W without the application of thermal solutions. Even with the use of foils to reduce the effective absorptivity, the heat is still approximately 200 W; hence the use of MLI is employed due to its low effective thermal conductivity of around $1 * 10^{-5}$ W/mK. The heat transfer through the insulation can be calculated using Equation 4.16, where the temperature of the MLI can be obtained by Equation 6.12. The absorbed heat from the environment now decreases to an order of magnitude of 10^{-1}, meaning that the electronics become the primary source of heat being absorbed by the REL. This leads to an absorbed heat range that varies between 8 and 67 W. Covering the REL with MLI leads to an area of 1.505 m^2, and with a density of 1.2 kg/m^2 [70], this gives a mass of 1.806 kg.

$$T_{MLI} = \left(T_{Env}^4 + \frac{\dot{Q}_{absorbed}}{\epsilon_{MLI}\cdot\sigma\cdot A_{MLI}}\right)^{1/4} \tag{6.12}$$

The final step in the analysis is to determine the heat to be emitted by the radiator. Ideally, the radiator must be able to emit the equivalent amount of heat being absorbed, which varies over the mission duration. To achieve this, it is possible to use louvers with bimetallic coils to control the emissivity of the radiator and hence control the heat being emitted. For an aluminium radiator with silver louver blades, the emissivity can be varied between 0.02-0.8, which increases sinusoidally with the blade angle [22]. The limiting performance element is the rate at which the louver blades can react to the varying temperature, since it cannot immediately adjust the blade angle. Hence, the angular rate of the blades has been assumed to be 60 ° in 10 seconds, so 6 $°/s$. For a calculated radiating area of 0.032 m^2, the temperature balance of each REL can determined over the mission duration, which is shown in Figure 6.19. It can be seen that both RELs stay within the temperature limits with a 5 K margin on each bound.

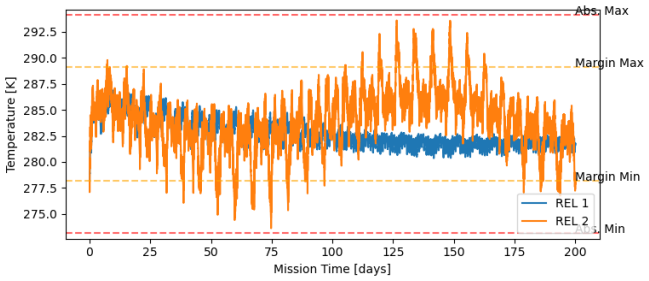

Figure 6.19: Variation of internal temperature of each REL over mission duration.

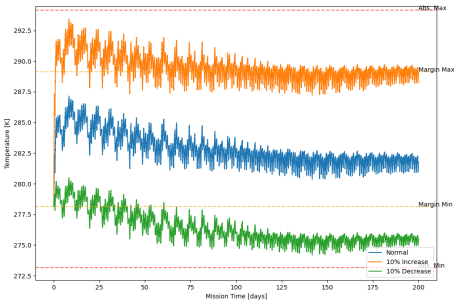

Figure 6.20: The sensitivity of the internal temperature to an increase / decrease of electric power consumption by 10% over the mission duration.

Model Limitations, Verification and Validation

One of the main assumptions the REL-THE thermal model makes is that the heat is assumed to be evenly distributed throughout the structure, i.e. there are no temperature concentrations in the structure. While this assumption has negligible effect for the heat absorbed from the environment, the heat transfer from the electronics to the radiator possesses a degree of inaccuracy. However, the effect of this assumption has been deemed acceptable for the level of this thermal analysis. To verify the model, hand calculations are performed for the equations as well as face validity of the results. It was not possible to validate the model with experimental data since similar models are not readily available. Ultimately, the results are deemed feasible but the model needs to be validated in the next iteration.

6.14.4. REL-THE Final Design Overview and Evaluation

With the thermal analysis and the sizing finished, the final design of the REL-THE can be presented. The sensitivity analysis performed and its results are described below, and the final design parameters are presented thereafter.

REL-THE Sensitivity Analysis

A sensitivity analysis has been performed on the thermal analysis and sizing of the REL-THE. For the REL-THE, the main variables that are susceptible to change are the orbital parameters and the power dissipation of the REL-EPS, which comes from the design of other subsystems. As a result of the change in orbital altitude, the albedo heat flux increases/decreases with the square of the altitude. However, since the MLI reduces the absorbed heat to the order of 10^{-1}, this has little effect on the thermal balance of the REL. For the change in power dissipation, the effect of an increase / decrease by 10% on the thermal balance can be seen in Figure 6.20. While these changes cause the temperature range to exceed the 5 K margins, the temperatures still lay within the absolute temperature bounds.

REL-THE Final Design Parameters and Evaluation

The final design parameters of the REL-THE are given in Table 6.32.

Table 6.32: Final design parameters of the REL-THE.

Component	Size [m^2]	Mass [kg]	Cost [$k€$]	Source
MLI	1.505	1.806	358.9	[70]
RAD	0.032	0.086		-
PIP	-	0.500		Assumed

7

Sustainable Development Strategy

This chapter encompasses the different aspects of the mission pertaining to sustainability and their relevance to the current times. In order to present the mission's approach to sustainability in a clear manner, this chapter has been divided into three sections. The first section, Section 7.1 contains sustainability matters regarding the environment the spacecraft interacts with. This is followed by Section 7.2 which covers the sustainability in an economic context. Finally, Section 7.3 compiles any and all social impact the mission may produce.

7.1. Environmental Sustainability

Due to the broad spectrum of environments the mission faces, the environments have been split into 'On-Earth' and 'Off-Earth' for documentation purposes.

7.1.1. On-Earth

The first aspect of the mission that could affect Earth's environment is the development of the mission. This includes events such as developing new technologies for scientific payloads or manufacturing prototypes for testing. Most of the scientific instruments selected to fly on the spacecraft bus have already been tested and developed, and as such the changes that have to be made to adapt them to a mission in Venus are minimal in comparison.

Once all elements that are encompassed by the mission are developed, the next step is manufacturing. This process may involve materials with intricate extraction processes, that could negatively affect the Earth's environment. Regarding this aspect, the mission minimises the use of harmful materials whenever possible.

The final phase affecting the terrestrial environment is the operations segment of the mission. Current technology limits the ways in which a spacecraft can be launched into space, thus the only realistic option is to use chemical propulsion. The currently-selected launcher, the Falcon 9, uses RP-1 as its fuel, which when burned does not produce large quantities of toxic fumes, reducing the harm done to the Earth's atmosphere. Regarding the launcher itself, its first stage is reusable, which is undoubtedly a positive for sustainability due to the reduction in wasted material. Furthermore, the effect of the mission on Earth's orbital cleanliness must be considered. No significant piece of debris is left orbiting Earth, as the first stage of the Falcon 9 launcher does not reach orbit and the second stage leaves Earth's gravity well altogether.

7.1.2. Off-Earth

Regarding off-earth operations, Venus is the main subject of this discussion, as it is the planet that the mission observes for 200 days. The transfer vehicle used by the mission follows an identical trajectory compared to the entry and descent vehicle (only separating briefly before atmospheric contact), and thus burns up in the atmosphere, avoiding the creation of debris orbiting Venus. Similarly, both RELs follow the same fate once the mission is over. Regarding the spacecraft bus itself, a lack of propulsion system ensures there is no direct gas exchange between the spacecraft and the Venusian atmosphere, avoiding the possibility of contamination. At end of life, the spacecraft is also discarded by allowing it to fall into the lower altitudes of Venus where it burns up.

7.2. Economic Sustainability

A major part of the sustainability aspect of the mission is the economic sustainability. First of all, as mentioned in the previous section most of the scientific instruments used in the spacecraft bus are existing instruments, thus little investment has to be made in order to adapt them for the Venusian atmosphere. Also mentioned in the previous section is the selected launcher, the Falcon 9, which has a reusable first stage. This not only cuts on environmental impact, but it also reduces the cost of launching the mission into space.

Moreover, a substantial amount of components in the data handling subsystems for all systems have a high

power efficiency, which reduces the energy needed, and thus reducing cost for all electrical power subsystems.

Finally, the development and manufacture of the components that compose this mission imply the involvement of a plethora of companies, both nationally and internationally. As a result, the execution of this mission is of service to the economic situation of the countries involved.

7.3. Social Sustainability

The social sustainability section of the mission can be classified into different aspects. The first being 'social awareness', which encompasses both the public's awareness of Venus as a planet to be explored, as well as the public's awareness towards the Earth's current atmospheric climate. Both are favoured through the accomplishment of this mission.

Another aspect of social sustainability is the effect this mission will have on communities indirectly involved in the mission. An example of this would be the effects on a community that has to be evicted from their land so that launch facilities can be built in order to complete the mission. In order to maintain a positive view from the public towards the LOVE mission it is preferable to minimize such events, which is one of the reasons why an already existing launch provider and booster was selected, as this should eliminate the need for such high-impact actions.

The final aspect to consider is the effects of finding life on Venus on society. If the data obtained by the mission provides evidence of the existence of life in the atmosphere of Venus, society may be affected as a result, as personal beliefs may be challenged by the mission's findings.

8

Conclusion

The LOVE mission aims at sending a science package of instruments to the atmosphere of Venus, more specifically in the main cloud deck, between 50 and 70 km above the surface. This package researches for 200 days on two main science objectives, namely the search for biomarkers that could support the thesis that microbial life exists in the atmosphere of the planet, and the atmospheric profiling of the planet.

The final design resulted in an entry and descent vehicle (EDV) which deploys a spacecraft bus (SCB) that uses a pumped hydrogen balloon to fly along an equatorial path between 50 and 62 km of altitude. This spacecraft is supported by two relay satellites (REL) orbiting on different planes at an altitude of 1701 km. Figure 8.1 shows a summary of the mission concept operations previously described. The overall estimated cost of the mission is 628 M Euros and the mission is set to launch in 2031 and end by 2035.

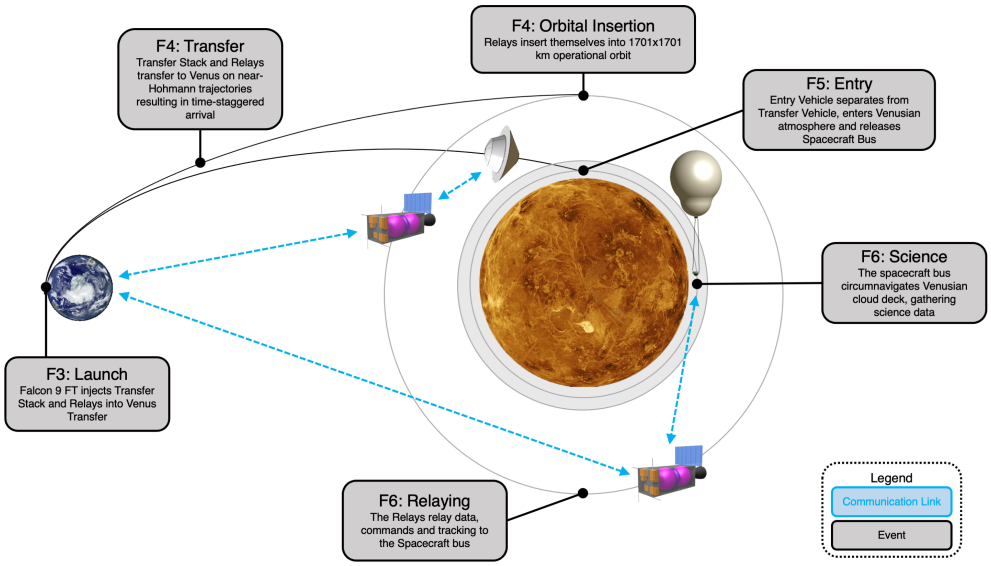

Figure 8.1: Concept Operations Diagram for the LOVE mission.

It was found during the design process that trying to obtain multiple measurements on or close to the Venusian surface leads to an unfeasible design. It was attempted to design a set of probes that could be dropped into the depths of the planet's atmosphere and reach the surface but the stringent temperature and pressure requirements led to a design with an unacceptable mass. On the flip side, resources vacated by the omission of the probes could be used to further the mission's utility for searching life through the addition of the polarimeter and the nephelometer.

Particular difficulty was the estimation the mass and power requirements of the hydrogen pump used to move the hydrogen between the superpressure and zero pressure chambers, and an approximate method had to be used. Moreover the power requirements for the spacecraft bus are driving for the overall design, having to use the pump to perform altitude changes in the night side of Venus meant a rather large battery of about 67kg had to be used, which represents about 18% of the the overall spacecraft bus mass.

The relay design was heavily influenced by the decision to transfer it to Venus by itself, since it was determined that using the TRV to insert the REL into orbit and then de-orbit to release the EDV on a trajectory into the Venusian atmosphere would be unfeasible. This resulted in the layout and configuration of the REL to be considerably heavier than was proposed in the midterm report, but still within the calculated volume. Given the new orbital parameters with an inclined orbit, this also implied that a more extensive communication strategy with Earth was needed to be devised. This updated communication strategy also flowed into the design of the REL subsystems.

Regarding the mission geometry, the main conclusions are that the requirements of ranging and maximizing contact time to the SCB are opposed, and a compromise had to be found. Furthermore, the SCB path along the equator is preferable due to its simplicity in terms of operations. Overall, it was also shown that the deviations from the equator due to meridional winds is relatively small, meaning that it can be expected for the SCB to follow an equatorial path even without propulsion.

Regarding the transfer, it is found that the combined transfer of all mission hardware to Venus leads to an infeasible design due to its excessive mass, leading to a change in the mission concept to have the two relays transfer to Venus separately, and the EDV following a hyperbolic trajectory before atmospheric entry.

References

[1] DSE Group 16. *Baseline Report: L.O.V.E. mission - Life On Venus Exploration*. TU Delft, 2022.

[2] DSE Group 16. *Midterm Report: L.O.V.E. mission - Life On Venus Exploration*. TU Delft, 2022.

[3] Airgas. *Safety Data Sheet - Helium*. 2021. URL: https://www.airgas.com/msds/001025.pdf (visited on 06/15/2022).

[4] Airgas. *Safety Data Sheet - Hydrogen*. 2020. URL: https://www.airgas.com/msds/001026.pdf (visited on 06/15/2022).

[5] Airship Wiki for the Small Blimp Community. *Lifting Gases*. 2010. URL: https://sites.google.com/site/airshipwiki/the-team (visited on 06/15/2022).

[6] *Atmos 22 Ultrasonic Anemometer*. URL: https://www.metergroup.com/en/meter-Environment/products/atmos-22-ultrasonic-anemometer.

[7] William Bains et al. "Production of ammonia makes Venusian clouds habitable and explains observed cloud-level chemical anomalies". In: *Proceedings of the National Academy of Sciences* 118.52 (2021), e2110889118.

[8] Blue Canyon Technologies. *BCT Data Sheet Components ACS*. 2022. URL: https://storage.googleapis.com/blue-canyon-tech-news/1/2022/04/BCT%5C_DataSheet%5C_Components%5C_ACS.pdf (visited on 06/15/2022).

[9] M. Bowden et al. "Experiments to investigate particulate materials in reduced gravity fields". In: (Nov. 1967).

[10] *Buckling of thin-walled truncated cones - NASA*. 1968. URL: https://ntrs.nasa.gov/api/citations/19690014753/downloads/19690014753.pdf.

[11] Ratnakumar Bugga et al. "Extended-range Variable Altitude Balloons for Venus atmospheric missions". In: *Acta Astronautica* (May 2022). ISSN: 00945765. URL: https://linkinghub.elsevier.com/retrieve/pii/S009457652200203X.

[12] Sonja Caldwell. *7.0 thermal control*. Oct. 2021. URL: https://www.nasa.gov/smallsat-institute/sst-soa/thermal-control.

[13] Anna Case. *COMMUNICATION SYSTEMS FOR CUBESAT MISSIONS*. URL: https://web.mst.edu/~kosbar/ITC/Previous_Student_Papers/SamplePaper24.pdf (visited on 06/13/2022).

[14] Performance Composites. *Mechanical Properties of Carbon Fibre Composite Materials*. URL: http://www.performance-composites.com/carbonfibre/mechanicalproperties_2.asp.

[15] D.M. Hassler et al. "The Radiation Assessment Detector (RAD) Investigation". In: *Space Sci Rev* 170 (2012), pp. 503–558.

[16] *DAVINCI Science*. URL: https://ssed.gsfc.nasa.gov/davinci/science.

[17] TU Delft. *AE1222-II: Aerospace Design & Systems Engineering Elements I - Spacecraft (bus) design and sizing*.

[18] Dupont de Nemours Inc. *Dupont Kapton*. 2020. URL: https://www.dupont.com/content/dam/dupont/amer/us/en/products/ei-transformation/documents/EI-10167-Kapton-General-Specifications.pdf (visited on 06/14/2022).

[19] Dupont de Nemours Inc. *Dupont Kapton - Summary of Properties*. 2022. URL: https://www.dupont.com/content/dam/dupont/amer/us/en/products/ei-transformation/documents/EI-10142_Kapton-Summary-of-Properties.pdf (visited on 06/14/2022).

[20] Dupont de Nemours Inc. *Dupont Kapton FN*. 2020. URL: https://www.dupont.com/content/dam/dupont/amer/us/en/products/ei-transformation/documents/EI-10160-Kapton-FN-Data-Sheet.pdf (visited on 06/14/2022).

[21] ECSS. *ECSS-E-HB-31-01 Part 7A: Insulations*. 2011.

[22] ECSS. *ECSS-E-HB-31-01 Part 9A: Radiators*. 2011.

[23] Todd Ely et al. "Comparison of Deep Space Navigation Using Optical Imaging, Pulsar Time-of-Arrival Tracking, and/or Radiometric Tracking". In: *The Journal of the Astronautical Sciences* 69 (2 Apr. 2022), pp. 385–472. ISSN: 2195-0571. DOI: 10.1007/s40295-021-00290-z. URL: https://link.springer.com/10.1007/s40295-021-00290-z.

[24] EnduroSat. *UHF Antenna III*. URL: https://www.endurosat.com/cubesat-store/cubesat-antennas/uhf-antenna/ (visited on 06/12/2022).

[25] ESA. *For the first time, an ESA deep space antenna controlled two spacecraft with one dish*. 2020. URL: https://phys.org/news/2020-02-esa-deep-space-antenna-spacecraft.html (visited on 06/14/2022).

[26] ESA ESTEC Concurrent Design Facility. *EnVision CDF Study - Executive Summary*. ESA.

[27] *ESA selects revolutionary venus mission envision*. URL: https://sci.esa.int/web/cosmic-vision/-/esa-selects-revolutionary-venus-mission-envision (visited on 04/29/2022).

[28] L. W. Esposito et al. "Sulfur Dioxide at the Venus Cloud Tops, 1978-1986". In: *Journal of geophysical research* 93.D5 (1988), pp. 5267–5276.

[29] Venkatapathy Ethiraj. *Thermal protection system technology and facility needs for demanding future planetary missions*. 2004.

[30] Javier Gomez-Elvira. *Mars Curiosity Rover: REMS*. 2012. URL: https://mars.nasa.gov/msl/spacecraft/instruments/rems/ (visited on 05/04/2022).

[31] GomSpace. *NanoPower BPX Datasheet*. URL: https://gomspace.com/UserFiles/Subsystems/datasheet/gs-ds-nanopower-battery_2600mAh.pdf (visited on 06/11/2022).

[32] Northrop Grumman. *LN-200S Inertial Measurement Unit*. URL: https://www.northropgrumman.com/what-we-do/ln-200s-inertial-measurement-unit/.

[33] J. L. Hall et al. *Prototype Development of a Variable Altitude Venus Aerobot*. 2021. URL: https://dartslab.jpl.nasa.gov/References/pdf/2021-08-02-venus-aerobot.pdf (visited on 06/15/2022).

[34] J.L. Hall et al. "Prototype design and testing of a Venus long duration, high altitude balloon". In: *Advances in Space Research* 42 (2008), pp. 1648–1655.

[35] J.E. Hallsworth et al. *Water activity in Venus's uninhabitable clouds and other planetary atmospheres*. June 2021. URL: https://doi.org/10.1038/s41550-021-01391-3.

[36] Jennifer Harbaugh. *Foam and cork insulation protects deep space rocket from fire and Ice*. June 2018. URL: https://www.nasa.gov/exploration/systems/sls/insulation-protects-sls-from-fire-and-ice.

[37] Ehsan Heidaryan et al. "Viscosity of pure carbon dioxide at supercritical region: Measurement and correlation approach". In: *The Journal of Supercritical Fluids* 56 (2 2011), pp. 144–151. DOI: doi:10.1016/j.supflu.2010.12.006.

[38] Richard Hodges et al. "A Deployable High-Gain Antenna Bound for Mars: Developing a new folded-panel reflectarray for the first CubeSat mission to Mars." In: *IEEE Antennas and Propagation Magazine* PP (Feb. 2017), pp. 1–1. DOI: 10.1109/MAP.2017.2655561.

[39] Sarah Holmes. *Iris Deep Space Transponder: MarCO's Telecom System*. URL: https://trs.jpl.nasa.gov/bitstream/handle/2014/50829/CL%5C%2319-2958.pdf?sequence=1 (visited on 06/12/2022).

[40] Texas Instruments. *MSP430F673x, MSP430F672x Mixed-Signal Microcontrollers*. 2000. URL: https://www.ti.com/lit/ds/symlink/msp430f6736.pdf (visited on 06/13/2022).

[41] Jacob Izraelevitz and Jeffery Hall. "Minimum-Mass Limits for Streamlined Venus Atmospheric Probes". In: *AIAA Journal of Spacecraft and Rockets* 57 (4 2020). DOI: doi:10.2514/1.A34437.

[42] James R. Wertz et al. *Space Mission Engineering: The New SMAD*. Microcosm Press, 2011.

[43] V.V. Kerzhanovich and S.S. Limaye. "Circulation of the atmosphere from the surface to 100 km". In: *Advances in Space Research* 5.11 (1985), pp. 59–83.

[44] T.W. Knacke. *Parachute Recovery Systems Design Manual*. 1st ed. Santa Barbara, California: Para Publishing, 1992.

[45] Kuraray. *Vectran - Liquid Crystal Polymer Fiber Technology*. Tokyo, Japan: Kuraray Co., 2014.

[46] Hall J. L. et al. *Prototype Development of a Variable Altitude Venus Aerobot*. Jet Propulsion Laboratory, California Institute of Technology, July 2021.

[47] A. G. Lavega et al. *The Atmospheric Dynamics of Venus*. July 2017. URL: https://web.lmd.jussieu.fr/~sllmd/pub/REF/2017SSRv..212.1541S.pdf.

[48] Alan Little. *MEDLI*. URL: https://mars.nasa.gov/msl/spacecraft/instruments/medli/ (visited on 06/13/2022).

[49] M.S. Gilmore et al. *Venus Flagship Mission Decadal Study*. Aug. 2020. URL: https://science.nasa.gov/science-red/s3fs-public/atoms/files/Venus%5C%20Flagship%5C%20Mission.pdf.

[50] Warren L. Martin and Tien M. Nguyen. *A COMPARISON OF MODULATION SCHEMES*. 1993. URL: https://deepspace.jpl.nasa.gov/files/phase1.pdf (visited on 06/21/2022).

[51] Materion. *AlBeMet Technical Fact Sheet*. URL: https://materion.com/-/media/files/beryllium/albemet-materials/maab-032albemettechnicaldatasheet.pdf.

[52] William McAdams. *Heat transmission*. McGraw-Hill, 1954.

[53] Menad Nait Amar et al. "Predicting thermal conductivity of carbon dioxide using group of data-driven models". In: *Journal of the Taiwan Institute of Chemical Engineers* 113 (2020), pp. 165–177. DOI: doi:10.1016/j.jtice.2020.08.001.

[54] Aerospace Specification Metals. *Aluminium 6061-T6*. URL: https://asm.matweb.com.

[55] Aerospace Specification Metals. *Titanium Ti-6Al-4V*. URL: https://asm.matweb.com.

[56] *Model of Venus Atmosphere*. Tech. rep. NASA, Dec. 1968. URL: https://ntrs.nasa.gov/api/citations/19690011554/downloads/19690011554.pdf (visited on 04/29/2022).

[57] NASA. *Iris V2 CubeSat Deep Space Transponder*. URL: https://www.nasa.gov/sites/default/files/atoms/files/brochure_irisv2_201507.pdf (visited on 06/11/2022).

[58] NASA. *Solar Cell and Array Technologies for Future Space Missions*. URL: https://solarsystem.nasa.gov/resources/296 (visited on 06/11/2022).

[59] NASA. *State-of-the-Art Small Spacecraft Technology*. 2020. URL: https://www.nasa.gov/smallsat-institute/sst-soa.

[60] NASA. *Vega 2 Balloon*. 2022. URL: https://nssdc.gsfc.nasa.gov/nmc/spacecraft/display.action?id=1984-128F (visited on 06/15/2022).

[61] *NASA FY 2023 budget estimates*. 2021.

[62] *Past missions to Venus*. URL: https://www.esa.int/Science_Exploration/Space_Science/Venus_Express/Past_missions_to_Venus.

[63] M.R. Patel et al. "Constraints on a potential aerial biosphere on Venus: II. Ultraviolet radiation". In: *Icarus* 373 (2022), p. 114796. ISSN: 0019-1035.

[64] C. H. Lucas Patty et al. "Circular spectropolarimetric sensing of vegetation in the field; possibilities for the remote detection of extraterrestrial life". In: (Feb. 2019). DOI: http://dx.doi.org/10.1089/ast.2019.2050. URL: http://arxiv.org/abs/1902.05859.

[65] *Phenolic Impregnated Carbon Ablators (PICA) as Thermal Protection Systems for Discovery Missions*. URL: https://ntrs.nasa.gov/api/citations/19970017002/downloads/19970017002.pdf (visited on 06/15/2022).

[66] A. Piccialli. *Cyclotrophic wind in the mesosphere of Venus from Venus Express observations*. Belgian Institute for Space Aeronomy, 2019.

[67] Dartnell Lewis R. et al. *Constraints on a potential aerial biosphere on Venus: I. Cosmic rays*. Sept. 2015. URL: https://ui.adsabs.harvard.edu/abs/2015Icar..257..396D/abstract.

[68] B. Ragent et al. "Pioneer Venus Sounder and Small Probes Nephelometer Instrument". In: *IEEE Transactions on geoscience and remote sensing* GE-18.1 (1980), pp. 111–117.

[69] Boris Ragent et al. "Pioneer Venus Sounder and Small Probes Nephelometer Instrument". In: *IEEE Transactions on Geoscience and Remote Sensing* GE-18 (1 1980), pp. 111–117. ISSN: 15580644. DOI: doi:10.1109/TGRS.1980.350292.

[70] RUAG. *Thermal Insulation Products*. 2020. URL: https://www.ruag.com/system/files/media_document/2020-02/Thermal%5C%20insulations%5C%20products_low_1.pdf.

[71] J.H. Saleh and J.F. Castet. *Spacecraft Reliability and Multi-state Failures: A Statistical Approach*. Georgia Institute of Technology: John Wiley and Sons, ltd, 2011.

[72] Satsearch. *ANT-100 UHF/VHF Monopole Antenna*. 2022. URL: https://satsearch.co/products/aac-clyde-ant-100-uhf-vhf-monopole-antenna (visited on 06/11/2022).

[73] Aerospace SBI. *Space - Propellant Tanks*. URL: https://www.sbi.at/en/applications/aeronautics/space-fuel-tanks.

[74] Luigi Scatteia. *Main Trends & Challenges in the Space Sector*. Dec. 2020.

[75] ECSS Secretariat. "Engineering design model data exchange (CDF)". In: ECSS-E-TM-E-10-25A (2010).

[76] Y.Z. Shen, G.C. Lin, and H.F. Tan. "A method for predicting the blasting pressure of balloons using the surface strain in low pressure". In: *Advances in Mechanical Engineering* 11.10 (2019), pp. 1–8.

[77] S.E. Solovyov and A.Y. Goldman. "Permeability of multi-layer structures". In: *e-Polymers* 1.23 (2004).

[78] A. Soria-Salinas, M.P. Zorzano, and Francisco Javier Martin-Torres. "Convective Heat Transfer Measurements at the Martian Surface". In: 2015.

[79] *Space: Investing in the final frontier*. URL: https://www.morganstanley.com/ideas/investing-in-space.

[80] SpaceX. *Falcon User's Guide*. 2021. URL: https://www.spacex.com/media/falcon-users-guide-2021-09.pdf.

[81] Steelhead composites. *Lightweight Hydrogen Storage*. 2022. URL: https://steelheadcomposites.com/hydrogen-storage/ (visited on 06/14/2022).

[82] Steelhead composites. *Lightweight Hydrogen Storage Brochure*. 2022. URL: https://steelheadcomposites.com/wp-content/uploads/2021/05/Hydrogen-Brochure-1001-E2101-Rev.-A.pdf (visited on 06/14/2022).

[83] Orbital Propulsion Centre <OR> I. Surname, I. Surname, and I. Surname. *400 N Bipropellant Apogee Motors*. 2020. URL: https://www.space-propulsion.com/spacecraft-propulsion/apogee-motors/index.html (visited on 06/15/2022).

[84] BAE systems. *RAD750® 6U CompactPCI single-board computer*. 2018. URL: file://Users/carloscastrogarcia/Downloads/RAD750%5C%206U%5C%20CompactPCI_datasheet.pdf (visited on 06/13/2020).

[85] T. Satoh et al. "Performance of Akatsuki/IR2 in Venus orbit: the first year". In: *Earth Planets Space* 69 (2017), p. 154.

[86] Sumitaka Tachikawa et al. "Advanced passive thermal control materials and devices for spacecraft: A Review". In: *International Journal of Thermophysics* 43.6 (2022). DOI: doi:10.1007/s10765-022-03010-3.

[87] H. Tatsumoto et al. *Characteristics of a cryogenic supercritical hydrogen pump with dynamic gas bearings at J□PARC*. 2022. URL: https://indico.cern.ch/event/244641/contributions/1563474/attachments/418403/581064/P3.1-7_ICEC_25ICMC_2014_tatsumoto-poster-2.pdf (visited on 06/15/2022).

[88] F.W. Taylor and D.M. Hunten. *Venus: Atmosphere*. University of Oxford and University of Arizona: Elsevier, 2014.

[89] Tensor Tech. *Introduction to FSS100 Nano Fine Sun Sensor Performance*.

[90] *Thermal and Fluid Analysis Workshop - Lecture 1, stagnation point heating*. URL: https://tfaws.nasa.gov/TFAWS12/Proceedings/Aerothermodynamics%5C%20Course.pdf (visited on 06/14/2022).

[91] The Engineering ToolBox. *Carbon Dioxide - Specific Heat of Gas vs. Temperature*. URL: https://www.engineeringtoolbox.com/carbon-dioxide-d_974.html.

[92] Utah State University. *Bring back Hydrogen lifting gas*. 2021. URL: https://www.thecgo.org/benchmark/bring-back-hydrogen-lifting-gas/ (visited on 06/15/2022).

[93] *Vectran - Product data sheet*. URL: https://fibrxl.com/fibrxl-performance/fibers/vectran/ (visited on 06/14/2022).

[94] VICI DBS. *Why is the Helium shortage important to us?* Scantec Nordic, 2020.

[95] Winbond. *3V 512M-BIT SERIAL SLC NAND FLASH MEMORY*. 2019. URL: https://eu.mouser.com/datasheet/2/949/w25n512gv_rev_c_021319-1608269.pdf (visited on 06/13/2022).

[96] B. Fegley Y. Hong. *The formation of Carbonyl Sulfide (OCS) in Venus' lower atmosphere*. URL: https://www.lpi.usra.edu/meetings/metsoc97/pdf/5090.pdf.

A

Mission-level Requirements Compliance Table

Below, the compliance table for the mission requirements is given. It is important to note that as a consequence of the large number of requirements generated (1447) and the early stage of development, compliance cannot be discussed on all levels, and for all requirements at this moment, as verification thereof will require either additional verification or is predicated on a more detailed state of design. Furthermore, compliance has already been established in previous reports for some requirements [2].

Table A.1: Mission-level requirements compliance table.

ID	Description	Compliant?	Where Shown?
MIS-REQ-2.1	The mission shall perform measurements of the middle atmosphere (main cloud deck) between 50 km and 62 km of altitude.	y	Subsection 2.4.1 & Section 4.3
MIS-REQ-2.2	The mission shall take measurements at a latitude of 0 deg ± 5 deg.	y	Subsection 2.4.1 & Subsection 4.3.3
MIS-REQ-2.4	The mission shall conduct 2 measurement cycles sweeping each defined path.	y	Subsection 2.4.1
MIS-REQ-2.5	The mission shall take measurements every 1km of horizontal distance travelled.	y	Section 3.2
MIS-REQ-2.6	The mission shall take measurements within a longitude range of 0 deg and 360 deg.	y	Subsection 2.4.1 & Subsection 4.3.3
MIS-REQ-2.7	The mission shall obtain measurements with a height resolution of at least 100 m.	y	Section 3.2
MIS-REQ-2.8	The mission shall be able to track its altitude with an accuracy of at least 0.1 km.	y	Section 4.11
MIS-REQ-2.9	The mission shall be able to measure atmospheric temperature with an accuracy of at least 1 K.	y	[2]
MIS-REQ-2.10	The mission shall be able to measure atmospheric pressure with an accuracy of at least 1 mbar.	y	[2]
MIS-REQ-2.12	The mission shall be able to measure meridional (North-South) wind speed magnitudes with an accuracy of at least 1.1 m/s.	y	Subsection 4.11.4
MIS-REQ-2.13	The mission shall be able to measure zonal (East-West) wind speed magnitudes with an accuracy of at least 1.1 m/s.	y	Subsection 4.11.4
MIS-REQ-2.14	The mission shall be able to measure vertical wind speed magnitudes with an accuracy of at least 1.1 m/s.	y	Subsection 4.11.4
MIS-REQ-2.15	The mission shall be able to track the altitude of the Sun above the horizon with an accuracy of at least 1 deg.	y	Subsection 4.11.4
MIS-REQ-2.16	The mission shall be able to determine the latitude at which measurements are taken on Venus with an accuracy of at least 1 deg.	y	Subsection 4.11.4
MIS-REQ-2.17	The mission shall be able to determine the longitude at which measurements are taken on Venus with an accuracy of at least 1 deg.	y	Subsection 4.11.4
MIS-REQ-2.18	The mission shall be able to measure meridional (North-South) wind speed magnitudes with a sensitivity of at least 0.1 m/s.	y	Subsection 4.11.4
MIS-REQ-2.19	The mission shall be able to measure zonal (East-West) wind speed magnitudes with a sensitivity of at least 1.1 m/s.	y	Subsection 4.11.4
MIS-REQ-2.20	The mission shall be able to measure vertical wind speed magnitudes with a sensitivity of at least 0.1 m/s.	y	Subsection 4.11.4
MIS-REQ-3.1	The mission shall measure the concentration levels of phosphine with a sensitivity of at least 1 ppb.	y	[2]
MIS-REQ-3.2	The mission shall measure the concentration levels of phosphine with an accuracy of at least 1 ppb.	y	[2]
MIS-REQ-3.3	The mission shall measure the concentration levels of phosphine from 50 km to 60 km of altitude	y	Subsection 2.4.1
MIS-REQ-3.5	The mission shall measure the concentration levels of phosphine over a period of at least 200 Earth days.	y	Subsection 2.4.1

Table A.1: Mission-level requirements compliance table.

ID	Description	Compliant?	Where Shown?
MIS-REQ-3.6	The mission shall measure the concentration levels of ammonia with a sensitivity of at least 1 ppm.	y	[2]
MIS-REQ-3.7	The mission shall measure the concentration levels of ammonia with an accuracy of at least 1 ppm.	y	[2]
MIS-REQ-3.8	The mission shall measure the concentration levels of ammonia from 48 km to 60 km of altitude.	y	[2]
MIS-REQ-3.10	The mission shall measure the concentration levels of ammonia over a period of at least 200 Earth days.	y	Subsection 2.4.1
MIS-REQ-3.11	The mission shall measure the concentration levels of carbonyl sulfide with a sensitivity of at least 1 ppm.	y	[2]
MIS-REQ-3.12	The mission shall measure the concentration levels of carbonyl sulfide with an accuracy of at least 1 ppmv.	y	[2]
MIS-REQ-3.13	The mission shall measure the concentration levels of carbonyl sulfide from 30 km to 40 km of altitude.	y	[2]
MIS-REQ-3.15	The mission shall measure the concentration levels of carbonyl sulfide for a period of at least 200 Earth days.	y	Subsection 2.4.1
MIS-REQ-3.16	The mission shall be able to detect circular polarization with an accuracy of at least 10^{-4}.	y	[2]
MIS-REQ-3.17	The mission shall be able to detect circular polarization with a sensitivity of at least 10^{-4}.	y	[2]
MIS-REQ-3.18	The mission shall measure circular polarization at least 200 Earth days.	y	Subsection 2.4.1
MIS-REQ-4.1	The mission shall measure the concentration levels of sulfur dioxide with a sensitivity of at least 10 ppb.	y	[2]
MIS-REQ-4.2	The mission shall measure the concentration levels of sulfur dioxide with an accuracy of at least 10 ppb.	y	[2]
MIS-REQ-4.3	The mission shall measure the concentration levels of sulfur dioxide from 50 km to 60 km of altitude.	y	Subsection 2.4.1
MIS-REQ-4.5	The mission shall measure the concentration levels of sulfur dioxide over a period of at least 200 Earth days.	y	Subsection 2.4.1
MIS-REQ-4.6	The mission shall measure the concentration levels of water with a sensitivity of at least 10 ppm.	y	[2]
MIS-REQ-4.7	The mission shall measure the concentration levels of water with an accuracy of at least 10 ppm.	y	[2]
MIS-REQ-4.8	The mission shall measure the concentration levels of water from 51 km to 62 km of altitude.	y	Subsection 2.4.1
MIS-REQ-4.10	The mission shall measure the concentration levels of water over a period of at least 200 Earth days.	y	Subsection 2.4.1
MIS-REQ-4.11	The mission shall measure ultraviolet irradiance with a sensitivity of at least $1 * 10^-7$ UV:PAR.	y	[2]
MIS-REQ-4.12	The mission shall measure ultraviolet irradiance with an accuracy of at least $1 * 10^-7$ UV:PAR.	y	[2]
MIS-REQ-4.13	The mission shall measure the ultraviolet irradiance from 49 km to 59 km of altitude.	y	Subsection 2.4.1
MIS-REQ-4.15	The mission shall measure the ultraviolet irradiance over a period of at least 200 Earth days.	y	Subsection 2.4.1
MIS-REQ-4.16	The mission shall measure the radiation incidence on Venus with a sensitivity of at least 0.01 Gy.	y	[2]
MIS-REQ-4.17	The mission shall measure the radiation incidence on Venus with an accuracy of at least 0.01 Gy	y	[2]
MIS-REQ-4.18	The mission shall measure the radiation incidence of Venus from 51 km to 62 km of altitude.	y	Subsection 2.4.1
MIS-REQ-4.20	The mission shall measure the radiation incidence over a period of at least 200 Earth days.	y	Subsection 2.4.1
MIS-REQ-4.21	The mission shall measure the presence of aerosols with an accuracy of at least 150 nm.	y	[2]
MIS-REQ-4.22	The mission shall measure the presence of aerosols in Venus' atmosphere from 50 km to 61 km of altitude.	y	Subsection 2.4.1
MIS-REQ-5.1	The mission shall detect natural olivine with a minimum particle volume of at least mm^3	y	[2]

Table A.1: Mission-level requirements compliance table.

ID	Description	Compliant?	Where Shown?
MIS-REQ-5.3	The mission shall detect and measure the presence of natural olivine over a period of at least 200 Earth days.	y	Subsection 2.4.1
MIS-REQ-5.4	The mission shall take a measurement for olivine every 4 hours for the duration of the mission lifetime.	y	Section 3.2
MIS-REQ-5.5	The mission's instruments shall take measurements of the chemical markers; phosphine, ammonia, carbonyl sulfide, sulfur dioxide, water and olivine within 1 s of each other.	y	Section 3.2
MIS-REQ-5.7	The mission's instruments shall take measurements of the chemical markers; phosphine, ammonia, carbonyl sulfide, sulfur dioxide, water and olivine with 0.1 s accuracy.	y	Section 3.2
MIS-REQ-6.1	The user shall be able to attain the data through an internet server.	?	To be designed
MIS-REQ-7.1	The mission shall deliver all science data to the user before 2035.	y	Subsection 2.4.1, Subsection 2.4.2, Subsection 2.4.3
MIS-REQ-8.1	The total mission cost shall not exceed 630M EUR (FY2022).	y	Subsection 2.8.3
MIS-REQ-9.1	The spacecraft shall have a probability of 90% of achieving the mission level science requirements.	y	Subsection 2.8.3
MIS-REQ-10.1	The mission shall not leave any mission segment in Venus' orbit.	y	Subsection 2.4.2, Subsection 6.10.5
MIS-REQ-11.1	The mission shall adhere to tailored "U-ST-20C Planetary Protection Standards" with regards to impact probability.	?	Contingent on following iteration
MIS-REQ-11.2	The mission shall adhere to U-ST-20C Planetary Protection Standards for Mars Surface missions with life detection tailored to a Venus mission.	?	Contingent on following iteration
MIS-REQ-12.1	The mission should minimize the use of high impact materials.	/	Requirement is recommendation
MIS-REQ-13.1	The mission shall make use of existing production processes.	?	Contingent on following iteration
MIS-REQ-13.2	The mission shall make use of existing production processes.	?	Contingent on following iteration
MIS-REQ-14.1	The mission shall adhere to the applicable national standards.	?	Contingent on following iteration
MIS-REQ-14.2	The mission shall adhere to the applicable national regulations.	?	Contingent on following iteration
MIS-REQ-14.13	The mission shall adhere to the applicable international standards.	?	Contingent on following iteration
MIS-REQ-14.4	The mission shall adhere to the applicable international regulations.	?	Contingent on following iteration
MIS-REQ-15.1	The mission shall make use of existing or foreseeable launchers.	y	Subsection 2.5.2
MIS-REQ-16.1	The mission shall adhere to the payload standards specificed by the selected launcher vehicle.	y	Subsection 2.8.3, Section 4.14, Section 5.13, Section 6.13
MIS-REQ-17.1	The mission shall make use of existing ground element(s).	y	Subsection 2.5.2